University of Reading

Hormonal Regulation of Adrenal Function by POMC-derived Peptides

A THESIS SUBMITTED FOR THE DEGREE OF DOCTOR OF PHILOSOPHY

THE SCHOOL OF BIOLOGICAL SCIENCES

Fatema Humoud AlShammari

February 2024

Declaration

I confirm that this is my own work, and the use of all material from other sources has been properly and fully acknowledged.

_____

Dedication

To my beloved kids, Humoud & Hessah, I love you to the moon and back!

Abstract

Over the last 40 years, numerous studies have reported the role of the N-terminal of proopiomelanocortin (N-POMC) in adrenal steroidogenesis and growth; however, little is known about the cell surface receptor that it activates. Identifying this receptor will help to understand the pathophysiology of certain adrenal disorders, such as familial glucocorticoid deficiency (FDG) and adrenal carcinomas. Recent data from the Bicknell lab identified the orphan G protein-coupled receptor 19 (GPR19) as a possible N-POMC receptor in adrenal cells. Preliminary data showed that overexpression of GPR19 leads to the accumulation of the protein inside the cell, so we proposed that it might require the co-expression of the melanocortin 2 receptor accessory protein (MRAP) to be translocated to the plasma membrane.

In this study, we generated three stably transformed cell lines in HEK-293: the first overexpresses GPR19, the second expresses MRAP, and the third overexpresses GPR19 and MRAP. The gene expression of GPR19 and MRAP was confirmed by RT-PCR, whilst the protein expression was confirmed by immunocytochemistry (ICC) and immunoblotting. ICC showed that in the cell line that expresses MRAP the fluorescent staining of GPR19 was greater on the plasma membrane in comparison to the cell lines that do not express it. ICC images of cells expressing GPR19/MRAP revealed that both are localised on the cell membrane and inside the cells. Co-IP results showed that GPR19 and MRAP precipitate together, and an N-$POMC_{1-28}$ antibody could precipitate the GPR19 cross-linked to N-$POMC_{1-28}$. Moreover, cells treated with N-$POMC_{1-28}$, either unlabelled or labelled with Alexa-Fluor 488 or biotin, showed a significant increase in signal intensity in the cell lines that overexpress GPR19 and/or MRAP in comparison to the wild-type. In competitive binding assays, the N-POMC fragments 1-49 and 1-77 were shown to compete with N-$POMC_{1-28}$. In addition, N-$POMC_{1-28}$ activates GPR19, and that leads to the reduction of cAMP levels in the cells, the increase of ERK1/2 phosphorylation and the activation of the downstream transcription factors, which

consequently stimulate cell proliferation. These results support the hypothesis that GPR19 is the receptor for N-POMC, and MRAP is required for full functionality. The identification of a receptor for N-POMC is significant and might be a potential target in adrenocortical carcinomas.

Acknowledgements

Words cannot express my gratitude to my supervisors, Dr. Andrew Bicknell and Dr. Elizabeth Lander, for their continuous encouragement, support, knowledge, and patience throughout this project.

I would like to thank the chair of my research committee, Prof. Phil Knight, and Prof. Philip Dash, for generously providing knowledge and feedback.

I would also like to say a big thank you to Ms Hong Lin, who is always available for help. I am very grateful for all the support you gave me.

A huge thank you to my colleagues Salim AlHarthi, Bokai Guo (Loki), Ali Alqallaf, Megan Donnelly, Leah Napier, and Jomanah Alqallaf, who have given me a huge amount of help and support over the years. Also, thanks to the entire staff, members, PhD students, and postdocs in the Hopkins building for providing a friendly and welcoming environment.

Deep thanks should also go to the academic librarian, Mr Tim Chapman, who provided training on using Endnote for referencing and support in using library e-resources.

A massive thank you to my wonderful mother. I wouldn't be the person I am today without you. I am so grateful to have you in my life.

To my amazing father, who always believed in me and encouraged me to follow my dreams. Rest in peace, Daddy!

I would like to say thank you to my handsome son, who is the light of my life and to my beautiful daughter, who fills my life with happiness. You are my everything.

A hug thanks to the rest of my family and to my best friends Manal, Dalal and Mardhiya. Their belief in me has kept my spirits and motivation high during this process.

Thank you endlessly and with love to my husband Abdulaziz Klaib. Thank you for your love, support, and never-ending patience. I am so blessed to have you in my life. Without your support and encouragement, the completion of this journey would not have been possible.

A deep thank you to all the staff of the Public Authority for Applied Education and Training and Kuwait Cultural Office for their support and help over the past years, especially during the tough months of the COVID-19 pandemic, and for generously funding this project.

Table of Contents

List of Figures

List of Tables

Abbreviations Used

AC	Adenylyl cyclase
ACE	Angiotensin-converting enzyme
ACTH	Adrenocorticotropic hormone
AGP	Adrenogonadal primordium
Akt	Protein kinase B
ALP	Alkaline phosphatase
APS	Ammonium persulfate
AsP	Adrenal secretory protease
BLAST	Basic local alignment search tool
B_{max}	Maximum density of receptors
CAH	Congenital adrenal hyperplasia
cAMP	Cyclic Adenosine Monophosphate
CLIP	Corticotrophin-like intermediate peptide
CME	Clathrin-mediated endocytosis
Co-IP	Co-immunoprecipitation
CREB	cAMP response element binding protein
CRH	Corticotrophin-releasing hormone
CTCF	Corrected total cell fluorescence
CYP11B1	P450 11β-hydroxylase
CYP11B2	Aldosterone synthase
CYP17A1	17α-hydroxylase
CYP21A2	21-hydroxylase
D1-D5	Dopamine receptors (D1, D2, D3, D4 and D5)
DEX	Dexamethasone
DHEA	Dehydroepiandrostenedione

DHEAS	Dehydroepiandrostenedione sulphate
DMSO	Dimethylsulfoxide
DNA	Deoxyribonucleic acid
DST	Disuccinimidyl tartrate
DTT	Dithiothreitol
DZ	Definitive zone
E. coli	Escherichia coli
EEA-1	Early endosome antigen-1
EGFP	Enhanced green fluorescent protein
ELISA	Enzyme-linked immunosorbent assay
Enho	Energy homeostasis-associated gene
ERK1/2	Extracellular signal-regulated kinases 1 and 2
FBS	Foetal bovine serum
FGD	Familial glucocorticoid deficiency
FGFβ	Fibroblast growth factor beta
Flp-In	Flp Recombinase-Mediated Integration technique
FRET	Fluorescence resonance energy transfer
FRT	Flp Recombination Target
FZ	Foetal zone
G0	Cell cycle gap 0 phase
G1	Cell cycle gap 1 phase
Gata4	GATA-binding protein 4
GEPIA	Gene Expression Profiling Interactive Analysis
GFP	Green fluorescence protein
GPCRs	Guanine protein-coupled receptors
GPR19	Guanine protein-coupled receptor 19

GPRASP	G protein-coupled receptor-associated sorting protein
GRKs	G protein receptor kinases
HAC15	Adrenocortical carcinoma cell line
HBSS	Hanks' Balanced Salt Solution
HEK-293	Human embryonic kidney-293 cell line
HPA-axis	Hypothalamic–pituitary–adrenal axis
HRP	Horseradish peroxidase
HSD3β2	3β-hydroxysteroid dehydrogenase
HSDs	Hydroxysteroid dehydrogenases
HSL	Hormone-sensitive lipase
IBMX	3-isobutyl-1-methylxanthine
ICC	Immunocytochemistry
IGF2	Insulin-like growth factor 2
IRES	Internal-ribosomal entry site
JNK	c-Jun N-terminal kinase
JP	Joining peptide
K_d	Equilibrium dissociation constant
Ki	Inhibitor dissociation constant
LB	Luria-Bertani
MAPK	Mitogen-activated protein kinase
MCR1-MCR5	Melanocortin receptors
MCS	Multiple cloning site
MEK	Mitogen-activated kinase/extracellular signal-regulated kinase
MRAP	Melanocortin receptor accessory protein
MSH	Melanocyte-stimulating hormone
MUP	4-methylumbelliferyl phosphate

NAD+	Adenine dinucleotide
NADP+	Nicotinamide adenine dinucleotide phosphate
NDP-MSH	[Nle4, D-Phe7] alpha-melanocyte-stimulating hormone
NHS ester	N-hydroxysuccinimide ester
N-POMC	N-terminal of POMC
OD	Optical density
ONPG	o-nitrophenyl-β-D-galactopyranoside
OX1R	Orexin receptor
P450scc	Cytochrome P450-dependent cholesterol sidechain cleavage
PBS	Phosphate buffered saline
PC1 and PC2	Prohormone convertases enzymes 1 and 2
PCs	Prohormone convertases
PDEs	Phosphodiesterases
PFA	Paraformaldehyde
PI3K	Phosphoinositide-3-kinase
PKA and C	Protein kinase A and C
PKR1 and PKR2	Prokineticin receptors
PNMT	Phenyl ethanolamine N-methyltransferase
POMC	Proopiomelanocortin
RAMPs	receptor activity modifying proteins
RAS	Renin–angiotensin system
RhoA	GTP Ras-homology A
RSK	Ribosomal S6 kinase
RSP	Regulated secretory pathway
RT-PCR	Real time- polymerase chain reaction
S phase	Cell cycle synthesis phase

SDS-PAGE	Sodium dodecyl sulphate–polyacrylamide gel electrophoresis
SEAP	Secreted placental alkaline phosphatase
Sf1	Steroidogenic factor 1
SRE	Serum response element
SRF	Serum response factor
SSTR1-SSTR5	Somatostatin receptors
StAR	Steroidogenic acute regulatory protein
TAE	Tris Acetate EDTA
TB	Transcription blocker
TBS	Tris-buffer saline
TBST	Tris-buffer saline tween-20
TEMED	N,N,N′,N′-Tetramethylethylenediamine
TF	Transcription factors
TFA	Trifluoroacetic acid
TMB	Tetramethylbenzidine
TPM	Transcripts per million
TZ	Transitional zone
WT	Wild type
Wt1	Wilms tumour suppressor-1
ZF	Zona Fasciculata
ZG	Zona Glomerulosa
ZR	Zona Reticularis
β-LPH	β-endorphin
β-MSH	β-melanocortin stimulating hormone

Chapter 1: Introduction

1.1. Pro-opiomelanocortin (POMC)

The pro-opiomelanocortin (POMC) gene and the peptides it encodes were first investigated in the pituitary gland of mammals. It is produced mainly by corticotroph cells in the anterior pituitary gland. Further studies reported that the POMC gene is expressed in several other tissues, including the hypothalamus, skin, testis, thyroid, placenta, pancreas, gut, kidney, adrenal and liver (Bicknell, 2008; Smith & Funder, 1988). POMC peptides in the circulation are derived mainly from the pituitary, and thus, the peptides produced in these other tissues have either an autocrine or paracrine action. The term pro-opiomelanocortin was first presented by Chrétien et al. (1979) to describe a precursor molecule that encodes the peptides adrenocorticotrophic hormone (ACTH), β-endorphin (β-LPH) and β-melanocortin stimulating hormone (β-MSH) and to reflect the fact that they are derived from the same precursor molecule even though they have different biological function, which was suggested earlier by Lowry et al. (1977).

The 267 amino acids sequence of human POMC preproprotein undergoes extensive, tissue-specific, post-translational processing by many different enzymes. The POMC processing is species-specific as there is some variation in the length of some of the POMC peptides, even though the gene structure is well conserved among species. The prohormone convertases (PCs) cleave POMC at specific lysine-arginine sites and are distributed in a tissue-specific manner in the pituitary and in the brain (Cawley et al., 2016; Harno et al., 2018; Zhou et al., 1993). There are eight potential dibasic cleavage sites within the POMC preproprotein structure and, depending on the type of PCs that are expressed in that tissue and the three-dimensional structure of POMC, allow easier access to the active site of the convertase.

The post-translational modification after cleavage by the PCs produces biologically active peptides that exert multiple physiological functions. Those modifications are catalysed by different enzymes, such as the carboxypeptidase E (CPE), that remove the basic amino acid (Lys and/or Arg) residues from the smaller POMC fragments. While the peptidyl-glycine α-amidating-monooxygenase (PAM) enzyme amidated the C-terminal after the removal of the basic amino acid residues by CPE. The N-terminal amino acid residues of some peptides are acetylated by the enzyme N-acetyltransferase (N-AT). This step is important to protect these peptides from degradation and for their biological activity (Harno et al., 2018; Zhou et al., 1993).

1.1.1. Processing of the Human POMC

1.1.1.1. Anterior Pituitary

In the anterior lobe of the human pituitary, the 267 amino acids sequence POMC (Fig. 1.1) is initially cleaved by pro-hormone convertase 1/3 (PC1/3) at the C-terminal side of the dibasic lysine-arginine site of the C-terminal of ACTH and the N-terminal of β-LPH to yield pro-ACTH and β-LPH. The second cleavage, at another lysine-arginine site, occurs between the C-terminal of the joining peptide (JP) and the N-terminal of ACTH that releases ACTH and an N-terminal peptide. The latter will be processed further by the same enzyme to release pro-γ-MSH, also known as N-POMC$_{1\text{-}76}$ and JP (Cawley et al., 2016; Harno et al., 2018). The processing of POMC in the anterior pituitary leads to the release of those four POMC peptides: N-POMC, JP, ACTH, and β-LPH. Gossard et al. (1980) reported the presence of a 26 amino acid signal sequence before the N-POMC sequence, which is suggested to be cleaved rapidly after or even during translation.

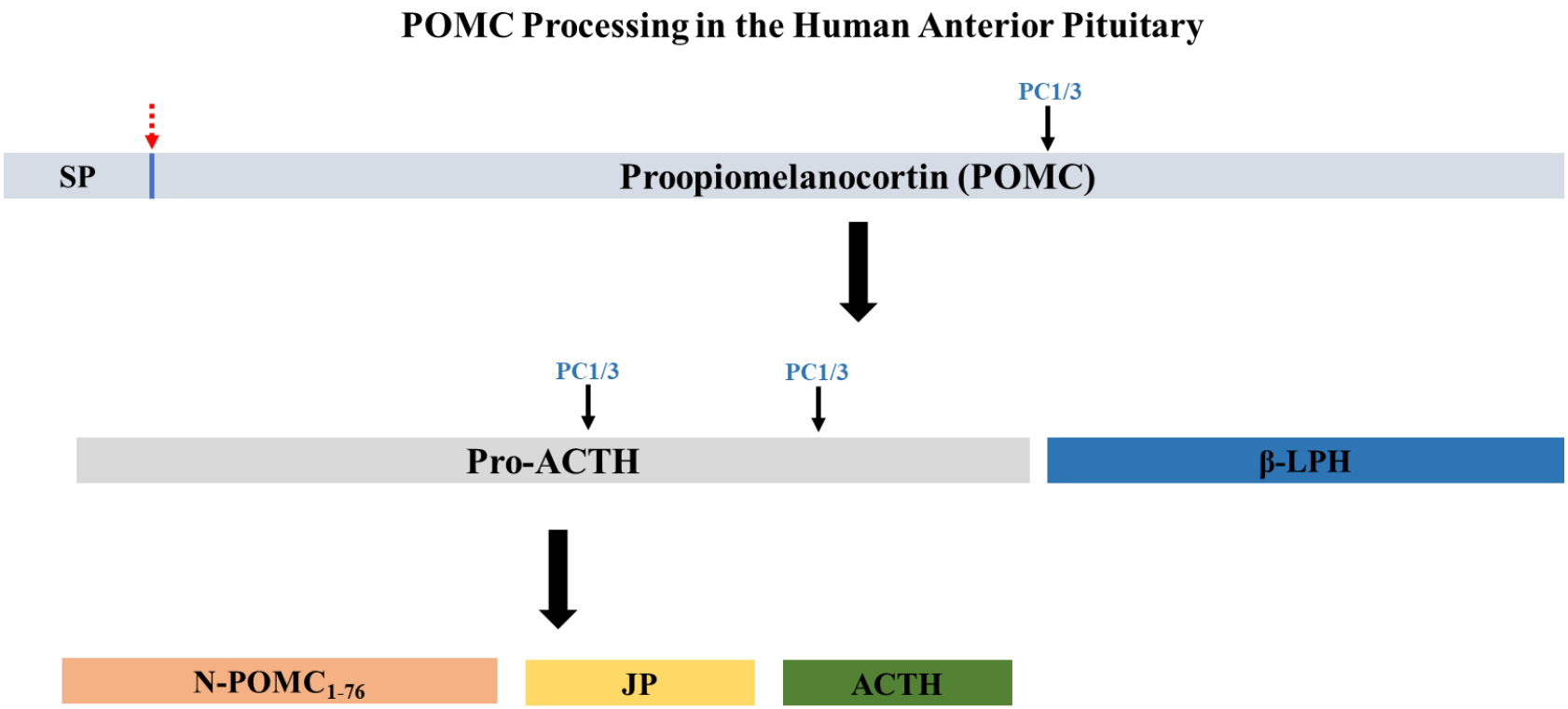

Fig. 1.1. Processing of the human POMC preproprotein in the anterior pituitary. The PC1/3 cleaved POMC at dibasic amino acid sites (lysine-arginine) to produce pro-ACTH and β-LPH. The pro-ACTH cleaved further by PC1/3 to produce N-terminal fragment N-POMC$_{1\text{-}76}$, joining peptide (JP) and ACTH. The first 26 amino acids, the sequence before N-POMC$_{1\text{-}76}$, is a signalling peptide (SP) that is suggested to be cleaved rapidly after or during translation.

1.1.1.2. Hypothalamus and Pars Intermedia

In the hypothalamus and pars intermedia of the pituitary, there is extensive processing of POMC in comparison to the anterior pituitary. As in the anterior pituitary, PC1/3 cleaves POMC to the four peptides mentioned earlier. This is followed by further cleavages by PC2 to produce smaller peptides (Fig.1.2).

1.1.1.2.1. Pro-γ-MSH Processing

Pro-γ-MSH or N-POMC was first known as the 16 K fragment in accordance with its apparent molecular weight on an electrophoresis gel (Eipper & Mains, 1980). The amino acid sequence of N-POMC is highly conserved among various mammalian and sub-mammalian species (Denef & Van Bael, 1998), where only the extreme C-terminal end differs, mainly because of one or more amino acid deletions. Rodent N-POMC consists of 74 residues, whereas the human N-POMC consists of 76 residues and bovine N-POMC of 77 residues. N-POMC contains two disulphide bridges at its N-terminal end, Cys2 paired to Cys24 and Cys8 paired to Cys20, inducing a hairpin tertiary structure (Seger & Bennett, 1986; Seidah & Chrétien, 1981). It has been reported that this disulphide bridge is essential for sorting POMC to the regulated secretory pathway (RSP) of the cell (Cool et al., 1995; Cool & Loh, 1994). It also has an O-linked glycosylation site at threonine (T45) and N-linked glycosylation at asparagine (N65) (Seger & Bennett, 1986; Seidah, Rochemont, Hamelin, Lis, et al., 1981) which is suggested to increase the half-life circulation of this peptide.

Human N-POMC$_{1-76}$ has a cleavage site of dibasic arginine-lysine, which would be cleaved by PC2 to produce two fragments: N-POMC$_{1-49}$ and Lys-γ-3-MSH (residues 50-76) (Zhou et al., 1993). Lys-γ-3-MSH is also known as γ-3-MSH as it was thought that PC2 would cleave the peptide after the lysine residue, but later studies show that γ-3-MSH starts with the lysine residue, and it is crucial for the full biological activity of this peptide (Harmer & Bicknell, 2005). The Lys-γ-3-MSH has an arginine-arginine dibasic amino acid cleavage site

that will undergo further processing to produce γ2-MSH, which will be modified further to γ1-MSH (Harno et al., 2018).

1.1.1.2.2. Joining Peptide Processing

Joining peptide (JP) was the last POMC fragment to be characterised. It was first described as a 31 amino acid missing POMC sequence identified from the human genomic DNA studies. Seidah and his group reported the isolation and sequence characterisation of this peptide from human pituitary extracts, and since then, it has been called a joining peptide (Seidah et al., 1981). They found that this peptide is 30 amino acid residues long and not 31 amino acid residues as in the DNA sequence. They proposed that the missing C-terminal glycine is cleaved during processing and then undergoes amidation at its C-terminal glutamic acid residue. It is secreted from the anterior pituitary as a homodimer (Bertagna et al., 1988), where the single cysteine residue that is only present in the human peptide structure allows dimerisation via the thiol groups, which makes it a unique POMC product. The biological role of the JP is unclear as its sequence shows a wide species difference (Bertagna et al., 1988; Jahnke et al., 1983) and whether the dimerisation of any physiological importance as the cysteine residue is only present in the human JP sequence (Bertagna et al., 1988).

1.1.1.2.3. ACTH Processing

ACTH consists of 39 residues is cleaved by PC2 to a shorter $ACTH_{1-17}$ and corticotrophin-like intermediate lobe peptide (CLIP), which represents the ACTH fragment 18-39 (Fig. 1.2). Then, the shorter $ACTH_{1-17}$ undergoes three enzymatic reactions to produce α-MSH (Harno et al., 2018). First, the enzyme CPE removes the C-terminal amino acids from $ACTH_{1-17}$ to generate $ACTH_{1-13}$, then amidation of the C-terminal of $ACTH_{1-13}$ by PAM to give des-acetyl α-MSH. This is then acetylated at the N-terminal by N-AT to generate α-MSH. The biological significance of CLIP is not well understood.

1.1.1.2.4. β-LPH Processing

β-LPH is also processed further to produce β-MSH and β-endorphin (Fig. 1.2). Initially, the dibasic site lysine-arginine between the C-terminal of γ-lipotropin (γ-LPH) and the N-terminal of β-endorphin is cleaved by PC2 (Cawley et al., 2016). The γ-LPH is then processed at a Lys-Lys site by the same enzyme to release β-MSH from its C-terminal. This Lys-Lys site is human-specific and is not present in the rat or mouse POMC sequence (Harno et al., 2018). Therefore, it is thought that β-MSH does not exist as a separate peptide in rodents. It is reported that shorter fragments of β-endorphin (1-31), 1-26 and 1-27 are also present in the pituitary and brain (Akil et al., 1985).

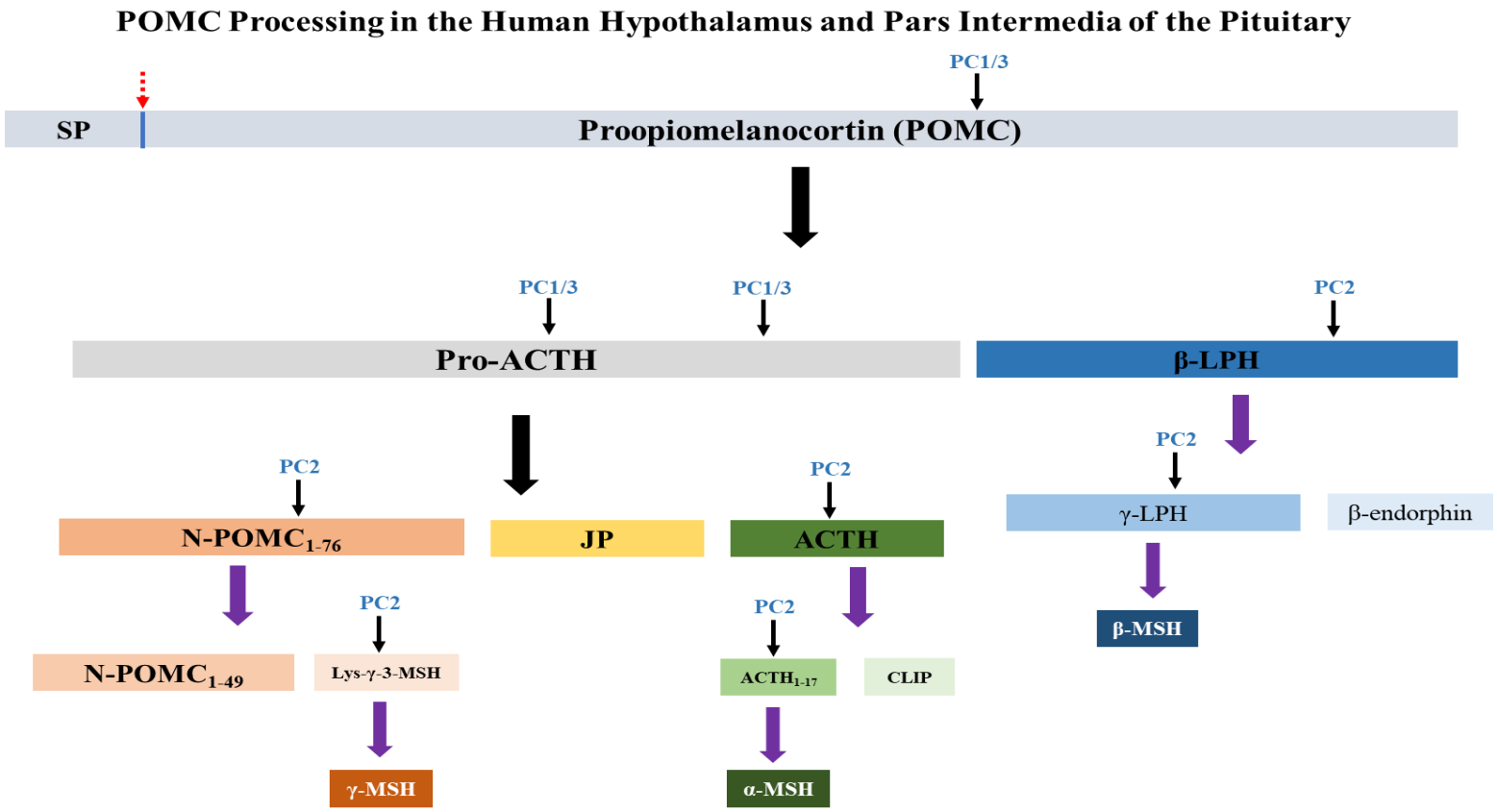

Fig. 1.2. Processing of the human POMC preproprotein in the human hypothalamus and pars intermedia of the pituitary. In the hypothalamus and pars intermedia, PC1/3 cleaves POMC into four peptides: N-POMC$_{1-76}$, JP, ACTH and β-LPH. The human N-POMC$_{1-76}$ is thought to be cleaved by PC2 to produce N-POMC$_{1-49}$ and Lys-γ-3-MSH. Moreover, Lys-γ-3-MSH can be cleaved by PC2 to produce γ-MSH. ACTH$_{1-39}$ is cleaved by PC2 to produce ACTH$_{1-17}$, which will be processed further to produce α-MSH and CLIP. β-LPH undergoes different cleavages by PC2 to produce two other active peptides, γ-LPH and β-endorphin. γ-LPH will be cleaved further by PC2 to β-MSH.

1.1.2. The Melanocortin Receptors

The POMC-derived peptides perform their biological activity through the melanocortin receptors (MCRs) and opioid receptors. The MCRs family consists of five members (MC1R-MC5R) that share high sequence homology and belong to class A of G-protein coupled receptors (GPCRs) that act primarily through cAMP as a second messenger. The MC1R, MC3R, MC4R, and MC5R were found to be activated by different MSH peptides and ACTH, while MC2R had an absolute specificity for ACTH. MSH peptides and ACTH contain a central tetrapeptide core Histidine-Phenylalanine-Arginine-Tryptophan (HFRW), which is essential for receptor binding and activation (Dores et al., 2016).

MC1R detected in the skin, brain, and immune system has a high affinity for α-MSH, and it can be activated by ACTH, β-MSH and γ-MSH. MC1R is involved in the regulation of pigmentation in the skin and in hair follicles. MC2R is detected in the adrenal gland, adipose tissue, and skin and shows a specific affinity to ACTH (that will be discussed in detail below). The MC3R is expressed in the hypothalamic region of the brain and has a role in energy homeostasis. It is also expressed in the peripheral tissues stomach, duodenum, pancreas, heart, testis, ovary, skeletal muscle, and kidney. The peptides α-, β-, γ-MSH and ACTH bind to MC3R. γ-MSH showed a high binding affinity for MC3R among the other MCRs (Dores et al., 2016; Gantz et al., 1993; Slominski et al., 2000). The MC4R is expressed in the brain and has a role in food intake and energy homeostasis. MC4R has an equal affinity for α-MSH and ACTH (Gantz et al., 1993). The MC5R is widely expressed in peripheral tissues such as adipose tissue, muscles, thymus, prostate, and skin. The physiological role of this receptor is not well understood. In mice, it was found that expression of MC5R is essential for normal thermoregulation and involved in the regulation of exocrine gland secretion (Chen et al., 1997). The primary

ligand of MC5R is α-MSH, but ACTH, β-MSH and γ-MSH also have binding affinity to this receptor (Gantz et al., 1993).

β-endorphin does not have the HFRW sequence and, therefore, does not signal through the MCRs; instead, it binds with high affinity to the μ-opioid receptor. The μ-opioid receptors are expressed in the central brain regions, including the cortex, hippocampus, hypothalamus, and brain stem, and are widely expressed in peripheral tissues, including the pancreas, testis, ovary, and kidney. β-endorphin has a role in energy homeostasis and feeding behaviour and acts as a local pain modulator (Harno et al., 2018; Slominski et al., 2000).

1.2. Adrenal Gland: Anatomy, Physiology and Growth

Adrenal glands are an important organ for well-being and survival where early studies found that animals could not survive bilateral adrenalectomy (Freed et al., 1931; Fukuda, 1952; Gaunt, 1933). They are a key component of the hypothalamic-pituitary–adrenal (HPA)-axis that plays a crucial role in the body to adapt to stress. They are endocrine tissues that produce active steroid hormones (glucocorticoids and mineralocorticoids), catecholamines and neuropeptides. The adrenals are located on top of the upper pole of the kidneys (Fig. 1.3), and the normal human adrenal is less than 1 cm in width and less than 4 cm in length. They are asymmetrical, with the right adrenal being pyramidal in shape and the larger left adrenal gland being crescent-shaped. The adult adrenal gland is enclosed within a capsule of fibroblasts and myofibroblasts and is composed of two combined endocrine tissues, the adrenal cortex and the medulla, each having different embryological origins (Yates et al., 2013).

1.2.1. Adrenal Gland Anatomy

1.2.1.1. Adrenal Cortex

The adrenal cortex surrounds the medulla on all sides and is composed of three distinct zones: zona glomerulosa (ZG), zona fasciculata (ZF), and zona reticularis (ZR). The adrenal cortex differentiates fully into those three zones by 3 years of age, where the ZG and ZF are present at birth, but the ZR develops later (Yates et al., 2013). These zones vary in their morphological features and the steroid hormones they produce.

The zona glomerulosa (ZG) is the outer zone of the cortex, and it is composed of a thin region of columnar cells arranged in round clusters. It serves as the unique source of the mineralocorticoid steroid hormone aldosterone as it is the only tissue that expresses aldosterone synthase (CYP11B2) (Yabu et al., 1991). Aldosterone production is mainly regulated by the renin-angiotensin system (RAS), but the HPA axis also causes circadian variation of aldosterone. This zone is essential for life as aldosterone is responsible for controlling blood volume and salt-water balance, and loss of this zone or the failure to secrete aldosterone may result in death (Gao et al., 2021).

The zona fasciculata (ZF) is the thickest zone of the cortex, as it makes up more than 70% of the cortex, and it is composed of polygonal epithelial cells that have many intracellular lipid droplets and arranged in radial columns separated by fenestrated capillaries. The ZF is the source of the glucocorticoid hormone, corticosterone in rats and mice and cortisol in humans, of which both have influential effects on metabolism, the cardiovascular system, and the immune system (Gao et al., 2021; Yates et al., 2013).

The zona reticularis (ZR) is the innermost layer of the cortex adjacent to the adrenal medulla. The ZR is composed of polyhedral cells arranged in a mesh-like structure. It is responsible for the biosynthesis of androgens such as

dehydroepiandrostenedione (DHEA), DHEA sulphate (DHEAS) and a low amount of androstenedione, which is primarily secreted in humans and higher primates (Gao et al., 2021). Recent studies have provided evidence that the ZR produces other androgens called 11-oxygenated androgens that include derivatives of androstenedione and testosterone e.g., 11β-hydroxyandrostenedione, 11-ketoandrostenedione, 11β-hydroxytestosterone and 11-ketotestosterone (Barnard et al., 2021; Rege et al., 2019). Those androgens can be used as a biomarker in disorders and diseases associated with androgen excess, such as congenital adrenal hyperplasia, castration-resistant prostate cancer and polycystic ovary syndrome (Barnard et al., 2021).

1.2.1.2. Adrenal Medulla

The adrenal medulla is the inner core of the adrenal gland and consists almost entirely of modified neuronal cells derived from the sympathetic nervous system (Yates et al., 2013). The medullary secretory cells are called chromaffin cells. The main secretory products are catecholamines, adrenaline and noradrenaline, which are secreted into the blood in response to activation by acetylcholine and calcium ions. The fact that the cortical cells and the chromaffin cells contact each other directly, as there is minimal, if any, connective tissue between them, demonstrates the possible paracrine interactions between the two endocrine systems (Ehrhart-Bornstein et al., 1998; Yates et al., 2013). In addition to the catecholamines, chromaffin cells produce, store, and release an array of neuropeptides where, some of which exert a stimulatory effect on cortical steroidogenesis while others are inhibitory (Ehrhart-Bornstein et al., 1998).

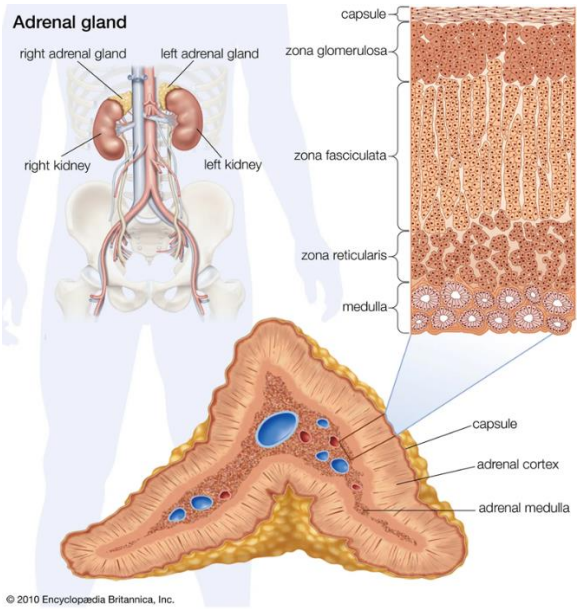

Fig. 1.3. Adrenal gland cross section demonstrating the adrenal zones. A thin fibrous capsule surrounds the adrenal cortex. The adrenal cortex consists of three zones, the zona glomerulosa (ZG), zona fasciculata (ZF), and zona reticularis (ZR). The ZG is the thinnest zone of the cortex. The ZF is the thickest zone of the cortex and is composed of columns of cortical cells. The cells of the ZR are smaller and less vacuolated compared to the ZF. The central region is the adrenal medulla, composed primarily of chromaffin cells (Obtained from Encyclopaedia Britannica).

1.2.2. Adrenal Steroidogenesis

Steroid hormones are synthesised in the adrenal glands, the gonads, and the placenta. The adrenal steroids are synthesised from cholesterol, the principal substrate for all steroid hormones, through a series of enzymatic reactions that take place in the inner membrane of mitochondria and in the smooth endoplasmic reticulum (Ghayee & Auchus, 2007; Yates et al., 2013). There are three mechanisms to acquire cholesterol for adrenal steroidogenesis: uptake of circulating lipoprotein-bound cholesterol, hydrolysis of lipid droplet-stored cholesterol esters, and de novo synthesis of cholesterol from acetyl-CoA (Payne & Hales, 2004). The steroidogenic enzymes are grouped into two major classes: cytochrome P450-dependent enzymes and hydroxysteroid dehydrogenases (HSD). The expression of those enzymes in the adrenal cortex determines the zonal-specific steroid hormone that it will produce and provides functional separation of the three zones.

1.2.2.1. Cytochrome P450-dependent Enzymes

Cytochrome P450 refers to a large group of enzymes which have approx. 500 amino acids and a single heme group, with a characteristic absorption peak at 450 nm in their reduced states in the presence of carbon monoxide (Payne & Hales, 2004). The recommended nomenclature for the cytochrome P450 genes is CYP for the human genes. CYP genes are located on chromosome 15q23-q24. Cytochrome P450-dependent cholesterol sidechain cleavage (P450scc) genes are expressed in all the primary steroidogenic tissues, the adrenal cortex and gonads, and non-classic steroidogenic tissues, such as the brain. There are two biochemical classes of P450 enzymes. Type I enzymes are expressed in mitochondria (e.g., P450scc), and type II enzymes are localised in the endoplasmic reticulum (e.g., cytochrome P450 21-hydroxylase also known as CYP21A2) (Ghayee & Auchus, 2007).

The conversion of cholesterol to pregnenolone is catalysed by a P450scc also known as CYP11A1, which is the initial and rate-limiting step of steroidogenesis (Fig. 1.4). This step is preceded by a key step which is the movement of cholesterol from the outer to the inner mitochondrial membrane via steroidogenic acute regulatory protein (StAR) where the P450scc enzyme is localised (Elustondo et al., 2017). Pregnenolone then leaves the mitochondrion and undergoes further transformation to other steroid intermediates in the endoplasmic reticulum.

Two key enzymes in the adrenal catalyse the terminal reactions in steroid biosynthesis, and their expression is limited to the adrenal cortex: P450 11β-hydroxylase (CYP11B1) and aldosterone synthase (CYP11B2) (Payne & Hales, 2004). Those enzymes are in the inner mitochondrial membrane, and thus, adrenal steroidogenesis requires the participation and coordination of both the mitochondria and the endoplasmic reticulum.

Aldosterone synthase appears to be expressed exclusively in adrenal ZG cells (Payne & Hales, 2004). It catalyses the synthesis of aldosterone from 11-deoxycorticosterone through three sequential reactions: 11β-hydroxylation of 11-deoxycorticosterone, hydroxylation of carbon 18, followed by oxidation of the hydroxyl group at carbon-18 to yield the carbon-18 aldehyde group, resulting in the formation of aldosterone.

The major site of CYP11B1 expression is in the adrenal ZF and ZR, whilst it is not expressed in the ZG (Payne & Hales, 2004). It can perform the first two catalytic reactions of CYP11B2; however, the 18-methyl oxidation generating aldosterone is unique to the type 2 isozyme. CYP11B1 catalyses the 11β-hydroxylation of 11-

deoxycorticosterone and 11-deoxycortisol to form corticosterone and cortisol, respectively, in the inner mitochondrial membrane.

In humans, the ZF and ZR highly express 17α-hydroxylase (CYP17A1), but not in the ZG, which can be described as the gatekeeper towards glucocorticoids and sex steroid biosynthesis and competes with 3β-hydroxysteroid dehydrogenase (HSD3β2) for substrate (Payne & Hales, 2004). This enzyme is not expressed in mouse or rat adrenal glands, leading to the production of corticosterone rather than cortisol.

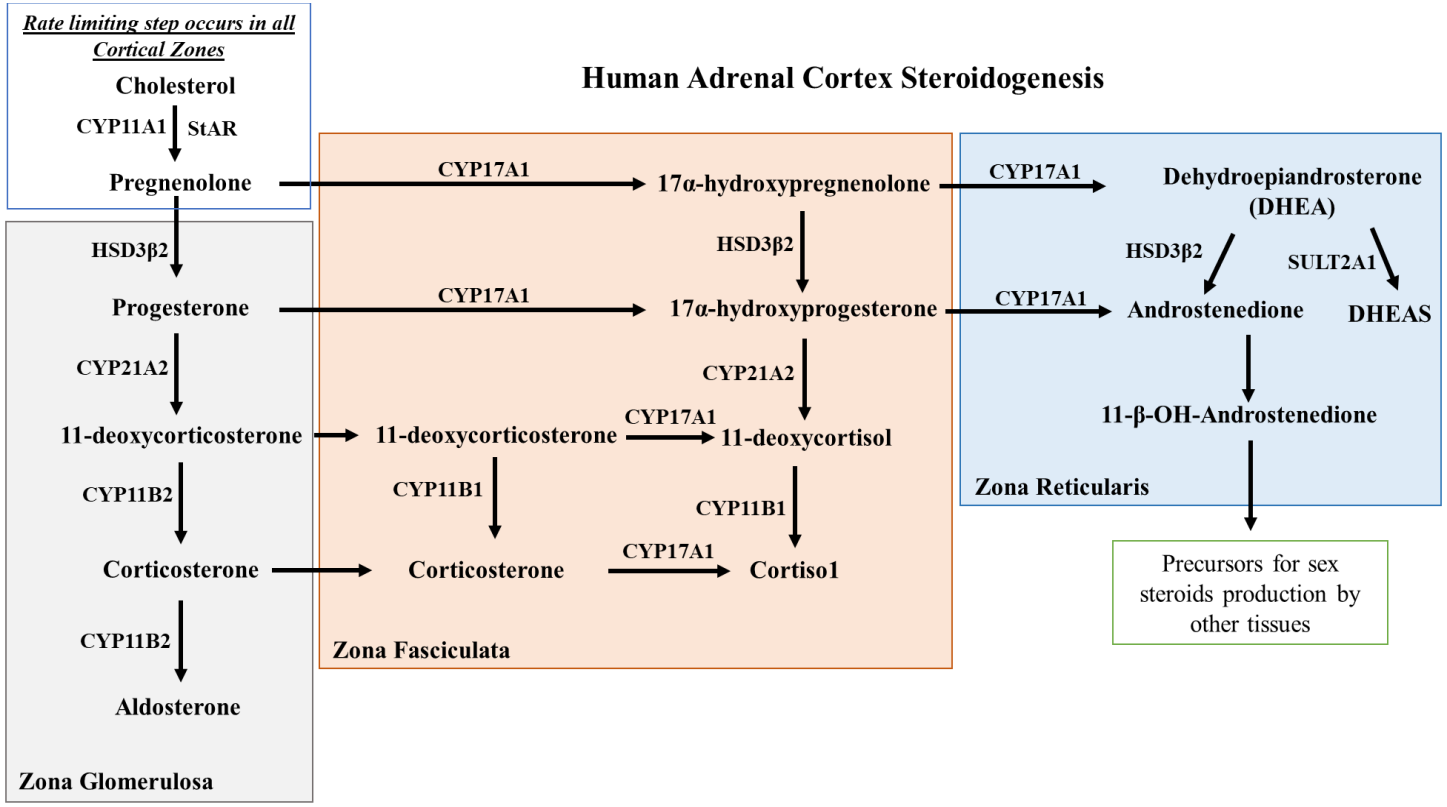

Fig. 1.4. Schematic representation of human adrenal steroidogenesis pathway in the three cortical zones. StAR: steroidogenic acute regulatory protein: shift cholesterol from the outer to the inner mitochondrial membrane, CYP11A1 or P450scc: Cholesterol side-chain cleavage enzyme, HSD3β2: 3-β-hydroxysteroid dehydrogenase, CYP17A1: 17-α-hydroxylase, CYP21A2: 21-hydroxylase, CYP11B1: 11β-hydroxylase, CYP11B2: Aldosterone synthase, SULT2A1: steroid sulfotransferase.

1.2.2.2. Hydroxysteroid Dehydrogenases (HSDs)

An array of hydroxysteroid dehydrogenases (HSDs) are involved in the reduction and oxidation of steroid hormones. They utilise nicotinamide adenine dinucleotide (NAD+) and nicotinamide adenine dinucleotide phosphate (NADP+) as hydrogen acceptors and NADH/NADPH as donors of reducing equivalents (Payne & Hales, 2004). One of the major differences between P450-enzymes and HSDs is that each P450-enzymes is a product of a single gene, whereas each HSD is expressed in several isoforms, and each isoform is a product of a distinct gene. The number of isoforms varies in different species, tissue distributions, catalytic activity (as a dehydrogenase or reductase), substrate and cofactor specificity, and subcellular localisation.

Both the ZG and ZF express high amounts of HSD3β2. It is a membrane-bound enzyme and is localised in both mitochondrial and microsomal membranes, depending on the type of cells in which it is expressed (Payne & Hales, 2004; Turcu et al., 2014). In the ZG, which does not express CYP17A1, HSD3β2 converts pregnenolone to progesterone, which is the substrate for 21-hydroxylase (CYP21A2). This step is crucial and determine the fate of the precursor to enter the aldosterone synthesis pathway. In the ZF, as both HSD3β2 and CYP17A1 are expressed, the precursor 17α-hydroxyprogesterone is produced and directed to enter the cortisol synthesis pathway.

Most of the adrenal androgens are secreted from the ZR in the form of DHEA and DHEAS for two reasons: first, the enzyme CYP17A1 has a 100-fold substrate preference to 17α-hydroxy pregnenolone rather than 17α-hydroxyprogesterone, second the conversion of DHEA to androstenedione is catalysed by HSBβ2 which has low expression in the ZR (Turcu et al., 2014). Aldosterone and cortisol leave the adrenal cortex as end products, while DHEA and DHEAS require further conversion to active steroid hormones, e.g., testosterone and oestrogens, in the gonads and other peripheral

tissues (Turcu et al., 2014). Rege et al. (2019) reported that adrenal androgen production is controlled by ACTH, and no other hormonal factor has been identified until now to stimulate adrenal androgen synthesis.

1.2.3. Biological Role of Adrenal Secreted Hormones

1.2.3.1. Aldosterone

Aldosterone is the primary mineralocorticoid produced by the ZG of the adrenal cortex. It stimulates renal salt and water reabsorption, as well as increased potassium and proton secretion and hence maintains blood volume and pressure. It also has effects on the cardiovascular system and can cause cardiac fibrosis (Yates et al., 2013). Its secretion is induced by ACTH and by elevated serum potassium levels. In response to low blood pressure, the kidney will release the hormone renin into the blood, which will convert angiotensinogen, secreted from the liver and continuously circulating in the plasma, to angiotensin I, which is physiologically inactive. Angiotensin I is converted to angiotensin II by an enzyme called angiotensin-converting enzyme (ACE), which is found primarily in the vascular endothelium of the lungs and kidneys (Brewster & Perazella, 2004; Yates et al., 2013).

Angiotensin II exerts many effects on different tissues by binding to angiotensin II receptor type I or II. On the ZG, Angiotensin II stimulates the release of aldosterone, which will cause an increase in sodium reabsorption and potassium excretion at the distal tubule and collecting duct of the nephron. The effect of angiotensin II-aldosterone on blood pressure may take hours to appear, while the effect of angiotensin II on other tissues to maintain blood pressure is a faster effect. When angiotensin II binds to its receptor in the systemic arterioles, it causes vasoconstriction, while in the kidney, it leads to increased sodium reabsorption (Ames et al., 2019). In the hypothalamus, the binding of angiotensin II to its receptor leads to an increase in thirst sensation, which causes an

increase in water intake and stimulates anti-diuretic hormone (ADH) release that will increase water reabsorption in the kidney (Coble et al., 2015). The net of those actions leads to increased blood pressure.

1.2.3.2. Cortisol

Cortisol has a crucial role in the glucose, protein, and fat metabolism of the body. Moreover, it has effects on the function of the cardiovascular system, the immune system, and the brain (Yates et al., 2013). The release of cortisol is in a diurnal rhythm where its level increases in the early morning and decreases throughout the rest of the day, and finally reaching its lowest levels between midnight and 4 am. Both acute and chronic stress leads to an increase in cortisol levels and, consequently, in dysregulation of this diurnal rhythm (Ortiz et al., 2022). Toxic stress that is associated with the dysregulation of cortisol levels in the long term, especially in childhood, leads to an increase in the risk of developing cardiometabolic diseases that include diabetes, obesity, dyslipidaemia, hypertension, and cardiovascular disease (Ortiz et al., 2022).

1.2.3.3. Androgens

The human androgens are synthesised mainly in the ZR of the adrenal cortex and the gonads. Because adult rat and mouse adrenal glands do not express the enzyme CYP17A1, they do not synthesise adrenal androgens. The adrenal androgens, such as DHEA, DHEAS, androstenedione (A4), androstenediol and 11β-hydroxyandrostenedione (11OHA), are produced from the adrenal glands in response to ACTH and provide a circulating pool to produce more potent androgens, such as testosterone and oestrogens, in the gonad (Yates et al., 2013). The biological function of androgens is linked to reproduction, the development of sexual characteristics and energy homeostasis. The size of ZR starts to expand around 4 to 5 years of age and continues to grow throughout the first two decades of life, which leads to an increase in the circulating

DHEAS. This process is called adrenarche, which is the transition period from prepuberty to adult life and is characterised by the appearance of pubic and axillary hair (Dumontet & Martinez, 2021; Turcu et al., 2014). As DHEA and DHEAS are mainly produced by adrenals, they are used as biomarkers for diseases caused by excess androgen of adrenal origin.

1.2.3.4. Catecholamines

Catecholamines include dopamine, noradrenaline, and adrenaline. The adrenal medulla secretes catecholamines that are responsible for the body's "fight or flight" response, and they are released into the bloodstream as circulating hormones (Yates et al., 2013). Besides the adrenal medulla, catecholamines are also synthesised in the sympathetic nervous system and the brain, and they act as neurotransmitters (Motiejunaite et al., 2021). In the medullary chromaffin cells, L-tyrosine is converted to L-dopa and then to dopamine by the action of tyrosine hydroxylase and DOPA decarboxylase, respectively. Dopamine will be converted to noradrenaline, and this is converted to adrenaline by the enzymes dopamine-β-hydroxylase and phenylethanolamine N-methyltransferase (PNMT), respectively (Yates et al., 2013). In humans, a large majority of the catecholamine that is secreted by the medulla is adrenaline as most of the chromaffin cells express PNMT. The secreted catecholamines activate α and/or β-adrenergic receptors in the cardiovascular system and cause rapid effects, including vasoconstriction, increased heart rate, and increase in systemic blood pressure that is all part of the "fight or flight" response (Motiejunaite et al., 2021; Yates et al., 2013).

1.2.4. Adrenal Development and Growth

From the late nineteenth century, the time that scientists started to be interested in studying the adrenal glands, there are numerous studies that have been published regarding embryonic adrenal development, adult adrenal growth maintenance and adrenal cortex zonation. The adrenal gland originates from two distinct embryological organs: the intermediate mesoderm, which gives rise to the adrenal cortex and the neurectoderm, which forms the adrenal medulla.

1.2.4.1. Embryonic Development of Adrenal Gland

Both the adrenal cortex and the gonads are generated from adrenogonadal primordium (AGP), which is derived from a specialised region of celomic epithelium known as the urogenital ridge, which also gives rise to the kidney. As the AGP grows, cells express transcription factor genes such as Wilms tumour suppressor-1 (Wt1), GATA-binding protein 4 (Gata4), and steroidogenic factor-1 (Sf1). As development proceeds, groups of cells separate from the coelomic epithelium and invade the mesenchymal layer in the intermediate mesoderm. The precursors next to the mesonephros migrate dorsolaterally to form the gonadal primordium and maintain expression of Sf1, Wt1, and Gata4 transcription factors. The medial cells that upregulate expression of Sf1 and downregulate expression of Wt1 and Gata4 migrate dorsomedially and converge to establish the adrenal primordium at the cranial pole of the mesonephros. Thereafter, the adrenal precursor cells combine with neural-crest-derived sympathoblasts, the precursors of chromaffin cells in the medulla, to form the adrenal anlagen (Kempná & Flück, 2008; Pihlajoki et al., 2015).

During this stage, the human foetal adrenal cortex consists of a small outer definitive zone (DZ), an inner foetal zone (FZ) and a transitional zone (TZ) that exists between those two zones. The FZ appears in the inner cortex and resembles the adult ZF

with high expression levels of steroidogenic enzymes such as CYP17A1 and CYP11A and produces large amounts of DHEA and DHEAS. These steroids serve as sources for the synthesis of placenta oestrogens that are essential for maintaining pregnancy (Kempná & Flück, 2008; Pihlajoki et al., 2015). The DZ in the outer cortex expresses relatively low levels of steroidogenic enzymes and emerges with FZ enlargement. In the prenatal stage, the TZ produces cortisol via the transient expression of HSD3β2. The cortisol from the TZ is required for the development of various organ systems in utero. The negative regulation of the foetal HPA axis by this early cortisol synthesis plays a role in protecting normal female sexual development by inhibiting the production of adrenal androgens at 8 to 9 weeks post-conception (Goto et al., 2006).

The cortisol derived from the cortex also induces the expression of the adrenaline-synthesizing enzyme PNMT in chromaffin cells of the medulla and transcriptionally regulates the expression of chromaffin cell-specific genes and neuron-specific genes. After birth, the medullary islands consist of chromaffin cells within the cortex that coalesce to form a contiguous medulla (Hammer et al., 2005; Pihlajoki et al., 2015).

After birth, the large FZ of the foetal adrenal regresses and disappears by 6 months of age, which causes a reduction of adrenal androgen secretion. The ZR starts to develop only after 4 years of age and gradually begins to synthesise androgens again from around age 6 to 8, a period known as adrenarche in humans and may not be fully differentiated before the age of 15 years. The DZ, possibly together with the TZ, develops into the fully differentiated ZG and ZF by the age of 3 years (Hammer et al., 2005; Kempná & Flück, 2008). The complex regulation underlying human adrenal gland zonation and development is still poorly understood.

1.2.4.2. Factors Involved in Adrenal Development and Growth

There are several factors and developmental signalling pathways involved in the regulatory mechanisms of foetal adrenal development, continuous adrenal cortex maintenance throughout life, homeostasis, and repair after injury. The development factors SF1, WT1 and DAX1 (dosage-sensitive sex reversal, adrenal hypoplasia critical region, on chromosome X, gene 1) and the signalling pathways Sonic Hedgehog (Shh) and wingless-type/ β-catenin (Wnt/ β-catenin) were found to mediate adrenal development and adult adrenal homeostasis.

SF1 is a nuclear receptor transcription factor that is a master regulator of AGP formation and plays a pivotal role in the regulation of adrenal and gonadal development, function, and maintenance (Hanley et al., 1999; Val et al., 2007; Lala et al., 1992; reviewed in Kim & Choi, 2020 and Relav et al., 2023). Complete deletion of the *Sf1* gene in mice leads to adrenal and gonadal agenesis and postnatal lethality due to adrenocortical insufficiency (Luo et al., 1994). On the other hand, overexpression of SF1 increases proliferation in human adrenocortical cells, and triggers adrenal tumour formation in mice and leads to a selective steroidogenic enzyme modulation (Doghman et al., 2007).

WT1 is a Zn finger transcription factor that is expressed very early in the developing AGP and the early expression of SF1 in the AGP is under the control of Wt1 (Bandiera et al., 2013). *Wt1* gene is specifically inactivated in Wilms' tumour, a paediatric kidney tumour, which supports its function as a tumour suppressor gene. Mutations in the *Wt1* gene in humans have been shown to cause defects in adrenal, gonad and kidney development (Bandiera et al., 2015; Haber & Housman, 1992).

DAX1 is an orphan nuclear receptor with unclear biological function. In humans, DAX1 expression occurs in the developing urogenital ridge, in the AGP as well as in the foetal and adult adrenal cortex. Besides the adrenal gland, DAX1 expression is restricted to the hypothalamus, pituitary, and testis (reviewed in Kempná & Flück, 2008 and Yates et al., 2013).

Studies have shown that knockdown of *Dax1* results in premature differentiation of adrenocortical progenitors in mice, further supporting the role of DAX1 in the maintenance of the stem cell population in the adrenal cortex. DAX1 was found to act as a co-repressor of *Sf1* expression, which is crucial for foetal cortex regression and normal adrenal development and function. Both SF1 and DAX1 were found to be expressed in all zones of the foetal adrenal as early as 4 weeks of gestation and maintained throughout pregnancy. The interaction between SF1 and DAX1 and their role in AGP development is still not fully understood. It is reported that overexpression of SF1 up-regulates, among other transcription factors, the expression of DAX1, which could represent a mechanism to limit the consequences of excessive SF1 stimulation (Doghman et al., 2007; Suntharalingham et al., 2015; reviewed in Relav et al., 2023).

Sonic Hedgehog (Shh) is the only Hedgehog ligand that is expressed in mouse and human adrenal glands (Huang et al., 2010). The expression of Sonic Hedgehog (Shh) is localised to a population of cortical subcapsular cells where tracing experiments have shown that Shh-positive cells contribute to the formation of the definitive cortex and centripetally displace older cells (King et al., 2009). Ching and Vilain (2009) showed that Shh and its downstream effectors, glioma-associated oncogenes (Gli1, Gli2, and Gli3), are expressed in the adrenal cortex throughout development and that Shh is required for normal adrenal organogenesis. They found

that the inactivation of Shh in the adrenal cortex resulted in severe hypoplasia and disorganisation of the adrenal cortex.

Various studies have demonstrated that the ZG is a heterogeneous progenitor cell compartment that is maintained by active Wnt/β-catenin signalling (reviewed in Little et al., 2021; Hammer & Basham, 2021). Lineage tracing experiments have identified Gli1 positive and Shh positive cells as two populations that contain adrenocortical progenitors (King et al., 2009), and reciprocal signalling between the Shh positive and Gli1 positive cells coordinates the hedgehog and Wnt signalling during adrenal homeostasis and regeneration (Finco et al., 2018). Finco et al. (2018) proposed that the Shh secreted by the Wnt-responsive progenitor cells in the ZG activates Shh signalling in the Gli1-positive capsular cells. This leads to the differentiation of Gli1positive cells, which are non-steroidogenic (Sf1 negative cells), to steroidogenic Sf1 positive cells and subsequently contribute to all steroidogenic lineages (King et al., 2009). In addition, Gli1 activation results in an increased expression of upstream Wnt ligands e.g., R-spondin 3 (Rspo3) in the capsule which amplifies ligand-dependent Wnt signalling and induces β-catenin activity that will signal to the Wnt-responsive progenitor cells in the ZG and serve as long-term retained progenitors that repopulate the adrenal cortex (reviewed by Kim & Choi, 2020 and Mateska, 2024).

1.2.5. Adrenal Diseases and Disorders

1.2.5.1. Adrenal Insufficiency

Adrenal glands play a critical role in the endocrine system by regulating and maintaining mineral balance, glucose metabolism, and early sexual differentiation. Defects in adrenal development or genetic mutations lead to adrenal insufficiency that causes severe consequences and diseases. Adrenal insufficiencies are divided into

primary, secondary, or tertiary depending on the tissue that causes the condition, either adrenal, pituitary or hypothalamus, respectively. The most common form of primary adrenal insufficiency is congenital adrenal hyperplasia (CAH). It is an inherited genetic disease where more than 95% of the cases are caused by a mutation in the CYP21A2 gene (Husebye et al., 2021). That gene codes for the enzyme steroid 21-hydroxylase that catalyses a key enzymatic reaction in adrenal steroidogenesis, which leads to deficiency in cortisol and aldosterone biosynthesis. This will lead to the disruption of cortisol feedback inhibition of the HPA-axis and result in excessive POMC peptide secretion from the anterior pituitary. Excess POMC peptide levels, in turn, lead to enlargement of the adrenal gland and excess of androgens secretion.

Familial glucocorticoid deficiency (FGD) is another type of primary adrenal insufficiency characterised by the failure of the adrenal cortex to produce glucocorticoids. Mutations in the genes of the ACTH receptor, melanocortin 2 receptor (MC2R), or its accessory protein MRAP (melanocortin receptor accessory protein) are responsible for 25% and 20% of the FGD cases, respectively (Metherell et al., 2005).

1.2.5.2. Cushing's Syndrome

Cushing's syndrome was described in 1932 by Harvey Cushing. It results from the chronic exposure of the adrenals to excessive circulating levels of glucocorticoids, causing endogenous hypercortisolism. It is divided into two forms: ACTH-dependent and ACTH-independent. The ACTH-dependent, also known as pituitary-dependent Cushing's disease, is characterised by excessive ACTH production and, accordingly, an increase in the levels of the other POMC peptides because of corticotroph adenomas of the pituitary. These high POMC peptide levels stimulate the adrenal cortex and result in increasing levels of circulating glucocorticoids, bilateral adrenocortical hyperplasia, and hypertrophy of the adrenal gland. ACTH-independent is caused by a heterogeneous group

of diseases characterised by low levels of plasma ACTH and could occur because of adrenal adenoma or carcinoma (Lacroix et al., 2015; St-Jean et al., 2018).

1.2.5.3. Hyperaldosteronism

Hyperaldosteronism, which is the excessive release of aldosterone from the ZG, can be divided into primary or secondary. The primary type is caused by a benign tumour of the adrenal gland, and now this type is recognised as the most common cause of secondary hypertension (Bioletto et al., 2022). This type leads not only to hypertension and electrolyte imbalance but is also associated with cardiometabolic complications (Gallo-Payet, 2016). It can be treated by either unilateral adrenalectomy or mineralocorticoid antagonist therapy (Almeida et al., 2020). Secondary hyperaldosteronism is caused by a diverse group of disorders, e.g., renin-producing tumour or renal artery stenosis, that increase the activation of the RAS, which leads to excess aldosterone production (Galasko, 2015).

1.3. Role of ACTH and N-POMC in Adrenal Steroidogenesis and Growth

1.3.1. ACTH

The synthesis and secretion of ACTH, a 39 amino acid peptide, from the anterior lobe of the pituitary gland is tightly controlled by the hypothalamus. During stress, the hypothalamic paraventricular neurons release corticotrophin-releasing hormone (CRH) and arginine vasopressin (Fig. 1.5). These two peptides stimulate the release of ACTH from the anterior pituitary that subsequently stimulates the ZF of the adrenal cortex to produce glucocorticoid hormones, corticosterone in rodents and cortisol in humans, and ZR to release androgens. Cortisol has a negative feedback inhibition effect on the hypothalamus and pituitary to suppress the release of CRH and ACTH, respectively.

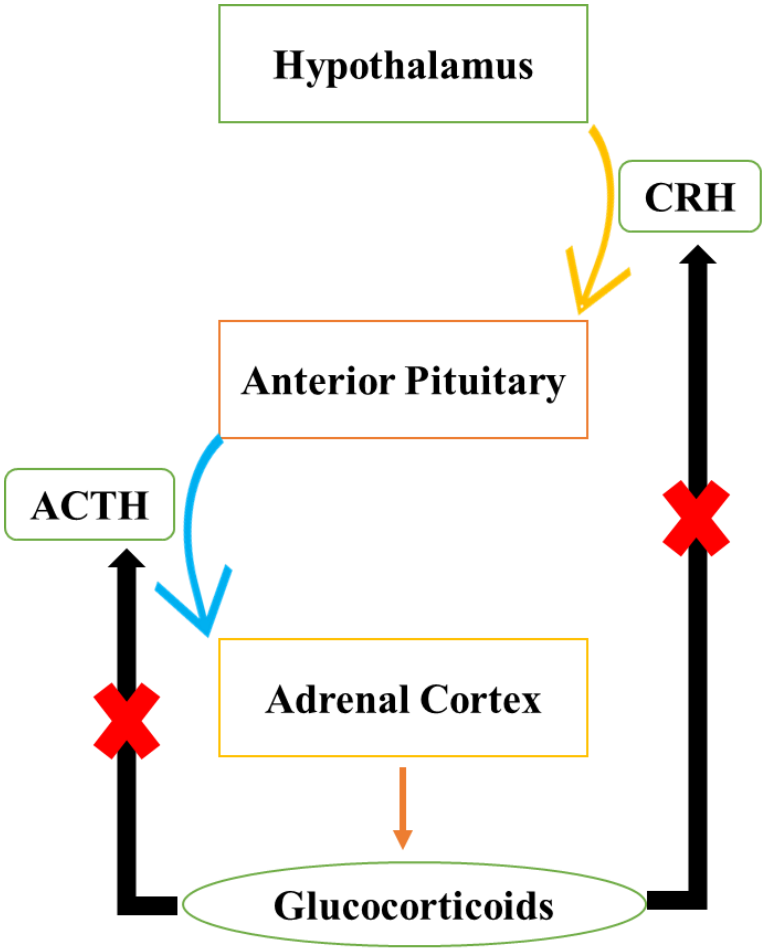

Fig. 1.5. Hypothalamic-pituitary-adrenal axis (HPA-axis). During stress, the hypothalamus releases corticotrophin-releasing hormone (CRH) that stimulates the release of ACTH from the anterior pituitary. ACTH subsequently stimulates the adrenal cortex to produce glucocorticoid hormones, which have a negative feedback inhibition effect on both the anterior pituitary and hypothalamus to inhibit the release of ACTH and CRH, respectively.

1.3.1.1. ACTH Receptor

ACTH acts by binding to the cell surface MC2R, the smallest member of the MCRs family, in the adrenal cortex. It is reported that MC2R is expressed mainly in the adrenal cortex and in other tissues such as bone, adipose tissue, ovaries, testes, skin, and the pituitary (Metherell et al., 2005). MC2R is highly specific for ACTH (Gallo-Payet, 2016) and mediates normal and stress-related ACTH responses.

It has been found that for the MC2R to be translocated from the endoplasmic reticulum to the plasma membrane, it requires an accessory protein termed the melanocortin receptor accessory protein (MRAP) (Metherell et al., 2005). MRAP is highly expressed in the adrenal gland, adipose tissue, testis, breast tissues and to a lesser extent in other tissues (Malik et al., 2015; Metherell et al., 2005; Zhang et al., 2018) and is expressed in two isoforms in the human genome: MRAP1 (Metherell et al., 2005) and MRAP2 (Chan et al., 2009). MRAP1 and MRAP2 are small transmembrane proteins that are orientated in a unique structure across the cell membrane to form anti-parallel homodimers or heterodimers (Chan et al., 2009; Sebag & Hinkle, 2007). The MC2R/MRAP1 complex exists primarily in the ZF of the adrenal cortex (Gorrigan et al., 2011), where glucocorticoids are produced. Zhang et al. (2018) reported that MRAP has an essential role in the regulation of ACTH-induced adipose lipolysis and whole-body energy balance. Furthermore, mutations in either MC2R or MRAP1 lead to familial glucocorticoid deficiency (Clark et al., 2016; Dores et al., 2016; Metherell et al., 2005; Novoselova et al., 2018) since MRAP1 is not only required for MC2R trafficking to the cell surface but also for ACTH binding to the receptor. Babischkin et al. (2016) found that high levels of oestrogen suppress the interaction between MC2R and MRAP and ACTH binding to MC2R.

1.3.1.2. Effect of ACTH on Adrenal Steroidogenesis

ACTH has a short half-life in the circulation and exerts an acute or chronic stimulation effect on the adrenocortical cells. In the acute effect, the increase in glucocorticoid secretion appears around 5 to 10 minutes after ACTH stimulation and reaches a peak after 15 to 30 minutes (Chung et al., 2011). ACTH binds to its receptor (MC2R), causing the activation of the adenylate cyclase that converts ATP to cAMP. cAMP is a second messenger that will activate the downstream signalling pathways, including the cAMP-dependent protein kinase A (PKA). PKA phosphorylates and activates cholesteryl ester hydrolases and StAR, which will increase the amount of cholesterol delivered to the inner mitochondrial membrane (Aumo et al., 2010). This causes an increase in the first and the rate-limiting step of steroidogenesis, which is the conversion of cholesterol to pregnenolone and an increase in the HSD3β2 enzyme activity that directs the precursor molecules to glucocorticoid synthesis. It was also found that this immediate steroidogenic response would depend on the expression levels of MRAP and MC2R at the cell membrane, and proteins can be readily trafficked to the plasma membrane (Chan et al., 2009).

Acute ACTH stimulation is characterised by an immediate release of the glucocorticoids after synthesis. Prolonged ACTH stimulation, hours to days, enhances adrenal expression of the enzymes and proteins of the steroidogenic machinery. In parallel, the blood flow within the adrenal gland will increase and induce adrenal hyperplasia (Ulrich-Lai et al., 2006). Essentially, the HPA-axis system is tightly regulated by the negative feedback of circulating glucocorticoids. The steroids inhibit the pituitary secretion of ACTH, ultimately turning off the adrenal production of steroid hormones.

1.3.1.3. Effect of ACTH on Adrenal Growth and Development

It is long known that removal or destruction of the anterior pituitary results in adrenal cortex atrophy with almost complete suppression of its secretory activity. Inversely, exogenous administration of ACTH can regenerate the adrenal cortex to its original size and activity (Geller, 1964). Since then, several reports have been published regarding the role of ACTH in adrenal growth and development. It has been found that ACTH is required to maintain pregnancy through its actions on steroidogenesis rather than its effects on adrenal growth as *Mc2r* null mice (Chida et al., 2007) have macroscopically detectable adrenal glands with markedly atrophied ZF at birth. However, ACTH has an indirect effect on the development of the human foetal adrenal gland. After 15 weeks of gestation, ACTH upregulates the expression of other growth factors, such as insulin-like growth factor 2 (IGF2) and fibroblast growth factor beta (FGFβ), which are found to be a potent mitogenic factor for foetal adrenal cells *in vitro* (Mesiano et al., 1993).

ACTH and other POMC peptides are required for postnatal proliferation and maintenance of adrenal structures and for adrenal steroid hormone production (Chida et al., 2007; Karpac et al., 2005). *In vivo* studies showed that chronic ACTH administration increases rat adrenal weight and steroid hormone production (Legros & Lehoux, 1983; Ulrich-Lai et al., 2006). Moreover, chronic ACTH administration in rats causes hyperplasia in the outer ZF and hypertrophy inner ZF and medulla (Ulrich-Lai et al., 2006). While low levels of ACTH, such as those seen in animals treated with dexamethasone, result in adrenal atrophy (Geller, 1964; Thomas et al., 2004; Wright et al., 1974).

In contrast, *in vitro* studies have shown that ACTH inhibits the growth of Y1 mouse adrenocortical tumour cells as well as normal adrenocortical cells in culture

(Hornsby, 1984; Masui & Garren, 1971). This suggests that ACTH acts as an indirect mitogen for the adrenal cortex in intact animals. It is reported that the mitogenic effect of ACTH is mediated via the induction of c-fos and c-jun gene expression and weak activation of the ERK pathway (Kimura & Armelin, 1990; Kimura et al., 1993; Rocha et al., 2003). The anti-mitogenic activity is mediated via cAMP and protein kinase A (PKA) and involves deactivation of the Akt pathway, c-Myc degradation, and increased expression of p27Kip1 (Lepique et al., 2004; Lotfi et al., 1997; Rocha et al., 2003). Le and Schimmer (2001) showed that stimulation of the cAMP-resistant mutant Y1 cells by ACTH led to the activation of the ERK pathway, indicating that PKA did not mediate the mitogenic action of ACTH.

1.3.2. Pro-γ-MSH (N-POMC)

N-POMC is co-secreted with ACTH from the anterior pituitary during the stress response. Early studies found that N-POMC could be involved in the physiological control of adrenal growth and steroidogenesis.

1.3.2.1. Role of N-POMC in Adrenal Growth and Development

It has been found that POMC peptides are required to maintain adrenal development during pregnancy, as *Pomc* knockout mice showed defective adrenal development (Karpac et al., 2005; Yaswen et al., 1999). This defect in adrenal development is linked to the role of the shorter N-POMC peptides, where the levels of those peptides increased in the circulation of foetal sheep during late gestation, which is a period characterised by rapid adrenal growth (Saphier et al., 1993). Moreover, it has been reported that the intra-foetal infusion of N-$POMC_{1-77}$ resulted in stimulated foetal adrenal growth and resulted in a specific increase in adrenal *CYP17A1* gene expression in late gestation, which suggests the role of N-$POMC_{1-77}$ in adrenal growth and steroidogenesis that occurs before birth (Ross et al., 2000).

In contrast, evidence from the *Pomc* knockout mice showed that adrenal glands were present in the animal, although they were significantly smaller than those found in wild-type animals. Moreover, they had a distinct cortex and medulla with disrupted cortical architecture, as the ZF was not clearly distinguishable from the ZG (Coll et al., 2004). They reported that injection of *Pomc* null mice for a period of 10 days with high ACTH doses (30 µg) twice daily did result in an increase in adrenal size and restored corticosterone but not aldosterone levels. However, examination of the adrenals showed that the increase in size was a result of cellular hypertrophy with no evidence of any hyperplasia. Moreover, subcutaneous treatment of *Pomc* knockout mice with synthetic N-POMC$_{1-28}$ (10 µg twice daily and for 10 days) had no impact on adrenal cortical morphology and plasma corticosterone levels (Coll et al., 2006). Treatment of the *Pomc* knockout mice with both N-POMC$_{1-28}$ and ACTH$_{1-24}$ together resulted in upregulation of steroidogenic enzymes, an increase of corticosterone levels, hypertrophy of the ZF and regression of the X zone, which is identical to the mice that were treated with ACTH$_{1-24}$ alone. The results of these experiments could be viewed as evidence against the role of the N-POMC peptides in adrenal growth. However, these results should be interpreted with some caution. As discussed by Bicknell (2016), the use of very high (300X physiological levels) pharmaceutical doses of the peptides should be questioned. The large doses of the peptides, either alone or in combination, could mask a much more subtle effect. Moreover, in long-term experiments, the stability of the disulphide bridge in concentrated solutions could be disrupted and affect the peptide's biological activity.

Early studies have shown that ACTH shares the mitogenic effect on adrenal glands with other peptides, which causes the compensatory growth response seen after unilateral adrenalectomy (Dallman et al., 1980). It has been found that 24 hours after unilateral adrenalectomy, i.e. the surgical removal of one adrenal gland, the weight, RNA,

and DNA contents in the remaining gland are dramatically increased. This phenomenon is called compensatory adrenal growth, and this mechanism has been used to investigate the mechanisms underlying adrenal growth (Dallman et al., 1980).

Estivariz et al. (1982) reported that treatment of rat adrenal cells with N-POMC$_{1-76}$ alone or in combination with ACTH did not affect DNA synthesis, while when they used smaller fragments of N-POMC$_{1-76}$, N-POMC$_{1-28}$ and N-POMC$_{2-59}$, they found that the DNA synthesis increased in dose dependant manner with N-POMC$_{2-59}$ being the more potent of the N-POMC peptides used. The idea that the mitogenic activity of POMC is in the extreme N terminal was further reported by Lowry et al. (1983). They treated female Wistar rats with various anti-POMC antisera 2 hours before unilateral adrenalectomy, and after 24 hours, the weight, DNA, and RNA content of the remaining adrenal gland were determined. They found that compared to control animals treated with rabbit serum, rats treated with anti-ACTH antiserum showed no effect in the increase in adrenal weight and DNA synthesis, but the increase in RNA content and plasma corticosterone concentration was inhibited significantly. On the other hand, treatment with anti-POMC$_{1-76}$ and anti-POMC$_{1-28}$ antisera inhibited DNA synthesis, suggesting a decrease in hyperplasia. Interestingly, when they used an anti-γ3-MSH (N-POMC$_{50-74}$) antibody, they found that the increase in the adrenal weight, RNA, and DNA was completely inhibited. Furthermore, they found that N-POMC$_{1-48/49}$ could stimulate DNA synthesis and mitogenesis. However, since the human anterior pituitary secretes N-POMC$_{1-76}$ into the circulation, this raises the question as to the potential source of these smaller fragments.

Lowry et al. (1983) proposed that N-POMC$_{1-76}$ is a mitogenic precursor that must be cleaved before it can express its mitogenic activity. After 20 years, Bicknell and co-workers provided evidence for this hypothesis by identifying an adrenal serine protease

enzyme that is responsible for the cleavage of pro-γ-MSH and named it adrenal secretory protease (AsP) (Bicknell, 2003; Bicknell et al., 2001). They also reported that the AsP enzyme bound to the cell surface and cleaves the circulating pro-γ-MSH to give N-$POMC_{1-52}$, which has been concluded to be the adrenal mitogenic factor (Bicknell, 2003; Bicknell et al., 2001). The idea that longer N-POMC fragments that include γ-MSH act as an adrenal mitogenic factor is also proposed by Lowry (2016) and called big γ-MSH based on the finding that the anti-γ3-MSH inhibited the increase of adrenal weight RNA and DNA. Big γ-MSH (N-$POMC_{1-61}$) is the N-terminally extended γ-MSH with phenylalanyl^{61}- amide at its C-terminal. This idea is supported by the fact that N-$POMC_{2-59}$ extracted from human pituitary glands (McLean et al., 1981) has been shown to be the most potent adrenal mitogenic factors among the other N-POMC fragments studied by Estivariz et al. (1982). Due to structural similarities between big γ-MSH and N-$POMC_{2-59}$, it is possible that the extracted fraction contains a heterogeneous mixture of both peptides.

N-$POMC_{1-28}$ is a short peptide that represents the first 28 amino acids sequence of the pro-γ-MSH and is an extraction artefact generated from proteolytic cleavage of the pro-γ-MSH during the large-scale extraction process of growth hormones from human pituitaries (Lowry, 2016; McLean et al., 1981). Further studies have shown that a synthetic N-$POMC_{1-28}$ with the disulphide bridges in the correct position between cysteine residues 2–24 and 8–20 can stimulate the growth of adrenocortical tumour cells (Fassnacht et al., 2003) while modified N-$POMC_{1-28}$ without disulphide bridges prevented atrophy of the adrenal cortex induced by depletion of circulating POMC peptides, suggesting that the disulphide bridges might be important but are not essential for N-$POMC_{1-28}$ to act as a mitogenic factor (Torres et al., 2010).

N-POMC$_{1-28}$ elicits its mitogenic effect by activating the mitogen-activated kinase/extracellular signal-regulated kinase (MEK) pathway with downstream signalling via extracellular signal-regulated kinases (ERK): ERK1 and ERK2 (de Mendonca et al., 2013; Fassnacht et al., 2003; Mattos et al., 2011; Pepper & Bicknell, 2009) (Fig. 1.6). Generally, the ERK pathway responds to growth factor signals by phosphorylation of ERK1/2 that will be translocated to the nucleus and directly phosphorylate transcription factors (TF) and upregulate the expression of c-Fos and/or c-Jun (Yang et al., 2013). Moreover, administration of N-POMC$_{1-28}$ to dexamethasone (a synthetic glucocorticoid to suppress POMC peptide secretion) treated rats induces synthesis phase (S phase) entry in all zones of the adrenal cortex (Torres et al., 2010) through the upregulation of cyclins D2, D3, and E that regulate the cell cycle progression from the gap 1 (G1) to the S phase (de Mendonca et al., 2013; Mendonca & Lotfi, 2011).

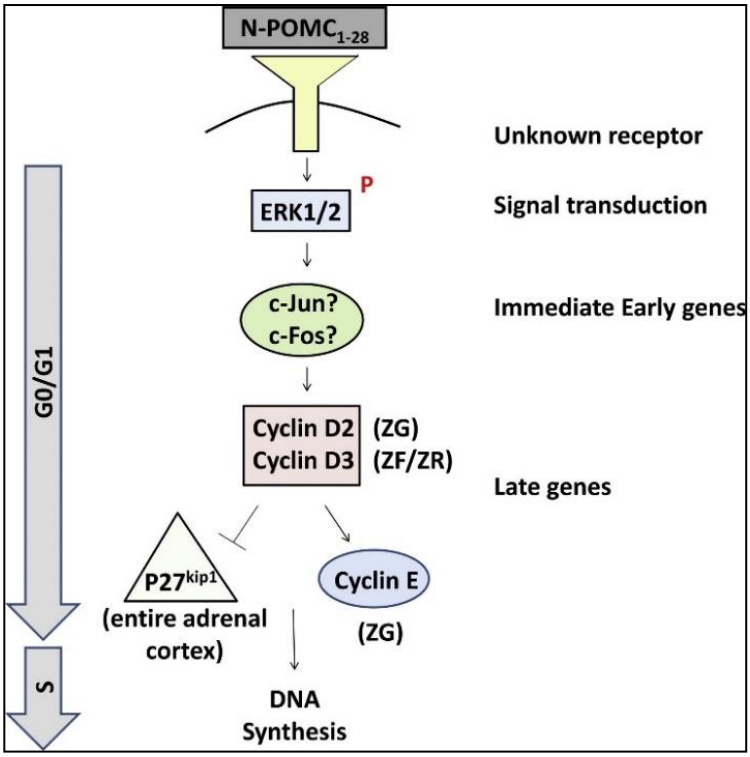

Fig. 1.6. The signalling model proposed by de Mendonca et al. (2013) of N-POMC$_{1-28}$ in rat adrenal glands during the transition from G1 to S phases. ERK 1/2: extracellular signal-related kinases 1 and 2, ZG: zona glomerulosa, ZF: zona fasciculata, ZR: zona reticularis, cell cycle phases Gap 0 (G0), Gap 1 (G1), and synthesis (S).

1.3.2.2. Role of N-POMC in Adrenal Steroidogenesis

The role of the different POMC peptides on adrenal steroidogenesis has been studied extensively. Interestingly, early studies found that pro-γ-MSH is indirectly involved in adrenal steroidogenesis by activating the enzyme hormone-sensitive lipase (HSL), the enzyme responsible for converting cholesterol ester to free cholesterol and increasing the cholesterol pool for steroid hormones synthesised during stress (Pedersen & Brownie, 1979; Pedersen et al., 1980). Consequently, it has been found that cortisol and aldosterone output is increased in rat and human adrenal cells if treated with both ACTH and pro-γ-MSH in comparison to the samples treated with ACTH only (Al-Dujaili et al., 1981). In contrast, the following studies reported that the pro-γ-MSH has a suppression effect on adrenal steroidogenesis (Coulter et al., 2000; Fassnacht et al., 2003).

1.3.2.3. N-POMC Receptor

The precise role of N-POMC on adrenal steroidogenesis and mitogenesis could be elucidated by identifying the receptor it acts through. Pedro de Montonca, a post-doctoral researcher in the Bicknell Lab at the University of Reading, started a study to identify the adrenal N-POMC receptor. They used cloning techniques together with a magnetic cell separation assay and ligand-binding assay to isolate an N-POMC receptor. Successively, they identified the G protein-coupled receptor 19 (GPR19), among other 38 orphan G protein-coupled receptors (GPCRs) that are expressed in rat adrenal gland, to be a possible receptor for N-POMC$_{1\text{-}28}$ in adrenal cells (unpublished data).

1.4. G protein-coupled Receptors (GPCR)

The superfamily G protein-coupled receptors (GPCRs), which are characterised by seven α-helical transmembrane structures, are the largest family among the signalling receptors in eukaryotes with more than 800 GPCRs in humans (Roux & Cottrell, 2014).

The GPCRs transduce the extracellular signals across the plasma membrane and into the cell cytosol in response to activation by a ligand. As a result, a broad range of downstream intracellular signals is activated, leading to both short-term effects (e.g., changes in intracellular cAMP or Ca+ levels) and long-term effects (e.g., transcription of a specific gene(s)) (Böhme & Beck-Sickinger, 2009).

The GPCR downstream effects on a cell signal are mediated through the heterotrimeric Gα, Gβ, and Gγ subunits that are stably associated only in the inactive, GDP-bound state. When a ligand occupies its GPCR binding pocket, conformational changes in the receptor occur that promote the exchange of the tightly bound GDP for GTP. Then, the activated Gα-GTP subunit dissociates from the Gβγ subunits to mediate the intracellular effects of ligand binding (van Biesen et al., 1996). Both the activated Gα-GTP and Gβγ subunits interact with downstream effectors such as adenylyl cyclase and phospholipases to modulate different signalling pathways (Smrcka et al., 2008). There are at least four different types of Gα subunits: Gαs, Gαi/0, Gαq and Gα12/13. The Gαs increase intracellular cAMP levels by activating the enzyme adenylyl cyclase that will activate the reaction of conversion ATP into cAMP. In contrast, Gαi/0 is generally described as inhibitory as it decreases adenylate cyclase activity. The Gαq/11 protein acts as a stimulator of phospholipase C that will activate protein kinase C (PKC) and increase intracellular Ca^{+} levels (Liu et al., 2021). The G12/13 proteins act as activators of the small GTP Ras-homology A (RhoA) that is regulated by a group of Rho guanine nucleotide exchange factors (RhoGEFs) that promote the exchange of GDP to GTP (Worzfeld et al., 2008).

The role of Gαs as an oncogene has been reported to be through the direct activation of adenylyl cyclase enzyme that will convert ATP into cAMP or by activating the soluble adenylyl cyclase (sAC) independent of G-proteins by high levels of

bicarbonate and calcium ions (Zhang et al., 2020). Where the increases in intracellular cAMP levels lead to protein kinase A (PKA) activation that subsequently leads to the activation of the cAMP response element binding protein (CREB). CREB is an important transcription factor that regulates the expression of several genes, including oncogenes c-Jun and cyclin D1 (Steven et al., 2020; Zhang et al., 2020). The cAMP–PKA–CREB pathway has been identified to play a tumour-promoting role in different tumour types, making it a target for human cancer therapy. In contrast, it has been reported that phosphodiesterases (PDEs) are responsible for the degradation of cAMP. Where intracellular cAMP concentrations depend on the relative balance between adenylyl cyclase and phosphodiesterase activities (Zhang et al., 2020).

It has been reported that activation of several GPCRs that are coupled to different types of Gα subunits leads to a synergistic crosstalk interaction between the activated signalling pathways. This crosstalk has been found to lead to the amplifying of intracellular signalling within parallel but separate pathways (Selbie & Hill, 1998). It is necessary when studying the interaction of a GPCR to its ligand to consider the basal state of the cellular model that is used and the simultaneous pathways that could be activated, as many agonists may be considered inactive in some cellular models and active in others. This could explain the conflict between the published reports regarding a specific GPCR agonist and the signalling pathway(s) it activates.

The activated GPCR undergoes desensitisation and internalisation to endosomes, which is a protective measure that is tightly regulated by the cell to control overstimulation and to sustain normal physiology (Rajagopal & Shenoy, 2018). The downstream signalling pathway of a GPCR is activated when an agonist binds to it and peaks within seconds to minutes, depending on the type of the GPCR. Moreover, stimulation of a GPCR over minutes results in its desensitisation where the response is

decreased in comparison to the initial response. Desensitisation is regulated by two major protein classes; the first class is the kinases that phosphorylate the receptor, such as G protein receptor kinases (GRKs), PKA and PKC (Rajagopal & Shenoy, 2018). The second protein class is the β-arrestins, which are responsible for recognising the phosphorylated receptor to initiate the internalisation process. Prolonged stimulation of GPCRs causes receptor internalisation into vesicles and is targeted to lysosomes for degradation. This is followed by the downregulation of receptor expression by decreasing mRNA levels (Smith & Pack, 2021).

The two major mechanisms that are implicated in GPCR internalisation from cell membrane to early endosomes are clathrin-mediated endocytosis (CME) and caveolae-mediated endocytosis. The CME is a complex process that involves the sequestration of the agonist-activated GPCR into the endocytic machinery that is bound to the β-arrestin protein (Hinze & Boucrot, 2018). Caveolae-mediated endocytosis involves flask-shaped cholesterol and sphingolipid-rich invaginations of the plasma membrane that is known as caveolae, with a core component of caveolin proteins that are used to concentrate the signalling molecules. It has been reported that each mechanism involves the trafficking of the activated GPCR to fuse with early endosomal membranes (Kiss & Botos, 2009).

1.4.1. GPR19

The human gene of GPR19 has been cloned and sequenced by O'Dowd et al. (1996) and found that it contained an intron less open reading frame of 1245 nucleotides, which encodes a 415 amino acid protein that is widely distributed in the brain and peripheral tissues. Since its cloning, few studies have been published regarding the ligand of GPR19 and its biological function and signalling pathway. Hoffmeister-Ullerich et al. (2004) studied the expression of GPR19 in mouse development and in adult tissues by northern blot analysis. They found that GPR19 is predominantly expressed in the brain

and testis and, to a lesser extent, in the liver, heart, and kidney. GPR19 mRNA expression is upregulated in different breast carcinomas when compared to the paired normal tissues (Rao & Herr, 2017). Kastner et al. (2012) found that GPR19 mRNA was differentially expressed during the cell cycle with a peak in S-phase and knockdown of GPR19 mRNA depressed cell proliferation.

It has been reported that GPR19 could be the potential receptor of adropin (Stein et al., 2016). Adropin is a 43-residue peptide hormone that was first isolated in 2008 by Kumar and his group from liver and brain tissues (Kumar et al., 2008). It has high expression in lung and breast cancer cells (Kastner et al., 2012; Rao & Herr, 2017). It is encoded by the energy homeostasis-associated gene (Enho), and it has a role in metabolic homeostasis. Recent studies show that adropin can reduce insulin resistance and hepatosteatosis in mice subject to diet-induced obesity (Ganesh Kumar et al., 2012) and inhibit water deprivation-induced drinking (Stein et al., 2016). Stein et al. (2016) noticed that the GPR19 siRNA-pre-treated rats consumed significantly more water following intracerebroventricular adropin administration than rats pre-treated with the control siRNA.

That raises the question if it is possible that both adropin and the N-POMC could activate the same receptor by binding to the same binding site. However, the study that reported adropin as the possible endogenous ligand of GPR19 did not have any direct evidence in the form of ligand-binding assay data showing that adropin binds to GPR19 (Kastner et al., 2012; Rao & Herr, 2017; Stein et al., 2016). Interestingly, by comparing the structure of adropin with N-POMC$_{1\text{-}28}$ (Fig. 1.7), we found that both have a similar number of polar and non-polar amino acids and have disulphide bridges that bring the peptide into a similar ‘C’ or hairpin shape. It is, therefore, possible that both could bind to the same receptor. Furthermore, the activated GPR19 receptor by adropin signals by

decreasing cAMP accumulation (Rao & Herr, 2017) and significantly increased the phosphorylation of ERK1/2 (Rao & Herr, 2017; Thapa et al., 2018), the same signalling pathway that N-POMC activates in the adrenal gland (Fassnacht et al., 2003; Mattos et al., 2011; Pepper & Bicknell, 2009).

This study aims to extend these initial studies. GPR19 is a membrane protein that must reach its site of action, the cell surface, to perform its function. Recent unpublished work in Bicknell's lab found that GPR19 over-expressed in human embryonic kidney 293 (HEK-293) cells remains inside the cell and does not localise to the cell membrane. This raises the possibility that, like the MC2R, GPR19 might need an accessory protein to correctly traffic to the cell surface.

MRAP is expressed in the human adrenal gland, and it is required for normal foetal adrenal differentiation and proliferation (Gorrigan et al., 2011), and mutations in MRAP were reported to cause FGD type 2 (Novoselova et al., 2018). Moreover, the *Mrap* null mice showed disrupted adrenal development with no apparent zonation in the adrenal cortex (Novoselova et al., 2018). In addition, studies showed that *Pomc* null mice have obesity, adrenal atrophy and altered pigmentation (Karpac et al., 2005; Yaswen et al., 1999). This reflects the role of POMC peptides, specifically N-POMC, in adrenal development. The similarities in the phenotypic characteristics of the MRAP-null mice and Pomc null mice trigger the idea of expressing MRAP in the HEK-293 cell, which does not express MRAP (Roy et al., 2007), and study if it is required for GPR19 translocation to the cell membrane.

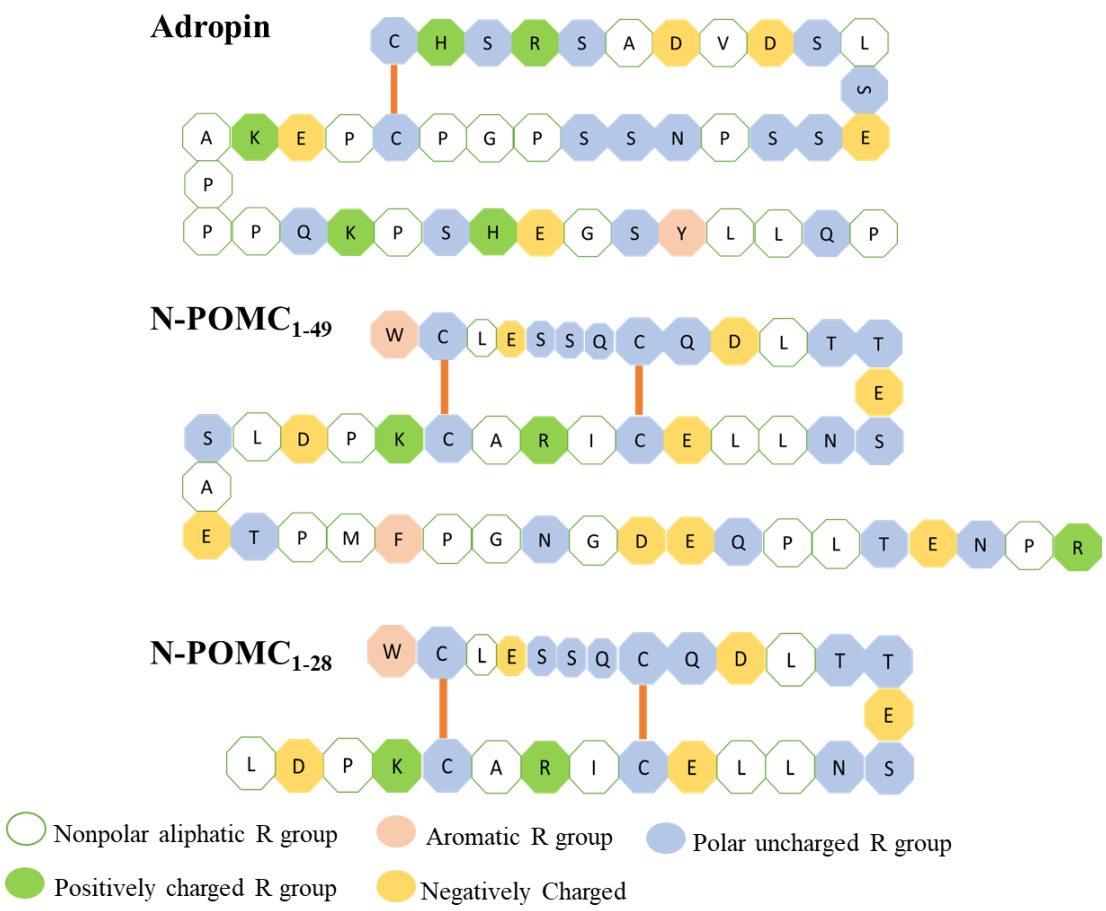

Fig. 1.7. The predicted shape of the mature protein of adropin, N-POMC$_{1-49}$ and N-POMC$_{1-28}$. The shape of the three peptides is almost similar. The sequence of adropin and N-POMC was drawn based on the NCBI Reference Sequence NP_940975.2 and CAG46625.1, respectively.

1.5. Hypothesis

GPR19 is the receptor for N-POMC, and it possibly requires MRAP to perform a role in adrenal growth.

1.6. Study Aims

To determine whether GPR19 is the receptor of N-POMC and to determine if it requires MRAP for its localisation to the cell membrane and for N-POMC binding to its receptor.

1.7. Objectives

Using the human embryonic kidney 293 (HEK-293) cell line as a cellular model to investigate the following:

1) To confirm if the genes of GPR19 and MRAP are expressed in the selected wild type (WT) and stably transfected cell lines with GPR19 and/or MRAP by RT-PCR.
2) To study the protein expression of GPR19 and MRAP in those cell lines by fluorescent staining (Immunocytochemistry, ICC) and quantified by western blotting.
3) To determine whether GPR19 and MRAP form a complex by studying their cellular co-localisation by ICC technique and reciprocal co-immunoprecipitation.
4) To quantify the binding ability of N-POMC$_{1-28}$ either unlabelled, Alexa Fluor-488 labelled, or biotin labelled in the WT cell line and compare it with the amount measured for the stably transfected cell lines with GPR19 and/or MRAP using ICC and ELISA assay.
5) To identify if the longer N-POMC fragments, N-POMC$_{1-49}$, and N-POMC$_{1-77}$, and adropin could compete with the binding of N-POMC$_{1-28}$.

6) To quantify the binding ability of biotin-labelled adropin to the WT cell line and compare it to the binding capacity of the stably transfected cells with GPR19 and/or MRAP. Then, identify if the binding ability of the biotin-labelled adropin could be competed with the N-POMC fragments: 1-28, 1-49, and 1-77.
7) To investigate the signalling pathway activated after the binding of N-POMC$_{1-28}$ to GPR19 using phosphorylation of ERK1/2, the cellular cAMP levels, recruitment of β-arrestin, and if it can induce cell proliferation using the SRE-SEAP vector model.

Chapter 2: General Methods

Unless stated otherwise, all materials and reagents were purchased from Sigma Aldrich (Gillingham, UK), Thermo Fisher Scientific (Loughborough, UK), and Melford (Ipswich, UK). Nucleic acid purification kits were purchased from Qiagen (Crawley, UK).

2.1. PCR Amplification Protocol

In a 0.5 ml microcentrifuge tube, a 25 µl PCR reaction mixture was prepared as follows: 1 µl of 10 µM forward and reverse primers, 12.5 µl of 2X Dream Taq Green PCR master mix (Thermo Scientific, K1081), 1 µl of the required template (approx. 20 ng/µl) or nuclease-free water if preparing a negative control, and 9.5 µl of nuclease-free water.

The PCR amplification reaction was conducted using Eppendorf MasterCycler® Nexus Gradient using the appropriate PCR conditions (as detailed separately) to amplify the target gene. The PCR products were then profiled by agarose gel electrophoresis.

2.2. Agarose Gel Electrophoresis

Agarose gel was prepared by dissolving 1% (w/v) agarose in 1X Tris Acetate EDTA (1X TAE) buffer and the solution was then heated until the agarose completely melted. SYBR Safe DNA Gel Stain (Invitrogen, S33102) was then added to the agarose solution with 1:10,000 dilution, and the gel was then left to set at room temperature (RT). The gel electrophoresis apparatus was filled with 1X TAE buffer until the gel was completely submerged. Approximately 1 µg of the sample was loaded; if required, 6X DNA loading dye (Thermo Scientific, R0611) was added to the sample with 1X final dilution before loading into the gel, and 10 µl of GeneRuler 1 kb Plus DNA Ladder (Thermo Scientific, SM1333) was added to a separate lane. Electrophoresis was

conducted for 30 – 40 min at 75 V. The products were visualised and imaged using a UV transilluminator (Syngene U: Genius 3).

2.3. Purification of DNA from Agarose Gel Slice

The QIAquick Gel Extraction Kit 250 (cat 28706, Qiagen) was used to purify DNA from agarose gel slices. The agarose gel was placed on a Dark Reader transilluminator (Clara Chemical Research), and the band of interest was excised from the gel using a scalpel blade and transferred to a 1.5 ml microcentrifuge tube. To the gel slice, 450 µl of Buffer QG was added and incubated at 50°C until it was completely dissolved. After that, 150 µl isopropanol was added to the sample and mixed. The mixture was then transferred into a QIAquick spin column with a 2 ml collection tube. The sample was centrifuged at 16,200 g for 1 min. Then the flow through was discarded, and 750 µl of PE buffer was added to the QIAquick spin column and centrifuged again for 1 min. To get rid of excess ethanol before extracting the DNA, the collection tube was replaced with a fresh one and centrifuged again. The DNA was eluted by placing the QIAquick spin column into a 1.5 ml microcentrifuge tube, and 30 µl of ultra-pure water was added directly above the QIAquick membrane, incubated at RT for 5 min, then centrifuged at 16,200 g for 1 min. Samples were stored at -20º C.

2.4. Restriction Enzyme Digestion

In this step, both the vector (plasmid) and the insert (purified DNA from procedure 2.3) were digested using restriction endonucleases. The endonucleases: 2 µl were added to 0.5 µl microcentrifuge tube, followed by the addition of 2 µl of the 10X Fast Digest green buffer (B72, Thermo Scientific) to have a 1X final dilution of the digestion buffer. Around 1 µg of the plasmid or the insert was then added to the tube, and the volume was increased to 20 µl with RNase-free water. The tube was incubated for 15

min at 37°C in a water bath. The samples then underwent agarose gel electrophoresis and were purified following the procedure in 2.2. and 2.3.; respectively.

2.5. Ligation

Digested plasmid and DNA insert were ligated using the Rapid DNA Ligation Kit (K1422, Thermo Fisher). First, the T4 DNA Ligase buffer was added to a 0.5 µl microcentrifuge tube at a final concentration of 1X. Then, the plasmid and the DNA insert were added to the tube with a 1:3 molar ratio, followed by the addition of 5 units of T4 DNA ligase and the volume made up to 20 µl with RNase-free water. The reaction mixture was mixed, centrifuged, and incubated at RT for 15 min. The mixture was then stored at -20°C and used for transformation to competent cells.

2.6. Competent E. coli Preparation

The Inoue method for 'Ultra Competent' cell preparation and transformation, published by Sambrook and Russell (2006), was used to prepare DH5α Escherichia coli (E. coli). Around 2 µl of DH5-α competent cell (EC0112, Thermo Fisher) was inoculated into 10 ml of Luria-Bertani (LB) medium (Appendix A.1). The tube was incubated for 6 hrs at 37ºC with vigorous shaking. After incubation, the starter culture was used to inoculate three 1-litre flasks, each containing 250 ml of LB medium. The first flask received 0.5 ml, the second received 1 ml, and the third received 2 ml of the starter culture. All three flasks were incubated overnight at 18-22ºC with shaking. The next morning the OD600 of the three cultures was measured and continued to be monitored every 45 min until an OD600 of 0.55 was achieved. The flask that achieved an OD600 of 0.55 was then chilled in an ice-water bath for 10 minutes, and the other two flasks were discarded. Then, the bacterial culture was divided into four 50 ml centrifuge tubes, and the cells were harvested by centrifugation at 2500 g for 10 min at 4ºC. The media was discarded, and the centrifuge tubes were stored upside down on a stack of paper towels

for 2 minutes to dry. The cell pellet of each tube was then resuspended in 20 ml of ice-cold Inoue transformation buffer (Appendix A.3) by swirling, and then the tubes were centrifuged at 2500g for 10 min at 4ºC. Again, the media was discarded, and the centrifuge tubes were stored upside down on a stack of paper towels for 2 minutes to dry. One pellet was re-suspended in 20 ml of ice-cold Inoue transformation buffer then the 20 ml buffer was transferred to the second cell pellet containing tube and so on to re-suspend and combine all pellets. After that, 1.5 ml of dimethylsulfoxide (DMSO) was added to the bacterial suspension, mixed by swirling, followed by incubation on ice for 10 min. Working quickly, 200 µl aliquots of the cell suspension were dispensed into a chilled, sterile 1.5 ml microcentrifuge tube. The competent cells were flash-frozen immediately in liquid nitrogen and then stored on dry ice. Finally, the tubes were stored at -80 ºC.

2.7. Transformation

An aliquot of the competent cells was obtained in 2.6. was thawed on ice. To a pre-chilled 1.5 ml microcentrifuge tube, 50 µl of the competent cell and 10 µl of the ligation mixture (obtained in 2.5) were added. Two controls, a positive control using empty plasmid (had no insert) and a negative control using water, were also prepared to provide a measure of the efficiency of the transformation procedure. The tubes were then incubated for 30 minutes on ice. The cells were then heat-shocked at 42 °C for 45 seconds and then cooled on ice for 1 min. Under aseptic conditions, 250 µl of LB was added to the cells and incubated at 37°C for 1 hr with shaking. After incubation, 300 µl of the LB culture was spread on an agar plate containing the appropriate antibiotic (Appendix A.4). The plates were then inverted and incubated overnight at 37°C.

2.8. Plasmid Amplification and Extraction

The amplified plasmid was extracted from the bacterial culture using either the Qiagen QIAprep Spin Miniprep kit (2.8.1) or the HiSpeed Plasmid Midi kit (2.8.2). The

buffers of each kit were prepared and stored according to the manufacturer's instructions before their use.

2.8.1. QIAprep Spin Miniprep Kit

Aseptically, one bacterial colony from the LB agar plates prepared in 2.7 was transferred to a 10 ml LB medium containing 0.1 mg/ml ampicillin (or another antibiotic). The medium is incubated at 37°C overnight with shaking. The next day, 1 ml of the bacterial culture was transferred to a 1.5 ml microcentrifuge tube and centrifuged for 1 min at 16,200 g. The supernatant was discarded, and the process was repeated a further two times to combine a pellet of 3 ml bacterial culture. The cell pellet was re-suspended in 250 µl of buffer P1, followed by the addition of 250 µl of buffer P2. The mixture was mixed by inverting the tube gently 4-6 times and incubated for 1 min at RT. Subsequently, 350 µl of buffer N3 was added, and the microcentrifuge tube was once again inverted 4-6 times and then centrifuged for 10 mins at 16,200 g. The supernatant was then transferred to a QIAprep Spin column, centrifuged for 1 min at 16,200 g, and the flow-through was discarded. This step was followed by two washing steps, first with 500 µl of buffer PB, then 750 µl buffer PE and in each step, the tube was centrifuged for 1 min at 16,200 g, and the flow-through was discarded. The QIAprep Spin column was then centrifuged at full speed for 1 min to remove residual wash buffer. The QIAprep Spin column was then transferred to a fresh 1.5 ml microcentrifuge tube, 50 µl of ultra-pure water was added directly above the column membrane, and the column was left to incubate for 5 min at RT. The plasmid was then eluted by centrifugation of the column for 1 min at 16,200 g. To confirm that the prepared plasmid contains the gene of interest, restriction site digestion was performed as in 2.4 and run on an agarose gel electrophoresis as described in 2.2. If the gel shows that the plasmid contains the gene of interest, a 15 µl at a

concentration of 50 ng/µl sample of the eluted plasmid was sent to Eurofins Genomics for sequencing.

2.8.2. HiSpeed Plasmid Midi Kit

Aseptically, 20 µl of the bacterial culture that was prepared in 2.7 was transferred to a 100 ml LB medium containing the appropriate antibiotic (Appendix A.4). The culture was incubated at 37°C overnight with shaking. The following day, the 100 ml bacterial culture was centrifuged at 6,000 g for 15 min at 4°C. The supernatant was discarded, and the pellet was re-suspended in 6 ml of buffer P1. To the resuspended bacterial pellet, 6 ml of buffer P2 was added, mixed by inverting the tube and then incubated at RT for 5 min. Subsequently, 6 ml of pre-chilled buffer P3 was added, and the cell lysate was once again mixed by inversion until it became colourless. The cell lysate was then transferred to a QIAfilter cartridge (provided with the kit) and left to equilibrate at RT for 10 min. During the incubation, a HiSpeed Tip was equilibrated with 4 ml of buffer QBT. After that, the cell lysate was filtered in the QIAfilter cartridge through the equilibrated HiSpeed Tip, and then the HiSpeed Tip was washed with 20 ml of buffer QC. The DNA was eluted by adding 5 ml of buffer QF to the HiSpeed Tip, and then 3.5 ml of isopropanol was added to the eluted DNA, followed by incubation at RT for 5 min. The eluted DNA-isopropanol mixture was filtered through the QIAprecipitator module and then washed with 2 ml 70% ethanol. To dry the sample from excess ethanol, air is forced through the module. Finally, the DNA was eluted by pushing 1 ml nuclease-free water through the module, and to increase the DNA yield of the eluted DNA, the same 1 ml water was re-filtered through the module again. DNA concentration was subsequently measured using a Nanodrop (2000).

2.9. General Cell Culture Procedure

Cell cultures were established by thawing frozen cell aliquots at 37°C using a water bath. The aliquot was transferred to a 15 ml centrifuge tube and centrifuged with 4 ml Hanks' Balanced Salt Solution (HBSS) at 200 g for 5 min and followed by resuspension of the pellet in 4 ml serum-containing growth media (as determined by the cell line). Cells were inoculated into a 75 cm^2 tissue culture flask, and the growth media was increased to 25 ml. The cells were grown to confluence in an incubator at 37°C and 5% (v/v) CO_2.

For passaging, first, the media was discarded, and the cells were washed gently with 5 ml of HBSS. This process was repeated twice. This was followed with the addition of 1 ml trypsin, and the cells were left to incubate at 37 °C and 5% CO_2 for 5 minutes. The cells were then detached from the flask by gentle tapping, and detachment was confirmed by microscopy. The cells were then seeded in a new 75 cm^2 tissue culture flask at a 1:10 dilution with pre-warmed serum containing growth media to 37 °C. Cells were passaged in this manner every 3-4 days for maintenance or alternately when specific experiments were being performed.

2.10. Long-Term Cell Preservation

Cells for preservation were grown to confluence. For a 75 cm^2 flask, the cells were washed twice with 5 ml HBSS and then detached from the flask by adding 1 ml trypsin. The cell suspension was then transferred to a 15 ml centrifuge tube, and 4 ml HBSS was added to it and centrifuged for five minutes at 200 g. The supernatant was then discarded, and the cells were resuspended in 2.7 ml of foetal bovine serum (FBS). 0.3 ml of DMSO was then added dropwise, and the cell suspension was slowly mixed. The cell suspension was aliquoted into 1 ml into cryovials and transferred to a Mr Frosty® (Thermo Scientific, Epson, Surrey, UK). The cells were then frozen overnight

at -80 °C and in the next day, the vials were transferred to liquid nitrogen dewar for permanent storage.

2.11. Total RNA Extraction

Total RNA was extracted using the RNeasy Plus Mini Kit (Qiagen), following the manufacturer's instructions. Briefly, cells grown in 6 well plates were harvested with 1 ml trypsin (TrypLE, Gibco) per well (< 5×10^{-6} cells). After a 5 min incubation at 37 °C and 5% (v/v) CO_2, the aliquot was transferred to an RNase-free microcentrifuge tube and centrifuged at 100 g for 5 min. The supernatant was discarded, and the pellet was washed with 1 ml HBSS and centrifuged at 100 g for 5 min. The pellet was re-suspended with 350 µl RLT Plus buffer. The cell lysate was then transferred to a gDNA Eliminator spin column to eliminate DNA from the RNA sample by placing the column in a 2 ml collection tube and centrifuging for 30 seconds at 9,600 g. To the flow-through, 350 µl of 70% (v/v) ethanol was added, mixed by pipetting, and transferred to the RNeasy spin column in a 2 ml collection tube. The tube was centrifuged for 15 s at 9,600 g, flow-through discarded, and 700 µl of RW1 buffer was added to the RNeasy spin column, which was centrifuged again for 15 s at 9,600 g. RPE buffer (500 µl) was then added, and the tube was centrifuged for 30 s at 9,600 g. A further 500 µl RPE buffer was added to the RNeasy spin column and centrifuged for 2 min at 9,600 g. The RNA was eluted by adding 30 µl RNase-free water directly to the spin column membrane and centrifuge for 1 min at 9,600 g. RNA concentration and purity were subsequently assessed using a Nanodrop (2000). RNA samples were stored at -80 °C.

2.12. cDNA Synthesis (RT-PCR)

cDNA was synthesised using the RevertAid First Strand cDNA Synthesis Kit (Thermo Scientific). An aliquot of 1 µg of the extracted RNA sample was mixed with 1 µl oligo (dT)18 primer (100 µM), and the volume was made up to 12 µl with nuclease-

free water. The following reagents were added subsequently to make the reaction volume up to 20 µl: 4 µl of 5 X reaction buffer (Appendix A.5), 1 µl RiboLock RNase Inhibitor (20 U/µl), 2 µl of 10 mM dNTP Mix and 1 µl RevertAid M-MuLV RT (200 U/µL). The reaction was incubated at 42°C for one hour and terminated by heating at 70°C for 5 minutes. Finally, the samples were stored at -20 ºC.

2.13. Immunocytochemistry (ICC)

Cells were cultured in 12 well plates containing 10 µg/ml poly-L-ornithine (Millipore, USA) coated coverslips. After 24 hours (hrs) of incubation, cells were washed with HBSS and fixed with 4% (w/v) paraformaldehyde (PFA, Appendix A.6) for 5 min, and then washed in 1X PBS (phosphate buffered saline). Cells were permeabilised with 0.2% (v/v) Tween-20 for 5 min and washed with 1X PBS. Non-permeabilised cells were alternatively incubated with 1X PBS. Cells were blocked with 10% (v/v) goat serum in 1X PBS for 45 min at RT and then incubated overnight at 4°C with primary antibodies in 1% (v/v) goat serum in 1X PBS. Coverslips were then incubated with secondary antibodies conjugated to Alexa Fluor dyes in 1% (v/v) goat serum in 1X PBS for 2 hrs at RT, then washed 3 times with 1X PBS. Coverslips were mounted in a fluorescent mounting medium with or without DAPI (Vector Laboratories, Inc, UK), which is used for nuclear visualisation. Cells were imaged using the Zeiss AxioImager fluorescent Microscope and/or the Nikon A1R Confocal Microscope.

2.14. Preparation of Total Cell Lysate

The cells were grown to 80-90% confluence in 6 well plates. The 6-well plate was placed on ice, then the cell media was discarded, and the cells were washed twice with ice-cold 1X PBS. The cells were then scraped in 0.5 ml/well 1X PBS, followed by combining two wells as one sample and transferred to an ice-cold 1.5 ml microcentrifuge tube. The samples were centrifuged at 100 g for 5 min at 4 °C. The pellet was resuspended

in 100 µl of 1:100 mixture of Halt Protease and Phosphatase inhibitor Cocktail (Thermo Scientific, USA) and RIPA buffer (Thermo Scientific, USA) and incubated in ice for 30 min. The samples were then centrifuged for 15 min at 16,000g and 4 °C, and the supernatant was transferred to a prechilled 1.5 ml microcentrifuge tube. The samples were stored at -80 ºC.

2.15. Sample Preparation for Western Blotting

Protein content in the total cell lysate, prepared as in 2.14, was detected using the Pierce BCA protein assay kit (Thermo Scientific, USA). The samples were prepared as 1 µg/µl in 2X sample buffer (Appendix A.8 or A.9), heated at 95 °C for 10 min and brought to RT. The samples were either loaded onto SDS-PAGE (sodium dodecyl sulphate-polyacrylamide gel electrophoresis) gel directly or stored at -20˚C until analysis.

2.16. Western Blotting

2.16.1. SDS-PAGE Gel Electrophoresis

A 20 µg of protein sample was separated by a BioRad Mini Protein-3 System using a 10% (v/v) resolving gel (Appendix A.11) and 4% (v/v) stacking gel (Appendix A.12). The Chameleon dual pre-stained protein ladder (*LI-COR, 928-60000*) was loaded, 5 µl, to monitor the apparent sizes of proteins detected. The proteins were separated by Laemmli discontinuous SDS-PAGE at 60 V for 15 min until the bands passed from the bottom of the wells, then at 120 V for 90 min at RT using 1X running buffer (Appendix A.14).

2.16.2. Electrophoretic Transfer Protocol

As the SDS-PAGE was completed, the separated proteins on the resolving gel were transferred to a nitrocellulose transfer membrane (0.45 µm, Amersham Protran) by assembling the following blotting sandwich (from anode to cathode): sponge pad, filter paper, transfer membrane, gel, filter paper, sponge pad. Any trapped air bubbles were

removed from each step by rolling over with a plastic tube. The sandwich was placed into the transblotting apparatus (Mini Trans blot cell BioRad), and the tank was filled with the transfer buffer (Appendix A.16). The transfer was run for 1 hr at 60 V and RT, the transfer tank contained an ice pack and a stirrer to keep the buffer circulating and to avoid build-up of heat or gas bubbles on the electrode.

2.16.3. Immunodetection of Blotted Proteins

After transferring the proteins to the nitrocellulose membrane, the nitrocellulose membrane was washed for 5 min with 1X Tris-Buffered Saline (1X TBS, Appendix A.18) and then blocked with 5% (w/v) dry skimmed milk dissolved in 1X TBS for 1 hr at RT with agitation. The membrane was then incubated with the primary antibody in 5% (w/v) dry skimmed milk dissolved in 1X Tris-Buffered Saline Tween-20 (1X TBST, Appendix A.19) overnight at 4 °C. The following day, the membrane was incubated with a secondary antibody in 5% (w/v) dry skimmed milk in 1X TBST for 2 hrs at RT. Finally, BioRad ECL reagent was used for protein band detection (as per the manufacturer's guideline), and the membrane was imaged using LI-COR Odyssey.

2.17. Statistical Analysis

All statistical data analysis was carried out using GraphPad Prism 8.3.1 software unless otherwise stated. The data presented as a mean and standard error of the mean of three independent experiments unless otherwise stated. One-way ANOVA and two-way ANOVA statistical tests were used to compare multiple groups of data, including the appropriate comparisons test. Controls, positive and/or negative, were used for almost all experiments and for each experimental condition, the data quoted was in relation to the relevant control. Data was considered statistically significant if the p-value was < 0.05.

Chapter 3: Development of a Cellular Model that Expresses GPR19 and MRAP

3.1. Introduction

3.1.1. Cellular Model

The reason for choosing one cellular system includes various reasons, among them the physiological nature of the cell line, the growth and transfection efficiency, as well as the relevance of the model to address the hypothesis. Nowadays, different mammalian stable expression cell line systems are available commercially that easily allow the integration and expression of the gene of interest. The Flp Recombinase-Mediated Integration technique system (Flp-In™) is one of the systems that is widely used to generate stable cell lines that express the gene or genes of interest by the integration of the gene of interest at a specific genomic location of Flp-In™ host cell line. This system is developed using the Saccharomyces cerevisiae-derived DNA recombination system. This DNA recombination system involves the insertion of a recombinase (Flp) and site-specific recombination called the Flp Recombination Target (FRT) site into the host mammalian cell line genome and the expression vector that carries the gene of interest. This FRT will facilitate the integration of the gene of interest into the specific site in the genome of the host cells. This system has many advantages where the generation of Flp-In™ stable cell line is rapid, efficient and generates isogenic stable cell lines (Invitrogen., 2010).

Three different vectors are used in the Flp-In system to generate isogenic stable mammalian cell lines that express the gene of interest (Invitrogen., 2010). First, the pFRT/*lac*Zeo target site vector (Fig. 3.1.) is used to generate a Flp-In™ host cell line. This vector contains: 1) a *lac*Z-Zeocin™ fusion gene where expression is controlled by the

SV40 early promoter that allows efficient and high-level expression of the *lac*Z-Zeocin ™ fusion gene in mammalian cells. The transfected host cell line is then selected for Zeocin™ resistance. 2) An FRT site that is inserted just downstream of the ATG initiation codon of the *lac*Z-Zeocin™ fusion gene. The FRT site serves as the binding and cleavage site for the Flp recombinase. The Zeocin™-resistant clones are then screened to identify those containing a single integrated FRT site so the resulting Flp-In™ host cell line contains an integrated FRT site and expresses the *lac*Z-Zeocin™ fusion gene.

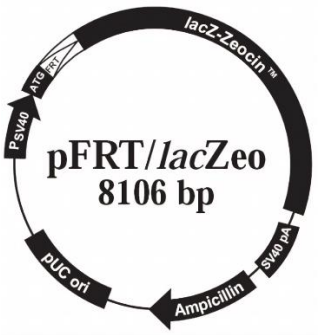

Fig. 3.1. The Flp-In™ pFRT/*lac*Zeo target site plasmid map. This plasmid contains *the lacZ-Zeocin™ fusion gene*, whose expression is controlled by the SV40 early promoter that allows efficient and high-level expression of the *lac*Z-Zeocin ™ fusion gene in mammalian cells, FRT site that is inserted downstream of the ATG initiation codon of the *lac*Z-Zeocin™ fusion gene that serves as the binding and cleavage site for the Flp recombinase. (Obtained from Invitrogen. (2010))

Second, the pcDNA™5/FRT expression vector (Fig. 3.2.), where the gene of interest will be cloned. This vector contains the following elements: 1) human cytomegalovirus (CMV) immediate-early enhancer/promoter that has the advantage of high-level constitutive expression of the gene of interest in a wide range of mammalian cells. 2) hygromycin resistance gene that is important for the selection of the stable cell

line, and it lacks a promoter and the ATG initiation codon. 3) multiple cloning sites to facilitate cloning the gene of interest. 4) a FRT site for Flp recombinase-mediated integration of the vector into the Flp-In™ host cell line.

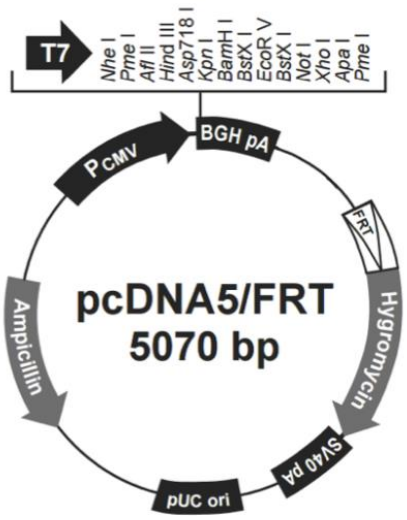

Fig. 3.2. The Flp-In™ pcDNA™5/FRT expression plasmid map. This plasmid contains a human cytomegalovirus (CMV) immediate-early enhancer/promoter site, hygromycin resistance gene for the selection of stable cell line, multiple cloning sites to facilitate cloning the gene of interest and FRT site for Flp recombinase-mediated integration of the vector into the Flp-In™ host cell line. (Obtained from Invitrogen. (2010)).

The third vector is the pOG44 plasmid (Fig. 3.3.), which constitutively expresses the Flp recombinase under the control of the human CMV promoter. This vector does not contain an antibiotic resistance marker to allow stable selection in mammalian cells.

After the insertion of the gene of interest into the pcDNA™5/FRT vector, it is co-transfected with pOG44 plasmid into the Flp-In™ host cell line (Fig. 3.4.). Upon co-transfection, the Flp recombinase expressed from pOG44 catalyses a homologous

recombination reaction between the FRT sites that is integrated on Flp-In™ host cell line and on pcDNA™5/FRT. This leads to the insertion of the pcDNA™5/FRT construct into the Flp-In™ host cell line genome at the integrated FRT site. This brings the hygromycin resistance gene downstream the SV40 promoter and the ATG initiation codon (from pFRT/*lac*Zeo) and inactivates the *lac*Z-Zeocin™ fusion gene. Thus, stable Flp-In™ expression cell lines can be selected for hygromycin resistance.

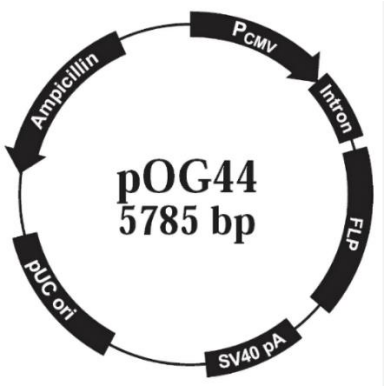

Fig. 3.3. The plasmid map of Flp-In™ pOG44. This plasmid expresses the Flp recombinase under the control of the human cytomegalovirus (CMV) promoter. (Obtained from Invitrogen. (2010)).

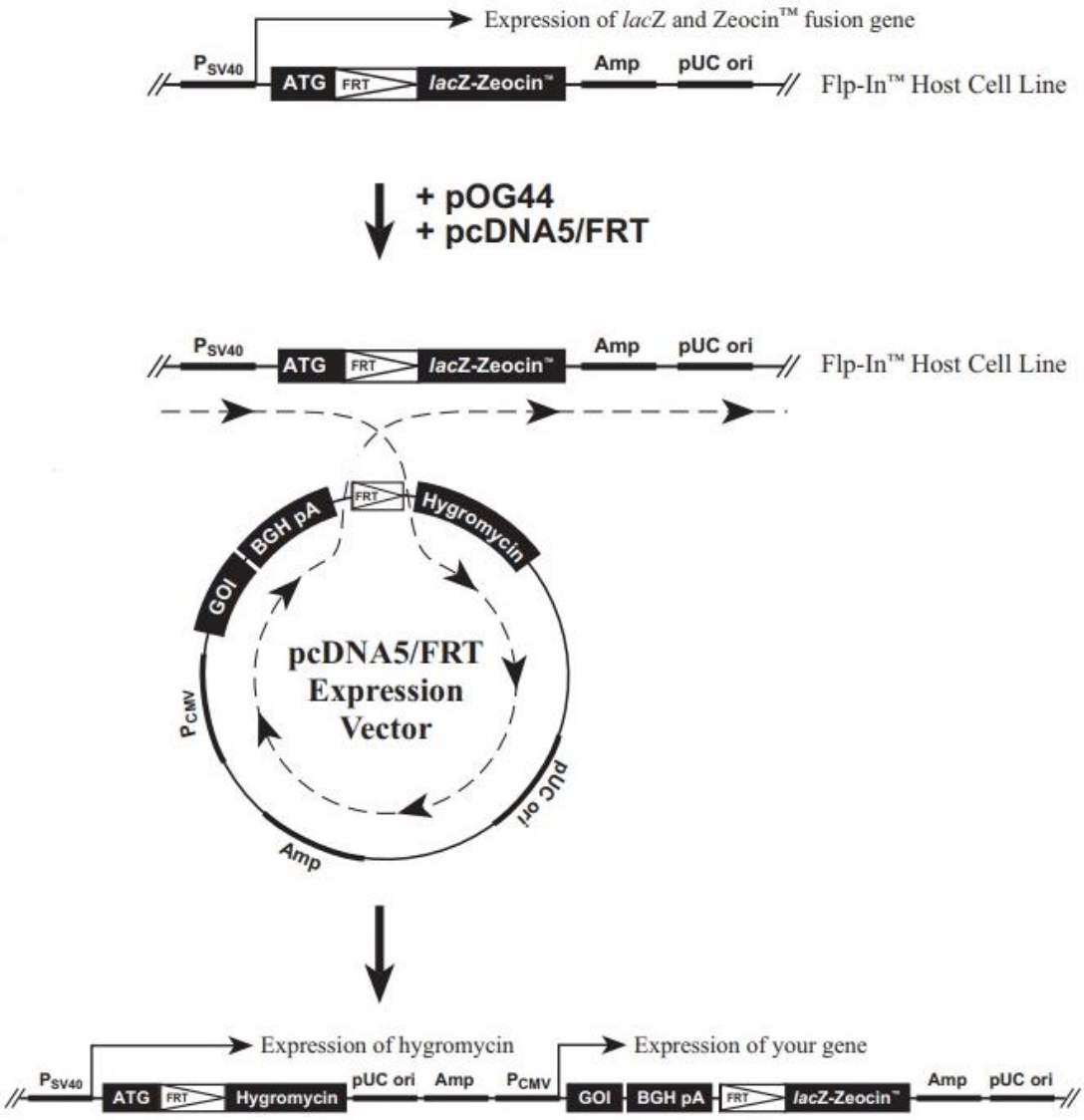

Fig. 3.4. Illustration of the Flp-In™ recombinase-mediated integration system. (Obtained from Invitrogen. (2010)).

3.1.1.1. Flp-In™ -293 as a Cellular Model

The Flp-In™ -293 was chosen as the cellular model to perform the experimental evidence to support the hypothesis. HEK-293 is a human embryonic kidney cell line. Since its development, this cell line has been widely used in cell biological research because of its ease of growth and transfection. HEK-293 cells can be used for heterologous expression, both transient and stable expression, of various proteins of interest. It was developed by the scientists Alex Van der Eb and Frank Graham in 1973 at the University of Leiden, Netherlands. This cell line was made by transforming human embryonic kidney cells with adenovirus type 5 DNA, which resulted in the incorporation of approximately 4.5 kilobases from the viral genome into human chromosome 19 of the HEK cells (Thomas & Smart, 2005). The number 293 came from Graham's habit of numbering his experiments, where the original HEK-293 cell clone was from his 293rd experiment. It has been published that HEK-293 expresses statistically significant levels of GPR19 mRNA (Atwood et al., 2011). However, it does not express MRAPα or MRAPβ (Roy et al., 2007). It is critical to choose the proper cellular model to characterise a receptor as it should express all the proteins and enzymes required for the post-translation modifications of this receptor as well as all the downstream mediated signalling machinery.

In our lab, two stably transfected HEK-293 cells were prepared by Dr. Elizabeth Lander using the Flp Recombinase-Mediated Integration technique to introduce a plasmid that carries rat GPR19 gene (rGPR19, Appendix B.1) into Flp-In™-293 to generate a HEK-293/GPR19 transformed cell line. The second stable cell line is transformed with a different plasmid that carries rGPR19 and mouse MRAP (mMRAP, Appendix B.2) genes to have the transformed cell line HEK-293/GPR19/MRAP. A third stably transfected HEK-293 cell line is transfected by a plasmid that carries only the

mMRAP gene that was prepared by me, which will be discussed later in the results section 3.4.

It is important to mention that the rGPR19 gene is amplified from rat cDNA by Pedro de Mendonca (a previous post-doctoral researcher in the Bicknell lab) and inserted in a plasmid containing the internal-ribosomal entry site (IRES) sequence followed by the coding sequence of the fluorescence protein mCherry (Fig. 3.5 A). This plasmid allows the expression of both proteins separately, and the expression of the rGPR19 is traced by checking the expression of the mCherry protein. This is followed by the preparation of two different pcDNA5 plasmids by Dr. Elizabeth Lander. Where the rGPR19 gene is amplified from the IRES-mCherry plasmid using primers that had restriction site cleavage at BamHI and HindIII (Table 3.1) and then inserted in pcDNA5 plasmid that is digested by BamHI and HindIII digestive enzymes (Fig. 3.5 B) and is used for the generation of the cell line that overexpressed GPR19.

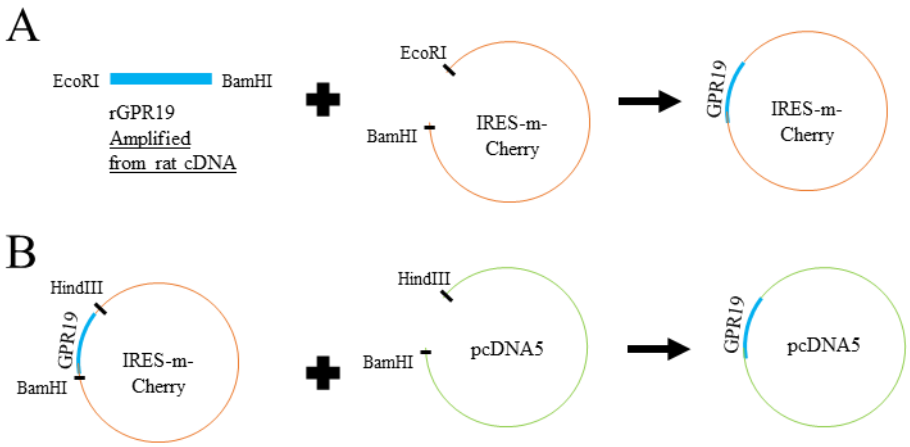

Fig. 3.5. The rat GPR19 (rGPR19) gene was amplified from rat cDNA by Pedro de Mendonca and inserted in IRES-mCherry plasmid (A). Then, it was cut using BamHI and HindIII digestion enzyme and inserted in pcDNA5 plasmid (B) to be used for the generation of an overexpressed GPR19 cell line.

Table. 3.1. Designed primers used for the amplification of the rGPR19 gene from IRES-mCherry plasmid that is carrying the rGPR19 gene.

Primer Type	**Primer Sequence (5`--3`)**
GPR19FHindIII	TAAGCAAAGCTTATTATGGGTTTTGATCACAGA
GPR19RBamHI	TGCTTAGGATCCTTAGAAATTAGACAAAAGTGT

The mMRAP gene was amplified from pcDNA3.1 plasmid donated by Dr Li Chan (William Harvey Research Institute, London) and inserted in pIRES-EGFP (enhanced green fluorescent protein) plasmid using BstX1 and NotI digestive enzymes (Fig. 3.6 A) with the EGFP gene to be lost during this digestion step. Then, the rGPR19 gene is amplified from the pcDNA5 plasmid and inserted in the same plasmid using EcoRI and BamHI digestive enzymes (Fig. 3.6 B). Both the mMRAP and the rGPR19 genes are cut from this plasmid using NotI and NheII digestive enzymes and inserted into the pcDNA5 plasmid (Fig. 3.6 C) to be used for the generation of the cell line that overexpresses GPR19 and express MRAP with IRES directing the expression of both proteins separately.

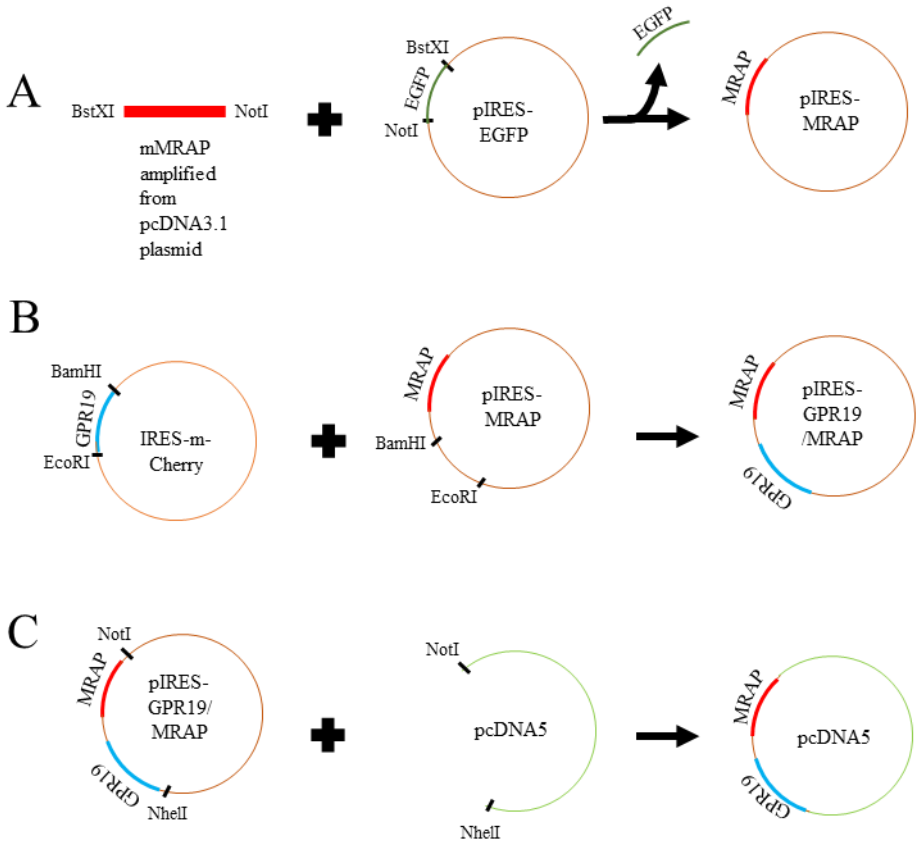

Fig. 3.6. The mMRAP gene is amplified from pcDNA3.1 plasmid, which is a donation from Dr. Li Chan (William Harvey Research Institute, London) and inserted in pIRES-EGFP plasmid using BstX1 and NotI digestive enzymes (A) where the EGFP is removed from the plasmid and MRAP gene is inserted. Then, the rGPR19 gene (for more information, see Figure 3.5) is inserted in the same plasmid using EcoRI and BamHI digestive enzymes (B). Both the mMRAP and the rGPR19 genes are cut from the IRES-EGFP plasmid using NotI and NheII digestive enzymes and inserted into pcDNA5 plasmid to be used for the generation of GPR19/MRAP overexpressing cell line (C).

3.2. Aims

1) To develop a stably transfected cell line that expresses the mMRAP gene beside the two cell lines that are over-expressed rGPR19 and over-expressed rGPR19 and mMRAP.
2) To confirm the endogenous gene expression of hGPR19 and the lack of hMRAP expression in the selected wild-type cell line and the expression of rGPR19 and mMRAP inserted genes in the generated stably transfected cell lines by RT-PCR.
3) To study the localisation of GPR19 and MRAP in those cell lines by fluorescent staining (ICC) and to quantify their total protein expression by western blotting.

3.3. Methods

3.3.1. mMRAP Gene Plasmid Construction

The mMRAP gene that is used for the MRAP stable expression cell line preparation was amplified from the GPR19/MRAP pcDNA5 plasmid (Fig. 3.7) and then introduced alone into the Flp-In™-293 cells using the Flp Recombinase-Mediated Integration technique.

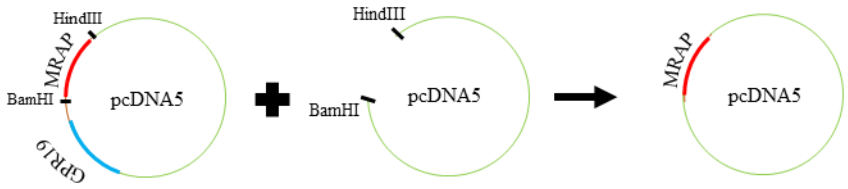

Fig. 3.7. The Mouse MRAP (mMRAP) gene containing plasmid is prepared by amplifying the mMRAP gene from the GPR19/MRAP plasmid using primers in Table 3.2, and both the amplified gene and pcDNA5 plasmid are digested by BamHI and HindIII digestive enzymes and then ligated together.

3.3.2. PCR Amplification Protocol

The PCR reaction mixture was prepared as discussed in section 2.1. The forward and reverse GPR19 and MRAP primers (Table 3.2 and 3.3) were designed using PrimerBlast (https://www.ncbi.nlm.nih.gov/tools/primer-blast/) and were purchased from Sigma.

The PCR amplification reaction was conducted using Eppendorf MasterCycler® Nexus Gradient as follows:

1) The PCR conditions used to amplify a target from a cDNA sample were as follows: initial denaturation at 94°C for 90 sec, followed by 35 cycles of three-

step cycles: denaturation at 94°C for 20 sec, primer annealing at 62°C for 20 sec, and extension at 68°C for 90 sec.

2) The PCR conditions used to amplify a target from a plasmid, e.g., the GPR19 and MRAP gene, were as follows: 5 cycles of the three-step cycle: denaturation at 94°C for 20 sec, primer annealing at 55°C for 20 sec, then extension at 68°C for 90 sec. These 5 cycles were followed by 35 cycles of a two-step cycle: denaturation at 94°C for 20 sec, annealing, and extension at 68°C for 90 sec.

The PCR products were then profiled by agarose gel electrophoresis (section 2.2).

Table 3.2. Designed primers used for amplification of the mMRAP gene from the GPR19/MRAP plasmid

Primer Type	Primer Sequence (5`--3`)	Product size
MRAPFHindIII	TAAGCAAAGCTTATGGCCAACGGGACCGACGC	319 bp
MRAPRBamHI	TGCTTAGGATCCTCAAGCGTAGTCTGGGACGT	

Table 3.3. Designed primers used for amplification of target genes in different cell lines.

Gene	NCBI Reference Sequence	Primer Type	Start	Stop	Primer (5`--3`)	Product Size (bp)
GAPDH	NM_002046.7	Forward	559	581	CAAGGTCATCCATGACAACTTTG	496
		Reverse	1054	1033	GTCCACCACCCTGTTGCTGTAG	
hGPR19*	NM_006143.3	Forward	266	285	GCAAGGGCTATTCCTGACCA	1434
		Reverse	1699	1679	TCCCTTGGAAAGTTGAGTGAA	
		Forward	432	451	CTGCACTGAAACAGCCACAC	1069
		Reverse	1500	1481	AGTTTTGGCCATGGAAGGGA	
rGPR19	NM_080579.1	Forward	189	208	CCCTGTGGTTACTGCTACCC	1067
		Reverse	1255	1236	TGGCCATCCTTGAACTGGTC	
hMRAP**	NM_206898.1	Forward	178	197	TGCCACAGACATGGCCAACG	213
	NM_178817.4		178	197		
	XM_006724028.3		108	127		
	XM_017028407.1		104	124		
	NM_206898.1	Reverse	371	390	ATCTGCGGGGAGGCGGACCA	
	NM_178817.4		371	390		
	XM_006724028.3		301	320		
	XM_017028407.1		297	316		
mMRAP	NM_029844.4	Forward	422	442	ACCTCATTCCTGTGGACGAGA	287
		Reverse	708	689	AGAAGGACTCTGCTGCGTTA	

* The two hGPR19 primer pairs have been designed where the first pair detects the full-length gene, and the second pair detects a middle sequence of the gene.

** The hMRAP gene has 5 different variants, and it was difficult to design one pair of primers to detect all the variants. One forward primer is designed to bind to four different variants.

3.3.3. Restriction Site Digestion and Ligation

The mMRAP amplified gene was purified from the agarose gel following the purification protocol in section 2.3. Then, both the Flp-In™ pcDNA™5/FRT expression plasmid and the purified gene were digested using the restriction endonucleases HindIII (FD0504, Thermo Scientific) and BamHI (FD0054, Thermo Scientific) following the protocol in section 2.4. The digested pcDNA5 plasmid and the purified genes are ligated following the ligation protocol in section 2.5.

3.3.4. Transformation, Plasmid Amplification and Extraction

The ligation mixture was obtained in section 3.3.3. was transformed into DH5α Escherichia coli (E. coli) competent cells following the protocol in section 2.7. The LB culture was spread on an ampicillin-containing agar plate (Appendix A.4). Colonies were picked, and plasmid was extracted using a QIAprep Spin Miniprep kit following the protocol in section 2.8.1. Around 15 µl at a concentration of 50 ng/µl of the extracted plasmid was sent to Eurofins Genomics for sequencing. If the sequence of the GPR19 and MRAP genes was correct and complete, a greater quantity of transfection-grade plasmid was prepared using the HiSpeed Plasmid Midi Kit following the protocol in section 2.8.2.

3.3.5. Flp-In™ -293 Stable Cell Line Generation

Flp-In™ -293 host cell line (Invitrogen, supplied through Thermo Scientific, Epson, Surrey, UK) was grown in 25 ml of serum-containing DMEM (Gibco) growth media (Table 3.4). Subsequently, the cells were seeded onto each well of a 6-well plate. Once the cells had reached a density of 50%, the media was removed, and the cells were transfected with the transfection mixture. The transfection mixture was prepared as follows: for a single well, 300 µl of serum-free DMEM was added to a sterile 1.5 ml microcentrifuge tube together with 9 µl Turbofect® (transfection reagent), vortexed and

incubated at RT for 5 min. Then, 2.7 ug of pOG44 and 0.3 μg of the desired pc5DNA plasmid that was prepared in section 3.3.4 were added to the solution, vortexed and incubated for 20 minutes at RT. The 300 μl of transfection mixture was then added dropwise to a single well and incubated for 5-6 hrs. The transfection mixture was then removed by aspiration, and a fresh 2 ml of serum-containing media was added to the cells. After 24 hrs, each transfected well was washed with 3 ml HBSS twice, and the cells were detached by adding 1 ml of trypsin and transferred into two 60 mm dishes or two wells of a 6-well plate. 5.5 ml of serum-containing DMEM media containing 200 μg/ml hygromycin B to select only the cells that were transfected with the pc5DNA plasmid was then added to each well, and the cells were incubated at 37°C and 5% CO_2. Every 3 to 4 days the medium was removed, and the cells washed with 3 ml HBSS, followed by replacement of the medium to remove the dead cells. After 14 days, the cells were trypsinised and transferred to a 25 cm^2 flask for expansion of the new cell line. Cells were passaged in this manner every 3 to 4 days for maintenance following the general cell culture procedure section 2.9.

Table 3.4. DMEM (Gibco) growth media for the wild-type and transfected cell lines

Reagents added to 500 ml DMEM, Gibco	WT cells		Transfected cells	
	Serum Media	Serum Free	Serum Media	Serum Free
foetal bovine serum (FBS, Gibco)	10% (v/v)	-	10% (v/v)	-
glutamine (GlutaMAX, Gibco)	1% (v/v)	1% (v/v)	1% (v/v)	1% (v/v)
streptomycin and penicillin (PenStrep, Gibco)	100 μg/ml and 100 U/ml	100 μg/ml and 100 U/ml	100 μg/ml and 100 U/ml	100 μg/ml and 100 U/ml
Hygromycin B (H75020-1, Melford)	-	-	100 μg/ml	100 μg/ml

3.3.6. GPR19 and MRAP mRNA Expression

To study the expression of the GPR19 and MRAP genes in the wild-type and transformed cells, total RNA was extracted using the RNeasy Plus Mini Kit (Qiagen) as described in section 2.11. Then, the cDNA was synthesised using RT-PCR, as described in section 2.12. The GPR19 and MRAP genes were amplified from the cDNA sample using the PCR protocol in section 3.3.2. The specific primers used for the amplification of hGPR19, rGPR19, hMRAP, and mMRAP are listed in Table 3.2.

3.3.7. GPR19 and MRAP Protein Expression in the Cell Lines

To investigate the protein expression of GPR19 and MRAP in the wild-type and transformed cell lines ICC and western blotting were used. It is important to note that the MRAP gene is tagged with an HA-Tag, so for ICC and western blotting, the anti-HA-Tag was used to detect its expression.

3.3.7.1. Immunocytochemistry (ICC)

The ICC technique was performed as described in section 2.13. The cells were incubated with 3 µg/ml of the primary antibodies that are listed in Table 3.5 and then incubated with the secondary antibodies conjugated to Alexa Fluor dyes: Alexa Fluor 488 goat anti-mouse IgG (A-11001, Invitrogen) and Alexa Fluor 546 goat anti-rabbit IgG (A-11010, Invitrogen), at 1:200 in 1% (v/v%) goat serum in 1X PBS. The cells were mounted in a fluorescent mounting medium without DAPI (Vector Laboratories, Inc, UK). DAPI is a dye that is used for nuclear visualisation. It has a broad spectrum that will interfere with the Alexa-488 dye, which will develop a false positive result. Cells were imaged using a Nikon A1R Confocal Microscope and an X60 lens.

Table 3.5. Primary antibodies used for ICC technique.

No.	Antibody	Catalogue Number	Immunogen and Epitope
1	Mouse Monoclonal anti-GPCR GPR19	[1B5] ab167140, abcam	Peptide conjugated with an epitope in the N-terminal portion.
2	Rabbit Polyclonal anti-HA tag	ChIP grade ab9110, abcam	YPYDVPDYA conjugated to KLH

3.3.7.2. Sample Preparation and Western Blotting

The cell lysate of the four cell lines was prepared following the procedure in sections 2.14 and 2.15. The western blotting was performed as in section 2.16. The primary antibodies that are used to detect GPR19, MRAP protein and the loading control antibody (anti-actin) are listed in table 3.6 with the dilution factor that was used. The rec-protein G-peroxidase conjugate (10-1223, Thermo Fisher) was used as a secondary antibody with 1:4000 dilution in 1X TBST containing 5% (w/v) skimmed milk.

Table 3.6. The primary antibodies that are used to detect GPR19 and MRAP in western blotting.

No.	Antibody	Catalogue Number	Immunogen and Epitope	Dilution Factor for WB
1	Mouse monoclonal anti-HA-Tag	A85278, antibodies	YPYDVPDYA conjugated to KLH	1:1000 5% (w/v) skimmed milk in 1X TBST
2	Rabbit Polyclonal anti-GPR19	A97504, antibodies	Synthetic peptide derived from human GPR19 (aa. 361-410)	1:2000 5% (w/v) skimmed milk in 1X TBST
3	Rabbit Monoclonal anti-β-actin	#4970, cell signalling	a synthetic peptide corresponding to residues near the amino-terminus of human β-actin protein.	1:1000 5% (w/v) skimmed milk in 1X TBST

3.4. Results

3.4.1. Generation of Stable Flp-In™-293 that Express mMRAP Gene

To generate this cell line, first, the mMRAP gene was amplified by PCR from the GPR19/MRAP pcDNA5 plasmid using the primers in Table 3.2. to produce a 319 bp product that was subsequently separated using agarose gel electrophoresis (Fig. 3.8). Then, the PCR product was purified from the agarose gel and both the Flp-In™ pcDNA ™5/FRT expression plasmid and the purified mMRAP gene were digested using the HindIII and BamHI endonucleases and analysed by agarose gel electrophoresis (Fig. 3.9). The restriction site digested plasmid and the gene were purified from the gel and then ligated together using the Rapid DNA Ligation Kit.

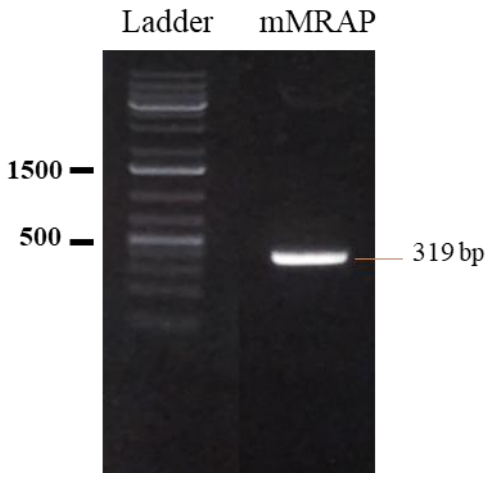

Fig. 3.8. Agarose gel electrophoresis of amplified mMRAP gene using PCR. The band match the expected size of the mMRAP gene of 319 bp, which confirms the amplification of the correct gene.

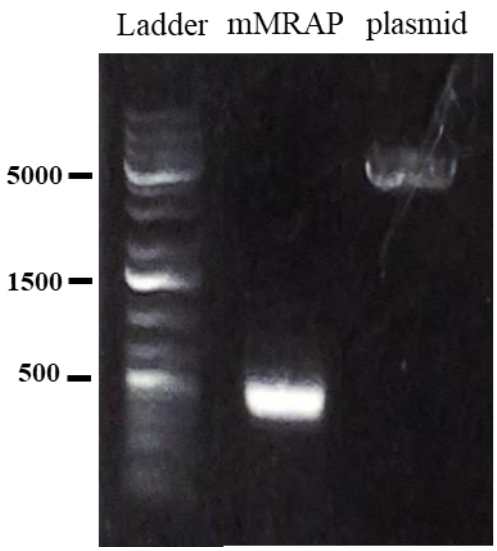

Fig. 3.9. Agarose gel electrophoresis of HindIII and BamHI endonucleases digested MRAP gene and Flp-In™ pcDNA™5/FRT expression plasmid. The band match the expected size of both the MRAP gene at 319 bp and the plasmid at 5070 bp.

This plasmid was then transformed into DH5-α competent cells, three colonies were picked and grown, and the plasmid was isolated using the QIAprep Spin Miniprep kit. The isolated plasmid was subject to restriction site digestion using the HindIII and BamHI endonucleases to confirm the presence of the MRAP gene in the plasmid (Fig 3.10). From this analysis, it was identified that the plasmid contained the desired insert and confirmed that it contained the complete MRAP gene sequence. A sample of the extracted plasmid was sent to Eurofins Genomics for sequencing. After confirming that the pcDNA5/FRT plasmid contains the correct and complete sequence of the mMRAP gene, a greater quantity of transfection grade was prepared using the HiSpeed Plasmid Midi kit to be used for Flp-In™-293 transfection.

After the cells were transfected with the pcDNA5/FRT plasmid carrying mMRAP, the cells were grown with DMEM media containing selection hygromycin B concentration (200 µg/ml) for 14 days. This concentration was chosen after growing the

cells in different hygromycin B concentrations, and it has been found that the 200 µg/ml hygromycin B concentration was the appropriate concentration to kill the un-transfected cells and to grow the transfected cells. After 14 days, the cells were transferred to a larger flask to allow expansion of the new stable cell line.

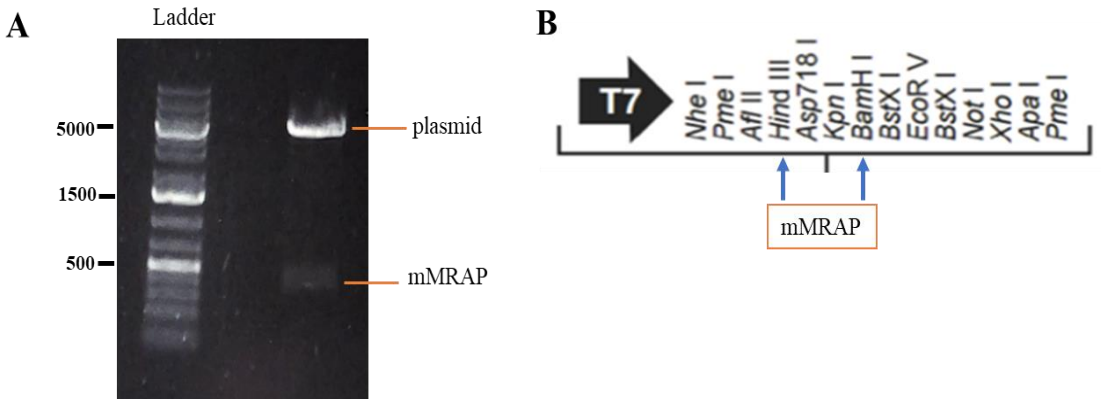

Fig. 3.10. A) Agarose gel electrophoresis showing Flp-In™ pcDNA™5/FRT expression plasmid in which mMRAP gene has been inserted. The plasmid has been digested with HindIII and BamHI endonucleases to confirm the presence of the insert at 319 bp. B) Map of the pcDNA5/FRT plasmid multiple cloning sites. The point of insertion of the mMRAP sequence into the pcDNA™5/FRT plasmid is in the correct orientation with respect to the CMV promoter.

3.4.2. GPR19 and MRAP mRNA Expression in Wild-Type and Transformed Cell Lines

The next aim of this project was to investigate the gene expression of GPR19 and MRAP in the wild-type cell line, HEK-293, and the transformed cell lines, GPR19, MRAP and GPR19/MRAP. This aim was achieved using RT-PCR. First, the purity and integrity of the extracted RNA sample were confirmed before the synthesis of first-strand cDNA of GPR19 and MRAP, as poor-quality RNA can give a false-negative result.

Nucleic acids (DNA and RNA) have absorbance maxima at 260 nm, while protein absorbs at 280 nm. Therefore, the 260/280 ratio is used as a good estimate of the level of protein contamination in the RNA sample. Pure RNA has a 260/280 absorbance ratio of 2. However, values between 1.8 and 2.0 are considered acceptable as pure RNA samples. The integrity of the extracted RNA sample was confirmed by running the RNA sample on a 1% (w/v) agarose gel electrophoresis to detect the two ribosomal RNA subunits. The upper ribosomal band (28S) should be about twice the intensity of the lower band (18S) (Fig. 3.11). If they were of the same intensity, this suggests that some degradation had occurred.

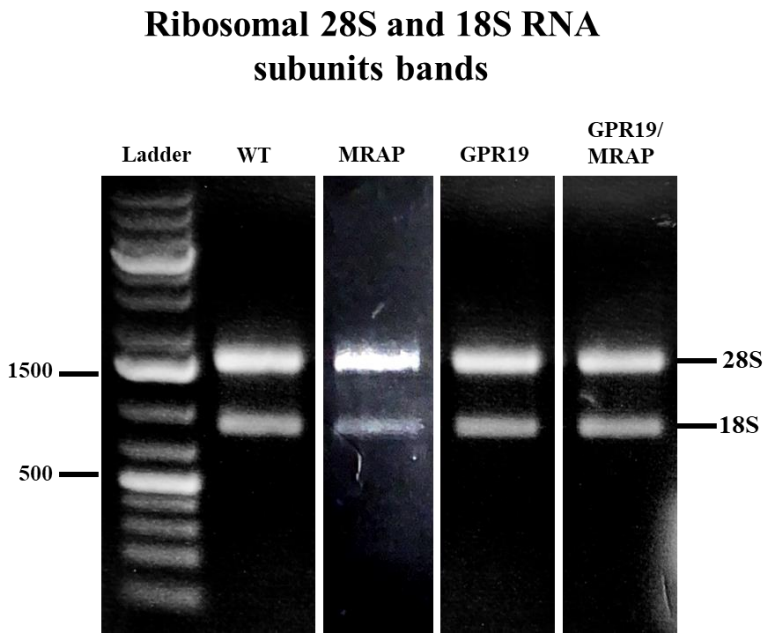

Fig. 3.11. Agarose gel electrophoresis of the isolated RNA sample from the four cell lines. The ribosomal 28S and 18S RNA subunit bands are indicated, which confirms the integrity of the isolated RNA sample; therefore, it can be used for cDNA synthesis of GPR19 and MRAP genes in those cell lines.

Moreover, to assess that the first-strand cDNA was efficiently synthesised, RT-PCR was performed for the housekeeping gene, glyceraldehyde 3-phosphate dehydrogenase (GAPDH). The GAPDH produces a band of approximately 500 bp (Fig. 3.12), which means the cDNA was successful; therefore, any negative result obtained from the RT-PCR of a gene of interest is due to the un-expression of that gene.

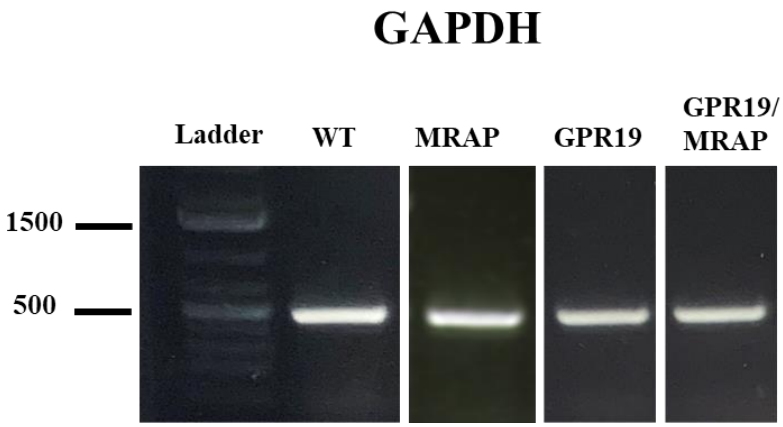

Fig. 3.12. Agarose gel electrophoresis of the cDNA samples from the four cell lines. The GAPDH band is indicated in the four cell lines, which means that the cDNA synthesis was successful and can be used for the synthesis of GPR19 and MRAP genes in those cell lines. Negative control runs side by side with the samples (images are not shown).

The presence of human mRNA transcripts encoding hGPR19 in the HEK-293 cell line was verified using the primer listed in Table 3.3, with the correct product size being obtained at approx. 1400 bp and 1000 bp in primer pairs 1 and 2, respectively (Fig. 3.13). The RT-PCR results for hMRAP agree with the finding of Roy et al. (2007) as neither MRAP isoforms are not expressed in HEK-293 (Fig. 3.14 A). The efficiency of the designed hMRAP primers was checked using the cDNA of the human breast, testis and

adrenal as it has been published that MRAPα and β are highly expressed in those tissues (Metherell et al. (2005). The RT-PCR gave a positive result for the primer pairs in all three tissues (Fig. 3.14 B). The expression of the inserted rGPR19 in the transformed cell lines, GPR19 and GPR19/MRAP was confirmed, as shown in Fig. 3.15. The expression of the inserted mMRAP in the MRAP and GPR19/MRAP transformed cell lines was also confirmed by using primers designed for mouse MRAP (Fig. 3.15 B and Fig. 3.16, respectively).

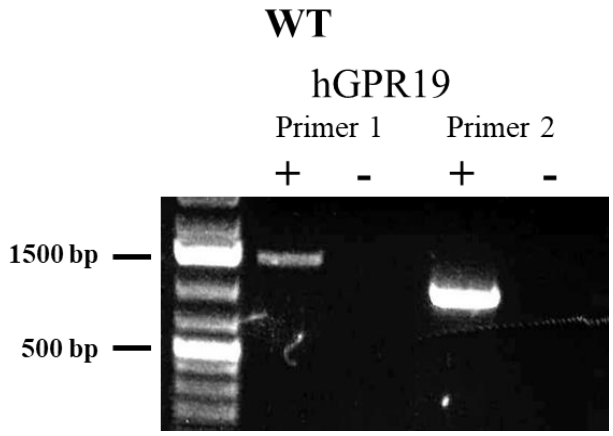

Fig. 3.13. Agarose gel electrophoresis of HEK-293 cell line for hGPR19 gene. The expression of the endogenous hGPR19 in the HEK-293 cell line is confirmed as the first pair of primers that amplifies the full-length hGPR19 gene gave a PCR product of 1400 bp, while the second pair of primers that amplifies the hGPR19 gene produce 1000 bp cDNA product.

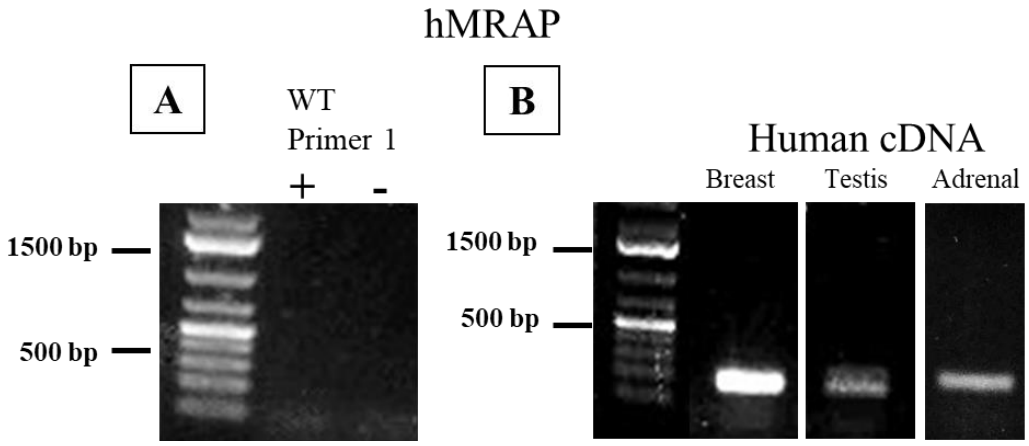

Fig. 3.14. Agarose gel electrophoresis of HEK-293 cell line for hMRAP gene. A: The RT-PCR of the endogenous hMRAP produce negative results as expected, as the MRAP gene is not expressed in the HEK-293 cell line. B: The RT-PCR results of human breast, testis and adrenal cDNA using hMRAP designed primers confirm that the designed primers can detect the hMRAP gene and the negative results that the WT cell line produces are due to no expression of MRAP. The three tissues produce a positive result and produce a band with a size of approx. 200 bp.

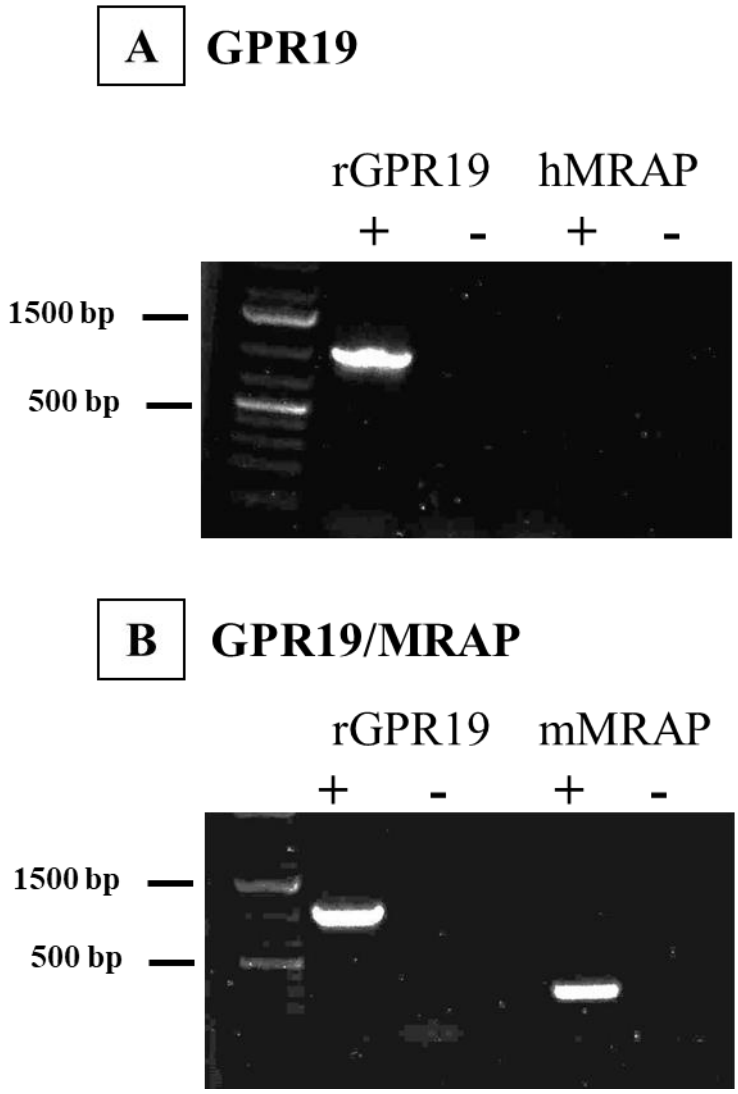

Fig. 3.15. Agarose gel electrophoresis of the transformed GPR19 and GPR19/MRAP cell lines for both rGPR19, hMRAP and mMRAP genes. A: The expression of the inserted rGPR19 gene in the transformed cell line that stably produces the rGPR19 gene is confirmed as a band of approx.1000 bp is produced. The RT-PCR of the hMRAP in this cell line produces negative results, as expected. The hGPR19 expression in this cell line has been confirmed (images not shown). B: The expression of both inserted rGPR19 and mMRAP in the GPR19/MRAP cell line is confirmed. The designed primer pair for the rGPR19 gene gave a product of approx. 1000 bp. Also, the expression of mMRAP is confirmed as a band of 300 bp is identified. The expression of the hGPR19 and the lack of the hMRAP expression in this cell line have been confirmed (images are not shown).

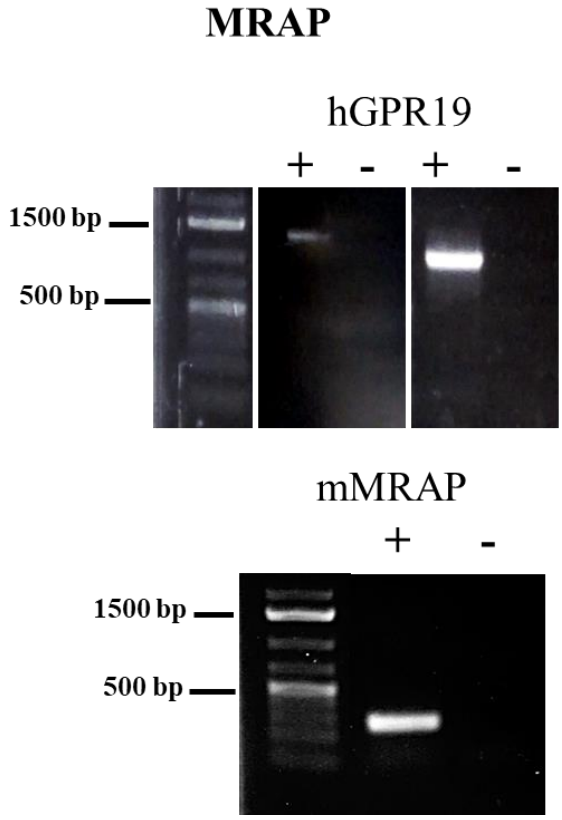

Fig. 3.16. Agarose gel electrophoresis of the transformed cell line with mMRAP gene. The expression of the endogenous hGPR19 in this cell line is confirmed as the first pair of primers, which covers the full length of the hGPR19 gene, gave a cDNA product of 1400 bp, while the second pair of primers, which covers part of the hGPR19 gene, produce 1000 bp cDNA product. Also, the expression of the inserted mMRAP gene is confirmed as a band of approx. 300 bp is identified. The lack of the hMRAP expression in this cell line has been confirmed (images are not shown).

3.4.3. GPR19 and MRAP Protein Expression in the Wild-Type and Transformed Cell Lines

Immunocytochemistry and western blot were used to study GPR19 and MRAP protein localisation and expression levels in the different cell lines, respectively. The immunofluorescence images using confocal microscopy revealed that the GPR19 protein is detected in the wild-type cell line and the three transfected cell lines.

The GPR19 protein expression in the wild-type cell line HEK-293 and the cells stably transfected with GPR19, MRAP and GPR19/MRAP were analysed using ICC, as shown in Fig 3.17. In the permeabilised condition, which detects total GPR19 expression, the transformed cell lines expressing the rGPR19 gene showed higher signal intensity in comparison to the wild-type cell line and to the transformed cell line with the mMRAP gene (Fig 3.17 A). On the other hand, the non-permeabilised condition, which detects GPR19 expression on the cell surface, shows that the cell lines that overexpress mMRAP or overexpress both MRAP and GPR19 had higher GPR19 signal intensity on the cell surface in comparison to the cell lines that do not express MRAP, i.e., the wild-type and GPR19 cell lines.

To confirm these findings statistically, the GPR19 protein expression in those four cell lines was calculated as the corrected total cell fluorescence (CTCF). CTCF was calculated in 5 cells from 3 independent images using ImageJ, and that was followed by statistical analysis of the data using two-way ANOVA and Šídák's multiple comparisons tests. The data represented in Fig 3.17 B confirms the overexpression of GPR19 in the cell lines that were transfected with rGPR19 in comparison to the WT cell line. Interestingly, the expression of MRAP alone does not increase the total expression of GPR19 inside the cells, but it increases the localisation of GPR19 to the cell membrane.

That finding confirms that GPR19 requires MRAP to be translocated to the cell membrane.

Interestingly, the inserted mMRAP gene gave a bright red stain in both MRAP and MRAP/GPR19 cell lines. Fig. 3.18 shows the total expression, the permeabilised condition images, and the cell surface expression, the non-permeabilised condition images, of the inserted mMRAP in the MRAP and GPR19/MRAP cell lines. The HA-tag is inserted in the C-terminal of the mMRAP gene. The HA-Tag antibody is used in the wild type and the GPR19 cell lines to demonstrate that it is specific and will not give false-positive results when it is used to detect the inserted mMRAP in the MRAP and GPR19/MRAP cell line.

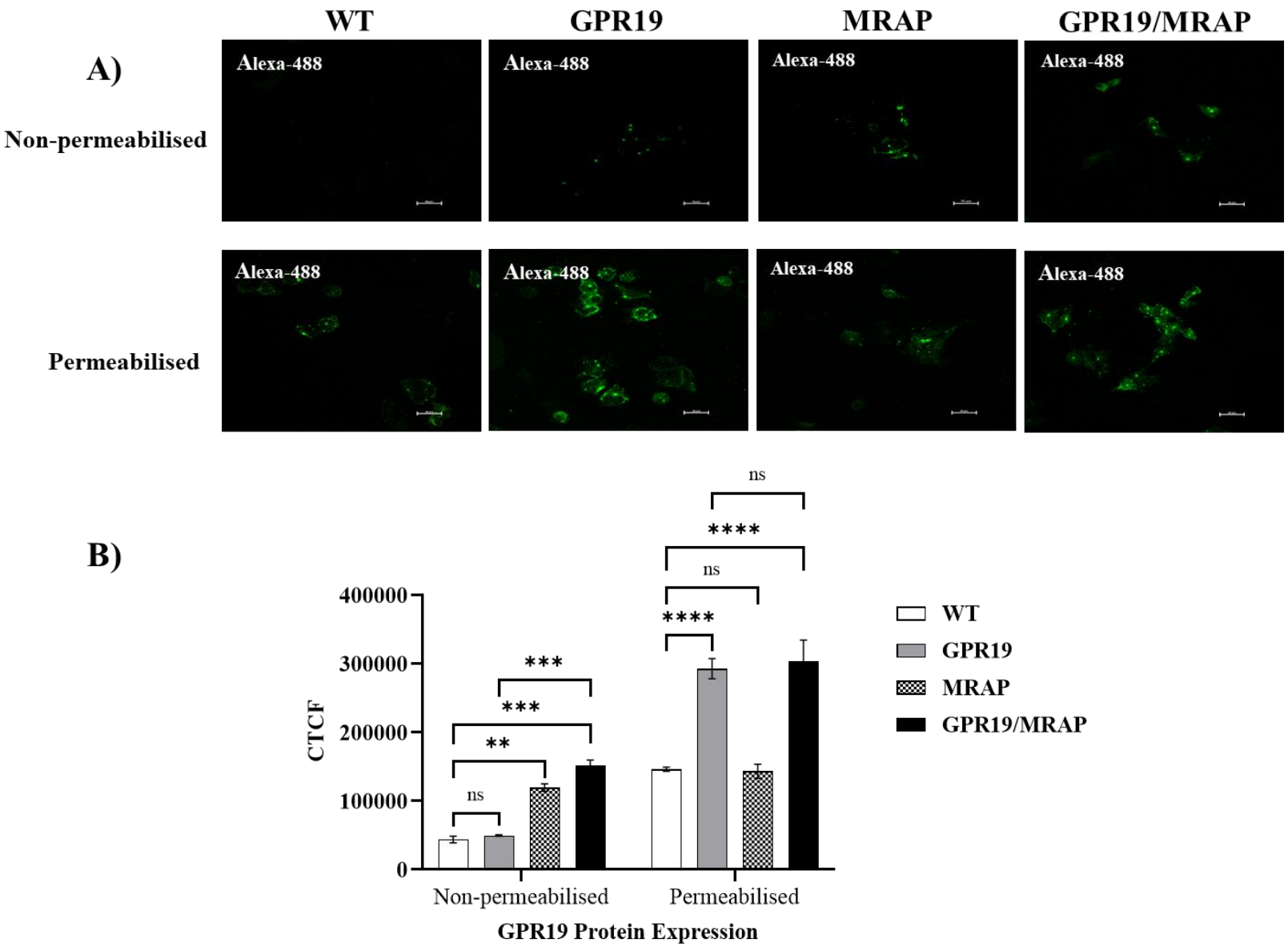
A)
WT
GPR19
MRAP
GPR19/MRAP
Non-permeabilised
Permeabilised
Alexa-488
B)
CTCF
400000
300000
200000
100000
0
ns
**
***
***
****
ns
****
ns
Non-permeabilised
Permeabilised
GPR19 Protein Expression
WT
GPR19
MRAP
GPR19/MRAP

Fig. 3.17. A) Distribution of GPR19 protein in the wild-type cell line HEK-293 and the stably transfected cells with GPR19, MRAP and GPR19/MRAP using ICC. GPR19 is stained with Alexa-488, where the non-permeabilised condition shows its distribution in the cell membrane, while the permeabilised condition with 0.2% (v/v) Tween-20 shows its total distribution. Images taken with a Nikon A1 Plus confocal microscope using NIS Elements software. Scale bars = 20 µm.

B) The corrected total cell fluorescence (CTCF) that represents the GPR19 protein expression in the four cell lines was calculated in 5 cells from 3 independent images. Statistical analysis was performed using two-way ANOVA and Šídák's multiple comparisons test. Data are expressed as mean ± SEM of three independent experiments. Results were considered statistically significant if the p-value was < 0.05.

.

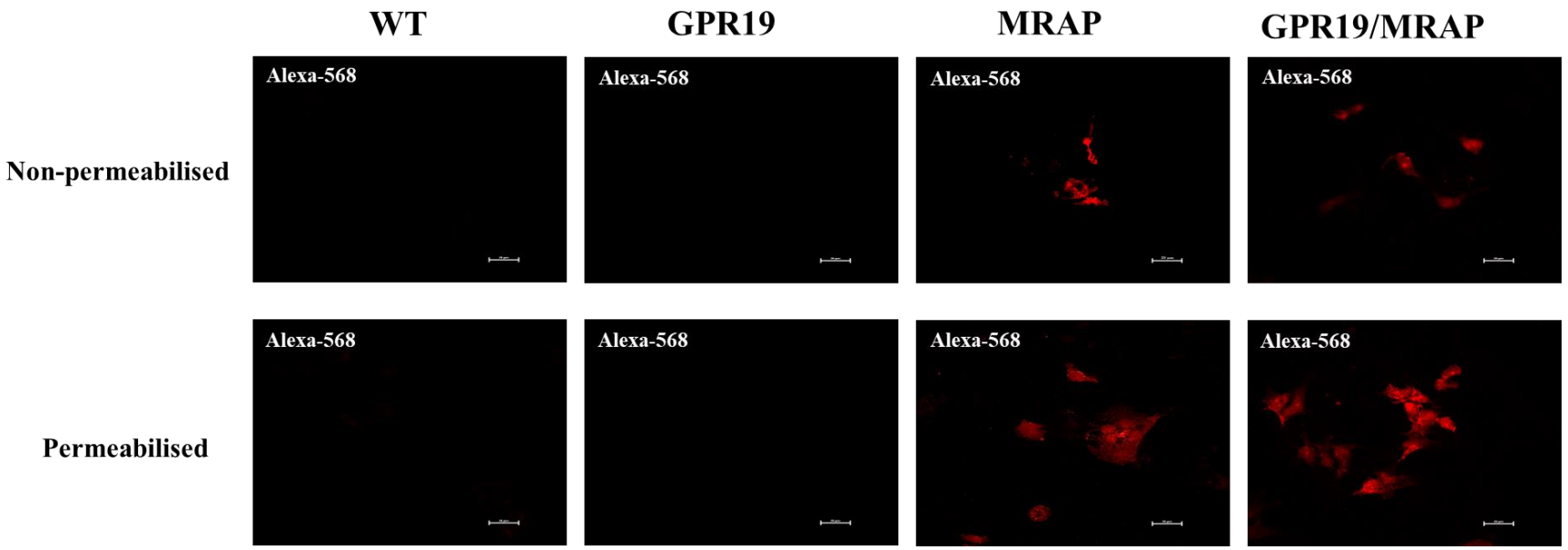

Fig. 3.18. Distribution of MRAP protein in the wild-type cell line HEK-293 and the stably transfected cells with GPR19, MRAP and GPR19/MRAP using immunocytochemistry. MRAP is stained with Alexa-546, where the non-permeabilised condition shows its distribution in the cell membrane, while the permeabilised condition with 0.2% (v/v) Tween-20 shows its total cellular distribution. Images confirm the expression of MRAP protein in the transformed cell lines MRAP and GPR19/MRAP but not in the WT and the transformed cell line GPR19. Images taken with a Nikon A1 Plus confocal microscope using NIS Elements software. Scale bars = 20 μm.

To study GPR19 protein expression in more detail, we used a western blot. The blot shows two bands of ~90 kDa and ~50 kDa (Fig. 3.19 A). The smallest band (50 kDa) corresponds to the predicted molecular weight of human and transfected rGPR19, and the other high molecular weight band (90 kDa) may result from dimerisation. The GPR19 protein content is normalised to β-actin protein content (Fig. 3.19 B), and fold above wild type GPR19 protein content is calculated, then 2-way ANOVA with Tukey's multiple comparisons test was applied. The GPR19 protein content of ~90 kDa band is significantly higher in the three stably transfected cell lines: the MRAP, GPR19 and GPR19/MRAP, in comparison to the wild-type cell line (Fig. 3.19 C). The ~50 kDa GPR19 band protein content is only significant in the cell lines that are transfected with the GPR19 gene, the GPR19 and GPR19/MRAP cell lines. These results showed only the increase in the higher molecular weight GPR19 band (90 kDa) in the cell line that is expressing the accessory protein MRAP, which could be explained as this band includes the biologically functional GPR19 receptor that is dimerised with another cell receptor. As expected, the protein expression and detection of the HA-tagged MRAP is only detected in the MRAP and GPR19/MRAP cell lines (Fig. 3.20).

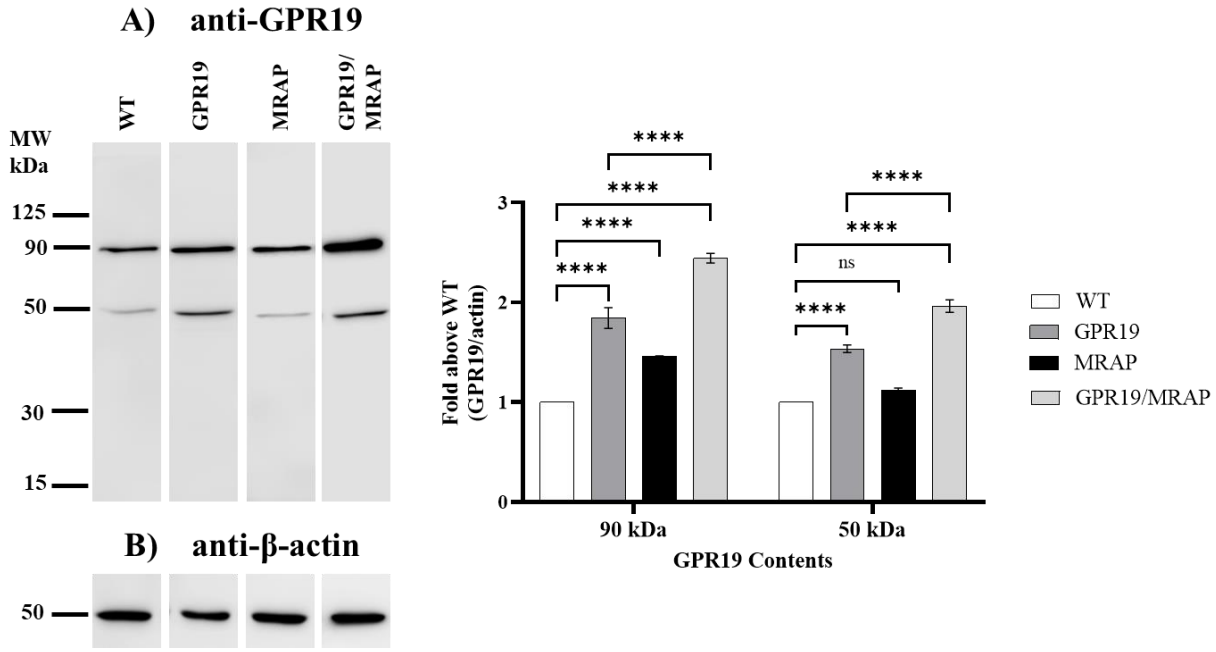

Fig. 3.19. Western blot analysis of GPR19 protein content in the wild-type cell line HEK-293 and the transfected cells with GPR19, MRAP and GPR19/MRAP. A) The four cells lysate are treated with rabbit polyclonal anti-GPR19 (A97504, antibodies) and two bands of ~ 90 kDa, and ~ 50 kDa are detected. B) Rabbit monoclonal anti-β-actin (# 4970, Cell Signalling). C) The GPR19 protein content is normalised to β-actin protein content, and fold above wild type GPR19 protein content is calculated, then statistically significant is evaluated using 2-way ANOVA with Tukey's multiple comparisons test. The 90 kDa GPR19 protein band is significantly increased in the three transformed cell lines in comparison to the wild type, while the 50 kDa GPR19 band increased in the cell lines that are transformed with GPR19 gene but not the cell line that is transformed with MRAP gene. Data represents three independent experiments and is shown as mean ± SEM. Results were considered statistically significant if the p-value was < 0.05. ns: not significant, **** $p > 0.0001$.

Fig. 3.20. The four cell lysates are treated with mouse monoclonal anti-HA Tag (A85278, antibodies). The HA-tagged MRAP, as expected, is only detected in the cell line that carries the MRAP pcDNA5 plasmid, the MRAP and GPR19/MRAP cell lines.

3.5. Discussion

The use of the Flp In™ system in the HEK-293 cell line allowed the generation of stable cell lines that express the gene(s) of interest efficiently and in a short period of time. The HEK-293 cell line was chosen since it expresses several types of GPCR receptors, including GPR19, that belong to different families, which makes it an attractive environment to express any GPCR (Atwood et al., 2011; Thomas & Smart, 2005), especially if post-translation modifications are critical for GPCR function (Markovic & Challiss, 2009). Moreover, various types of GPCR signalling-related gene products such as the G proteins α, β, and γ, and their targets and downstream effectors, as well as the proteins that regulate GPCR signalling, are expressed in this cell line (Atwood et al., 2011). Furthermore, HEK-293 is suitable for both transient transfection and stable cell line selection. For those features, the HEK293 was chosen as the cellular model to express the receptor GPR19 and determine if N-POMC is its natural ligand and to study its down-stream signalling.

Successfully, three cellular models that overexpress rGPR19, mMRAP and rGPR19/mMRAP genes were developed, which provided tools to investigate and confirm our hypothesis. Atwood et al. (2011) reported that HEK-293 expresses statistically significant levels of GPR19 mRNA, and Roy et al. (2007) reported that this cell line does not express the MRAP gene. The mRNA expression of the GPR19 and MRAP in the HEK-293 has been studied here using RT-PCR. The reported results here concur with these findings as we successfully amplified the hGPR19 gene in HEK-293 cells using RT-PCR, and the lack of the hMRAP gene was confirmed. Furthermore, the gene expression of the inserted rGPR19 and mMRAP in the three cell lines was also confirmed by RT-PCR. Therefore, any changes in the response of those cell lines in comparison to

the wild-type cell line in the subsequent experiments will be linked to the overexpression of the GPR19 and/or the expression of MRAP.

The subcellular distribution patterns have become an essential component of GPCR characterisation as these might have multiple regulatory consequences. For signal transduction to be initiated by a GPCR, it must be present at the cell surface. This prerequisite provides a mechanism for regulation. Indeed, dysregulation of this process of control means if a GPCR does not reach the cell surface and/or is down-regulated incorrectly, this can lead to aberrant cell signalling and potentially lead to disorders and diseases such as familial glucocorticoid deficiency (FGD). FGD is a disorder that causes ACTH resistance and severe glucocorticoid deficiency that is reported to be caused by either mutation of the ACTH receptor, the melanocortin receptor 2 (MC2R), and/or mutations in the accessory protein MRAP that is required for ACTH signalling (Sebag & Hinkle, 2007).

In this study, to confirm that the inserted rGPR19 and mMRAP genes are translated to protein and that protein is localised in its expected cellular compartments, which is the cell membrane, the GPR19 and MRAP protein distribution in the four cell lines was detected by ICC using non-permeabilised and permeabilised conditions. The cell membrane localisation of GPR19 has been reported in different cell lines by Bresnick et al. (2003), Roy et al. (2011) and Stelcer et al. (2020). The immunofluorescence staining images of the wild-type cell line revealed that GPR19 protein is mainly accumulated inside the cell with little staining detected on the cell membrane. The same is observed in the cell line that over-expresses GPR19, where the images show intense staining of the GPR19 inside the cells, which confirms the over-expression of the receptor inside the cell, but much of it does not localise to the cell membrane. Metherell et al. (2005) reported similar results when they studied the expression of the MC2R receptor. They found that

expression of the MC2R receptor in CHO-K1 cells leads to its accumulation inside the cells, while expression in the Y6 cell line leads to its localisation to the plasma membrane (Metherell et al., 2005). Then, they found that the expression of MRAP increased the co-localisation of both MC2R and MRAP in the plasma membrane, and it is inactive when it is expressed in cells that lack MRAP (Sebag & Hinkle, 2007). This finding highlighted that it is important to study the cellular distribution of the receptor after expressing it in a cellular model, as failure in receptor translocation to the cell surface due to the lack of the accessory protein or the translocation machinery in the used cellular model may generate a misleading result.

It has been reported by Sebag and Hinkle (2007) that MRAP is a transmembrane protein with an antiparallel dimeric structure. The ICC images confirm that the inserted mMRAP gene is expressed and translocated correctly to its expected cellular compartment. Interestingly, when the MRAP is expressed in the HEK-293 cell line, we notice a higher GPR19 staining signal on the cell surface. This increase in GPR19 translocation to the cell membrane suggested that MRAP plays a role in this process. The process of GPCR trafficking from the endoplasmic reticulum to the cell membrane is a complicated process that involves hundreds of proteins and enzymes, and much more to be discovered (Achour et al., 2008; Magalhaes et al., 2012; Milligan, 2009; Thompson et al., 2014).

The western blot shows that GPR19 migrates as two bands of ~90 kDa and ~50 kDa. Where the smallest band corresponds to the predicted molecular weight of human and transfected rGPR19, while the high molecular weight band may result from dimerisation of either homodimer and/or heterodimer with other GPCR or with other protein that is responsible for GPR19 translocation to the cell membrane. Although it is difficult to study the cellular distribution of those two bands separately, it might be

possible that the higher molecular weight form of the GPR19 (~90 kDa) is the form that trafficked to the cell membrane using translocation machinery that is available in the HEK-293 cell line which is an interesting research area to be investigated.

While the smaller size GPR19, the 50 kDa form, is accumulated inside the cell. This translocation machinery can support the translocation of the low 90 kDa GPR19 level in the WT cell line, but it is insufficient to support the translocation of the high level of the 90 kDa GPR19 in the over-expressed GPR19 cell line. The significant increase of the 90 kDa bands in the cell line that over-expressed GPR19 could explain the increase of the signal intensity of the GPR19 detection in the cell membrane in comparison to the WT cell line using the ICC technique in this cell line. Moreover, we can notice that the cell lines that express MRAP show an increase in the GPR19 high molecular weight band but not the smaller one. This can be explained as MRAP does not increase the expression of the GPR19 protein in the cells, but it plays a role in increasing the form of GPR19 that can be translocated to the cell surface. This finding is in accordance with the ICC results, where the GPR19 staining in the cell membrane increased in this cell line in comparison to the WT cell line, while the GPR19 staining inside the cells did not increase.

Several studies have recognised that GPCRs interact with other proteins that have roles in receptor biosynthesis, cellular distribution, trafficking, signalling, desensitisation, internalisation, and degradation. These include other GPCRs, GPCR kinases (GRKs), arrestins, receptor activity modifying proteins (RAMPs), and G protein-coupled receptor-associated sorting protein (GPRASP) (Böhme & Beck-Sickinger, 2009; Brady & Limbird, 2002). Moreover, it has been reported that GPCR can exist as a monomer, a dimer of the same receptor (homodimer) or with another receptor (heterodimer) or even in a higher-order oligomer (Gurevich & Gurevich, 2018; Milligan, 2001; Milligan et al., 2019). Class A GPCRs were believed to function as monomers.

Recent data published by Kasai et al. (2018) and Tabor et al. (2016) suggested that the dopamine D2 receptor, a class A GPCR, exists in a dynamic equilibrium between monomer and homodimer near the physiological receptor expression levels and agonist addition increased the dimer fraction of the receptor. This suggests that the homodimer's formation of the GPCR may play some important roles in receptor-ligand binding, signalling and receptor trafficking.

A recent study performed by Li et al. (2021) reported that GPR19 dimerised with MC3R that is not expressed in the HEK-293 cell line (Atwood et al., 2011). It is possible that GPR19 is traffic as a dimer with another GPCR that is expressed in the HEK-293 cell line, as it has been hypothesised that GPCR dimer might promote other translocation (Achour et al., 2008). This requires further investigation beyond the scope of this study. Furthermore, it has been reported that the protein sequence of GPR19 had significant sequence similarity with both the dopamine D2 receptor family and the neuropeptide Y receptors (O'Dowd et al., 1996), where the movement of those receptors from the cytoplasm to the plasma membrane can be regulated by agonist activation (Achour et al., 2008). Holtbäck et al. (1999) reported that treatment of cells with neuropeptide Y leads to the increased translocation of the α-adrenergic receptors to the cell membrane. GPR19 translocation to the cell membrane is often likely to be regulated by such a mechanism.

A key question is whether MRAP and GPR19 form a complex. This question will be answered in the next chapter, where the co-localisation and immunoprecipitation of those two proteins will be studied by ICC and co-immunoprecipitation. This will add to our understanding of how GPR19 and MRAP interact together.

Chapter 4: Characterisation of MRAP as a GPR19 Accessory Protein

4.1. Introduction

4.1.1. Detection of Protein-Protein Interactions

Understanding Protein-protein interaction is one of the major objectives of cell biology. Proteins dynamically interact with other cellular components to fulfil their diverse cellular roles (Berggård et al., 2007; Liddington, 2004). The function of unknown proteins can be predicted based on their interaction with other protein(s) of known function (Liddington, 2004). Moreover, identifying a protein-protein complex is an important step in identifying the signal transduction pathway of this complex (Rao et al., 2014). Over the years, various methods have been developed to study protein-protein interactions and among the widely used methods are the study of the cellular co-localisation of the proteins of interest and whether they form a complex with other proteins by co-immunoprecipitation (Co-IP) (Berggård et al., 2007; Rao et al., 2014).

4.1.2. The Receptor GPR19

GPR19 is a membrane receptor that features a hydrophobic core of 7 transmembrane-spanning α-helices, which is a characteristic of all G protein-coupled receptors (GPCRs). The GPR19 receptor is classified, based on sequence alignments of the transmembrane core, as a member of the GPCR family A that includes the rhodopsin, adrenergic and dopaminergic receptors, and receptors for other small organic ligands (Hoffmeister-Ullerich et al., 2004). GPCRs activate intracellular transducer G proteins that allow the transduction of signal information to classes of ion channels and enzymes that alter the rate of synthesis or degradation of intracellular second messengers (that will be discussed in Chapter 6).

Furthermore, a range of other proteins, such as RAMPs and MRAP (Achour et al., 2008), have been identified to interact with GPCRs to determine their cellular distribution and to regulate the trafficking of GPCRs within the cell. It has also been recognised that GPCRs can exist as homo- or hetero-dimers or as oligomers (Bouvier, 2001; Milligan, 2009; Sleno & Hébert, 2018; Terrillon & Bouvier, 2004). For signal transduction to be initiated by a GPCR, it must be present at the cell surface. This prerequisite provides a mechanism for regulation. Indeed, dysregulation of the process that controls if a GPCR reaches the cell surface and if it internalises or is down-regulated properly can lead to abnormal cell signalling and potentially lead to disorders and diseases such as adrenal insufficiency and congenital hypothyroidism caused by mutations in the MC2R and thyrotropin receptor genes; respectively (Marti-Solano, 2023; Ulloa-Aguirre et al., 2022).

The study of both the expression pattern and the cellular distribution of a given receptor can be helpful in assigning its specific function and identifying its endogenous ligand. The expression pattern of GPR19 has been studied on the mRNA level and shows that it is predominantly expressed in human and mouse brain and testis and to a lesser extent in liver, adrenal, heart, and kidney (Hoffmeister-Ullerich et al., 2004; O'Dowd et al., 1996).

The cell membrane localisation of the GPR19 receptor in the MCF-7 (human breast tumour cell line) and MDA-MB-231 (breast cancer cell line) cell lines had been confirmed after transfection of the cells with GPR19-V5 plasmid (Rao & Herr, 2017). To our knowledge, the published reports with the aim to identify the natural ligand of GPR19 and its signalling pathway(s) (Hossain et al., 2016; Kastner et al., 2012; Martin et al., 2015; Rao & Herr, 2017), the cellular trafficking of GPR19 to the cell membrane after

over-expression in the cellular model used and whether if it requires an accessory protein to be translocated to the cell membrane has not been studied before.

4.1.3. The Accessory Protein MRAP

GPCR trafficking from the endoplasmic reticulum to the cell membrane is tightly regulated by a variety of interacting proteins, and many studies have reported the different mechanisms that GPCRs use for trafficking. Some receptors can form a dimer, either a homodimer or heterodimer or an oligomer with other receptors and proteins throughout the trafficking process to the cell surface (Kunselman et al., 2021; Sleno & Hébert, 2018; Weinberg & Puthenveedu, 2019). While some GPCRs require a specific accessory protein for their trafficking and receptor response to its ligand, as in the case of the ACTH receptor (MC2R).

Metherell et al. (2005) found that expression of the MC2R gene in CHO-K1 cells leads to the accumulation of the protein within the cells, and it is not translocated to the plasma membrane. In contrast, expression in the Y6 cell line demonstrated localisation into the plasma membrane and forming a functional signal-transducing receptor. This finding suggests that there is a factor that is expressed in the Y6 cells but not in the CHO-K1 cells that is responsible for the translocation of MC2R from the endoplasmic reticulum to the cell membrane. They found that MRAP, a small transmembrane protein, is that factor, and it is required not only for the trafficking of MC2R to the cell membrane but also for signal transduction. Furthermore, mutations in either MC2R or MRAP result in the autosomal recessive disorder familial glucocorticoid deficiency type 2 (Metherell et al., 2005). This study highlighted that over-expression of a GPCR in a cellular model is not always enough to study its ligand binding or signalling pathway without taking into consideration studying its cellular distribution as failure in receptor translocation to the

cell surface due to the lack of trafficking proteins in the cellular model may generate a misleading result.

MRAP is expressed as two homologues, MRAP1 and MRAP2, where MRAP2 has 39% amino acid identity to MRAP1 in the N-terminal and transmembrane domains (Chan et al., 2009). The human MRAP1 gene consists of six exons where either exon 5 or exon 6 is alternatively spliced to encode the isoforms MRAP1-α or MRAP1-β (Jackson et al., 2015). MRAP2 is primarily expressed in the human brain and the adrenal gland (Chan et al., 2009), whereas MRAP1 is expressed in more varied tissues such as the adrenal cortex, testis, breast, thyroid, lymph node, ovary, and fat (Metherell et al., 2005). MRAP has a unique topology in the cell membrane as it forms an antiparallel dimer (Sebag & Hinkle, 2007). Chan et al. (2009) found that both MRAP homologues can modulate the signalling of all 5 melanocortin receptors (MCRs) and can form a homodimer, e.g., MRAP/MRAP or MRAP2/MRAP2, and a heterodimer, e.g., MRAP/MRAP2.

As mentioned in Chapter 3, we found that GPR19 over-expressed in HEK-293 cells remains inside the cell and does not localise to the cell membrane. In contrast, we noticed an increase of GPR19 staining in the cell membrane in the cell lines that are expressing MRAP. This raises the possibility that GPR19, like the MC2R, might need the accessory protein MRAP to correctly traffic to the cell surface. In this chapter, we will study the co-localisation of GPR19 with MRAP using the ICC technique. Moreover, we will study if GPR19 and MRAP form a complex using reciprocal co-immunoprecipitation.

4.2. Aims

1) To study if GPR19 and MRAP co-localise in the cell membrane and inside the cell using confocal microscopy.
2) To identify if GPR19 and MRAP form a complex using reciprocal co-immunoprecipitation.

4.3. Methods

4.3.1. Co-localisation of GPR19 and MRAP Using ICC

The same slides that were prepared in Chapter 3, section 3.3.7.1, to study the cellular distribution of GPR19 and MRAP were used to study the localisation between GPR19 and MRAP in the transfected cell lines that express it. The slides were imaged using a Nikon A1R Confocal Microscope with an X60 lens, and the images were merged to investigate the co-localisation.

4.3.2. Reciprocal Co-IP

The GPR19/MRAP cell line was used to confirm if these two proteins form a complex, while the WT cell line was used as a negative control. The cells were grown to 80-90% confluence in 6 well plates. Then different samples were prepared as follows (Fig. 4.1.):

a) The 6-well plate was placed on ice, and the cells were washed twice with ice-cold 1X PBS and then scraped into 0.5 ml/well 1 XPBS; two wells were combined as one sample and transferred to an ice-cold 1.5 ml microcentrifuge tube. The samples were centrifuged at 100 g for 5 min at 4°C. The pellet was resuspended in either 300 µl of 1:100 mixture of Halt Protease and Phosphatase inhibitor Cocktail and RIPA buffer or 1% (w/v) n-dodecyl-β-D-maltoside (#89902, Thermo Scientific) prepared in 1X PBS and incubated in ice for 30 min.

b) The cells were prepared as non-treated or treated with 1 nM N-$POMC_{1-28}$ for 10 min in the 5% (v/v) CO_2 and 37°C incubator. After 10 min, the cells were washed twice with 1X PBS, then 400 µl of disuccinimidyl tartrate (DST) crosslinker (#20589, Thermo Fisher) was added to each well with a final concentration of 5 mM and incubated for 30 min at RT. The

crosslinking reaction was quenched by adding Tris (pH 7.5) with a final concentration of 20 mM and incubated in RT for 15 min. The cells were scraped and transferred to an ice-cold 1.5 ml microcentrifuge tube, where two wells were combined as one sample. The samples were centrifuged at 100 g for 5 min at 4°C. The pellet was washed twice with 1 ml 1XPBS and then resuspended in 300 µl of 1:100 mixture of Halt Protease and Phosphatase inhibitor Cocktail and RIPA buffer and incubated on ice for 30 min.

c) The cells were treated with 1 nM N-POMC$_{1-28}$ for 10 min in the 5% (v/v) CO_2 and 37°C incubator. After 10 min, the cells were washed twice with 1X PBS, then 400 µl of DST crosslinker (#20589, Thermo Fisher) was added to each well with a final concentration of 5 mM and incubated for 30 min at RT. The crosslinking reaction was quenched by adding Tris (pH 7.5) with a final concentration of 20 mM and incubated at RT for 15 min. The cells were scraped off the dish and transferred to an ice-cold 1.5 ml microcentrifuge tube, where two wells were combined as one sample. The samples were centrifuged at 100 g for 5 min at 4°C. The pellet was washed twice with 1 ml 1X PBS and then resuspended in 300 µl of 1:100 mixture of Halt Protease and Phosphatase inhibitor Cocktail and RIPA buffer and incubated in ice for 30 min.

The samples prepared were then centrifuged for 15 min at 16,000 g and 4°C. The supernatant was transferred to a clean 1.5 ml microcentrifuge tube. To supernatants that were prepared by the protocol in steps a and c, 5 µg of primary antibody (Table 4.1) was added and kept at 4°C on a rotary wheel overnight. On the next day, 50 µl of protein G-agarose resin (P7700, Sigma) was prepared as described by the manufacturer and was added to the supernatant and kept at 4°C on the rotary wheel for 2 hrs. The samples were

then centrifuged at 2000 g for 1 min at 4°C. The supernatant was discarded while the pellet was washed three times with the lysis buffer and labelled as an *eluted-IP* pellet. To the eluted IP pellet and the samples prepared in step b, 50 µl of non-reduced (Appendix A.8) or reduced 2X SDS sample buffer (Appendix A.9) were added. The samples were analysed by western blotting following the protocol in Chapter 2, section 2.16. The rec-protein G-peroxidase conjugate (10-1223, Thermo Fisher) was used as a secondary antibody with 1:4000 dilution in 5% (w/v) skimmed milk in 1X TBST.

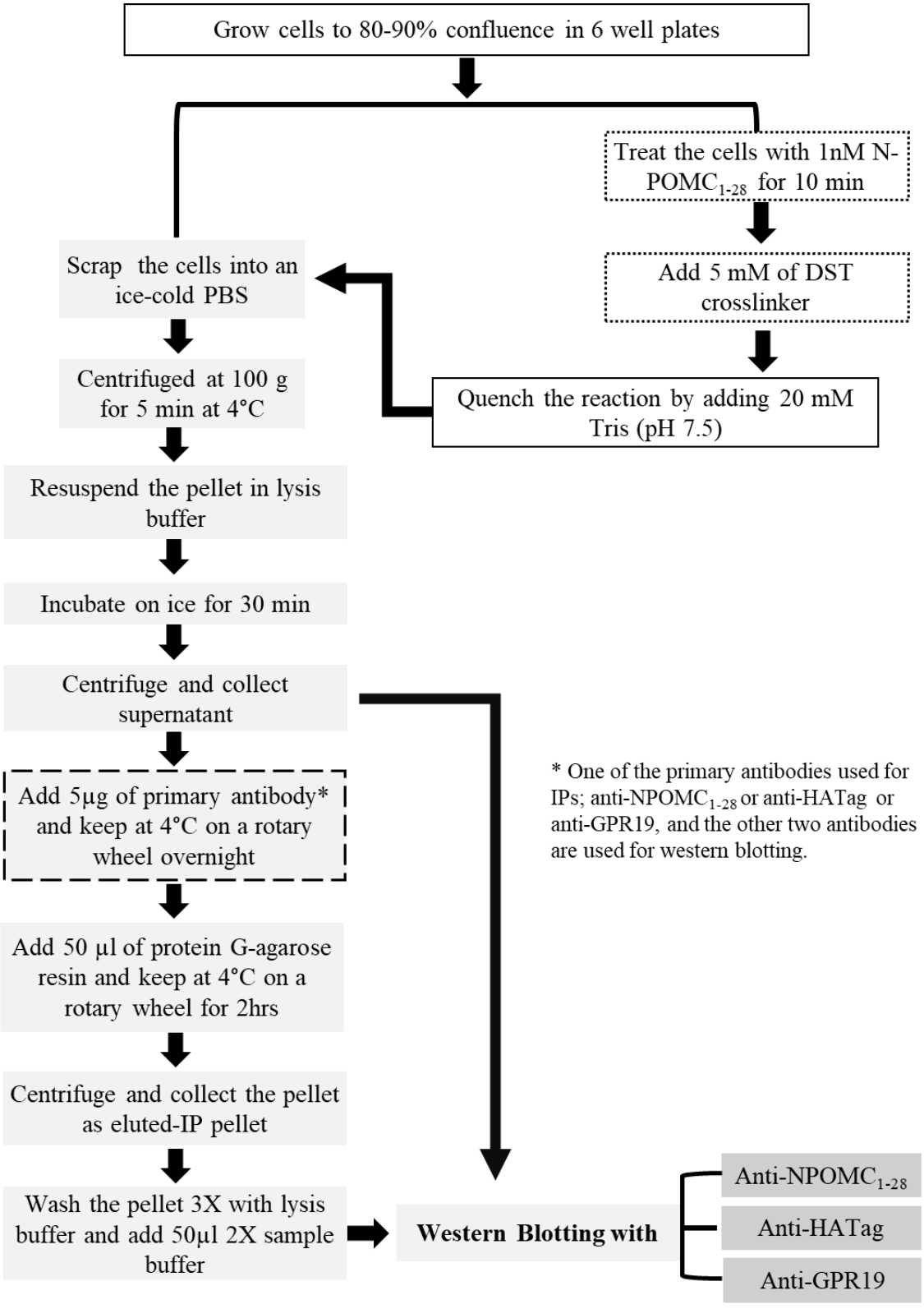

Fig. 4.1. Reciprocal co-immunoprecipitation (Co-IP) sample preparation protocol.

Table 4.1. Primary antibodies are used for IPs and western blotting techniques.

Antibodies used for IP and WB				
No.	**Antibody**	**Catalogue Number**	**Immunogen and Epitope**	**Dilution Factor for WB**
1	Mouse monoclonal anti-HA-Tag	A85278, antibodies	YPYDVPDYA conjugated to KLH	1:1000 5% (w/v) skimmed milk in 1X TBST
2	Rabbit Polyclonal anti-GPR19	A97504, antibodies	Synthetic peptide derived from human GPR19 (aa. 361-410)	1:2000 5% (w/v) skimmed milk in 1X TBST
3	Rabbit anti-N-$POMC_{1-28}$	Prepared in our lab	Antibody was raised by immunising rabbits with purified bovine N-$POMC_{1-49,}$ and antibodies to N-$POMC_{1-28}$ were affinity purified using solid-phase 1-28	1:1000 5% (w/v) skimmed milk in 1X TBST

4.4. Results

4.4.1. Co-localisation of GPR19 and MRAP

As shown in the previous chapter, the protein expression of both GPR19 and MRAP in the cell lines that were transfected with MRAP and GPR19/MRAP genes was confirmed. Moreover, the ICC results of the wild-type and the over-expressed GPR19 cell lines showed that most of the GPR19 protein was retained within the cell, while the images of the cell lines that express MRAP show more GPR19 protein staining localised to the cell membrane. This raised the question of whether those two proteins co-localise in the cell membrane or inside the cells.

The ICC images show that both GPR19 and MRAP co-localised in the cell membrane (Fig. 4.2.) in the non-permeabilised cells. Moreover, the images show that both proteins are also co-localised inside the cells (Fig. 4.3.) in the permeabilised cells with 0.2% (v/v) Tween-20. Because GPR19 and MRAP co-localised, we tested whether they form a complex by reciprocal co-immunoprecipitation.

4.4.2. Reciprocal Co-IP

As shown in Chapter 3, GPR19 migrates as two bands of 90 kDa and 50 kDa, while HA-Tagged MRAP migrates as one band of 15 kDa when resolved by SDS-PAGE. The reciprocal co-immunoprecipitation experiment was performed using:

1) Two lysis buffers: RIPA or 1% (w/v) n-dodecyl-β-D-maltoside, as the lysis buffer may lead to the dissociation of the complex during sample preparation.

2) 2) Antibodies to detect GPR19, MRAP, and N-POMC$_{1-28}$. One antibody is used for the immunoprecipitation step, and the other two are used for detection with western blotting.

3) With and without cross-linker DST.

4) Two cell lines were used: the GPR19/MRAP cell line was used to investigate the binding complex between GPR19 and MRAP, while the WT cell line was used as a negative control.

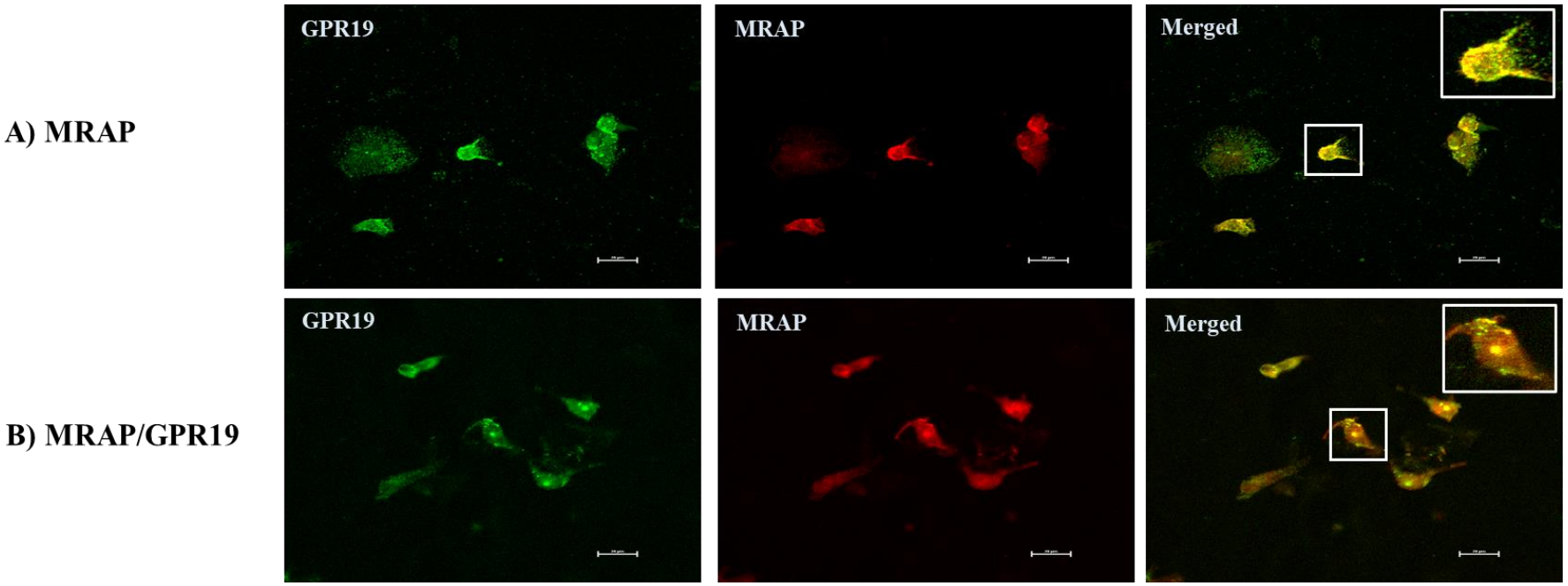

Fig. 4.2. Co-localisation of GPR19 with MRAP proteins in the non-permeabilised stable cell lines that express MRAP (A) and GPR19/MRAP (B). GPR19 was stained with Alexa-488, and MRAP was stained with Alexa-546. Images reveal that GPR19 and MRAP proteins were co-localised in the cell membrane, indicating that those two proteins form a complex that may have potential biological activity. Images taken with a Nikon A1 Plus confocal microscope using NIS Elements software. Scale bar = 20 µm.

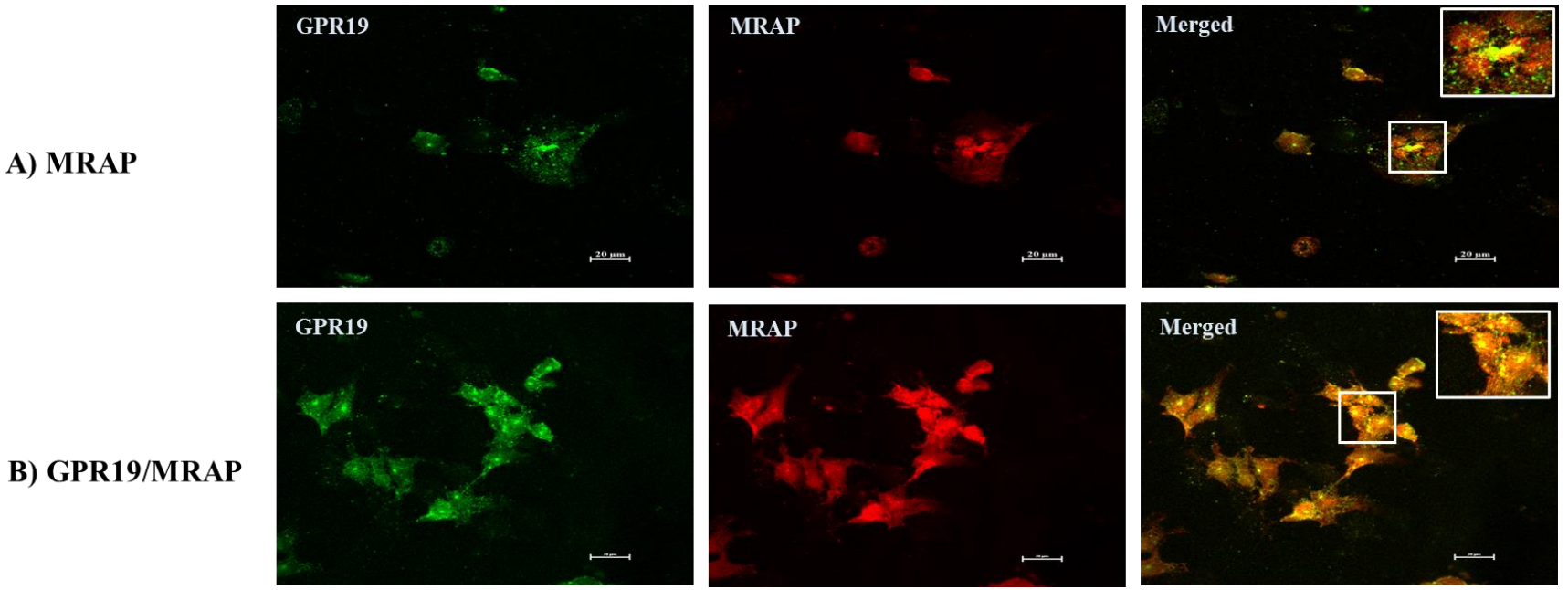

Fig. 4.3. Co-localisation of GPR19 with MRAP proteins in permeabilised stable cell lines that express MRAP (A) and GPR19/MRAP (B) with 0.2% (v/v) Tween-20. GPR19 was stained with Alexa-488, and MRAP was stained with Alexa-546. Images reveal that GPR19 and MRAP proteins were co-localised inside the cells, indicating that two proteins form a complex that may have potential biological activity. Images taken with a Nikon A1 Plus confocal microscope using NIS Elements software. Scale bar = 20 µm.

The first reciprocal co-immunoprecipitation experiment was performed with the total cell lysate prepared by RIPA lysis buffer. Then, the mouse anti-HA Tag antibody (to target HA-tagged MRAP) was added to the cell lysate, and the complex was precipitated by protein G-agarose resin, eluted, and detected using rabbit anti-GPR19 antibody. We found that GPR19 did not precipitate (Fig.4.4. A), and a band at 30 kDa was developed. We tested whether this band was cross-reactivity of the protein G-agarose resin with the antibody used, so a small amount of the protein G-agarose resin was run in SDS-PAGE after adding appropriate amounts of 2X SDS sample buffer alongside total cell lysate of the GPR19/MRAP cell line and detected using rabbit anti-GPR19 and mouse anti-HA Tag antibodies. We found that the protein G-agarose resin can interact with both antibodies (Fig. 4.4 B and C), where it gives a distinctive band at ~30 kDa, which is in between the GPR19 band (50 kDa) and HA-Tagged MRAP band (15 kDa) Using the secondary antibody alone showed no binding (data not shown). We hypothesised that RIPA buffer might disrupt the association between GPR19 and MRAP, and using a milder lysis buffer, 1% (w/v) n-dodecyl-β-ᴅ-maltoside prepared in 1X PBS, could give different results, but the results were identical (Fig.4.4. D). The immunoprecipitation alone does not show any complex between GPR19 and MRAP, and this could be because the lysis buffer leads to the dissociation of MRAP from GPR19.

After that, we decided to use the DST cross-linker before lysing the cells. DST is a homo-bifunctional crosslinker with a short spacer arm (4 Å in length). It contains amine-reactive N-hydroxysuccinimide (NHS) ester groups and is lipophilic, which makes it useful for intracellular and intramembrane protein conjugation. The cross-linking reaction occurs as NHS esters react with primary amino groups ($-NH_2$) present on the side chain of lysine (K) residues and the N-terminus of the polypeptides.

Here, two sets of experiments were conducted: cells that were treated with the DST cross-linker and cells that were treated first with N-POMC$_{1-28}$ for 10 min, then the cross-linker DST was added to the cells. After that, the cells were lysed with RIPA buffer and prepared with non-reducing and reducing 2X sample buffer. The samples were analysed by western blotting using an anti-GPR19 antibody, anti-HA-TAG to detect MRAP and an anti-N-POMC$_{1-28}$ antibody. The results of the non-treated cells are like those of the treated cells; therefore, the images will not be shown here. The blotting reveals that two GPR19 bands (Fig. 4.5 A) can be detected in the non-reduced and reduced sample buffer. In both conditions, the 15 kDa HA-Tagged MRAP were detected (Fig. 4.5 B), while no band was detected after using the anti-N-POMC antibody (Fig. 4.5 C). We expect to detect a band on the western blot that was different from the GPR19 and MRAP bands, including the receptor, the accessory protein, and the ligand. So, we decided to use both the DST cross-linker, co-immunoprecipitation, and western blot after treating the cells with N-POMC$_{1-28}$.

The cells were treated with N-POMC$_{1-28}$, DST cross-linker and lysed with RIPA buffer and then immunoprecipitation was performed using one of the three antibodies separately and followed by preparation of the sample with either non-reduced or reduced 2X sample buffer and the eluted proteins were detected with the other two antibodies. First, the samples were analysed using only the secondary antibody, rec-protein G-peroxidase conjugate, to confirm that there was no cross-reactivity between the secondary antibody and the antibody used for immunoprecipitation. The blotting (Fig. 4.6 A) reveals a black band between the 70 and 50 kDa ladder bands with the anti-GPR19 and anti-N-POMC$_{1-28}$ antibodies in the non-reduced samples only, which suggests cross reactivity.

The co-immunoprecipitation with anti-HA-Tag and anti-N-POMC$_{1-28}$ antibodies specifically co-precipitated the two GPR19 bands size in the reduced condition and the

~90 kDa in the non-reduced condition (Fig. 4.6 B). In the reciprocal immunoprecipitation experiment with anti-GPR19 and anti-N-POMC$_{1-28}$, the MRAP band (15 kDa) co-precipitates with the anti-GPR19 in both the reduced and non-reduced samples (Fig. 4.6 C). Interestingly, a ~50 kDa band co-precipitated in the reduced sample with both the anti-GPR19 and anti-N-POMC$_{1-28}$; this band was probably the GPR19 band. The cells were treated with 1 nM N-POMC$_{1-28}$ before the cross-linking step, and the HA-Tag and GPR19 co-immunoprecipitated samples with anti-N-POMC$_{1-28}$ antibody underwent a western blot. Interestingly, the ~50 kDa band can be detected in both reduced samples, which strongly suggests it to be the GPR19 band (Fig. 4.6 D). These findings strongly indicated that GPR19 (the receptor), MRAP (the accessory protein of GPR19) and N-POMC$_{1-28}$ (the ligand) are forming a complex.

The WT cell line was used as a negative control to confirm the above finding, as this cell line expresses GPR19 but not MRAP. The co-immunoprecipitation with anti-HA-Tag did not precipitate any band with anti-GPR19 and anti-N-POMC$_{1-28}$ (Fig. 4.7 A and C), and the reciprocal immunoprecipitation also gave no results (Fig. 4.7 B) confirming the specificity of the HA-Tag antibody. The co-immunoprecipitation with anti-N-POMC$_{1-28}$ specifically co-precipitated the 50 kDa GPR19 band in the reduced samples (Fig. 4.7 A). Interestingly, the same band was co-precipitated in the reciprocal immunoprecipitation with anti-GPR19 (Fig. 4.7 C). This finding confirms that N-POMC$_{1-28}$ binds to 50 kDa GPR19. The difference here is that the 90 kDa band was not co-precipitated with the anti-N-POMC$_{1-28}$ as in the cell line that expresses MRAP (Fig 4.6 B). That finding suggests that N-POMC$_{1-28}$ will not be able to bind to the higher molecular weight (90 kDa) form of GPR19 if MRAP is not expressed in the cell but is still able to bind to the smaller molecular weight (50 kDa) GPR19.

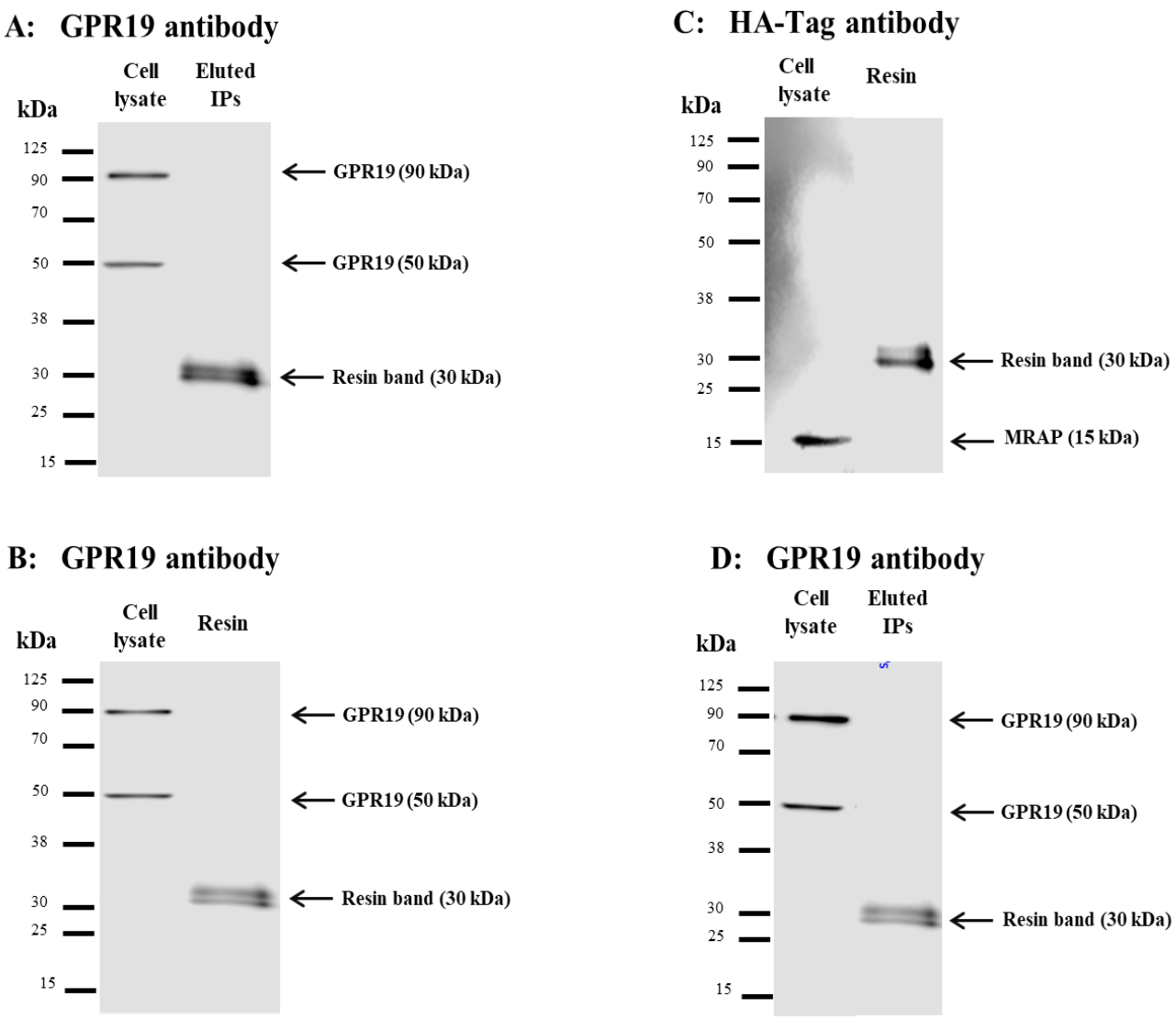
A: GPR19 antibody
Cell lysate
Eluted IPs
kDa
125
90
70
50
38
30
25
15
GPR19 (90 kDa)
GPR19 (50 kDa)
Resin band (30 kDa)
C: HA-Tag antibody
Cell lysate
Resin
kDa
125
90
70
50
38
30
25
15
Resin band (30 kDa)
MRAP (15 kDa)
B: GPR19 antibody
Cell lysate
Resin
kDa
125
90
70
50
38
30
25
15
GPR19 (90 kDa)
GPR19 (50 kDa)
Resin band (30 kDa)
D: GPR19 antibody
Cell lysate
Eluted IPs
kDa
125
90
70
50
38
30
25
15
GPR19 (90 kDa)
GPR19 (50 kDa)
Resin band (30 kDa)

Fig. 4.4. Co-immunoprecipitation of GPR19 and MRAP in the stably transfected cell line with GPR19/MRAP. The total GPR19/MRAP cell lysate was prepared by RIPA buffer. (A) After 30 min incubation with the lysis buffer, the samples were centrifuged, and to the supernatant, 5 µg of mouse anti-HA tag antibody (A85278, antibodies) was added and stored overnight at 4ºC. The next day, protein G-agarose resin was added to the supernatant, which was kept at 4°C for 2 hrs. The samples were then centrifuged, and the pellet was collected and resuspended in a proper volume of 2X SDS sample buffer containing 5% (v/v) β-mercaptoethanol. B and C) 50 µl of the resin was mixed with an equal amount of the reduced 2X SDS sample buffer and ran side-by-side with total cell lysate of the GPR19/MRAP cell line and detected using the anti-GPR19 (B) and anti-HA-Tagged (C) antibodies. The resin gives a distinctive band at ~30 kDa, which is in between the GPR19 band (50 kDa) and the HA-Tagged MRAP band (15 kDa). D) The total GPR19/MRAP cell lysate was prepared with 1% (w/v) n-dodecyl-β-ᴅ-maltoside prepared in 1X PBS following the sample preparation protocol as in A.

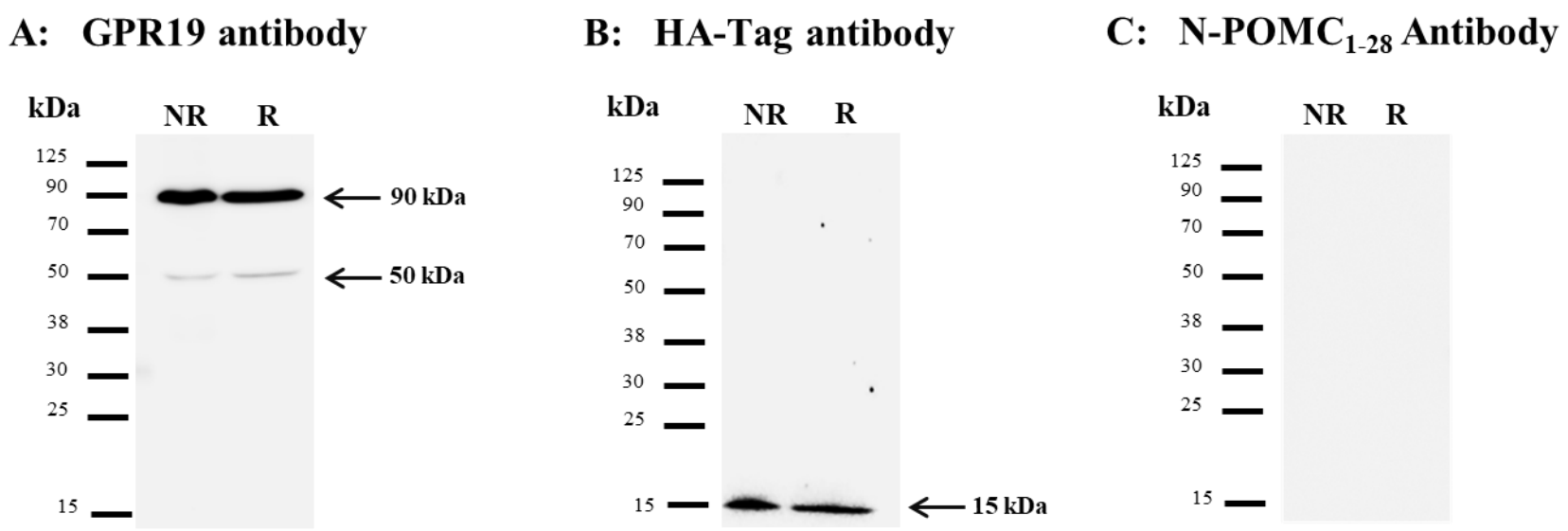

Fig. 4.5. Western blot of crosslinked GPR19 and MRAP in the stably transfected cell line with GPR19/MRAP. The GPR19/MRAP cells were treated with 1 nM N-POMC$_{1-28}$ for 10 min in the 5% (v/v) CO_2 and 37°C incubator. After 10 min, the cells were treated with disuccinimidyl tartrate (DST) crosslinker (#20589, Thermo Fisher) at a final concentration of 5 mM and incubated for 30 min at RT. The crosslinking reaction was quenched by adding Tris (pH 7.5) with a final concentration of 20 mM and incubated at RT for 15 min. The cells were scraped and transferred to an ice-cold 1.5 ml microcentrifuge tube and centrifuged at 100 g for 5 min at 4°C. The pellet was resuspended in 300 µl of 1:100 mixture of Halt Protease and Phosphatase inhibitor Cocktail and RIPA buffer and incubated on ice for 30 min. The samples were then centrifuged for 15 min at 16,000 g and 4°C. To the supernatant, 50 µl of non-reduced (NR) or reduced (R) 2X SDS sample buffer was added. The samples were analysed by western blotting using A) anti-GPR19 antibody, B) anti-HA-TAG to detect MRAP or C) anti-N-POMC$_{1-28}$ antibody.

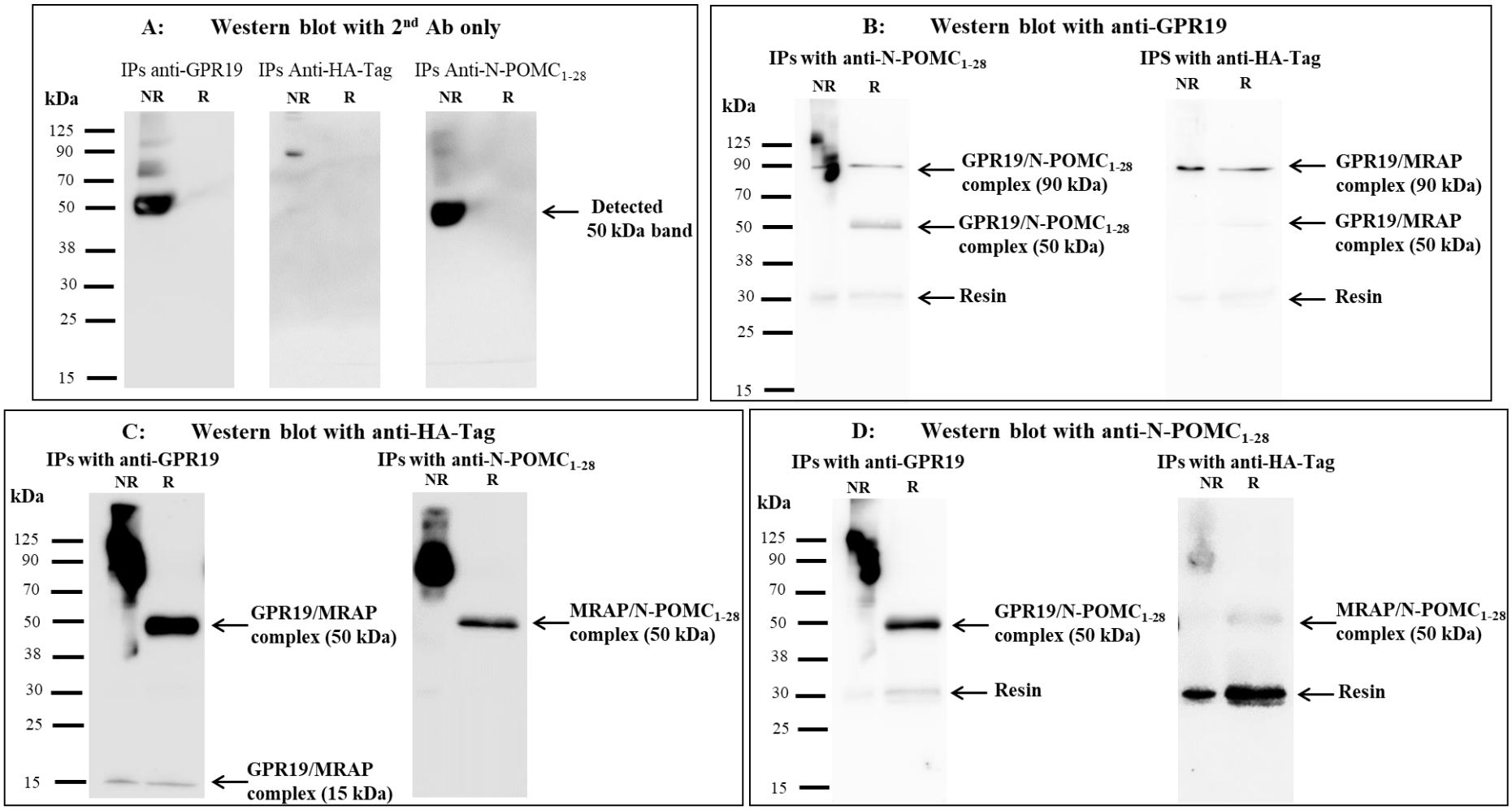
A: Western blot with 2nd Ab only
IPs anti-GPR19
IPs Anti-HA-Tag
IPs Anti-N-POMC1-28
NR R NR R NR R
kDa
125
90
70
50
38
30
25
15
Detected 50 kDa band
B: Western blot with anti-GPR19
IPs with anti-N-POMC1-28
IPS with anti-HA-Tag
NR R NR R
kDa
125
90
70
50
38
30
25
15
GPR19/N-POMC1-28 complex (90 kDa)
GPR19/N-POMC1-28 complex (50 kDa)
Resin
GPR19/MRAP complex (90 kDa)
GPR19/MRAP complex (50 kDa)
Resin
C: Western blot with anti-HA-Tag
IPs with anti-GPR19
IPs with anti-N-POMC1-28
NR R NR R
kDa
125
90
70
50
38
30
25
15
GPR19/MRAP complex (50 kDa)
GPR19/MRAP complex (15 kDa)
MRAP/N-POMC1-28 complex (50 kDa)
D: Western blot with anti-N-POMC1-28
IPs with anti-GPR19
IPs with anti-HA-Tag
NR R NR R
kDa
125
90
70
50
38
30
25
15
GPR19/N-POMC1-28 complex (50 kDa)
Resin
MRAP/N-POMC1-28 complex (50 kDa)
Resin

Fig. 4.6. Co-immunoprecipitation of GPR19 and MRAP in the stably transfected cell line with GPR19/MRAP. The GPR19/MRAP cells were treated with 1 nM N-POMC$_{1-28}$ for 10 min in the 5% (v/v) CO_2 and 37°C incubator. After 10 min, the cells were treated with disuccinimidyl tartrate (DST) crosslinker (#20589, Thermo Fisher) at a final concentration of 5 mM and incubated for 30 min at RT. The crosslinking reaction was quenched by adding Tris (pH 7.5) with a final concentration of 20 mM and incubated at RT for 15 min. The cells were scraped and transferred to an ice-cold 1.5 ml microcentrifuge tube and centrifuged at 100 g for 5 min at 4°C. The pellet was washed in 1X PBS and then resuspended in 300 µl of 1:100 mixture of Halt Protease and Phosphatase inhibitor Cocktail and RIPA buffer and incubated on ice for 30 min. The samples were then centrifuged for 15 min at 16,000 g and 4°C. To the supernatant, 50 µl of non-reduced or reduced 2X SDS sample buffer was added. A) The samples were analysed using only the secondary antibody, rec-protein G-peroxidase conjugate (10-1223, Thermo Fisher), to confirm that there was no cross-reactivity between the secondary antibody and the antibody that was used for immunoprecipitation that would give a false positive result. The blotting reveals a black band between the 70 and 50 kDa ladder bands with the anti-GPR19 and anti-N-POMC$_{1-28}$ antibodies in the non-reduced samples only. B) The samples were analysed using anti-GPR19. C) The samples were analysed using anti-HA-TAG to detect MRAP. D) The samples were analysed using anti-N-POMC$_{1-28}$.

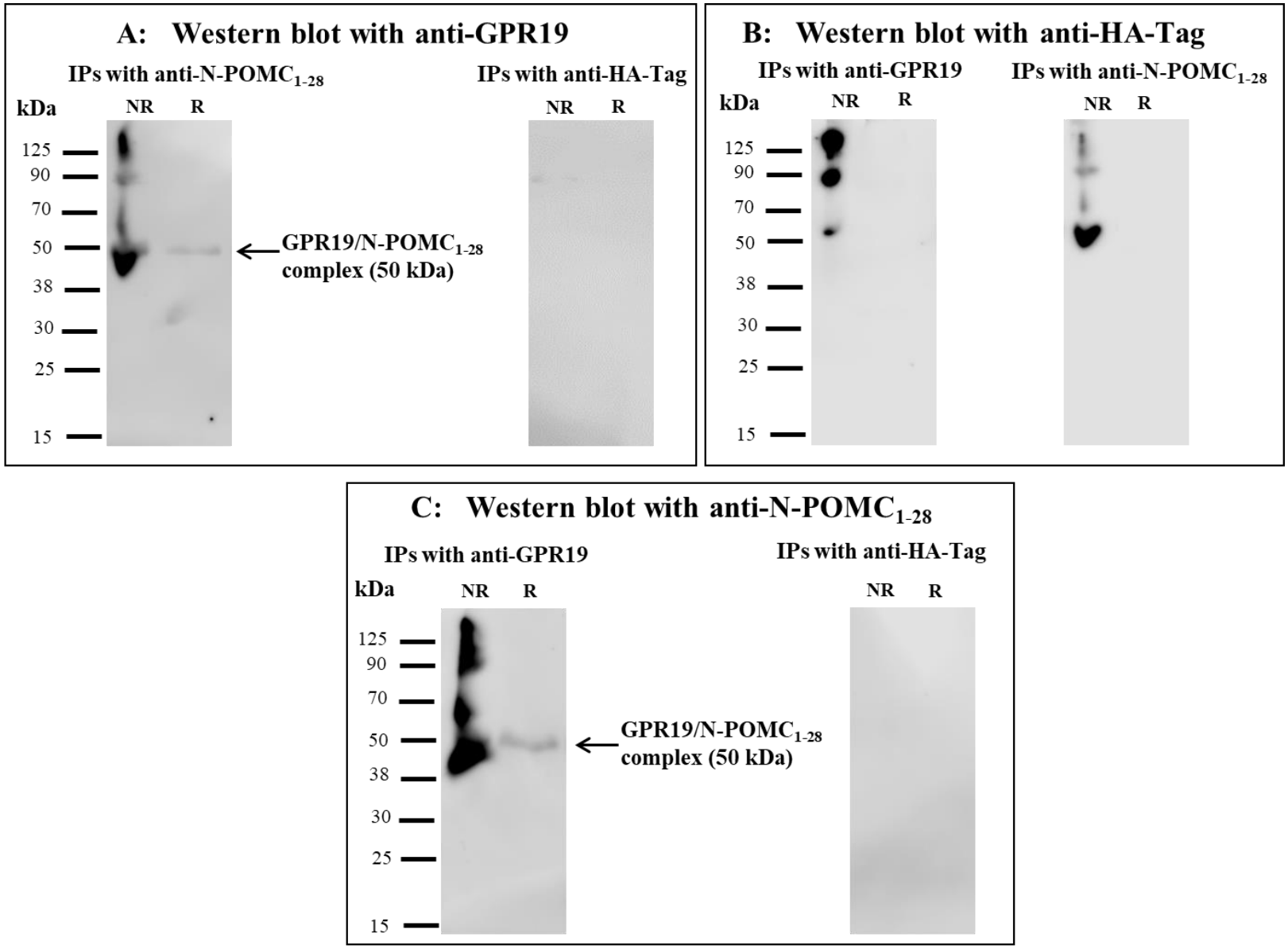
A: Western blot with anti-GPR19
IPs with anti-N-POMC1-28
IPs with anti-HA-Tag
kDa
NR R
NR R
125
90
70
50
38
30
25
15
GPR19/N-POMC1-28
complex (50 kDa)
B: Western blot with anti-HA-Tag
IPs with anti-GPR19
IPs with anti-N-POMC1-28
kDa
NR R
NR R
125
90
70
50
38
30
25
15
C: Western blot with anti-N-POMC1-28
IPs with anti-GPR19
IPs with anti-HA-Tag
kDa
NR R
NR R
125
90
70
50
38
30
25
15
GPR19/N-POMC1-28
complex (50 kDa)

Fig. 4.7. Co-immunoprecipitation of WT cell line. The WT cells were treated with 1 nM N-POMC$_{1-28}$ for 10 min in the 5% (v/v) CO_2 and 37°C incubator. After 10 min, the cells were washed with 1X PBS, then disuccinimidyl tartrate (DST) crosslinker (#20589, Thermo Fisher) was added with a final concentration of 5 mM and incubated for 30 min at RT. The crosslinking reaction was quenched by adding Tris (pH 7.5) with a final concentration of 20 mM and incubated in RT for 15 min. The cells were scraped and transferred to an ice-cold 1.5 ml microcentrifuge tube and centrifuged at 100 g for 5 min at 4°C. The pellet was washed 1X PBS and then resuspended in 300 µl of 1:100 mixture of Halt Protease and Phosphatase inhibitor Cocktail and RIPA buffer and incubated on ice for 30 min. The samples were then centrifuged for 15 min at 16,000 g and 4°C. To the supernatant, 50 µl of non-reduced or reduced 2X SDS sample buffer was added. A) The samples were analysed using anti-GPR19. B) The samples were analysed using anti-HA-TAG to detect MRAP. C) The samples were analysed using anti-N-POMC$_{1-28}$.

4.5. Discussion

The data shown in this chapter indicate that GPR19 and MRAP form a complex, as both are co-localised in the cell membrane and inside the cell. Moreover, the co-immunoprecipitation results show that the anti-GPR19 antibody can precipitate the MRAP band, while in the reciprocal experiment, we found that the anti-HA-Tagged MRAP can precipitate the two GPR19 bands.

MRAP was initially identified as an essential accessory protein for the translocation of the MC2R to the cell membrane and to increase the binding affinity of ACTH to MC2R (Metherell et al., 2005). The following studies reported that MRAP is expressed in two variants, MRAP1 and MRAP2, and is widely expressed in different human tissues (Fagerberg et al., 2014; Metherell et al., 2005) and in other species, including mice, rats, and zebrafish (Asai et al., 2013; Gorrigan et al., 2011; Sebag et al., 2013). Moreover, it is reported that MRAP is not specific to the MC2R and regulates both the expression and the response of the other melanocortin receptors, namely MC1R, MC3R, MC4R and MC5R (Chan et al., 2009). In addition, MRAP2 was found to regulate the signalling of other non-melanocortin GPCRs such as orexin receptor (OX1R), prokineticin receptor 1 (PKR-1) (Chaly et al., 2016; Rouault et al., 2017) and growth hormone secretagogue receptor-1a (GHSR-1a) (Srisai et al., 2017). Interestingly, MRAP does not always act as a positive regulator of those receptors where it is reported that expression of MRAP downregulates the surface expression of MC1R, MC4R, MC5R (Chan et al., 2009; Sebag et al., 2013), OX1R (Rouault et al., 2017), and PKR-1 (Chaly et al., 2016).

In the previous chapter, we showed that GPR19 staining in the cell membrane increased in the HEK-293 cell line that was stably transfected with MRAP. In this chapter, we tested whether it is likely that MRAP partners with GPR19 and whether

MRAP expression increased GPR19 expression in the cell membrane using co-localisation imaging and reciprocal co-immunoprecipitation.

Co-localisation may indicate that the two proteins in a cell are occupying the same structure, while in digital imaging, it means that two proteins signal within the same pixel in the image (Zinchuk et al., 2007). In confocal microscopy, the co-localisation of two fluorescent dyes in a sample is represented in the image by pixels containing both colour contributions. We wanted to test the hypothesis that MRAP could form a complex with GPR19 and act as a potential accessory protein to facilitate its translocation to the cell membrane in a similar mechanism as MRAP trafficking MC2R to the cell surface (Webb et al., 2009; Webb & Clark, 2010).

We investigated the subcellular localisation of MRAP using HEK-293 cells stably transfected with the mMRAP gene with a HA-Tag at the C terminus or with rGPR19 and the same mMRAP gene with a HA-Tag at the C terminus. To prevent the nonspecific signal bleed through, which will complicate the interpretation of the acquired image and can lead to false results, particularly in the studies of co-localisation and fluorescence quantification, the secondary antibodies used were labelled by fluorophores that had distinct fluorescence spectra. The secondary antibody used to detect GPR19 was conjugated to Alexa Fluor-488, which has an excitation max at 495 nm and an emission max of 519 nm, and the antibody to detect HA-Tagged MRAP was conjugated to Alexa Fluor-546, which has an excitation max at 556 nm and emission max at 573 nm. Moreover, DAPI has a broad emission curve that may overlap and bleed into other channels e.g., FITC (fluorescein isothiocyanate) and Alexa Fluor-488 (Swaim, 2010). In addition, there are reports about the photoconversion of DAPI to form green and red fluorescent products (Jež et al., 2013; Roberts, 2019) that consequently will overlap with the fluorescence emission of the other fluorescence dyes used and cause a false positive

result. For those reasons, we decided not to use DAPI in the slides that were prepared to study the co-localisation of GRP19 and MRAP.

The co-localisation images revealed that both GPR19 and MRAP proteins co-localised in the cell membrane (Fig 4.2) and inside the cell (Fig. 4.3). From this finding, the increase in the GPR19 cell surface expression in the cell line that expresses MRAP can be explained as MRAP being the required factor, not expressed in the HEK-293 cell line, needed to translocate GPR19 to the cell membrane; otherwise, it will accumulate inside the cell as in the case of the cell line that overexpresses GPR19 alone. These results provide sufficient evidence to suggest that GPR19 and MRAP are working together to perform cellular function, and such findings will help to predict their trafficking mechanism and their interaction with other signalling pathways that will alter the levels of the cellular second messengers such as cAMP and Ca^{+} (Roux & Cottrell, 2014).

Furthermore, to confirm that GPR19 and MRAP form a complex, we used the reciprocal co-immunoprecipitation (Co-IP) technique. This technique involves the detection of the protein complex by using one antibody for immunoprecipitation of the complex and a second antibody for immunoblot analysis of the co-precipitated complex. Co-IP is used in many studies to confirm the formation of a complex between two proteins, either a receptor and its accessory protein such as MC2R and MRAP (Metherell et al., 2005; Sebag & Hinkle, 2007), and the melanocortin receptors (MC1R, MC3R, MC4R and MC5R) and MRAP (Chan et al., 2009), or two receptors such as the receptors MC3R and MC4R with other GPCRs (Li et al., 2021).

In this report, we used this technique to provide direct evidence that GPR19 can form a complex with MRAP when both are co-expressed in the GPR19/MRAP cell line. Previously, we showed in Chapter 3 that GPR19 migrates as two bands of 90 kDa and 50 kDa. The smaller band is expected to be the functional form of the GPR19 receptor, and

the higher band could be a dimer with other GPCRs (will be discussed below). The HA-Tagged MRAP migrates as one band of 15 kDa. We found that using immunoprecipitation alone is not enough to precipitate a complex, either using the RIPA lysis buffer or the milder lysis buffer 1% (w/v) n-dodecyl-β-D-maltoside (Fig. 4.4). Moreover, the use of the cross-linker DST alone is not enough to precipitate a complex (Fig. 4.5). While, when both the cross-linker DST and the immunoprecipitation techniques were combined, we were able to detect an interaction between those proteins as shown in Fig. 4.6 where the two GPR19 bands precipitated with the anti-HA-Tag and the HA-Tag MRAP band precipitated with the anti-GPR19 antibody. These findings strongly suggest that GPR19 and MRAP are forming a complex.

Interestingly, the co-immunoprecipitation results of the WT cell line that naturally expresses GPR19 but not MRAP reveal the precipitation of a 50 kDa GPR19 band in both experiments with anti-GPR19 and the reciprocal experiment with anti-N-POMC$_{1-28}$. From this finding, we can propose that MRAP is not required for N-POMC$_{1-28}$ to bind to GPR19. Moreover, in the previous chapter, we reported that the expression of MRAP in the HEK-293 cell line leads to an increase in the concentration of the higher molecular weight GPR19 (90 kDa) form, which we thought to be a hetero-GPR19 dimer, in comparison to the WT cell line. This form of GPR19 can be precipitated by both anti-HA-Tag and anti-N-POMC$_{1-28}$ in the GPR19/MRAP cell line but not in the WT cell line. This finding could be explained as N-POMC$_{1-28}$ could bind to the GPR19 if it is expressed alone at the cell surface, while if it is in a dimer with other protein(s), it requires MRAP to facilitate the binding of N-POMC$_{1-28}$ to GPR19, in the same way, MC2R requires MRAP for ACTH binding (Metherell et al., 2005).

To our knowledge, the only report that mentions GPR19 dimerising with another receptor is the study published by Li et al. (2021). The aim of this study was to identify

the GPCR that heterodimerised with MC3R and MC4R in the mouse hypothalamus. They reported that GPR19, among another 23 GPCRs, heterodimerised with MC3R but not with MC4R, and the surface expression of GPR19 increased as the expression ratio of MC3R increased in the cells. While the surface expression of MC3R decreased as the GPR19 expression increased in the cells. Moreover, they transfected cells with a fixed amount of MC3R and different ratios of GPR19 and followed the cAMP accumulation inside the cells as MC3R is a coupled Gαs receptor that, upon activation, the level of cAMP inside the cells increases. They found that dimerisation between MC3R and GPR19 slightly enhanced cAMP accumulation.

This finding is of interest as Gantz et al. (1993) reported that MC3R is expressed in the human brain, specifically in the cortex, thalamus, hippocampus, and hypothalamus, and in the placenta but not expressed in the adrenal tissue. It is known that MC3R is activated by POMC-derived peptides, γ1- and γ2-MSH peptides, as well as α-MSH (Roselli-Rehfuss et al., 1993). It is reported that both MRAP and MRAP2 interact with MC3R, and the expression of MRAP and MRAP2 either alone or in combination does not alter the cell-surface expression of MC3R (Chan et al., 2009). In the same study, they found that expression of MRAP2 alone or in combination with MRAP in a cell line that is expressing MC3R and then treated with the ligand NDP-alpha-MSH ([Nle4, D-Phe7] alpha-melanocyte-stimulating hormone) leads to a significant reduction in cAMP generation in comparison to the cell line that expressing MC3R alone.

GPR19 is expressed during mouse embryonic development and is highly expressed in the adult brain, particularly in the olfactory bulb, the hippocampus, hypothalamic nuclei, and the cerebellum (Hoffmeister-Ullerich et al., 2004). GPR19 is one of the genes that is downregulated in the brain by water deprivation (Tang et al., 2011). Moreover, Stein et al. (2016) demonstrated *in vivo* that reduction in GPR19

mRNA levels in the medial basal hypothalamus of male rats resulted in the loss of the inhibitory effect of adropin, the peptide proposed as a ligand for GPR19, on water deprivation-induced thirst. Moreover, Mushala et al. (2023) reported that GPR19 plays a role in energy homeostasis as they noticed an increase in total energy expenditure in GPR19 knockout mice in comparison to control mice. Hence, both MC3R and GPR19 are expressed in the brain, and all three, MC3R (Cone, 2006), GPR19 (Mushala et al., 2023) and adropin (Kumar et al., 2008), play a role in energy homeostasis. The study of GPR19/MC3R dimerisation and the involvement of MRAP in the formation of this dimer may yield important insight into the physiological role of this dimer on the brain's response to POMC-derived peptides and to adropin, which requires further characterisation.

The data in this chapter shows that the two forms of GPR19 can be co-precipitated by the anti-N-$POMC_{1-28}$ antibody but cannot precipitate the HA-Tag MRAP band, which indicates that N-$POMC_{1-28}$ binds to GPR19 but not MRAP. Moreover, it shows that N-POMC can bind to GPR19 if it is a monomer or a complex with other proteins. In contrast, anti-N-$POMC_{1-28}$ antibody can co-precipitate a ~50 kDa band when western blotted with the HA-Tag MRAP, which suggests that this is the GPR19 form that both MRAP and N-$POMC_{1-28}$ bind to.

MRAP has previously been shown to potentiate MC2R signalling to promote adrenal steroidogenesis (Metherell et al., 2005; Roy et al., 2007). As discussed earlier, MRAP is not specific to MC2R and can bind to other GPCRs, including GPR19, which is confirmed in this study. Stelcer et al. (2020) linked the high GPR19 expression in tumour-derived adrenocortical cells and the inhibitory effect of adropin to the secretion of adrenal hormones. Interestingly, Fassnacht et al. (2003) reported that the treatment of the human adrenocortical cancer cell line (NCI-h295) with N-$POMC_{1-28}$ led to a

concentration-dependent reduction of steroid hormone production. In addition, they reported that treatment of the cells with N-POMC$_{1-28}$ had no effect on the steroidogenesis regulatory enzymes and transcription factors StAR, P450scc, SF-1 and DAX-1. In contrast, Stelcer et al. (2020) reported that adropin decreases the gene and the protein expression of StAR and CYP11A1, the side-chain cleavage enzyme that catalyses the first and the rate-limiting step of steroidogenesis. The inhibitory effect of both N-POMC$_{1-28}$ and adropin in adrenocortical steroidogenesis through the activation of GPR19 and whether it performs that effect as a monomer or as a dimer with other GPCR and the role of MRAP in this process remains an open question.

Before answering that question, we need to confirm first that the orphan GPR19 protein acts as the membrane receptor for N-POMC$_{1-28}$ and adropin. In the next chapter, we will establish a link between the overexpression of GPR19 and the expression of MRAP and the response of the cells to N-POMC$_{1-28}$ using ICC and ELISA assays. Moreover, N-POMC$_{1-28}$ binding specificity to GPR19 will be assessed through a competitive-binding assay. Here, the amount of N-POMC$_{1-28}$ bound to GPR19 is measured in the presence of other putative ligands, e.g., N-POMC peptides: N-POMC$_{1-49}$ and N-POMC$_{1-77}$ or adropin. If the receptor is indeed specific for N-POMC$_{1-28}$, and if the binding of N-POMC$_{1-28}$ bound to the receptor can be competed off with other ligands. In this experiment, we can predict if MRAP plays a role in switching GPR19 to a N-POMC$_{1-28}$ specific receptor by comparing the binding specificity of N-POMC$_{1-28}$ in the cell line that expresses GPR19 alone and the cell line that expresses both GPR19 and MRAP. Moreover, the binding specificity of the other N-POMC peptides, N-POMC$_{1-49}$, N-POMC$_{1-77}$, and adropin to GPR19 will be investigated.

Chapter 5: Identification of N-POMC as a GPR19 Ligand

5.1. Introduction

5.1.1. Receptor-Ligand Interaction

The interaction between a receptor and its ligand is a complex process that involves conformational changes and multiple noncovalent bond formations. Receptor-ligand binding assays provide a quantitative measure of receptor expression and receptor affinity for almost any ligand. Binding assays are essential for studying GPCR biochemistry and for the development and characterisation of new drugs in the pharmacological industry.

The law of mass action is used to describe ligand binding and pharmacodynamic models. Where the binding between the ligand and the receptor occurs due to diffusion, the correct orientation and sufficient energy (Dong et al., 2015; Finlay et al., 2020). The equilibrium is reached when the rate at which new ligand-receptor complex equals the rate at which they dissociate. Ligand-receptor complexes are characterised by many properties, such as specificity, affinity, saturation, and biological response. Receptors often bind to one preferred natural ligand which means it is specific to that ligand. This is not always the case, as it has been found that some natural ligands and toxins, such as α-bungarotoxin, can bind to different receptors (Attie & Raines, 1995).

Ligand specificity can be assessed by competitive-binding assays where the amount of ligand bound to a receptor is measured in the presence of another putative ligand. If the receptor is indeed specific for the original ligand, the amount of ligand bound is not affected by the presence of the other ligands (Motulsky & Neubig, 2010). The binding of the ligand to other sites, other than the receptor, is called nonspecific

binding. The nonspecific binding can occur due to the binding of the ligand to other cellular molecules or to the plates, tubes, or other materials used to perform the experiment. Usually, non-specific binding increases in a linear relationship with the ligand concentration. It can be measured by using an unlabelled ligand at a high concentration, e.g., 100 times the used concentration of the labelled ligand. This will block all the specific binding sites, and the labelled ligand only binds non-specifically. Ideally, nonspecific binding is only 10% to 20% of the total ligand binding, which is the sum of specific and nonspecific binding (Flanagan, 2016; Motulsky & Neubig, 2010).

Moreover, receptor-ligand interactions are distinguished from other nonspecific interactions by their high affinity. Where affinity is the strength of the binding of a ligand to its receptor. It is known that a receptor has a limited number of binding sites and is, therefore, saturated at high ligand concentrations. The saturation experiment is performed by using an increasing series of concentrations of the ligand, and then the equilibrium constants are measured. The equilibrium dissociation constant (K_d) is a measure of the strength of the interaction of a ligand to its receptor, and it is used to describe the ligand affinity. The K_d value is the concentration of the ligand that occupies half of the receptors at equilibrium (Dong et al., 2015; Finlay et al., 2020). The K_d value also measures the equilibrium between the ligand-receptor complex and the dissociated components:

$$[R] + [L] \underset{}{\overset{Kd}{\rightleftharpoons}} [RL]$$

$$Kd = \frac{[R]\,[L]}{[RL]}$$

Where [R] is the free receptor concentration, [L] is the free ligand concentration, and [RL] is the receptor-ligand complex.

The K_i value, which is the dissociation constant, represents the binding of an inhibitor to the receptor, and it depends on the kinetic mechanism of inhibition, either competitive, non-competitive, uncompetitive, or mixed inhibition. In competitive inhibition, the inhibitor binds only to the free receptor but not to the receptor-ligand complex. In uncompetitive inhibition, the inhibitor binds only to the receptor-ligand complex. Mixed inhibition involves inhibitor binding to both free receptor and receptor-ligand complex with different binding constants. In non-competitive inhibition, the inhibitor binding has no effect on ligand binding as it binds to a different site than the active site where the ligand binds (Hulme & Trevethick, 2010).

The maximum density of receptors (B_{max}) provides an estimated measure of the total number of receptors that can bind to a ligand (Hulme & Trevethick, 2010). It is usually expressed in terms of ligand bound per milligram of protein. It is estimated by plotting a hyperbolic curve of the specific binding against the ligand concentrations that are high enough to approach full receptor occupancy.

The receptor-ligand interaction leads to a physiological response. This will be discussed in detail in the following chapter, and with its cellular internalisation. Internalisation of the receptor after ligand activation could affect the results of the ligand-binding assay. This can be reduced or prevented by using one of the following approaches. First, perform the experiment at low temperatures, e.g., 4 to 15 ºC, as it has been reported that the internalisation process is slower in low temperatures. Second, use of reagents that prevent or stop the internalisation process, such as Pitstop2 (von Kleist et al., 2011). Third, the use of the cell membrane extracts, rather than a whole cell which prevents internalisation, is not always a good choice as the receptor 3D structure may be affected during the extraction process (Oliver & Jamur, 2010).

5.1.2. Ligand Binding Assays

Radioactive ligand binding assays were widely used to define receptor function at the molecular level. This technique remains the most sensitive quantitative technique to determine receptor expression levels in both intact cells and membrane extracted samples. It is also used for many pharmacological analyses, including the determination of binding kinetics. It is a powerful technique that is used for the identification of ligands for the orphan GPCRs. These receptors are artificially expressed in cell lines and linked to a reporter system to identify when a ligand binds to the receptor (Attie & Raines, 1995; Civelli et al., 2013). This "reverse pharmacology" technique has been very successful in de-orphanizing and identifying the cognate ligand of many GPCRs, such as dopamine receptors (D1, D2, D3, D4 and D5) and melanocortin receptors (MC1R, MC2R, MC3R, MC4R and MC5R) (Civelli et al., 2013).

In recent years, alternative techniques, such as non-radioactive ligand binding assays, have been developed to reduce the use of radioactive isotopes due to the danger to human health and the environment and the expensive cost of its waste disposal (Böhme & Beck-Sickinger, 2009). Commonly used non-radioactive labelling reagents for the creation of ligand conjugates are biotin and fluorescent reagents. Those reagents are available commercially as individual ligand-binding reagents or as kits. The choice of a reagent to conjugate to a ligand depends upon the functional groups that are available for modification and on the application to be undertaken.

Cell-enzyme-linked immunosorbent assay (cell-ELISA) is a simple, rapid, inexpensive, and highly sensitive quantitative technique that is used to quantify the expression of proteins or receptors on the cell surface (Lourenço & Roque-Barreira, 2010). The assay is performed directly in a cell culture plate to obtain information about

the relative abundance of an antigen in a cell population. This is followed by the direct labelling of cells with a primary antibody and then with a secondary antibody conjugated to a detection enzyme like horseradish peroxidase (HRP). The optical density of the HRP reaction is measured, and it is proportional to the amount of antigen expression on the cell surface. Moreover, it can be used to study changes in receptor total and cell surface expression selectively using permeabilised and non-permeabilised conditions, respectively.

5.1.3. Proteins and Peptides Labelling Technique

Bioconjugation is a powerful technique that involves the attachment of two molecules together, usually through a covalent bond, to create a complex. Bioconjugation is used to modify, label, or crosslink biomolecules where the resulting conjugate will have a characteristic not normally found among the naturally occurring molecules (Hermanson & ebrary, 2013). Nowadays, most of the activities in biological research cannot be done without the use of one or more bioconjugated reagents. A basic understanding of the reactions of bioconjugation is essential to understand how to form a successful conjugate for a particular application. Where the key step is the selection of the proper crosslinking reagent that, in turn, contains the appropriate reactive group(s), which will couple with the functional group(s) available on the molecule to be linked together.

N-hydroxysuccinimide ester (NHS ester), either labelled with fluorescent molecules or biotin, is the most used amine-reactive crosslinker. It is used to label the primary amines ($R\text{-}NH_2$) of proteins, amine-modified oligonucleotides, and other amine-containing molecules (Hermanson & ebrary, 2013). The reaction of a carboxylate group of the NHS ester with the amine group of the molecule to be labelled leads to the

formation of a stable amide labelled molecule and NHS leaving group (**Fig. 5.1**). In peptides and protein molecules, NHS ester crosslinking reagents couple principally with primary amines at the N-terminals and the secondary amines of lysine side chain, forming stable amide and imide linkages, respectively.

Alexa Fluor™ fluorescent dyes with excitation suited for a specific wavelength are used for stable signal generation and imaging using flow cytometry and fluorescence microscopy, respectively. The NHS ester labelled with Alexa Fluor™ is widely used for covalently conjugating the fluorescent dye to a protein or antibody, where the resulting Alexa Fluor™ conjugate will be used to assay or track its interaction with other biomolecules (Hermanson & ebrary, 2013).

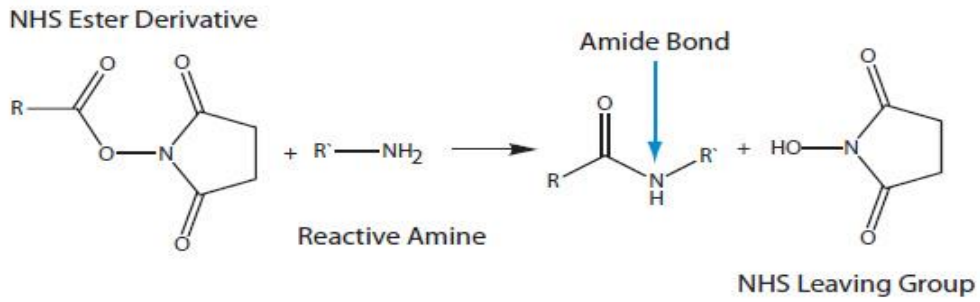

Fig. 5.1. General N-hydroxysuccinimide ester (NHS ester) reaction with primary amine.

The strong non-covalent binding of avidin to biotin has made it a useful tool to be used in diverse applications in immunology, histochemistry, *in situ* hybridisations, affinity chromatography, and many other techniques. In this assay, a biotinylated molecule, either an antibody or a protein, is first applied to the sample and then detected by using labelled avidin. A variety of avidins labelled with detection conjugates, including fluorescent, enzyme, iodine, ferritin, or gold conjugates, are available commercially. Avidin is a positively charged glycoprotein found in egg-whites that is made up of four identical subunits where each has one binding site for biotin (Hermanson & ebrary, 2013). This interaction gives the advantage of enhancing the signal intensity of the immunoassay. Moreover, avidin-biotin strong non-covalent interaction is resistant to break-down and to denaturation under extreme conditions which makes it useful in bioconjugation applications. The only disadvantage of using avidin is its nonspecific binding to other non-biotin molecules due to its high isoelectric point (pI) and carbohydrate content. Streptavidin is the bacterial counterpart of avidin. It is a non-glycosylated protein that also binds to four biotin equivalents per molecule with high affinity and low reversibility. As streptavidin has no carbohydrate content and has lower pI in comparison to avidin, this overcomes the disadvantage of the nonspecific binding of avidin. Streptavidin-biotin binding, therefore, has advantages over avidin-biotin binding as it shows a lower signal-to-noise ratio (Hermanson & ebrary, 2013).

5.1.3.1. Labelling of N-POMC$_{1-28}$

N-POMC$_{1-28}$ is a short peptide that represents the first 28 amino acids sequence of the N-POMC. N-POMC$_{1-28}$ is not a natural product of POMC processing where it had been extracted from proteolytic cleavage of the pro-γ-MSH during the large-scale extraction process of growth hormones from human pituitaries (Lowry, 2016; McLean et al., 1981). The sequence of N-POMC is stabilised by two disulphide bridges, Cys2 paired

to Cys24 and Cys8 paired to Cys20, inducing a hairpin tertiary structure (Bennett et al. (1986), Fig. 5.2). The disulphide bridges are essential for targeting POMC to the regulated secretory compartment of the cell (Cool & Loh, 1994). The N-POMC amino acid sequence is extremely well conserved among various mammalian and sub-mammalian species where only the extreme C-terminal end differs because of one or more amino acid deletions e.g., rat N-POMC consists of 74 residues, human of 76 residues and bovine of 77 residues (Denef & Van Bael, 1998). Early studies reported the role of N-POMC, either the full length or the smaller fragments, in adrenal growth and mitogenesis (Estivariz, Carino et al., 1988; Estivariz et al., 1982; Estivariz, Morano, et al., 1988; Lowry et al., 1983). It has been proposed that pro-γ-MSH secreted from the pituitary undergoes a post-secretion cleavage where the cleavage occurs after the arginine residue, resulting in the generation of N-POMC$_{1-49}$ and Lys-γ3-MSH (residues 50-76) (Bicknell, 2016; Seger & Bennett, 1986).

The receptor of N-POMC remains unknown; however, it has been found that the C-terminal fragment of N-POMC, γ3-MSH, is the physiological ligand of the melanocortin receptor MC3R (Lorsignol et al., 1999; Roselli-Rehfuss et al., 1993). In this project, receptor-ligand binding assays are performed to confirm that GPR19 is the receptor of N-POMC as it is identified among other orphan GPCRs expressed in the adrenal cortex to be N-POMC receptor (Bicknell, unpublished data). To perform those assays, the N-POMC$_{1-28}$ will be labelled using an NHS ester either conjugated with a fluorescent dye or biotin, then the cells are treated with this labelled form of N-POMC$_{1-28}$, and the cell binding capacity is determined. Labelling of N-POMC$_{1-28}$ with NHS ester could lead to the labelling at the N-terminal amino acid and/or at the lysine (K) side chain group.

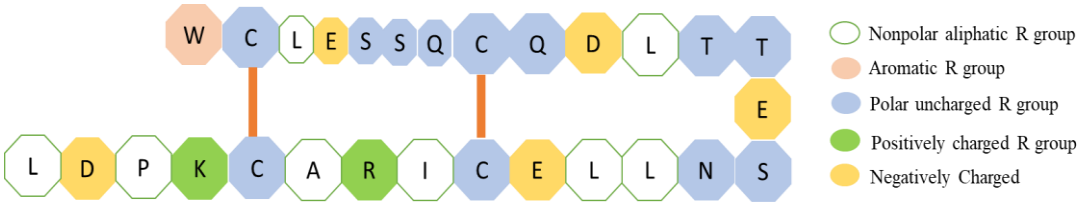

Fig. 5.2. N-POMC$_{1-28}$ amino acids sequence. It contains two disulphide bridges, Cys2 paired to Cys24 and Cys8 paired to Cys20 (shown in orange), inducing a hairpin tertiary structure (Bennett et al., 1986). The NHS ester labelling occurs at the N-terminal amino acid tryptophan (W) and the side chain of the amino acid lysine (K).

5.1.3.2. Labelling of Adropin

The full adropin peptide is made up of 76 amino acids that are coded by the Energy Homeostasis Associated (Enho) gene, which is 100% conserved in humans, mice, and rats (Ali et al., 2022). The first 33 amino acids are described as a signal peptide while the sequence from 34 to 76 amino acids is described as the bioactive sequence (Fig. 5.3). It contains one disulphide bridge where Cys34 paired to Cys56 inducing a hairpin tertiary structure (Kumar et al., 2008) like the structure of the N-POMC$_{1-28}$. It has been reported that adropin is secreted by human tissues, e.g., the brain, heart, and liver (Thapa et al., 2018; Thapa, Xie, Manning, et al., 2019; Thapa, Xie, Zhang et al., 2019), and by cell lines, e.g., HEK-293 (Kumar et al., 2011). In contrast, a study by Wong et al. (2014) showed that adropin was a membrane-bound peptide rather than a secreted peptide. Since its discovery, research into adropin has concentrated on its physiological role. Several studies and reports indicated the involvement of adropin in lipid and carbohydrate metabolism, insulin resistance, functioning of the cardiovascular system and inflammation (Ali et al., 2022). Moreover, Lovren et al. (2010) reported the ability of

adropin to stimulate the proliferation and differentiation of the human umbilical vein endothelial cells.

Adropin has been stated as a putative endogenous ligand for GPR19 (Stein et al. (2016), Jasaszwili et al. (2019); Rao and Herr (2017), Stelcer et al. (2020)). However, there is no evidence for the peptide binding to GPR19, including a de-orphanisation study by Foster et al. (2019) and no published receptor-ligand binding studies. To explore whether adropin is a GPR19 ligand, adropin was labelled using an NHS ester conjugated with biotin, which could lead to the labelling at the N-terminal amino acid and/or at one or the two lysine (K) side chain residues. This labelled adropin will be used to perform receptor-ligand binding ELISA assay and a competitive assay against N-POMC fragments.

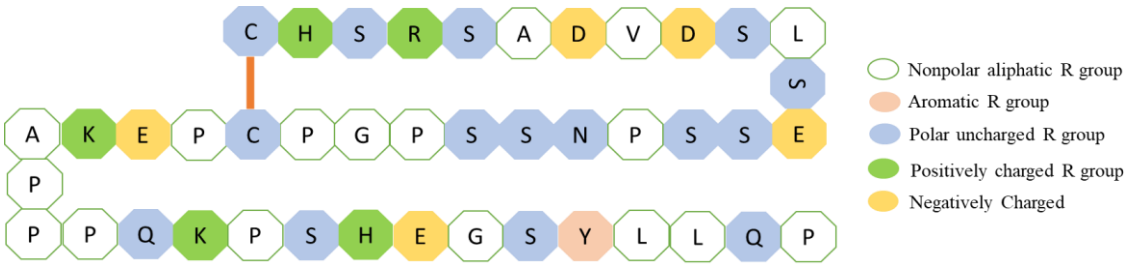

Fig. 5.3. Human adropin 34-76 amino acids sequence. It contains one disulphide bridge, Cys34, paired to Cys56 (shown in orange), inducing a hairpin tertiary structure (Kumar et al., 2008). The NHS ester labelling occurs at the N-terminal amino acid cystine (C) and the side chain of the two lysine residues (K).

5.2. Aims

1) To measure the binding ability of the florescent labelled N-POMC$_{1-28}$ to the wild-type HEK-293 cell line and compare it to the cells transfected with GPR19, MRAP, and GPR19/MRAP using the ICC technique.
2) To quantify the binding ability of unlabelled N-POMC$_{1-28}$ and adropin to the wild-type HEK-293 cell line and compare it to the binding capacity of the transfected cells with GPR19, MRAP, and GPR19/MRAP using an ELISA assay.
3) To determine the binding capacity of biotin labelled N-POMC$_{1-28}$ to the wild-type HEK-293 cell line and compare it to the binding capacity of the transfected cells with GPR19, MRAP, and GPR19/MRAP using an ELISA assay. Then compete, the binding of biotin labelled N-POMC$_{1-28}$ with unlabelled N-POMC$_{1-28}$, N-POMC$_{1-49}$, N-POMC$_{1-77}$ and adropin.
4) To quantify the binding ability of biotin-labelled adropin to the wild-type HEK-293 cell line and compare it to the transfected cells with GPR19, MRAP, and GPR19/MRAP using ELISA assay. Then, the biotin-labelled adropin was competed with unlabelled N-POMC$_{1-28}$, N-POMC$_{1-49}$, and N-POMC$_{1-77}$.

5.3. Methods

5.3.1. N-POMC$_{1-28}$ Labelling with Alexa Fluor-488

Synthetic N-POMC$_{1-28}$ peptide was custom synthesised from Bachem (Merseyside, UK) and labelled with Alexa Fluor-488 NHS Ester by mixing a 3:1 molar ratio of the peptide with Alexa Fluor-488 NHS Ester. First, 1.2 mg of N-POMC$_{1-28}$ peptide was dissolved in 500 µl of freshly prepared 0.1 M sodium bicarbonate buffer (pH 8.3), and 400 µg of Alexa Fluor-488 NHS Ester (Succinimidyl Ester, A20000, Invitrogen) was dissolved in 50 µl DMSO. The two solutions were mixed well and incubated at RT for an hour. After that, 1 ml of peptide extraction buffer (Appendix C.1) was added to the N-POMC-Alexa Fluor-488 mixture. The labelled ^{488}N-POMC$_{1-28}$ peptide was purified using a Sep-pak C18 cartridge (Waters, USA). Briefly, a 1 ml column was wetted using methanol before equilibrating with 5 ml of 0.1% (v/v) trifluoroacetic acid (TFA). The mixture was applied, and the column was washed with 5 ml of 0.1% (v/v) TFA. The column was eluted in a stepwise fashion using an elution buffer containing 0.1% (v/v) TFA and increasing percentages of acetonitrile starting from 10% to 80%. The labelled ^{488}N-POMC$_{1-28}$ was eluted with the 0.1% (v/v) TFA containing 40% (v/v) acetonitrile elution buffer. Helium gas was used to evaporate the acetonitrile from the fraction that contains the ^{488}N-POMC$_{1-28}$, and then that fraction was neutralised by adding 0.5 ml of 0.1 M sodium bicarbonate solution (pH 8.3). The concentration of the ^{488}N-POMC$_{1-28}$ was calculated using the following equation:

$$\text{Concentration of the peptide (M)} = \frac{A280 - A498}{e} \times CF$$

The principle of this equation depends on the fact that the amino acid tryptophan that is present in the N-POMC$_{1-28}$ peptide can absorb light at the wavelength 280 nm, and Alexa Fluor-488 dye has an excitation maximum at wavelength 495 nm. The N-POMC$_{1-}$

$_{28}$ has one tryptophan residue, which has an extinction coefficient (*e*) of 5050 $cm^{-1}M^{-1}$. The correction factor (*CF*) of the Alexa Fluor-488 dye at 280 nm (A_{280} free dye/A_{max} free dye) is provided as 0.11.

5.3.2. Biotinylating of N-POMC$_{1-28}$ and Adropin

5.3.2.1. Labelling of Peptides

Synthetic N-POMC$_{1-28}$ was labelled with EZ-link™ NHS-biotin (N-Hydroxysuccinimidobiotin) by mixing more than 12-fold molar excess of biotin to peptide. First, 135 µg of N-POMC$_{1-28}$ peptide was dissolved in 650 µl of freshly prepared 0.1 M sodium bicarbonate buffer (pH 8.3), and 122 µg of EZ-link™ NHS-biotin (#20217, Thermo Scientific) was dissolved in 100 µl DMSO. Subsequently, 50 µl of the biotin solution was mixed well with the N-POMC$_{1-28}$ peptide solution and incubated at RT for an hour; the tube was mixed every 10 min.

The adropin synthetic peptide was purchased from Cambridge Research Biochemicals and labelled with EZ-link™ NHS-biotin by mixing more than 12-fold molar excess of biotin to the peptide. First, 110 µg of adropin peptide was dissolved in 500 µl of freshly prepared 0.1 M sodium bicarbonate buffer (pH 8.3), and 341 µg of EZ-link™ NHS-biotin was dissolved in 100 µl DMSO. Then, 100 µl of the biotin solution was mixed well with the adropin peptide solution and incubated at RT for 2 hrs, and the tube was mixed every 10 min.

5.3.2.2. Elution of the Labelled Peptides

To the biotin-labelled peptides, 100 µl of peptide extraction buffer was added and then purified using high-performance liquid chromatography (HPLC, Spectra Series P200 and UV100, Spectra-Physics) that is connected to 4.6 mm x 250 mm C18 column (Thermo Fisher). The biotinylated N-POMC$_{1-28}$ eluted with a linear gradient of 0.5

ml/min flow rate of the mobile phase, which is made up of two eluents: eluent A is 0.1% (v/v) TFA in acetonitrile and eluent B is 100% acetonitrile. The biotinylated adropin eluted with a linear gradient of 1.5 ml/min flow rate of the mobile phase, which is made up of 90% eluent A (0.1% (v/v) TFA in water) and 10% eluent B (0.1% (v/v) TFA in acetonitrile). The detection of peptides was done by measuring absorbance at 280 nm. The eluted fractions were collected after 35 mins at 40% eluent A and 60% eluent B, and the acetonitrile was evaporated from the eluted fractions using Helium gas.

5.3.2.3. Determine the Concentration of the Eluted Peptides

The absorbance at 284 nm of the biotinylated peptide was measured against 0.1% (v/v) TFA. The Beer-Lambert equation was used to calculate the concentration of biotinylated peptide:

$$\text{Concentration of the peptide (M)} = \frac{A284}{e*l}$$

Where A284 is the absorbance at 284 nm, e is the extinction coefficient, and l is the optical path length.

The principle of this equation depends on the fact that the amino acids tryptophan and tyrosine can absorb light at the wavelength 280 nm, which has an extinction coefficient (e) of 5050 cm-1M-1 and 1440 cm-1M-1, respectively. N-POMC$_{1\text{-}28}$ has one tryptophan residue in its sequence, while adropin has one tyrosine residue.

5.3.2.4. ELISA Assay for Biotin and the Peptide in the Eluted Fractions

In a 96-well plate, 2 µl of each fraction was added to 98 µl of freshly prepared in 0.1 M $NaHCO_3$ mixed well and incubated at RT for 3 hrs. The plate was then blocked by adding 200 µl of 0.1% (w/v) BSA in 0.1 M $NaHCO_3$ and incubated at RT for 2 hrs. The

wells were washed 3 times with 200 µl 1X TBST for each wash. To check if the eluted fraction contains biotin, 200 µl of the Ultra streptavidin-HRP (N504, Thermo Scientific) at 1:500 in 0.1% (w/v) BSA in 1X TBST was added, and the plate incubated for 1 hr at RT. Then, the plate was washed 3 times with 1X TBST, 200 µl for each wash. To confirm that the eluted fraction also contained the peptide, 200 µl of the rabbit anti-N-POMC$_{1-28}$ antibody was raised by immunising rabbits with purified bovine N-POMC$_{1-49}$ and antibodies to N-POMC$_{1-28}$ were affinity purified using solid-phase 1-28, which is N-POMC$_{1-28}$ covalently linked to cyanogen bromide activated Sepharose resin (*prepared by Andrew Bicknell*), or rabbit anti-adropin (PA5-72781, Invitrogen) primary antibody at 1:500 dilution prepared in 0.1% (w/v) BSA in 1X TBST was added, and the plate was incubated for 1 hr at RT. The wells were then washed 3 times with 1X TBST, 200 µl for each wash, and 200 µl 1:1000 diluted goat anti-rabbit IgG horseradish peroxidase (ab97051, abcam) secondary antibody that was prepared in 0.1% (w/v) BSA in 1X TBST was added per well and incubated for 2 hrs at RT. The plate was then washed 3 times with 1X TBST, 200 µl for each wash. The ELISA reaction was started by adding 200 µl of Tetramethylbenzidine (TMB) solution (Appendix C.2) that contained 0.05% (v/v) H_2O_2. The reaction was stopped once a blue colour had developed (approx. 5-10 mins) before the addition of 100 µl of 0.5 M HCl, which stopped the reaction and turned it yellow. The absorbance at 450 nm was subsequently read using a plate reader (Molecular Devices).

5.3.3. Detection of Labelled ^{488}N-POMC$_{1-28}$ by ICC

Cells were cultured in 12 well plates containing 10 µg/ml poly-L-ornithine (Millipore, USA) coated coverslips. After 24 hrs of serum starvation, the cells were incubated for 6-7 min with 200 µl of 30 µM Pitstop 2™ solution (ab120687, abcam), prepared as recommended by the manufacturer. The pitstop2™ solution was discarded,

and then the cells were induced with 1 nM ^{488}N-POMC$_{1-28}$ for 10 min in the 5% (v/v) CO_2 and 37°C incubator. After 10 min, the coverslips were washed twice with ice-cold 1X PBS, and the cells were fixed with 4% (w/v) PFA for 5 min at 4°C. Coverslips were mounted in a fluorescent mounting medium without DAPI (Vector Laboratories, Inc, UK). Cells were imaged at 40X lens using the Zeiss AxioImager fluorescent Microscope.

5.3.4. Fixed-Cell ELISA

This assay was performed following a protocol described by Jones et al. (2007) with modifications. Briefly, cells were cultured in 6 well plates for 48 hrs. After 24 hrs of serum starvation, the cells were incubated for 6-7 min with 300 µl of 30 µM Pitstop 2™ solution (ab120687, abcam), prepared as recommended by the manufacturer. The pitstop2™ solution was discarded, and then the cells were incubated with a 10-fold serial dilution of N-POMC$_{1-28}$ starting from 1 *p*M to 1 nM for 10 min in a 5% (v/v) CO_2 at 37°C incubator. After 10 min, the cells were washed twice with ice-cold 1XPBS and then fixed with 4% (w/v) PFA for 5 min at 4°C. The cells were washed twice with ice-cold 1X PBS, then scraped into 0.5 ml/well 1X PBS and transferred to a 1.5 ml microcentrifuge tube. The tubes were centrifuged at 400 g and 4°C for 5 min. After discarding the supernatant, the cells were blocked at RT for 1 hr with 0.5 ml 10% (v/v) goat serum prepared in 1X PBS. To the blocking buffer, 0.5 µl rabbit anti-N-POMC$_{1-28}$ primary antibody was added to a final 1:1000 dilution factor and incubated overnight at 4°C. The next day, the microcentrifuge tubes were centrifuged at 100 g for 5 min, and the cells were washed 3 times with 1X PBS. The cells were incubated with the goat anti-rabbit IgG horseradish peroxidase (ab97051, abcam) secondary antibody at 1:5000 10% (v/v) goat serum for 2 hrs at RT and then washed 3 times with 1X PBS, 0.5 ml for each wash. In a 96-well plate, 10 µl of each sample was used to perform the ELISA reaction. The reaction was started by adding 200 µl of Tetramethylbenzidine (TMB) solution (Appendix C.2) that contains

0.05% (v/v) H_2O_2. The reaction was stopped after 15 min; during this time, the reaction mixture turned blue by adding 100 µl of 0.5 M HCl, and then the absorbance at 450 nm was read using a plate reader (Molecular Devices). For standardisation, the absorbance at 540 nm was determined in 10 µl of each sample using a BCA protein kit assay.

5.3.5. Non-Radioactive Ligand Binding Assay Using Biotinylated Peptide

Cells were cultured in 96 well plates containing 10 µg/ml poly-L-ornithine (Millipore, USA). After 48 hrs of incubation, the cells were blocked with DMEM containing 1% (w/v) BSA for 30 min in a 5% (v/v) CO_2 at 37°C incubator. The Pitstop 2™ solution was added to the blocking buffer directly with 30 µM final dilution and incubated for 6-7 min. The solution was discarded, and then the cells were treated with serial dilutions of biotinylated peptide for 10 min in a 5% (v/v) CO_2 at 37°C incubator. To find the non-specific binding, the cells were treated with unlabelled peptide 100X fold the concentration of biotinylated peptide concentrations. For the competitive assay, the cells were treated with a fixed concentration of biotinylated peptide equal to the K_d value and serial dilutions of unlabelled N-POMC$_{1-28}$, N-POMC$_{1-49}$, pro-γ-N-POMC (both N-POMC$_{1-49}$ and N-POMC$_{1-77}$ were purified from bovine pituitary tissue, purified by Andrew Bicknell) or adropin. After 10 min, the cells were washed twice with 200 µl 1X PBS followed with the addition of Ultra streptavidin-HRP (N504, Thermo Scientific) at 1:500 1% (w/v) BSA in 1X PBS for 1 hr at RT and then washed 3 times with 1X PBS, 200 µl for each wash. The reaction was started by adding 200 µl of TMB solution containing 0.05% (v/v) H_2O_2. The reaction was stopped after 15 min; during this time, the reaction mixture turned blue, adding 100 µl of 0.5 M HCl, and then the absorbance at 450 nm was read using a plate reader (Molecular Devices).

5.4. Results

In this chapter, we investigated whether N-POMC can bind to the GPR19 receptor. In these experiments, the internalisation of plasma membrane receptors was inhibited by incubating the cells with 30 μM Pitstop 2™ for 7 min. Pitstop 2™ competitively inhibits the clathrin terminal domain to selectively inhibit CME, which will prevent the GPCR internalisation after ligand binding.

5.4.1. Labelled Peptides

The biotin-labelled peptides are eluted as more than one peak, as was expected due to the different combinations of the labelling sites that are available in each peptide with the preference to be labelled at the lysine side chain rather than the N-terminal. Since N-POMC$_{1-28}$ could be labelled at either the N-terminal amino acid and/or at the lysine (K) side chain group, three possible labelling combinations were expected to form during the labelling step. The HPLC elution profile of the biotinylated N-POMC$_{1-28}$ (Fig. 5.4) shows 4 peaks, with the third peak being the dominant one. The presence of both the N-POMC$_{1-28}$ peptide and biotin in each fraction was studied by ELISA assay. The results revealed that peak 3, which was collected as fraction 3, has the highest peptide and biotin signal intensity (data not shown). The concentration of N-POMC$_{1-28}$ in this fraction was determined, and it is used to perform the non-radioactive ligand binding assay to study the binding ability of the cells to this peptide and if the longer fragment, 1-49 and 1-77, or adropin could compete for this peptide.

The adropin peptide has two lysine (K) amino acids; therefore, one of them or both could be biotinylated in addition to the N-terminal. This could develop up to six possible labelling combinations. Surprisingly, the HPLC elution profile of the biotinylated adropin (Fig. 5.5) shows 9 overlapping peaks that were collected as 9 fractions. The ELISA assay results showed that all the fractions contain adropin peptide

and biotin, with fractions 4, 5, 6, 7 and 8 having the highest signal (data not shown), so 100 µl of each fraction was combined, and the final concentration was measured. The combined fractions were used to detect if the cells showed any adropin binding ability.

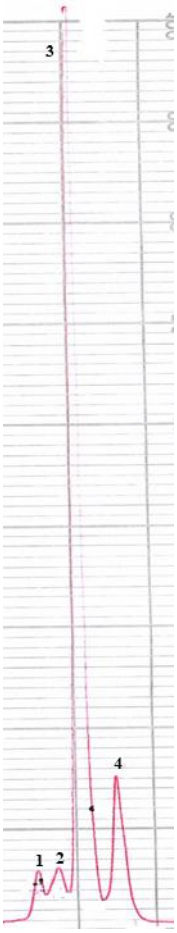

Fig. 5.4. The eluted biotin labelled N-POMC$_{1-28}$ using HPLC (Spectra Series P200 and UV100, Spectra-Physics). It was eluted as 4 peaks collected separately as 4 fractions. Peak 3, the peak with the highest intensity, was found to contain the highest concentration of biotinylated N-POMC$_{1-28}$.

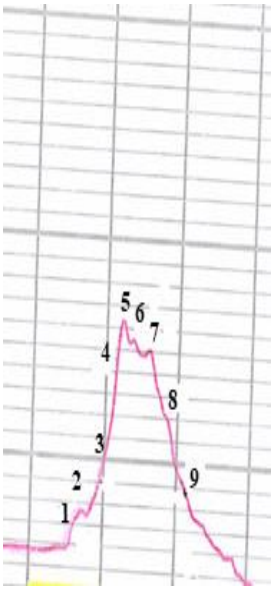

Fig. 5.5. The eluted biotin-labelled adropin using HPLC (Spectra Series P200 and UV100, Spectra-Physics). It was eluted as 9 overlapping peaks that were collected as 9 fractions.

5.4.2. Binding of Labelled ^{488}N-POMC$_{1-28}$ to GPR19

The WT cell line and the three stably transfected cells with GPR19, MRAP and GPR19/MRAP were treated with 1 nM ^{488}N-POMC$_{1-28}$. At first, the fluorescent mounting media containing DAPI was used, and we noticed that DAPI bled through the 488 nm wavelength, so fluorescent mounting media without DAPI was used. The corrected total cell fluorescence (CTCF) was calculated in 5 cells from 3 independent images of one slide of three independent experiments, and then one-way ANOVA and Tukey's multiple comparisons test were applied. Figure 5.6 shows that ^{488}N-POMC$_{1-28}$ signal intensity in the cell line expressing GPR19, MRAP and MRAP/GPR19 was at a significant level in comparison to the WT cell line. Moreover, the signal intensity in the cell lines that express MRAP and GPR19/MRAP was significantly higher ($p < 0.001$) than the cell line that overexpressed GPR19 only. Interestingly, the cell line that was expressing MRAP

without overexpression of GPR19 showed a significantly higher ^{488}N-POMC$_{1-28}$ signal in comparison to the cell line that was overexpressing GPR19. This finding reflects the availability of the N-POMC receptor in the cell membrane where the cells that express more GPR19 receptor signal with more ^{488}N-POMC$_{1-28}$.

We tried to label the cells with a lower and higher concentration than the 1 nM ^{488}N-POMC$_{1-28}$, but it was unsuccessful. In the lower concentrations, it was difficult to have a good image, especially in the WT cell line. In the higher concentrations, the image had a high background, which made it difficult to identify the cells from the background. That leads us to use a different technique to study the binding ability of those cell lines to different N-POMC$_{1-28}$ concentrations.

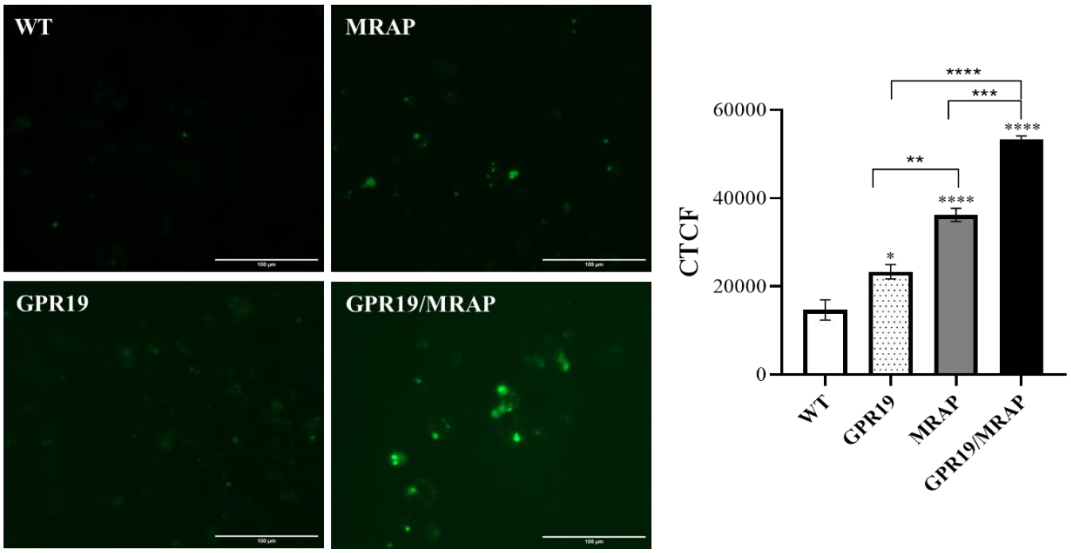

Fig. 5.6. Binding of Alexa-Fluor 488 labelled N-POMC$_{1-28}$ to the WT HEK-293 in comparison to stably transfected cells with GPR19, MRAP and GPR19/MRAP. Cells were imaged at 40X lens using the Zeiss AxioImager fluorescent Microscope, scale bar 100 µm. The corrected total cell fluorescence (CTCF) is calculated in 5 cells from 3 independent images of one slide. Statistical analysis was performed using one-way ANOVA and Tukey's multiple comparisons test. Data are expressed as mean ± SEM of three independent experiments. Results were considered statistically significant if the p-value was < 0.05.

5.4.3. Binding Ability of N-POMC$_{1-28}$ to Its Receptor

This work aimed to investigate whether overexpression of just GPR19 could increase N-POMC binding to the HEK-293 cell membrane or if there is a requirement for MRAP. The four cell lines were treated with increasing concentrations of unlabelled N-POMC$_{1-28}$, starting from 1 *p*M to 1 nM. Many standardisation steps were performed to reach the final protocol that was used in this study. We found that using a 6-well plate to culture the cells was better than using a 12-well plate, as more cells are required to perform both the ELISA and the protein content assays in the cell samples. Moreover, the assay was performed at concentrations lower than 1 *p*M and higher than 1 nM of N-

POMC. The signal at the lower concentrations was very low and could not be distinguished from the background, while the signal at higher concentrations showed saturation, especially in the wild-type cell line. The blocking step was found to reduce the non-specific binding of the primary and secondary antibodies. The best dilution factor that should be used for both the primary and secondary antibodies was also tested using the titration method (data not shown). It was difficult to have the same number of cells per sample as the HEK-293 cells are easily detached from the plate, so to standardise the results, the same amount of protein was used to perform the ELISA assay.

The results were statistically analysed using 2-way ANOVA and Dunnett's multiple comparisons test, as shown in Figure 5.7. The results show that overexpression of GPR19 alone was not enough to give a significant difference in N-POMC$_{1-28}$ binding to the cell membrane in comparison to the wild-type cell line. In contrast, overexpression of GPR19 with MRAP results in a significant difference in N-POMC$_{1-28}$ binding to the HEK-293 cell membrane, with as low as 10 *p*M of N-POMC$_{1-28}$. Interestingly, a stably transformed cell line that expresses MRAP shows a significant binding ability response to N-POMC$_{1-28}$, like the transformed cell line with GPR19 and MRAP. This finding highlights that MRAP plays a role in facilitating the binding of N-POMC to its receptor GPR19.

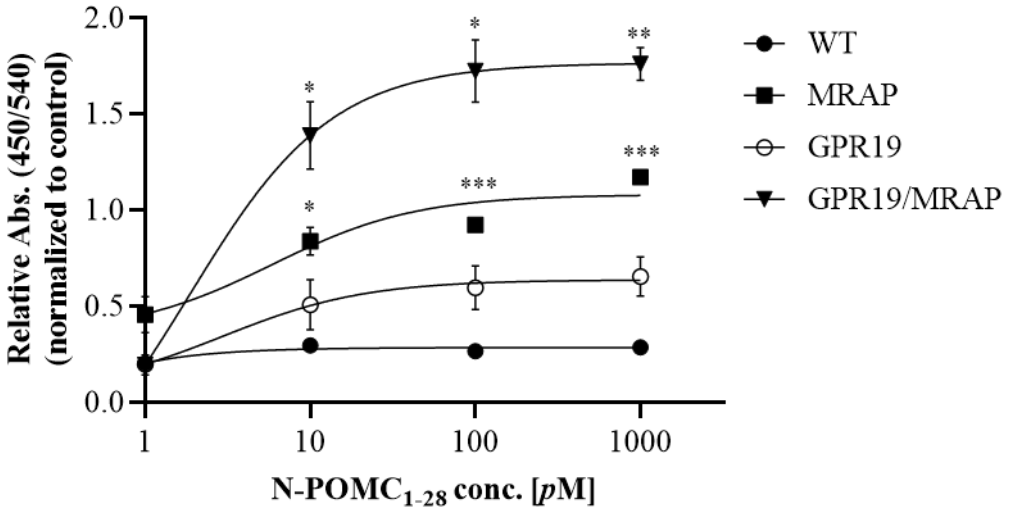

Fig. 5.7. The relative absorbance (450 nm/540 nm, normalised to control) of the WT HEK-293 in comparison to stably transfected cells with GPR19, MRAP and GPR19/MRAP using fixed-cell ELISA. The cells were treated with 30 µM Pitstop 2™ solution (ab120687, abcam) for 6-7 min, then treated with serial concentrations of N-POMC$_{1\text{-}28}$ starting from 1 *p*M to 1 nM with 10 times dilution factors. The cells were fixed for 5 min with 4% (w/v) PFA and incubated with rabbit anti-N-POMC$_{1\text{-}28}$, then incubated with goat anti-rabbit IgG horse radish peroxidase (ab97051, abcam). The ELISA reaction was performed by adding a TMB solution that contains 0.05% (v/v%) H_2O_2, and the absorbance was read at 450 nm. A BCA protein assay kit was used to determine the amount of protein in samples for standardisation (absorbance 540 nm). Statistical analysis was performed using 2-way ANOVA and Dunnett's multiple comparisons test. Data are expressed as mean ± SEM of three independent experiments. Results were considered statistically significant if the p-value was < 0.05.

5.4.4. Binding Ability of the N-POMC fragments (1-49 and 1-77) and Adropin to GPR19

N-POMC$_{1-28}$ is not a natural peptide hormone but is described as an extraction artefact (Lowry, 2016) since it had been identified during growth hormone purification from human pituitaries. In this section, we will investigate which other N-POMC fragments, N-POMC$_{1-49}$ and pro-γ-MSH (bovine N-POMC$_{1-77}$), can bind to GPR19. The non-radioactive ligand binding assay was used first to study the binding ability of the cell lines to biotinylated N-POMC$_{1-28}$ and to confirm the finding of the fixed-cell ELISA assay. The specific binding of the cells to the biotinylated N-POMC$_{1-28}$ was determined by treating the cells with serial dilutions of biotinylated N-POMC$_{1-28, \text{ which}}$ is calculated as the total binding. Then, the non-specific binding was determined by treating the cells with unlabelled N-POMC$_{1-28}$ 100-fold more than the biotinylated N-POMC$_{1-28}$ concentrations. Figure 5.8 represents the total, non-specific and specific binding of biotinylated N-POMC$_{1-28}$ in the four cell lines. The non-specific binding shows a linear response with increased concentrations of unlabelled N-POMC$_{1-28}$ and less than 20% of the total binding, which is accepted as good-quality data. The specific binding of the wild-type cell line and the cell line that overexpresses GPR19 (Fig. 5.8 A and B) shows a saturated curve with increasing concentration of biotinylated N-POMC$_{1-28}$. In contrast, the cell lines that are expressing MRAP (Fig. 5.8 C and D) show an increasing response that does not reach a plateau. From the shape of the curve, it is expected to reach saturation if a higher concentration is used. Due to the limitation of the peptide labelling and extraction procedures, unfortunately, we were not able to prepare higher peptide concentrations to perform such an assay.

The data were statistically analysed using 2-way ANOVA and Dunnett's multiple comparisons test and represented in Fig. 5.8 E. Statistically, all the transformed cells with

GPR19, MRAP, GPR19/MRAP showed a significant dose-dependent binding response to the N-$POMC_{1-28}$ in comparison to the wild-type cell line with as low as 0.15 nM N-$POMC_{1-28}$ concentration.

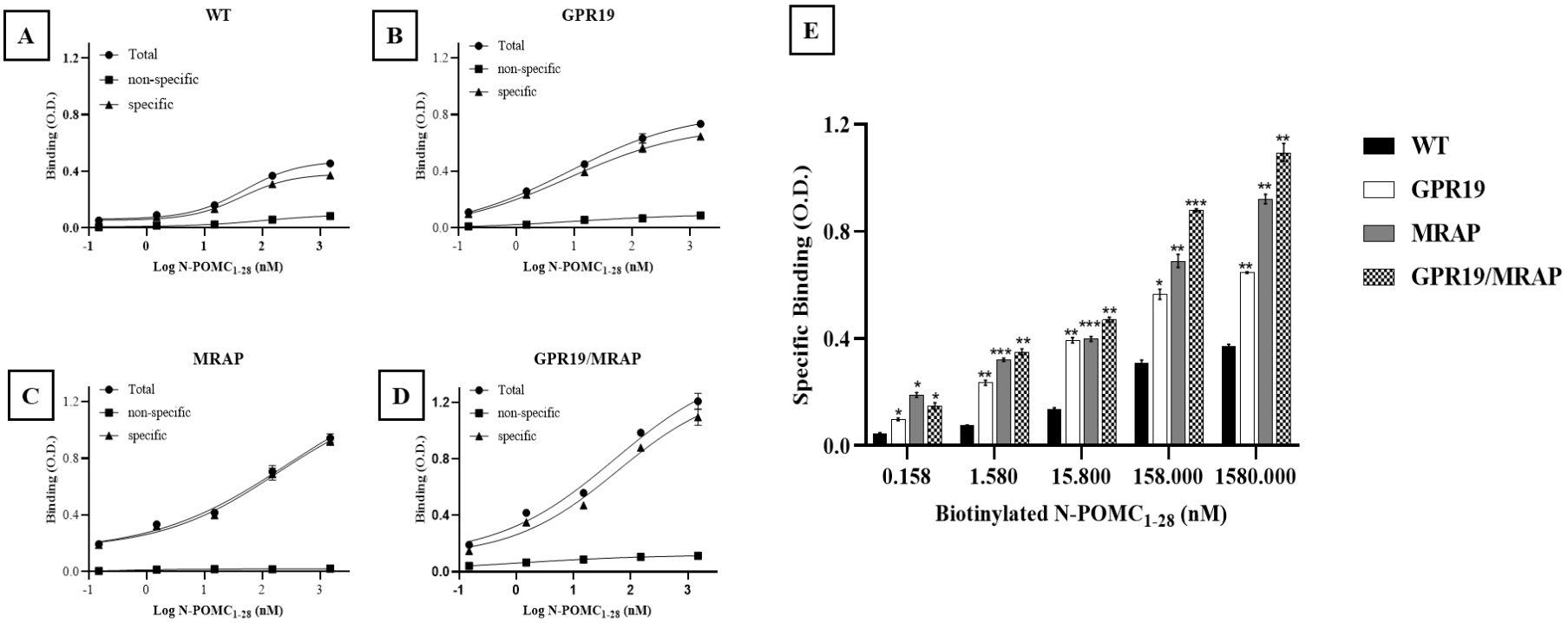

Fig. 5.8. The binding ability of biotinylated N-POMC$_{1-28}$ (optical density at 450 nm, normalised to control) to the WT HEK-293 in comparison to transformed cells with GPR19, MRAP and GPR19/MRAP using the non-radioactive ligand binding assay. Cells were treated with 30 µM Pitstop 2™ solution and then treated with serial concentrations of biotinylated N-POMC$_{1-28}$ starting from 0.15 nM to 1500 nM with 10 times dilution factors. The non-specific binding is determined by treating the cells with unlabelled N-POMC$_{1-28}$, which is 100-fold the concentration of biotinylated N-POMC$_{1-28}$. The biotinylated N-POMC$_{1-28}$ binding is detected using Ultra streptavidin-HRP (N504, Thermo Scientific) at 1:500 dilution in 1% (w/v) BSA in 1X PBS. Statistical analysis was performed using 2-way ANOVA and Dunnett's multiple comparisons test. Data are expressed as mean ± SEM of three independent experiments of three replicates. Results were considered statistically significant if the p-value was < 0.05.

Interestingly, the MRAP-expressing cell lines showed in the three N-POMC$_{1-28}$ binding assays (Fig. 5.6, Fig. 5.7, and Fig 5.8), significant N-POMC$_{1-28}$ binding capacity in comparison to the wild-type cell line. Such an effect of MRAP on the MC2R receptor to increase its ligand, ACTH, binding is reported by Metherell et al. (2005) and Malik et al. (2015), where they found that MRAP is required for full functionality of the ACTH receptor, MC2R. MRAP is required for the translocation of the MC2R to the cell surface and for ACTH to bind to MC2R. In the previous chapter, we demonstrated the role of MRAP in increasing the cell surface expression of GPR19 in the cell lines that express MRAP. Moreover, in the cell line that expresses MRAP without overexpressing GPR19, we found that MRAP increased the GPR19 translocation to the cell membrane without increasing GPR19 cellular expression. This finding suggests that, like the ACTH receptor, the N-POMC receptor GPR19 requires MRAP for cell surface translocation and to increase the affinity of the receptor to its ligand.

The equilibrium dissociation constant (K_d) is the concentration of the ligand that occupies half of the receptors at equilibrium and is calculated from a saturation curve (Maguire et al., 2012). This indicates the affinity of a ligand to its receptor, where if the K_d value is low, only low concentrations of the ligand are required to occupy the receptor, so the affinity is high and vice versa. Statistical analysis using the non-linear regression equation for one-site specific binding (Fig. 5.9) shows that the binding affinity of the transformed cell lines to N-POMC$_{1-28}$ increased in comparison to the wild-type cell line. The cell lines that are overexpressing GPR19 and express MRAP show Kd values of 12.34 nM and 10.62 nM (Fig. 5.9 B and C); respectively, this is two times lower than the K_d value of wild-type cell line (K_d = 24.12 nM, Fig. 5.9 A). In comparison, the transformed cell line with GPR19/MRAP has a K_d value of 7.52 nM (Fig. 5.9 D), which is around two times lower than the K_d value of the cells that overexpress GPR19 and three

times the K_d value of the wild-type cell line. This finding indicates that the expression of MRAP, alone or with overexpression of GPR19, increases the binding affinity of the cells to N-POMC$_{1-28}$.

Comparison of the curves of specific binding clearly indicates that the GPR19 (B_{max} = 0.7511, Fig. 5.9 B) and GPR19/MRAP (B_{max} = 0.9140, Fig. 5.9 D) cell lines contained a significant amount of GPR19 receptor in comparison to the wild-type cell line (B_{max} = 0.3682, Fig. 5.9 A). Interestingly, the cell line that transformed with the MRAP gene showed a similar amount of GPR19 receptor in the cell membrane (B_{max} = 0.835, Fig. 5.9 C) as the cells that overexpressed GPR19, and the cell line that overexpressed GPR19 and MRAP.

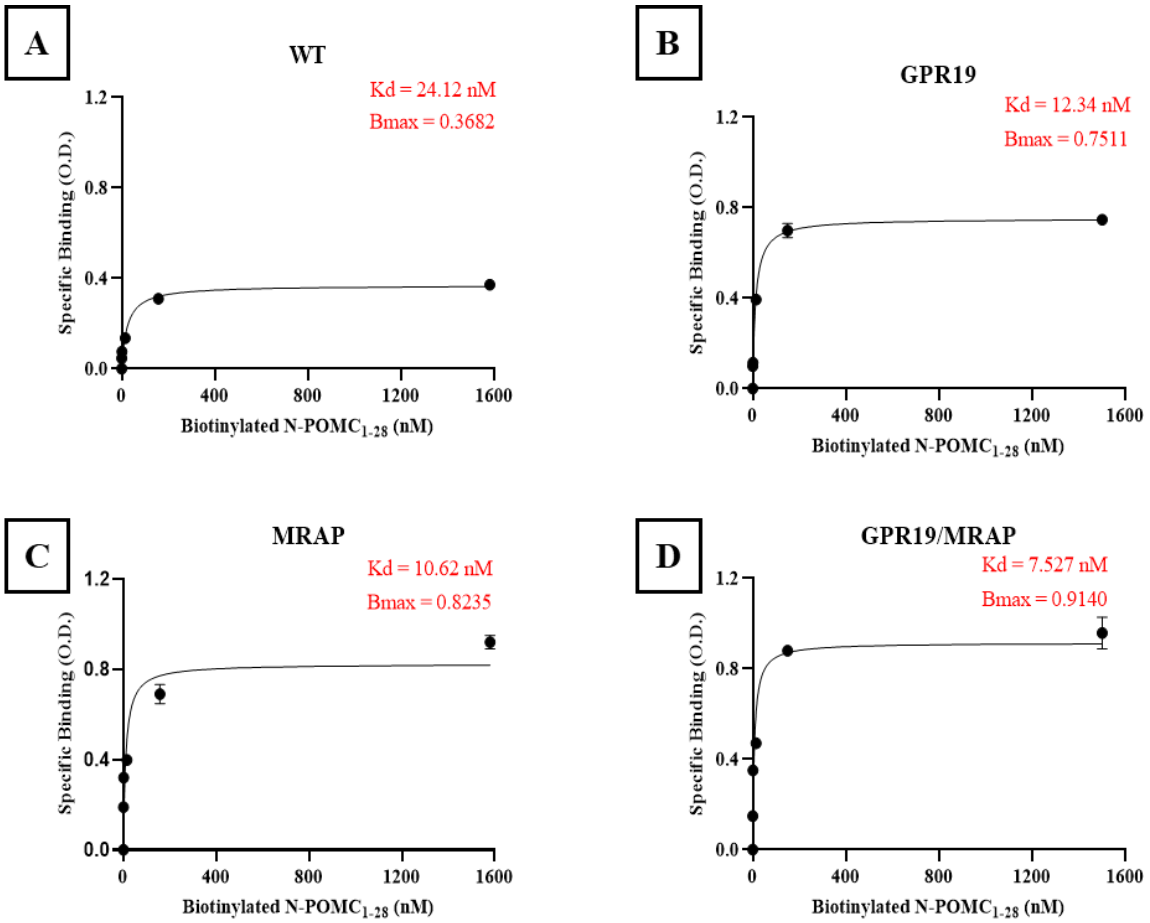

Fig. 5.9. Non-linear regression using one-site specific binding of the specific N-POMC$_{1\text{-}28}$ binding in the four cell lines to calculate K_d and Bmax value.

In the present study, we searched for other N-POMC fragments that could bind to GPR19 using the competitive binding assay against biotinylated N-POMC$_{1-28}$. For the competitive assay, the cells were treated with 15 nM biotinylated N-POMC$_{1-28}$ and a serial dilution of unlabelled N-POMC$_{1-28}$ or N-POMC$_{1-49}$ or N-POMC$_{1-77}$. The optical density (OD) is normalised to the OD of the cells that are treated with 15 nM biotinylated N-POMC$_{1-28}$ alone, which is normalised to 100%. Then, the non-linear regression one-site fit Ki equation is applied to calculate the effect of the addition of unlabelled N-POMC$_{1-28}$, N-POMC$_{1-49}$, and N-POMC$_{1-77}$ on the binding percentage. This model fits the Ki of the unlabelled ligand directly by entering the concentration of biotinylated N-POMC$_{1-28}$ and the K_d value for each cell line as constants, and GraphPad Prism directly fits the Ki of the competitor compound. In general, the results of the four cell lines showed dose-dependent depletion of N-POMC$_{1-28}$ after the addition of either N-POMC$_{1-49}$ or N-POMC$_{1-77}$ (Fig. 5.10).

The four cell lines responded to the inhibition differently, where the wild-type cell line showed around two times more binding affinity (Ki value) to N-POMC$_{1-49}$ or N-POMC$_{1-77}$, respectively, in comparison to N-POMC$_{1-28}$ (Fig. 5.10 A). This result indicates that both N-POMC$_{1-49}$ and N-POMC$_{1-77}$ bind to the same binding site as N-POMC$_{1-28}$. Moreover, the binding affinity for N-POMC$_{1-49}$ and N-POMC$_{1-77}$ increased to 25 and 10, respectively, times more in the cell line that is overexpressing GPR19 (Fig. 5.10 B) in comparison to the affinity of the same cell line to N-POMC$_{1-28}$. Interestingly, the affinity for N-POMC$_{1-49}$ peptide increased dramatically to 29 and 36 times more in the cell lines that are expressing MRAP (Fig. 5.10 C) and GPR19/MRAP (Fig. 5.10 D), respectively, in comparison to the Ki value of N-POMC$_{1-28}$ in the same cell line. Furthermore, the affinity to N-POMC$_{1-77}$ in the cell line that expressed MRAP increased to up to 13 times more than the affinity to N-POMC$_{1-28}$.

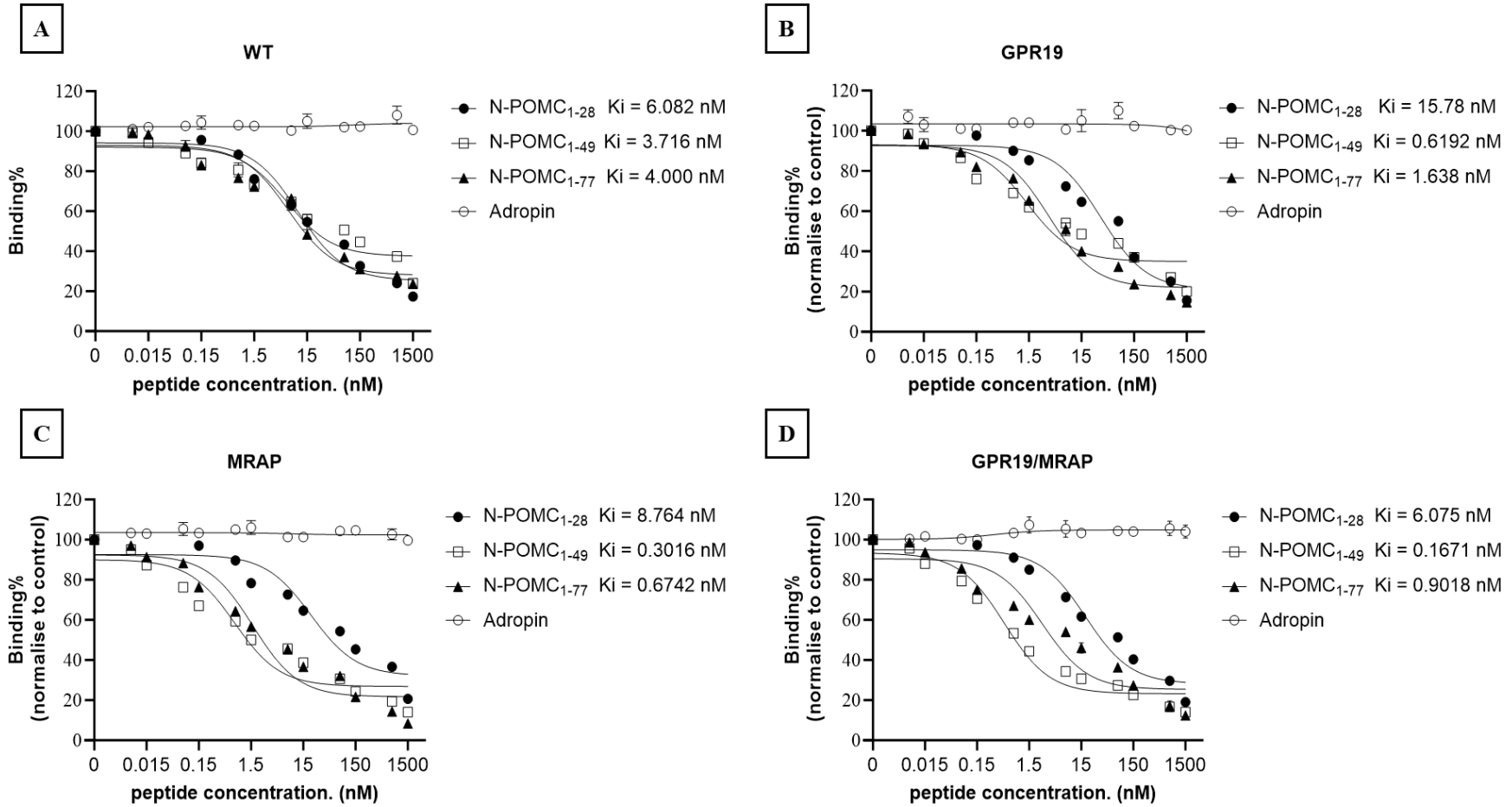

Fig. 5.10. Binding% of the unlabelled N-POMC$_{1-28}$, N-POMC$_{1-49}$, N-POMC$_{1-77}$ and adropin competing 15.8 nM biotinylated N-POMC$_{1-28}$. The Ki value is calculated using the non-linear regression equation one-site Fit Ki value. Data are expressed as the mean ± SEM of three independent experiments of three replicates.

To determine whether adropin, as published by Stein et al. (2016), Jasaszwili et al. (2019), Rao and Herr (2017) and Stelcer et al. (2020) is a possible agonist for GPR19, the cells were treated with serial dilutions of unlabelled adropin to determine whether it could compete with biotinylated N-POMC$_{1-28}$. Surprisingly, the results (Fig. 5.10) show that adropin did not compete with the biotinylated N-POMC$_{1-28}$ peptide in any of the four cell lines. This finding could be explained as either adropin binds to a different receptor other than the N-POMC receptor or it binds to GPR19 at a different site that N-POMC$_{1-28}$ does not bind to. If both bind to the same binding site, it seems that N-POMC$_{1-28}$ is a stronger GPR19 agonist and cannot be competed by adropin.

To our knowledge, no published data have studied the binding ability of adropin to its possible receptor, GPR19. Since HEK-293 cells produce adropin (Ganesh Kumar et al., 2012), treating the cells with unlabelled adropin and then determining the binding ability of this peptide to the cells using an anti-adropin antibody is impractical as it produces a high background in the control samples (data not shown).

Thus, adropin was labelled with biotin, and the biotinylated adropin was used to study its binding ability in the four cell lines using the same protocol as the binding ability of the biotinylated N-POMC$_{1-28}$. The results (Fig 5.11 A, B, C, D) demonstrated a linear specific binding response and not saturable curve as expected, with increasing biotinylated adropin concentrations in all the cell lines. As the calculation of K_d and B_{max} values required a saturation curve (Hulme & Trevethick, 2010), such a statistical analysis cannot be performed with this data. The interesting finding of this assay was that the cell line that was overexpressing GPR19 showed a significant dose-dependent response to the biotinylated adropin in comparison to the wild-type cell line (Fig 5.11 E) after applying 2-way ANOVA and Dunnett's multiple comparisons tests. This finding indicates that the binding ability of adropin increases significantly as the GPR19 expression is increased.

Moreover, it seems that expression of MRAP in the cells prevents the binding of adropin to its receptor, whether it is GPR19 or another receptor, as it gives a non-significant response with the increased adropin concentrations, that could be explained as MRAP converting the GPR19 to be more N-POMC specific receptor.

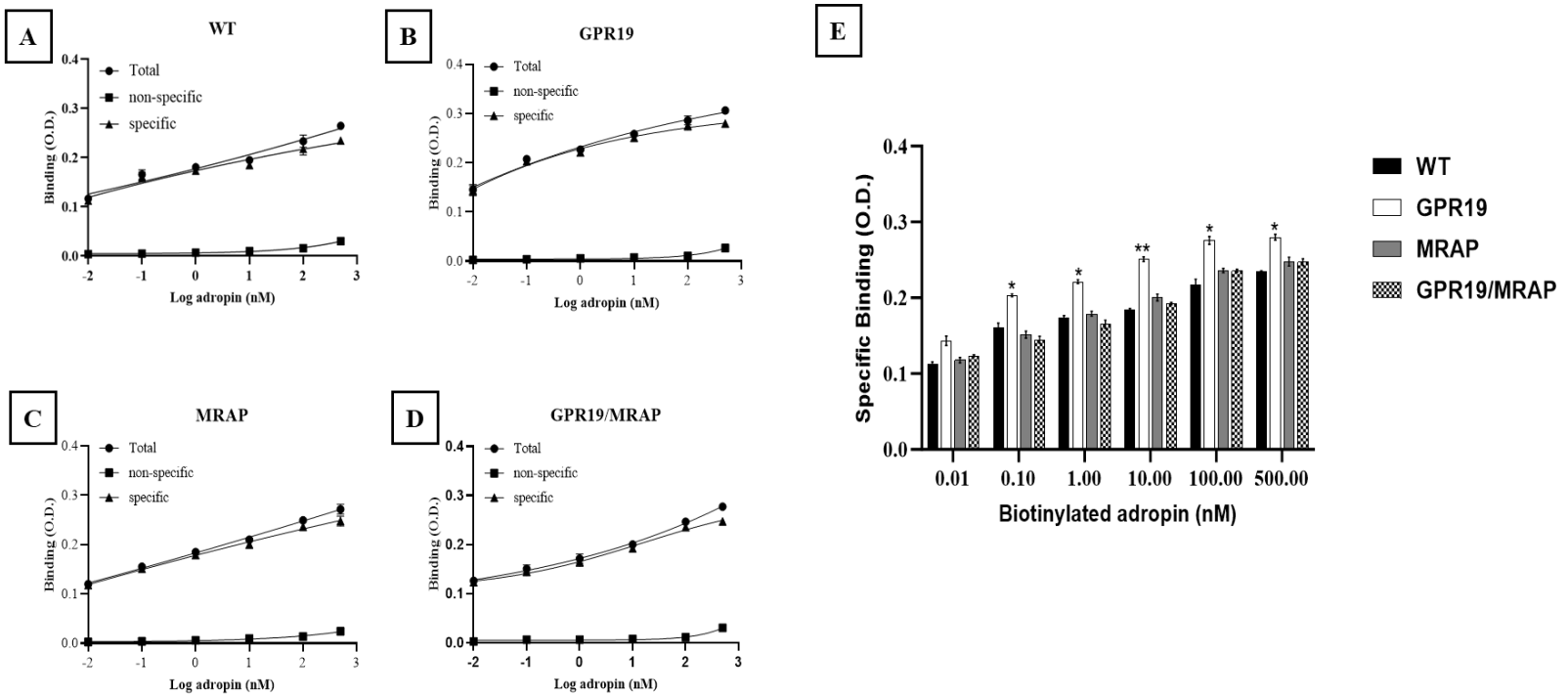

Fig. 5.11. The binding ability of biotinylated adropin (optical density at 450 nm, normalised to control) to the WT HEK-293 in comparison to the transformed cells with GPR19, MRAP and GPR19/MRAP using non-radioactive ligand binding assay. Cells were treated with 30 µM Pitstop 2™ solution and then treated with serial concentrations of biotinylated adropin starting from 0.01 nM to 500 nM. The non-specific binding is determined by treating the cells with unlabelled adropin, which is 100-fold the concentration of biotinylated adropin. The biotinylated adropin binding is detected using Ultra streptavidin-HRP (N504, Thermo Scientific) at 1:500 dilution in 1% (w/v) BSA in 1X PBS. Statistical analysis was performed using 2-way ANOVA and Dunnett's multiple comparisons test. Data are expressed as mean ± SEM of three independent experiments of three replicates. Results were considered statistically significant if the p-value was < 0.05.

This was followed by studying the competitive ability of the N-POMC fragments to biotinylated adropin binding to the cells. The cells were treated with 10 nM biotinylated adropin and a serial dilution of unlabelled N-POMC$_{1-28}$, N-POMC$_{1-49,}$ or N-POMC$_{1-77}$. This was followed by the same detection assay and statistical analysis as the competitive assay of the biotinylated N-POMC$_{1-28}$. As can be seen in Fig. 5.12, all the N-POMC peptides competed with adropin binding from the cells, especially N-POMC$_{1-28}$. The biotinylated adropin binding percentage was reduced by more than 80% with 10 nM of unlabelled N-POMC$_{1-28}$ in all four cell lines. Meanwhile, N-POMC$_{1-49}$ required up to 100 nM, and N-POMC$_{1-77}$ required up to 500 nM to reduce the biotinylated adropin binding percentage by 80%.

It has been shown previously that adropin cannot compete with N-POMC$_{1-28}$ (Fig. 5.10), while N-POMC fragments can compete with adropin (Fig. 5.12) in all the cell lines that were used to perform these experiments. In addition, adropin only showed a significant dose-dependent response in the cell line that was overexpressing GPR19 and not in the cell lines that were expressing MRAP. These results suggest that MRAP converts GPR19 to be an N-POMC receptor rather than adropin. On the other hand, the results cannot confirm if adropin is the GPR19 cognate agonist. Further experiments, such as using a cell line that does not express GPR19, could be used to confirm if GPR19 is acting as an adropin receptor, which is not the aim of this study.

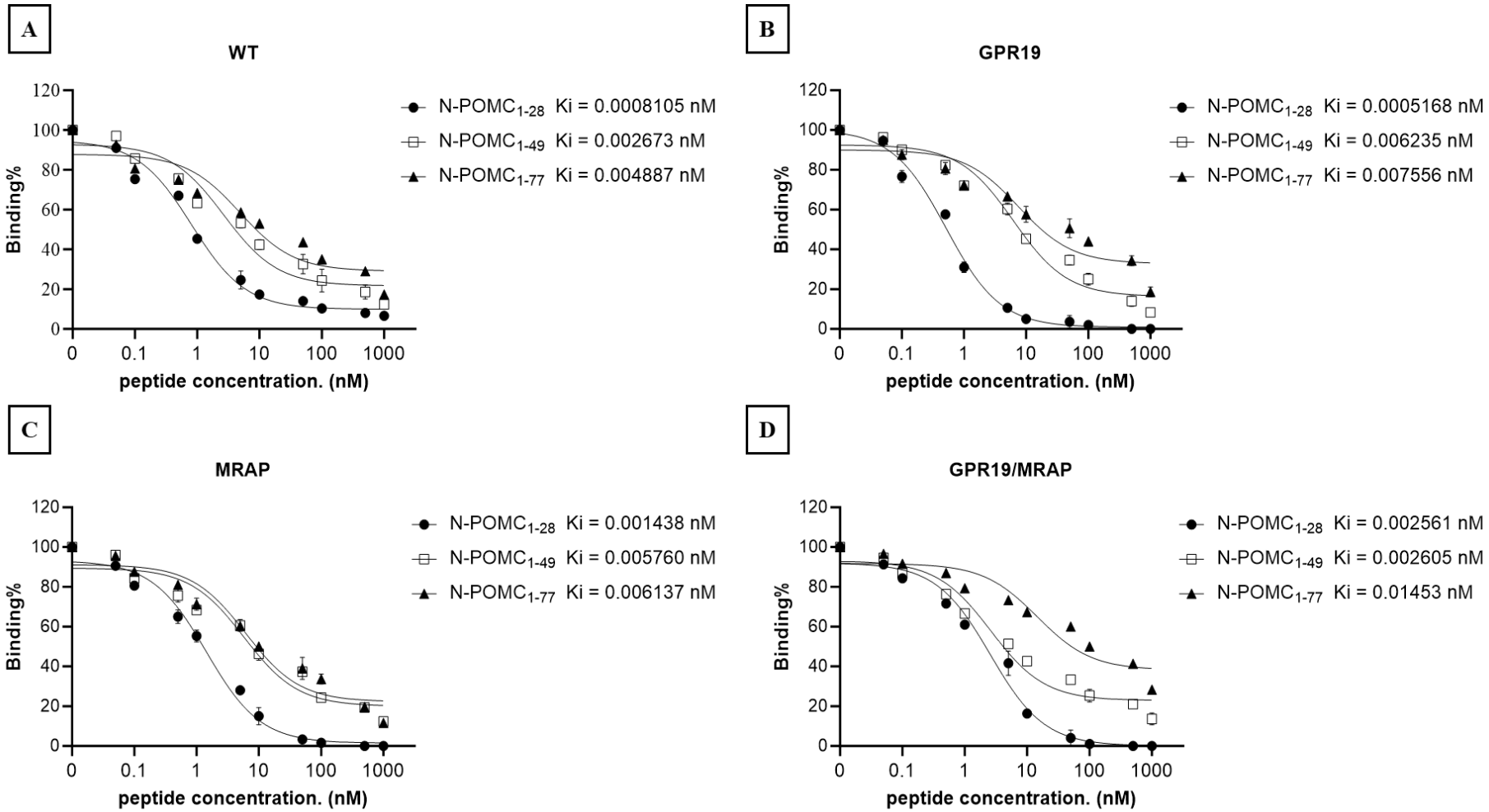

Fig. 5.12. Binding% of the unlabelled N-POMC$_{1-28}$, N-POMC$_{1-49}$ and N-POMC$_{1-77}$ competing 10 nM biotinylated adropin. The Ki value is calculated using the non-linear regression equation one-site Fit Ki value. Data are expressed as the mean ± SEM of three independent experiments of three replicates.

5.5. Discussion

In this chapter, a link between the overexpression of GPR19, the expression of MRAP and the binding of N-POMC to the HEK-293 cell line has been established. Unpublished data from the Bicknell group had identified the receptor GPR19 to be a possible receptor for N-POMC$_{1-28}$ in adrenal cells. In the previous chapter, the ICC images showed that GPR19 and MRAP proteins are co-localised in the cell membrane and inside the cells. Moreover, the Co-IPs results showed GPR19 and MRAP forming a complex, and the GPR19 bands could be precipitated using an anti-N-POMC$_{1-28}$ antibody after treating the cells with N-POMC$_{1-28}$ and using the crosslinker DST.

It has been reported that GPR19 is expressed in numerous distinct regions of the adult and foetal brain (Hoffmeister-Ullerich et al., 2004), specifically in the pituitary and the hypothalamus, where the POMC peptides are processed and secreted. It is also found that GPR19 is expressed in different peripheral tissues (O'Dowd et al., 1996). According to GEPIA (Gene Expression Profiling Interactive Analysis) web server for cancer and normal gene expression profiling based on RNA-seq data, expression of GPR19 in normal human adrenal gland is relatively low in comparison to the brain tissue, 0.37 TPM (transcripts per million) vs 3.79 TPM; respectively, and to adrenal carcinoma, 9.69 TPM. While MRAP1 is strongly expressed in the adrenal gland with 232.78 TPM in comparison to 1.09 TPM for MRAP2. The expression pattern changes dramatically in adrenal carcinoma cells, where the expression of MRAP1 decreased to 12.59 TMP while the expression of MRAP2 increased to 52.08 TPM. The expression pattern of GPR19 and its accessory protein MRAP is of clinical significance in identifying normal adrenal cortex from the adrenocortical carcinoma tissues.

Previous studies have shown the N-POMC fragments 1-28 and 2-54 to be potent adrenal mitogens (Estivariz, Carino, et al., 1988; Estivariz et al., 1982; Fassnacht et al.,

2003; Lowry et al., 1983). Because the pituitary secretes pro-γ-MSH alongside ACTH during the stress response and the growth-promoting activity appears to reside in the N-terminal sequence, a hypothesis was proposed that adrenal growth and mitogenesis were controlled by a post-secretion cleavage of pro-γ-MSH. Bicknell et al. (2001) identified AsP with its expression being limited to the adrenal cortex, mainly in the capsule and zona glomerulosa, which is involved in adrenal growth. They performed several experiments using mouse Y1 adrenal cells to show that the growth of these cells after treating them with pro-γ-MSH is dependent on the expression of this protease. Moreover, they found that AsP cleaves pro-γ-MSH between the amino acid valine 52 and methionine 53 to release the adrenal mitogenic fragment N-POMC$_{1-52}$. It is also suggested that the cleavage may occur after the arginine 49 and result in the generation of N-POMC$_{1–49}$ and Lys-γ3-MSH (50–76 residues in rats) (Harmer & Bicknell, 2005).

It has been reported that the steroidogenesis that takes place in the adrenal gland requires the coordination of several POMC peptides and has been extensively studied since the 1950s. Pedersen et al. (1980) reported that besides ACTH, pro-γ-MSH could activate the HSL enzyme that hydrolyses cholesterol ester to free cholesterol to enter the steroidogenic pathway. Interestingly, they found that administration of the trypsin-treated pro-γ-MSH to hypophysectomised rats was found to result in an increase in adrenal HSL activity and increased steroid hormone secretion in response to ACTH to 130% of the control animals (Pedersen & Brownie, 1980). Al-Dujaili et al. (1981) reported a similar effect where they found that N-POMC$_{1-77}$ could increase the release of both cortisol and aldosterone in rat and human adrenal cells. Torres et al. (2010) showed that administration of modified synthetic N-POMC$_{1-28}$ that lacked the disulphide bridges to dexamethasone-treated rats induces S-phase entry in all zones of the adrenal cortex.

Meanwhile, the synthetic N-POMC$_{1-28}$ with disulphide bridge has a mitogenic effect only in the ZG and ZR, but not ZF, of the adrenal cortex (Mendonca & Lotfi, 2011).

Several studies have been performed to characterise the receptors through which the different POMC peptides act in adrenal growth and steroidogenesis. It has been found that ACTH and MSH peptides, which are produced from the precursor POMC, are selectively binding to a family of G protein-coupled receptors known as the melanocortin receptors (MCRs). ACTH binds specifically to MC2R, and it requires the accessory protein MRAP for full functionality (Metherell et al., 2005; Roy et al., 2007). The melanocortin peptides α-MSH, β-MSH, γ1-MSH, γ2-MSH and γ3-MSH have been reported to have different binding affinities to the MCRs (Denef & Van Bael, 1998). Interestingly, it has been found that the C-terminal fragment of the pro-γ-MSH that is known as γ3-MSH, residue 51–74 in rats, acts through the MC3R receptor (Gantz et al., 1993), and it is the only member of the MCRs that have significant affinity for this peptide in rat adrenal. In addition, they found that ACTH, α-MSH and β-MSH show an agonist activity on the MC3R receptor. Unlike those peptides, N-POMC does not seem to be an agonist of MC3R (Harmer & Bicknell, 2004; Tilemans et al., 1997). Tilemans et al. (1997) reported the role of N-POMC$_{1-74}$ as a paracrine growth factor in the development of lactotrophs, and its action cannot be mediated by γ3-MSH. This data suggested that N-POMC does not act simply as an extended N-terminal form of γ3-MSH and that a specific receptor for N-POMC may exist.

In contrast, a binding study performed by Pedersen and Brownie (1983) reported that N-POMC competed γ3-MSH for an adrenal receptor binding site, which suggests that both peptides occupy the same receptor. Interestingly, in the same assay, they found that the smaller bovine N-POMC fragment (1-36 residues) does not compete with the γ3-MSH. Thus, that raises the possibility that each of the three peptides, the full-length N-

POMC, the N-terminal (residues 1-49) and the C-terminal (residues 51-74 in rat), have physiological roles and act through different receptors.

A study that is performed by Vassilatis et al. (2003) grouped GPR19 with other receptors that are predicted to be activated by peptides. Our data strengthened this finding by successfully demonstrating that the wild-type and the three transformed cell lines showed the binding capacity to N-POMC1-28 either if it is unlabelled, fluorescently labelled or biotin labelled. In these experiments, the internalisation of the plasma membrane receptors was inhibited by incubating the cells with 30 µM Pitstop2™, which will competitively inhibit the clathrin terminal domain to selectively inhibit CME. The cells that were treated with 1 nM Alexa Fluor-488 labelled N-$POMC_{1-28}$ revealed that the binding capacity of the cell lines that overexpressed GPR19, MRAP and GPR19/MRAP to N-$POMC_{1-28}$ is statistically significantly greater in comparison to the WT cell line (Fig. 5.6). Moreover, the cells that overexpressed GPR19/MRAP showed a significant binding capacity in comparison to the other two transformed cell lines with only GPR19 or MRAP. Moreover, the fixed-cell ELISA assay results showed a significant dose-dependent response of the MRAP and GPR19/MRAP cell lines to the unlabelled N-$POMC_{1-28}$ in comparison to the wild-type and overexpressing GPR19 cell lines. Interestingly, similar results have been found when using biotin labelled N-$POMC_{1-28}$. These findings suggested that GPR19 is the associated receptor of N-$POMC_{1-28}$, and the expression of MRAP increases the binding of N-$POMC_{1-28}$ to GPR19. The effect of MRAP on the binding affinity of a ligand to its receptor will be discussed below.

As mentioned earlier, N-$POMC_{1-28}$ is an extraction artefact; therefore, the ability of the longer N-POMC fragments, 1-49 and 1-77, to bind to GPR19 was investigated. In the competitive binding assay, the cells were treated with 15 nM of biotinylated N-$POMC_{1-28}$ and then competed with serial dilutions of unlabelled N-$POMC_{1-49}$ and N-

$POMC_{1-77}$. Generally, both N-$POMC_{1-49}$ and N-$POMC_{1-77}$ competed with N-$POMC_{1-28}$ with the peptide's order of potency at GPR19 as follows: N-$POMC_{1-49}$ > N-$POMC_{1-77}$ > N-$POMC_{1-28}$. Thus, this data concludes that natural and synthetic N-POMC fragments perform their biological function through GPR19.

The role of MRAP (MRAP1 and MRAP2) in modulating the melanocortin receptors' ligand affinity, signalling, and dimerisation has been reported in different species. Chan et al. (2009) reported that both MRAP1 and 2 interacted with all five of the MCRs, and the expression of this accessory protein led to a significant reduction in the cell surface expression of MC4R and MC5R but did not alter the cell surface expression of MC1R or MC3R. Moreover, they noticed a significant reduction in cAMP responses to the ligand NDP-MSH in the cells that co-express the receptor MC4R or MC5R with MRAP1 or MRAP2 or both. Co-expression of both MRAP isoforms with the receptor MC1R or MC3R also leads to a significant decrease in cAMP responses to the same ligand in those cells, and co-expressed of MRAP2 with MC3R shows a similar response.

By contrast, Sebag et al. (2013) reported that the cell surface expression of zebrafish MC4R at the plasma membrane of transfected HEK-293T cells was not changed by zebrafish MRAP2a expression, but it caused up to an 80% decrease in α-MSH binding to MC4R. Expression of MRAP2a did not significantly change the affinity of MC4R for α-MSH, which suggested that MRAP2a reduces ligand binding by decreasing the number of the binding sites but not by altering affinity. In agreement, Asai et al. (2013) found that α-MSH increased PKA activity 5-fold above the basal level in the CHO cells that co-express MRAP2 and MC4R. Moreover, the presence of MRAP2 increased signalling through MC3R at high α-MSH doses. Moreover, the effect of MRAP expression on MC2R activity is addressed by Metherell et al. (2005) and by Malik et al.

(2015). They reported that expression of MRAP is required to bind to MC2R in a correct orientation to be active and to increase cAMP levels after ACTH stimulation.

Recently, MRAPs were also found to regulate the trafficking and activity of other non-melanocortin GPCRs, such as the prokineticin receptors (PKR1 and PKR2) and the Somatostatin receptors (SSTR1- SSTR5). PKRs are expressed in several tissues, including the hypothalamus, and it is reported that these GPCRs are involved in regulating food intake. Chaly et al. (2016) reported that MRAP2 inhibits PKR1 and PKR2 trafficking and signalling *in vitro*. The SSTRs are GPCRs that are activated by the hypothalamic neuroendocrine hormone somatostatin. The SSTR is coupled to Gαi and reduces cAMP levels in cells during activation, as in GPR19. Wang et al. (2022) found that mouse SSTR2 could form heterodimers with SSTR3 and SSTR5, and MRAP1 selectively interacts with SSTR3 and SSTR5 but not SSTR2. Interestingly, they found that expression of MRAP1 inhibited the dimerisation of SSTR2/3 and SSTR2/5. Moreover, the phosphorylation of ERK and the inhibition of cell proliferation were enhanced in the presence of MRAP1. It is clear from those studies that MRAP (1 and/or 2) can regulate multiple GPCRs trafficking and signalling other than MCRs.

Multiple studies have reported that adropin is a proposed agonist of the receptor GPR19, even though a direct interaction could not be confirmed in a de-orphanisation study by Foster et al. (2019). In the non-radioactive ligand binding assay, no saturable binding of biotinylated adropin was detected, and this could be explained as the HEK-293 cell line secreting adropin, and that could compete with the added biotinylated adropin over the binding site. On the other hand, this could be explained as GPR19 not being an adropin receptor and adropin binding to another receptor that exists in the HEK-293 cell line. The low significant dose-dependent increase, which is linear and not saturable as in the case with increased concentration of N-POMC$_{1\text{-}28}$, in adropin binding

capacity in the cell line that is overexpressing GPR19 could be related to the role of GPR19 in increasing the binding affinity of adropin to its receptor, that may form a dimer with GPR19, and that is suppressed by MRAP binding to GPR19. Moreover, adropin shows no ability to compete with N-POMC$_{1-28}$ for the GPR19 receptor binding site, while N-POMC fragments 1-28, 1-49 and 1-77 could compete with biotinylated adropin. In fact, this finding is interesting and could be explained as GPR19 acting as a receptor of both the N-POMC fragments and the adropin due to the similar 3D structure of those peptides, and this is only in the cells that express GPR19 alone while co-expression of MRAP convert GPR19 to be an N-POMC specific receptor. Moreover, those findings suggest that N-POMC is a strong GPR19 agonist, and that could explain why adropin could not compete with the binding of N-POMC$_{1-28}$ while the N-POMC fragments could compete with adropin.

On the other hand, GPR19 could be the only N-POMC receptor, and adropin could bind to another receptor that exists in the cell line used. This adropin receptor might form a dimer with GPR19, and co-expression of MRAP suppresses this dimer formation, like the effect of MRAP expression on SSTR2 that has been reported by Wang et al. (2022). They found that expression of MRAP inhibits the dimerisation of SSTR2 with SSTR3 and SSTR5. The data suggest that MRAP expression may inhibit the dimer formation between GPR19 (N-POMC receptor) and adropin receptor; subsequently, the cell surface expression of the adropin receptor is reduced. This effect is shown as a reduction in the binding capacity of adropin to its receptor, specifically in the cell lines that express MRAP. This idea is supported by the results of Fig 5.11, as the cell lines that express MRAP show less adropin binding capacity than the WT cell line in most of the adropin concentrations that were used. It will be recommended to perform an experiment using a cell line that does not express GPR19, identify the binding ability of the N-POMC

fragments and adropin to this cell line, and confirm whether adropin is binding to GPR19 or not.

Overall, the results reported herein strongly suggest that GPR19 is a peptide receptor, and N-POMC is potentially the endogenous ligand for GPR19. Both adropin and N-POMC shared sequence similarities and had a similar hairpin tertiary structure at their N-terminal sequence. Their similar 3D structures mean these peptides bind to the binding site of GPR19, with N-POMC having a higher affinity for GPR19 than adropin.

Chapter 6: Interactions Between N-POMC-GPR19 and Signal Transduction

6.1. Introduction

6.1.1. GPR19 Signalling Pathway

The GPR19 gene located on human chromosome 12p12.3 region is frequently rearranged in various malignancies (Montpetit & Sinnett, 1999). The gene contains an intron-less open reading frame of 1245 nucleotides, which encode a 415 amino acid protein that has structural similarities to the D2 dopamine receptor and the neuropeptide Y receptor (O'Dowd et al., 1996). It has significant expression during mouse embryonic development, in the central nervous system, and in various peripheral tissues (Hoffmeister-Ullerich et al., 2004; O'Dowd et al., 1996). The hydrophobic analysis of the receptor amino acid sequence revealed that the GPR19 receptor contains three putative glycosylation sites, which is a consensus sequence for phosphorylation by protein kinase C (PKC) in the intracellular loops (O'Dowd et al., 1996).

It has been reported that GPR19 receptor signals by increasing the phosphorylation of protein kinase B (Akt) and the extracellular signal-regulated kinases 1 and 2 (ERK1/2) that are involved in cell cycle progression and cell proliferation (Hossain et al., 2016). The authors identified GPR19 along with 4 other orphan GPCRs to mediate the Akt and ERK1/2 phosphorylation induced by the glycerophospholipids plasmalogens (PIs) to prevent neuronal cell death. This finding has been confirmed by the knockdown of the GPR19 gene and then treating the cells with PIs, which leads to no effect on the levels of phosphorylated ERK in the neuronal cells. Interestingly, they found that overexpression of GPR19 and the other 4 GPCRs increased ERK and Akt

phosphorylation in neuronal and non-neuronal (e.g., HEK-293T) cells compared with the mock group and the signal was enhanced after treating the cells with Pls.

Moreover, Bresnick et al. (2003) reported that the GPR19 receptor signals by decreasing cAMP accumulation. They used the fluorescence resonance energy transfer (FRET) technique to test the signalling mechanism of different orphan GPCR receptors in a calcium-sensitive CHO-reporter cell line and a cAMP-sensitive HEK-reporter cell line. They found that GPR19 did not give a response in either cell line, suggesting that this receptor might be a Gαi-coupled receptor. Moreover, they co-transfected the GPR19-expressing cell line with a plasmid that encodes the chimeric G protein, Gqi5, into the calcium-responsive CHO reporter line. They determined a strong signal in this cell line, which suggests that the GPR19 receptor is linked to inhibiting adenylate cyclase.

Overstimulation of a GPCR due to repeated or continuous stimulation with its agonist leads to its desensitisation as a protective measure, where overstimulation results in cellular toxicity or uncontrolled cellular growth (Magalhaes et al., 2012). Acute or short-term desensitisation occurs over minutes of stimulation and involves phosphorylation of the receptor by GPCR kinases (GRKs) that allows the binding of β-arrestins to the receptor and prevents the G proteins interaction with the GPCR and hence reduce receptor signalling. Long-term desensitisation, also known as downregulation, occurs over ten minutes to hours of GPCR stimulation. GRKs and β-arrestins are responsible for both short-term and long-term desensitisation. Once a GRK phosphorylates a receptor, β-arrestins bind to the receptor with high affinity, which promotes receptor internalisation into clathrin-coated vesicles, its trafficking and degradation in lysosomes and decreased receptor mRNA levels (Rajagopal & Shenoy, 2018; Scott & Laporte, 2019). A study by Southern et al. (2013) observed constitutive

recruitment of β-arrestin to GPR19 and all other studied orphan GPCRs and suggested that this is a common feature of most GPCRs.

6.1.1.1. Adropin Stimulate GPR19 Signalling Pathway

A recent study by Rao and Herr (2017) reported that GPR19 can phosphorylate ERK (1/2) in breast cancer-derived cell lines. They indicated adropin, a peptide hormone expressed in the brain and liver, as the cognate ligand of GPR19. They found that adropin decreases the cAMP accumulation in a dose-dependent manner and leads to a significant increase in ERK1/2 phosphorylation in the GPR19 overexpressing cell line compared to the control cells. Moreover, it has been reported that knockdown of GPR19 led to a significant decrease in the phosphorylation of ERK1/2, along with its downstream target p90 ribosomal S6 kinase (p90RSK) after 72 hrs (Thapa et al., 2018). In the same study, they stimulated H9c2 cells, a cardiac cell line derived from rat atrial tissue, with 0.5 µg/ml adropin and found that it significantly increased ERK1/2 and p90RSK phosphorylation after 24 hrs. The adropin phosphorylation of both the ERK1/2 and p90RSK was completely blocked when the cells were pre-treated with the ERK1/2 kinase inhibitor: U0126.

Similar data has been reported by Stelcer et al. (2020). Instead, they used the adrenocortical carcinoma cell line (HAC15), which expresses both the adropin precursor gene (ENHO) and GPR19, to study the effect of adropin on adrenal steroidogenesis. They found that the cell proliferation via ERK1/2 and Akt pathway was completely inhibited when the HAC15 treated with adropin in the presence of ERK1/2 and phosphoinositide-3-kinase PI3K/Akt inhibitors, U0126 and LY294002; respectively. Moreover, they found that incubation of the cells for 24 hrs in 10^{-8} M adropin, 10^{-7} M ACTH or 25 µM forskolin did not affect the expression of the ENHO and GPR19 receptor genes. In addition, they found that treatment of HAC15 cells with 10^{-8} M adropin for 24 hrs caused a significant

decrease in forskolin-stimulated aldosterone and cortisol secretion in relation to untreated cells. They reported that adropin reduces the secretion of the steroidogenic hormones by decreasing the expression of the *StAR*, the protein that facilitates cholesterol translocation into the inner mitochondrial membrane, and the expression of the side-chain cleavage enzyme complex (*CYP11A1*), that catalyses the transformation of cholesterol to pregnenolone, where both are essential for the first and the rate-limiting step of steroidogenesis; respectively. In addition, they found that the proliferation rate of HAC15 cells incubated with adropin increased significantly after 48 hrs of incubation using flow cytometry involving cell labelling with BrdU and after 50 hrs of incubation using the xCelligence method. In those studies, adropin is considered a possible ligand for GPR19, while the coupling between adropin and GPR19 remains controversial (Foster et al., 2019; Southern et al., 2013).

6.1.2. N-POMC Signalling Pathway

Interestingly, more than forty years ago, studies found that the N-POMC is indirectly involved in adrenal steroidogenesis by activating hormone-sensitive lipase, the enzyme responsible for converting cholesterol ester to free cholesterol and increasing the cholesterol pool for steroid hormone synthesised during stress (Pedersen & Brownie, 1979; Pedersen et al., 1980). Consequently, it has been found that the cortisol and aldosterone output is increased in rat and human adrenal cells if treated with both ACTH and pro-γ-MSH together in comparison to the samples treated with ACTH only (Al-Dujaili et al., 1981). The following studies have shown that N-POMC$_{1\text{-}28}$, with the disulphide bridges in the correct position between cysteine residues 2–24 and 8–20, can stimulate the growth of adrenocortical tumour cells (Fassnacht et al., 2003) while the modified N-POMC$_{1\text{-}28}$ without disulphide bridges prevented atrophy of the adrenal cortex induced by depletion of circulating POMC peptides suggesting that the disulphide bridges

might be important but are not essential for the N-POMC$_{1-28}$ to act as a mitogenic factor (Torres et al., 2010).

Many studies reported that N-POMC$_{1-28}$ elicits its mitogenic effect by activating the mitogen-activated protein kinase (MAPK) cascade: the RAS-RAF-MEK-ERK signal transduction pathway (de Mendonca et al., 2013; Fassnacht et al., 2003; Mattos et al., 2011; Pepper & Bicknell, 2009) which is the same signalling pathway previously reported that the activated GPR19 receptor may signal through. Moreover, administration of N-POMC$_{1-28}$ to dexamethasone-treated rats induces synthesis phase (S phase) entry in all zones of the adrenal cortex (Torres et al., 2010) through the upregulation of cyclins D2, D3, and E that regulate the cell cycle progression from the G1 to S phase (de Mendonca et al., 2013; Mendonca & Lotfi, 2011).

6.1.3. Reporter Gene Assay

The signalling mechanisms following the activation of the receptor GPR19 are not completely understood. The reporter gene system has been widely used to characterise GPCRs to identify their natural ligand (de-orphanisation), intracellular signalling pathways and the transcription factors that it down or up regulates. Activation of a GPCR with a specific ligand alters the levels of the second messengers, e.g., cAMP, IP3, Ca^{2+}, RhoA, and ERK1/2, which in turn activate certain transcription factors. The reporter gene system has a specific response element on its genome in which the stimulus binds to and activates the reporter gene, rather than a cellular gene, that their product can be quantified (Azimzadeh et al., 2017).

The SEAP Reporter System (Clontech Laboratories, Inc. is Takara Bio Company, Japan) was used in this study to quantify the transcriptional activity of GPR19 after N-POMC$_{1-28}$ activation. The profiling vector pSRE-SEAP (Fig. 6.1) is designed to monitor the induction of the MAPK signal transduction pathway, which is widely used in research

to follow cell proliferation and cell cycle differentiation. This vector is designed to provide a direct measurement of the activation of this pathway. As mentioned earlier, the activation of GPR19 leads to ERK1/2 signalling pathway activation that can be assayed using this vector after N-$POMC_{1-28}$ treatment of the cells. This vector contains three tandem copies of the SRE (serum response element) consensus sequence fused to a TATA-like promoter (P_{TAL}) region from the Herpes simplex virus thymidine kinase (HSV-TK) promoter. After the transcription factor binds to the SRE, transcription is induced, and the reporter gene SEAP (secreted placental alkaline phosphatase) is activated.

The SEAP reporter gene encodes a truncated form of the placental enzyme that lacks the membrane anchoring domain, thereby allowing the protein to be efficiently secreted from transfected cells into cell culture media and, therefore, provides many advantages. It allows for the determination of reporter activity without disturbing the cells as it does not require the preparation of cell lysate, as a single set of cultures can be used both for the SEAP assay and for further investigations such as RNA and protein analysis. Moreover, it can be used for kinetic studies by repeatedly collecting culture medium from the same sample (Kain, 1997). SEAP has the unusual properties of being extremely heat stable, and therefore, the endogenous alkaline phosphatase activity can be eliminated by heating the samples at 65°C. SEAP activity can be detected via chemiluminescent or fluorescence detection assay, and the choice between them depends on the fact that the assay should provide a convenient and highly sensitive method for the quantitation of transcriptional activity (Alam & Cook, 2003; Cullen, 2000).

Upstream the SEAP gene, there is a TATA-like promoter (P_{TAL}) region that is essential to provide optimal induction of the reporter gene. The SEAP coding sequence is followed by the SV40 late polyadenylation signal to ensure proper, efficient processing

of the SEAP transcript in eukaryotic cells. Moreover, a synthetic transcription blocker (TB) region is located upstream of SRE, composed of adjacent polyadenylation and transcription pause sites, which is important to reduce the transcription background of the SEAP gene (Groskreutz & Schenborn, 1997). The vector backbone also contains an ampicillin resistance gene for propagation and selection in E. coli.

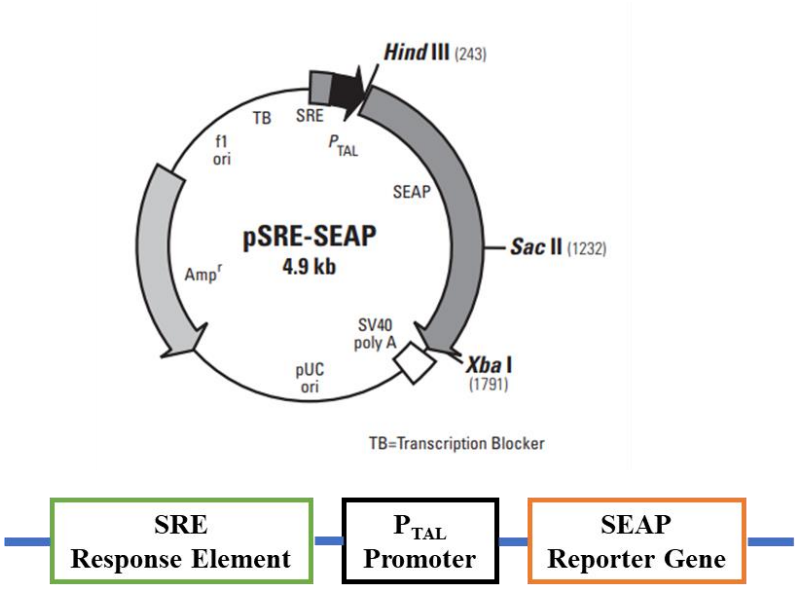

Fig. 6.1. The pSRE-SEAP profiling vector map. This vector contains three tandem copies of the SRE consensus sequence representing the response element fused to a TATA-like promoter (P_{TAL}) region followed by the reporter SEAP gene. The SEAP coding sequence is followed by the SV40 late polyadenylation signal to ensure efficient processing of the SEAP transcript in eukaryotic cells. A synthetic transcription blocker (TB) region is located upstream of the SRE region, which is important to reduce the transcription background. It contains an ampicillin resistance gene for propagation and selection in E. coli. Reproduced from Clontech Laboratories (1999).

It is important to include the proper controls for the transfection and the detection methods before the beginning of the reporter gene experiments, and it is important to use a high-efficiency transfection reagent that is compatible with the cell line being transfected. Moreover, it is critical to perform the experiment in triplicate and subsequently assayed to minimise the variability among experimental groups. It is highly recommended to include an internal transfection control that is co-transfected with the SEAP vector and expresses an activity that can be clearly differentiated from SEAP activity and can be easily assayed. It is used to monitor the transfection efficiency and to ensure that the transfection has worked by measuring its protein level or activity in the cells. The enzyme β-galactosidase is among the most widely used reporter genes as an internal control to normalise the transfection and activity of other reporter genes.

It is also important to include a negative control to determine the uninduced background levels of the reporter gene activity, e.g., SEAP. The pSEAP2-Basic (Fig. 6.2) is a negative control vector that contains the SEAP gene without a promoter or enhancer. It is also acceptable to use the un-transfected cells as a negative control (Kain, 1997). Where the culture medium from the cells that were un-transfected or transfected with pSEAP2-Basic vector is assayed, and the values obtained from such control should be subtracted from the treated cells results.

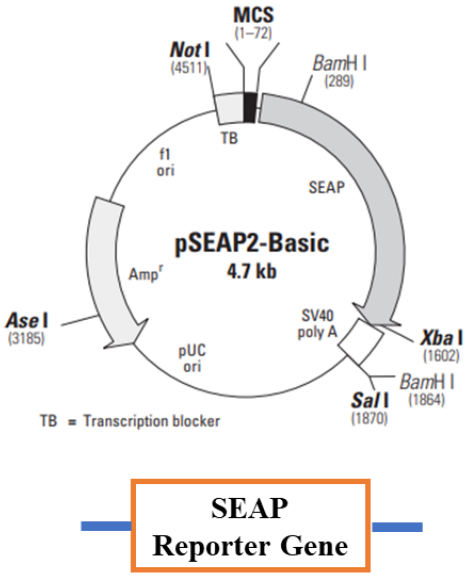

Fig. 6.2. The pSEAP2-Basic negative control vector map. It lacks eukaryotic promoter and enhancer sequences. The multiple cloning site (MCS) allows promoter DNA fragments to be inserted upstream of the SEAP gene. Enhancers can be cloned into either the MCS or unique downstream sites. The transcription blocker (TB) sequence upstream of the MCS reduces the potential read-through of upstream promoters, which are part of the backbone. Reproduced from Clontech Laboratories (2005).

The positive control vector can be used as a transfection positive control where the positive result confirms that the vector transfection is successful. Moreover, it can be used to optimise the detection method (Kain, 1997). The pSEAP2 (Fig. 6.3) is a positive control vector that expresses SEAP in most cell types, which provides an important positive control in most experiments. SEAP is under the control of the SV40 early promoter and the SV40 enhancer. As in the pSRE-SEAP vector, the pSEAP2 contains the SV40 late polyadenylation signal, a synthetic TB, and an ampicillin resistance gene.

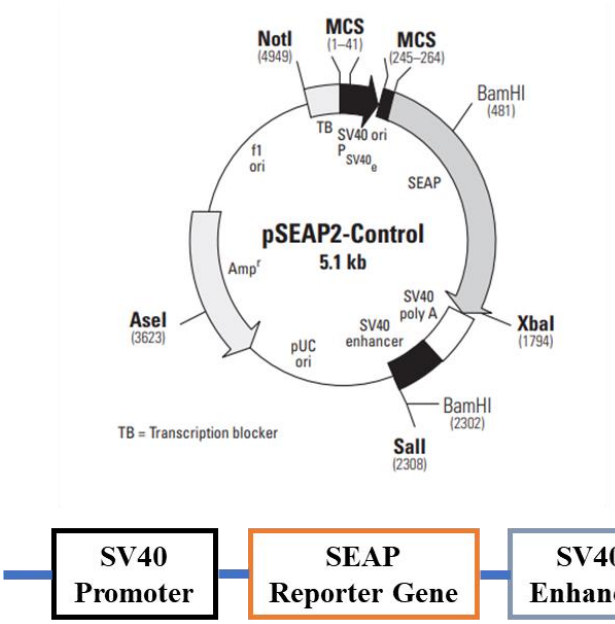

Fig. 6.3. The pSEAP2 control vector map. A positive control vector expressing SEAP under the control of an SV40 early promoter was inserted upstream of the SEAP gene, and the SV40 enhancer was inserted downstream. The SEAP coding sequence is followed by the SV40 late polyadenylation signal to ensure efficient processing of the SEAP transcript in eukaryotic cells. A synthetic transcription blocker (TB), composed of adjacent polyadenylation and transcription pause sites, is located upstream of the multiple cloning site (MCS) to reduce background transcription. It contains an ampicillin resistance gene for propagation and selection in E. coli. Reproduced from Clontech Laboratories (2005).

6.2. Aims

1) To determine the dose-dependent effect of N-POMC$_{1-28}$ and N-POMC$_{1-49}$ on ERK1/2 phosphorylation in the wild-type cell line. Then, identify if the overexpression of GPR19 and/or expression of MRAP could alter the cell response to those peptides. Moreover, to investigate the time-dependent effect of N-POMC$_{1-28}$ on ERK1/2 phosphorylation.
2) To investigate whether N-POMC$_{1-28}$ could induce ERK1/2 phosphorylation using the SRE-SEAP vector in the WT cell line and then study if the overexpression of GPR19 and/or expression of MRAP could alter the cell response.
3) To investigate the effect of treating the cells with 1 nM N-POMC$_{1-28}$ or 1 nM adropin on the cellular cAMP level.
4) To identify N-POMC$_{1-28}$/GPR19 pairing based on potential signalling through the β-arrestin pathway.

6.3. Methods

6.3.1. Detection of Total and Phosphor-ERK1/2

6.3.1.1. Preparation of Cell Lysates

The cells were grown to confluence in 6-well plates, and serum starved for 24 hrs. The first set of cells was treated with different concentrations of N-POMC$_{1-28}$ or N-POMC$_{1-49}$ prepared in 0.1% (w/v) BSA DMEM media, starting from 1 *p*M to 1 nM with 10X dilution factor difference between them. For the time-dependent experiment, the cells were treated with 10 *p*M of N-POMC$_{1-28}$ at different time intervals: 30 sec, 5, 10, 20, 30, and 60 min. As a control, cells were treated with 0.1% (w/v) BSA DMEM media alone and incubated for the same period to confirm that any effect was due to the addition of the N-POMC peptides. After the N-POMC induction of the cells for the appropriate time, the solution was discarded, and the plate was incubated on ice. The cells were washed twice with ice-cold 1X PBS, then scraped into 0.5 ml/well of 1XPBS with two wells combined as one sample and transferred to an ice-cold 1.5 ml microcentrifuge tube. The samples were centrifuged for 5 min at 100 g and 4°C. Then, the pellet was resuspended in 100 µl of 1:100 mixture of Halt Protease and Phosphatase inhibitor Cocktail (Thermo Scientific, USA) and RIPA buffer (Thermo Scientific, USA) and incubated in ice for 30 min and then centrifuged for 15 min at 16,000 g in 4°C. The supernatant was collected, and the protein content was determined using a BCA protein kit assay (Thermo Scientific, USA). To each sample, appropriate volumes of reduced 2X SDS sample buffer (Appendix A.9) and 1X PBS were added to give a final protein concentration of 1 µg/µl. The samples were heated at 94°C for ten minutes, then cooled on ice for at least 5 minutes and either loaded on the SDS-PAGE gel directly following the protocol in Chapter 2, sections 2.16.1, or stored at -20˚C until analysis.

6.3.1.2. Western Blotting

The proteins were transferred to nitrocellulose membrane (0.45µm, Amersham Protran) following the protocol in Chapter 2, section 2.16.2 and membranes blocked with 5% (w/v) dry skimmed milk, dissolved in 1X TBS for 1 hr at RT with agitation. The membrane was washed three times with 1X TBS for 5 minutes at RT and then incubated with primary antibody (Table 6.1 A) in 5% (w/v) BSA in 1X TBST overnight at 4°C. The following day, the membrane was washed in 1X TBS three times and incubated with a secondary antibody (Table 6.1 B) in 5% (w/v) dry skimmed milk in 1X TBST for 2 hrs at RT. Finally, the membrane was washed in 1X TBS three times, 10 minutes each, and the BioRad ECL reagent was used for protein band detection according to the manufacturer's instructions. The membrane was imaged using LI-COR Odyssey.

Table 6.1: The primary and secondary antibodies used for western blotting

Antibody	Dilution Factor
A: Primary Antibodies	
Rabbit anti-p44/42 MAPK (ERK1/2) (#9102, Cell Signalling)	1:1,000
Rabbit monoclonal anti-phospho-p44/42 MAPK (ERK1/2) (Thr202/Tyr204) (#4370, Cell Signalling)	1:2,000
B: Secondary Antibody	
Rec-protein G-peroxidase conjugate (10-1223, Thermo Fisher)	1:4,000

6.3.1.3. Statistical Analysis

The protein band intensity was measured using Image J software. All statistical data analysis was carried out using GraphPad Prism 8.3.1 software. Data is presented as mean ± SEM of three independent experiments. For the dose-dependent experiment, the two-way ANOVA followed by Tukey's multiple comparisons test was used to compare the cell responses to N-POMC fragments. In the time-dependent experiment, multiple t-tests were used to compare the results of one cell line and the two-way ANOVA, followed by Tukey's multiple comparisons test to compare the results of the four different cell lines. Data was considered statistically significant if the p-value was <0.05.

6.3.2. Reporter Gene Assays

6.3.2.1. Transfection of Cells with Plasmids

The cells were cultured in 12 well plates for 24 hrs in serum-containing DMEM (Gibco) growth media to achieve 60-70% confluency. After 24 hrs, the serum-containing media was discarded, and 200 µl/well of transfection mixture was gently pipetted onto the cells and incubated in the incubator at 5% (v/v) CO_2 and 37°C for 5 hrs. The transfection mixture was prepared as follows: for a single well, add 200 µl of serum-free DMEM into a sterile 1.5 ml microcentrifuge tube and 1 µg of pSV-β-galactosidase vector (E1081, Promega, Fig 6.4) with 1 µg of the profiling vector pSRE-SEAP (Cat No. 631901, Clontech Laboratories, Inc.) or 1 µg of the positive control pSEAP2 (Cat No. 631717, Clontech Laboratories, Inc.) and vortex. Then, 4 µl Turbofect® (transfection reagent) was added, vortexed and incubated at RT for at least 15 min. Cells transfected with 1 µg of pSV-β-galactosidase vector alone were used as a negative control to measure the background signal associated with the cell culture media. The transfection reagent was then removed by aspiration, and 1 ml of fresh serum-containing media was added to the cells. After 24 hrs from the start of the transfection step, the cells were serum starved

for 16-18 hrs by discarding the serum-containing media and adding 1 ml of serum-free media.

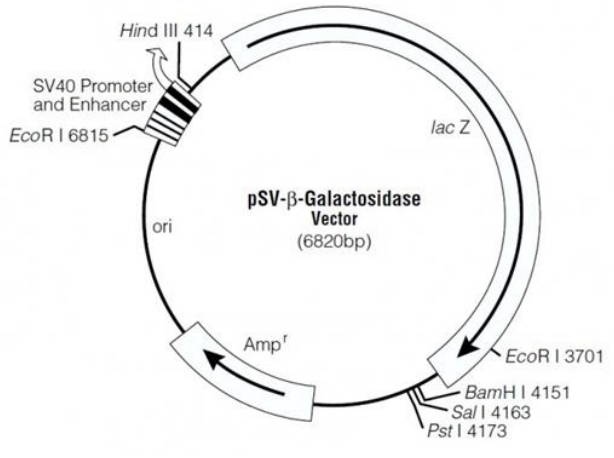

Fig. 6.4. pSV-β-Galactosidase Vector Map used as a transfection control vector.

6.3.2.2. Cells Treatment with N-POMC$_{1-28}$

The media was discarded, and the cells were treated with 200 µl of 1 nM N-POMC$_{1-28}$ prepared in 0.1% (w/v) BSA DMEM and incubated in the 5% (v/v) CO_2 and 37°C incubator for 24 hrs. The control samples were incubated with 200 µl 0.1% (w/v) BSA DMEM. After 24 hrs, 75 µl of the media was collected, and the samples were frozen at -20°C. Those samples were used to measure the alkaline phosphatase (SEAP) activity as described in section 6.3.2.3. To the cells, 200 µl of HBSS was added, and the cells were then scraped and transferred to a prechilled 1.5 ml microcentrifuge tube. The samples were frozen at -20°C and will be used to measure the β-galactosidase activity in the cell samples as in section 6.3.2.4.

6.3.2.3. Alkaline Phosphatase (SEAP) Assay

The media samples were thawed at RT and then centrifuged at 100 g for 5 min. 25 µl of the supernatant was transferred to a 1.5 ml microcentrifuge tube, and 25 µl of alkaline phosphatase (ALP) buffer (Appendix D.1) was added to each sample and mixed thoroughly. The samples were incubated for 30 min at 65°C (using a heating block). The samples were then cooled to RT by placing them on ice for 2-3 min, equilibrated to RT, and then 50 µl samples were transferred to a 96-well plate. The 96-well plate was kept in the spectrophotometer for 10 min at 37 °C. Then, 100 µl of 0.03 mM 4-methylumbelliferyl phosphate (MUP, M6491, Invitrogen) diluted in ALP buffer was added to all the samples. The excitation/ emission (EX/EM) at 355/460 nm was read every 5 min for 60 min at 37 °C.

6.3.2.4. β-galactosidase Assay

The frozen cell samples were thawed on ice and then centrifuged at 100 g for 5 min at 4 °C. The supernatant was discarded, and the pellet was resuspended in 70 µl of 1:100 mixture of Halt Protease and Phosphatase inhibitor Cocktail (Thermo Scientific, USA) and RIPA buffer (Thermo Scientific, USA) and incubated on ice for 30 min. The samples were then centrifuged for 15 min at 16,000 g at 4 °C, and the supernatant was transferred to a prechilled 1.5 ml microcentrifuge tube. In 96-well plate, the samples were diluted as 10 µl sample and 40 µl ddH_2O. Then, 110 µl of the freshly prepared buffer A (Appendix D.2) was added to all the samples and mixed by pipetting. The plate was covered and kept at 37 °C for 10 min. Then, 50 µl of 4 mg/ml o-nitrophenyl-β-D-galactopyranoside (ONPG, #34055, Thermo Scientific) prepared in 100 mM NaH_2PO_4 buffer (pH 7.5) was added to each sample and the absorbance at 420 nm was read every 10 min for 60 min using a plate reader (Molecular Devices).

6.3.3. cAMP Assay

The cells were cultured in 6 well plates for 48 hrs in serum-containing DMEM (Gibco) growth media. After 48 hrs, the cells were serum starved for 24 hrs, then treated with 300 µl of 0.5 mM 3-isobutyl-1-methylxanthine (IBMX) and 5 µM forskolin prepared in 0.1% (w/v) BSA DMEM and incubated for 20 min. After that, the solution was discarded, and the cells were treated with 300 µl of 1 nM N-$POMC_{1-28}$ or 1 nM adropin prepared in 0.1% (w/v) BSA DMEM and incubated for 10 min. The control samples were incubated with 300 µl of 0.1% (w/v) BSA DMEM. Immediately after 10 min, the solution was discarded, and 282 µl of 0.1 M HCl was added, followed by incubation at RT for 20 min. The cells were scraped from the plate, transferred to a microcentrifuge tube, and centrifuged for 15 min at 16,000 g at 4°C. The supernatant was transferred to a prechilled 1.5 ml microcentrifuge tube, flash frozen in liquid nitrogen and then stored at -80 °C freezer until analysis. The cAMP content of the samples was quantified using a cAMP Assay Kit (Competitive ELISA, ab65355, abcam) per the manufacturer's instructions.

6.3.4. β-arrestin Assay Using Fixed-Cell ICC

Cells were cultured in 12 well plates containing 10 µg/ml poly-L-ornithine (Millipore, USA) coated coverslips. After 24 hrs, the media was discarded, and the cells were transfected with the transfection mixture. The transfection mixture was prepared as follows: for a single well, 200 µl of serum-free DMEM was added into a sterile 1.5 ml microcentrifuge tube with 1 µg GFP-beta-arrestin and vortexed. Subsequently, 4 µl Turbofect® (transfection reagent) was added, vortexed and incubated at RT for at least 15 min. The serum-containing media was discarded, and 200 µl/well was gently pipetted onto the cells, followed by incubation for 5 hrs. The transfection reagent was then removed by aspiration, and 1 ml of serum-free media was added to the cells. After 24 hrs of serum starving, the cells were treated with 200 µl of 1 nM N-$POMC_{1-28}$ prepared in

0.1% (w/v) BSA DMEM and incubated for 10 min with 5% (v/v) CO_2 at 37 °C. Control samples were incubated with 200 µl of 0.1% (w/v) BSA DMEM. After 10 min of incubation, the cells were washed with 1XPBS and fixed with 4% (w/v) PFA (Appendix A.6) for 5 min and then washed twice with 0.5 ml 1X PBS. Cells were permeabilised with 0.5 ml of 0.2% (v/v) Tween-20 for 5 min and washed twice with 0.5 ml 1X PBS. Cells were blocked with 10% (v/v) goat serum in 1XPBS for 60 min at RT and then incubated overnight at 4°C with 300 µl mouse anti-EEA1 primary antibody (# 610457, BD Transduction Laboratories™) at 1:200 in 1% (v/v) goat serum in 1X PBS. Coverslips were incubated with 300 µl of goat anti-mouse secondary antibody conjugated to Alexa Fluor-555 (A-21422, Invitrogen) prepared in 1% (v/v) goat serum in 1X PBS for 2 hrs at RT. Then, the cells were washed 3 times with 1X PBS, and the coverslips were mounted in a fluorescent mounting medium without DAPI (Vector Laboratories, Inc, UK). Cells were imaged using a Nikon A1R Confocal Microscope.

6.4. Results

6.4.1. Effect of N-POMC$_{1–28}$ in ERK1/2 Phosphorylation

6.4.1.1. Following ERK1/2 Phosphorylation by Western Blotting

Since N-POMC$_{1–28}$ and N-POMC$_{1-49}$ have been shown in previous studies to increase ERK1/2 phosphorylation (Fassnacht et al., 2003; Pepper & Bicknell, 2009) and the receptor GPR19 signals through the same pathway (Hossain et al., 2016; Rao & Herr, 2017; Stelcer et al., 2020; Thapa et al., 2018) we were interested in identifying if those peptides could also activate this signalling pathway in the HEK-293 cell line. Moreover, we were interested in investigating the effect of overexpression of GPR19 and/or MRAP on the phosphorylation of ERK1/2. To standardise the western blotting detection method, the p44/42 MAPK (ERK1/2) control cell extracts (#9194, Cell Signalling) were used as a positive control for the detection of the total (non-phosphorylated) p44/42 MAPK (ERK1/2) and as a negative control for the detection of phosphorylated p44/42 MAPK (ERK1/2). Figure 6.5 (A) confirms that the used anti-rabbit p44/42 MAPK (#9102, Cell Signalling) antibody can detect both non-phosphorylated and phosphorylated ERK1/2 and the anti-rabbit phospho-p44/42 MAPK (Thr 202/Tyr204, #4370, Cell Signalling) can specifically detect the phosphorylated ERK1/2 (Fig. 6.5 B). This is also used to confirm the size of the detected bands, and any other detected bands could be explained as nonspecific binding.

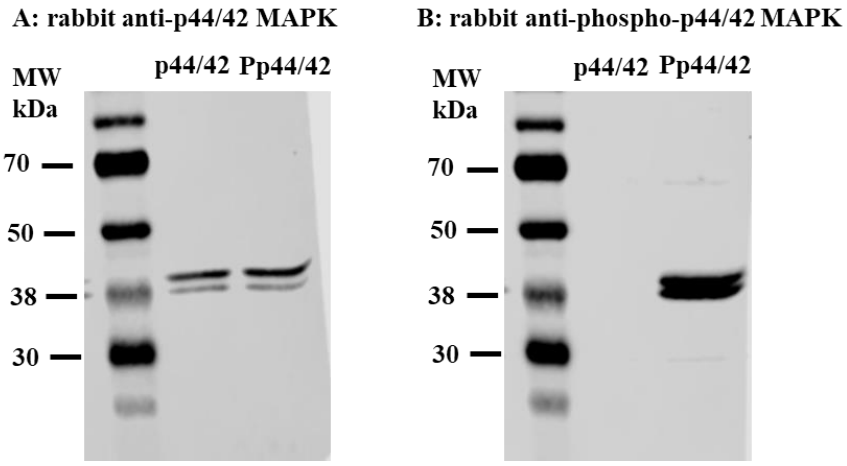

Fig. 6.5. Western blot analysis of non-phosphorylated p44/42 MAPK (ERK1/2) control cell extract to serve as negative control (p44/42) and phosphorylated p44/42 MAPK control cell extract to serve as positive control (Pp44/42) (#9194, Cell Signalling), treated with (A) rabbit anti-p44/42 MAPK (#9102, Cell Signalling) and (B) rabbit anti-phospho-p44/42 MAPK (Thr 202/Tyr204, #4370, Cell Signalling). Rec-protein G-peroxidase conjugate (10-1223, Thermo Fisher) is used as the secondary antibody.

Cells were treated with a serial dilution of N-POMC fragments for 10 min as Fassnacht et al. (2003), and Pepper and Bicknell (2009) reported that the maximum phosphorylation of ERK1/2 after N-POMC fragments, either 1-28 or 1-49, treatment was detected between 10 to 20 min. Then, the ERK1/2 band density was measured using Image J and the phosphorylated ERK1/2 density was divided by the total ERK1/2 density and then normalised to the control where cells were treated by the same media used to dilute the N-POMC fragment, to reveal any stress effect that was caused by the media. Moreover, normalising the results to the control samples of the same cell line showed the effect of overexpression of GPR19 on ERK1/2 phosphorylation, which has been reported by Hossain et al. (2016). The authors reported that overexpression of GPR19 and four other GPCRs in neuronal and HEK-293T cells led to an increase in ERK1/2

phosphorylation in comparison to the cells that did not overexpress this gene. For standardisation, the cells were serum starved for 24 hrs to minimise the levels of endogenous phosphorylated ERK1/2 present in these cells and to make the population of proliferating cells more homogenous before being stimulated with N-POMC peptide.

The results were statistically analysed using one-way ANOVA, and Dunnett's multiple comparisons test was applied to compare the findings of the three independent experiments of the same cell line. The wild-type cell line showed a non-significant increase in the ERK1/2 phosphorylation over the different N-POMC$_{1-28}$ concentrations that were used (Fig.6.6 A). This finding could be explained as the serum starving period (24 hrs), which was used to reduce the basal cellular activity, was not enough. In the reported results by Fassnacht et al. (2003) and Pepper and Bicknell (2009) they serum starved the cells for 36 hrs and 48 hrs, respectively, and they used different cell lines, NCI-h295 and mouse Y1 cell lines, respectively. It is reported that each cell line responds to serum starving differently, and prolonged serum starving causes environmental stress that triggers phosphorylation of ERK1/2 (Pirkmajer & Chibalin, 2011), so for the HEK-293, it is preferred not to increase the serum starving period to more than 24 hrs.

Alternatively, these results could not be related to the serum starving period, and they could reflect the levels of the N-POMC receptor (GPR19) that is present in the cells. Low levels of N-POMC receptor (GPR19) produced a weak and quick response that began and ended before the 10 min, which gave a non-significant result. Probably the last explanation is more reasonable as the cell line that overexpresses GPR19 showed a significant response with N-POMC$_{1-28}$ concentrations 1 *p*M and 10 *p*M (Fig. 6.6. B) while the transfected cell line with MRAP (Fig. 6.6. C) and the GPR19/MRAP cell line (Fig. 6.6. D) that both have high GPR19 expression in the cell membrane in comparison to the

WT cell line as shown in Chapter 3 showed a significant increase in ERK1/2 phosphorylation with 1 *p*M, 10 *p*M and 100 *p*M N-POMC$_{1-28}$ concentrations.

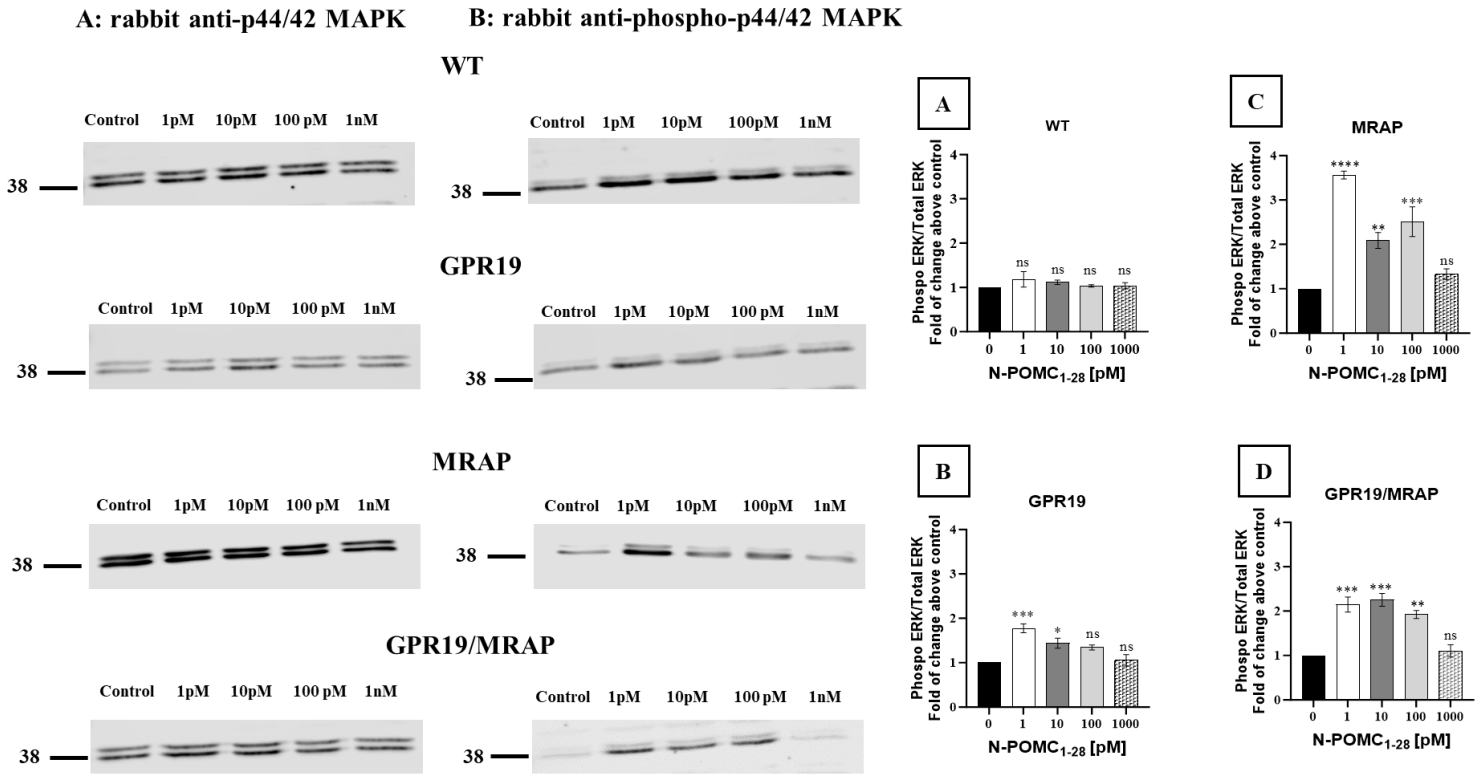

Fig. 6.6. Western blot analysis of total ERK1/2 and phosphorylated ERK1/2 using rabbit anti-p44/42 MAPK and rabbit anti-phospho-p44/42 MAPK, respectively, in HEK-293 (wild-type) and transformed cells with MRAP, GPR19 and GPR19/MRAP. The cells are treated for 10 min with serial dilutions of N-POMC$_{1-28}$ starting from 1 *p*M to 1 nM with 10X dilution factors. The control cells are treated with 1% BSA DMEM media. One-way ANOVA, followed by Dunnett's multiple comparisons test, is used to compare the findings within the same cell line. Data are expressed as mean ± SEM of three independent experiments. Results were considered statistically significant if the p-value was < 0.05. ns: not significant, * p-value > 0.03, ** p-value > 0.002, *** p-value > 0.0002 **** p-value > 0.0001.

The two-way ANOVA followed by Dunnett's multiple comparisons test was applied to compare the responses of the four cell lines to the different N-POMC$_{1-28}$ concentrations. Interestingly, the three transfected cells with GPR19, MRAP and GPR19/MRAP showed a significant increase in ERK1/2 phosphorylation in comparison to the WT cell line when the cells were treated with 1 *p*M N-POMC$_{1-28}$ (Fig. 6.7). At 10 *p*M and 100 *p*M of N-POMC$_{1-28}$ treatment, cells transfected with MRAP and GPR19/MRAP showed a significant response in comparison to the WT cell line. This finding strongly suggests that GPR19 is the receptor of N-POMC as overexpression of this receptor increased the cell response to N-POMC$_{1-28}$, and MRAP plays a role in increasing the sensitivity of the cells to N-POMC.

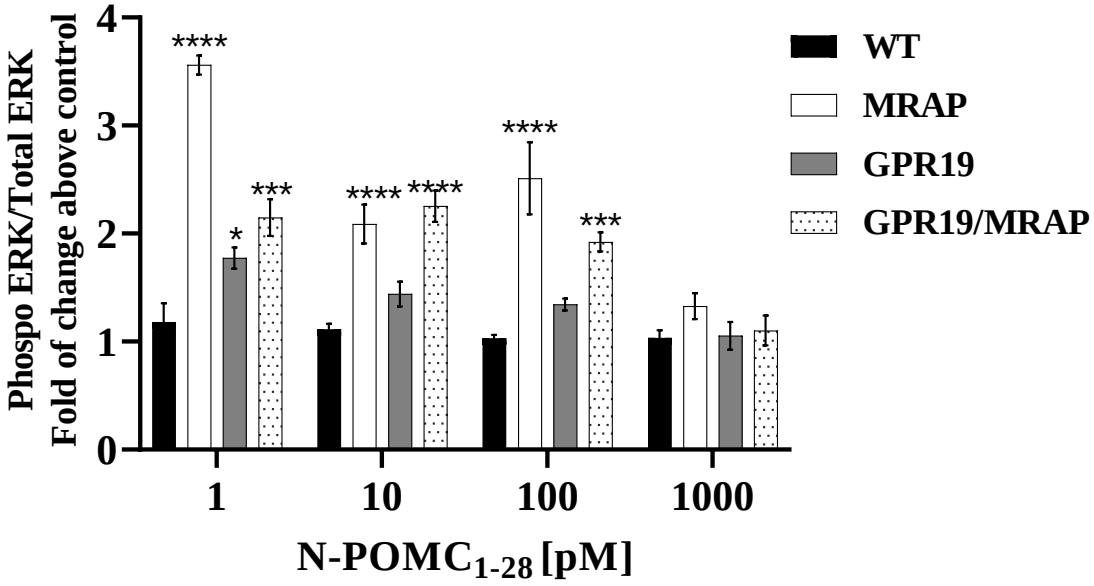

Fig. 6.7. Comparing the dose-dependent treated cells with N-POMC$_{1-28}$ within the four cell lines using two-way ANOVA followed by Dunnett's multiple comparisons tests. Results were considered statistically significant if the p-value was < 0.05. * p-value > 0.03, ** p-value > 0.002, *** p-value > 0.0002, **** p-value > 0.0001.

As mentioned earlier, Pepper and Bicknell (2008) reported that the N-POMC$_{1-49}$ peptide could also activate this pathway in mouse Y1 adrenocortical cell line, and they noticed that the cells show slightly slower response to N-POMC$_{1–49}$ than that observed for N-POMC$_{1–28}$. We were interested in investigating if the WT cell line would show a similar response and if the overexpression of GPR19 and/or MRAP could alter this response. The cells were serum starved for 24 hrs and then treated with serial N-POMC$_{1-49}$ concentrations for 10 min. N-POMC$_{1-49}$ was found to stimulate ERK1/2 phosphorylation in the WT cell line significantly when the cells were treated with 1, 10 and 100 *p*M (Fig. 6.8 A) for 10 min, while this effect was not observed when the WT cells were treated with serial N-POMC$_{1–28}$ concentrations for 10 min (Fig. 6.6 A). Interestingly, the cells that overexpressed GPR19 (Fig. 6.8 B) showed a significant dose-dependent response when treated with N-POMC$_{1-49}$, like the WT cell line.

In contrast, the two cell lines that express MRAP (Fig. 6.8 C and D) show a significant increase in ERK1/2 phosphorylation only at the lowest N-POMC$_{1-49}$ concentration 1 *p*M. When treated with N-POMC$_{1-28}$, there was a significant increase in ERK1/2 phosphorylation at 1, 10, and 100 *p*M. It seems that the cells that express MRAP are more sensitive to N-POMC$_{1-28}$ than to N-POMC$_{1-49}$. The results of the four cell lines were compared using two-way ANOVA followed by Dunnett's multiple comparisons tests (Fig. 6.9), and it shows that the cells overexpressing GPR19 gave a significant increase in ERK1/2 phosphorylation after treatment with 1 *p*M in comparison to the WT cell line. The other two cell lines show either no significant or a lower ERK1/2 phosphorylation in comparison to the wild-type cell line.

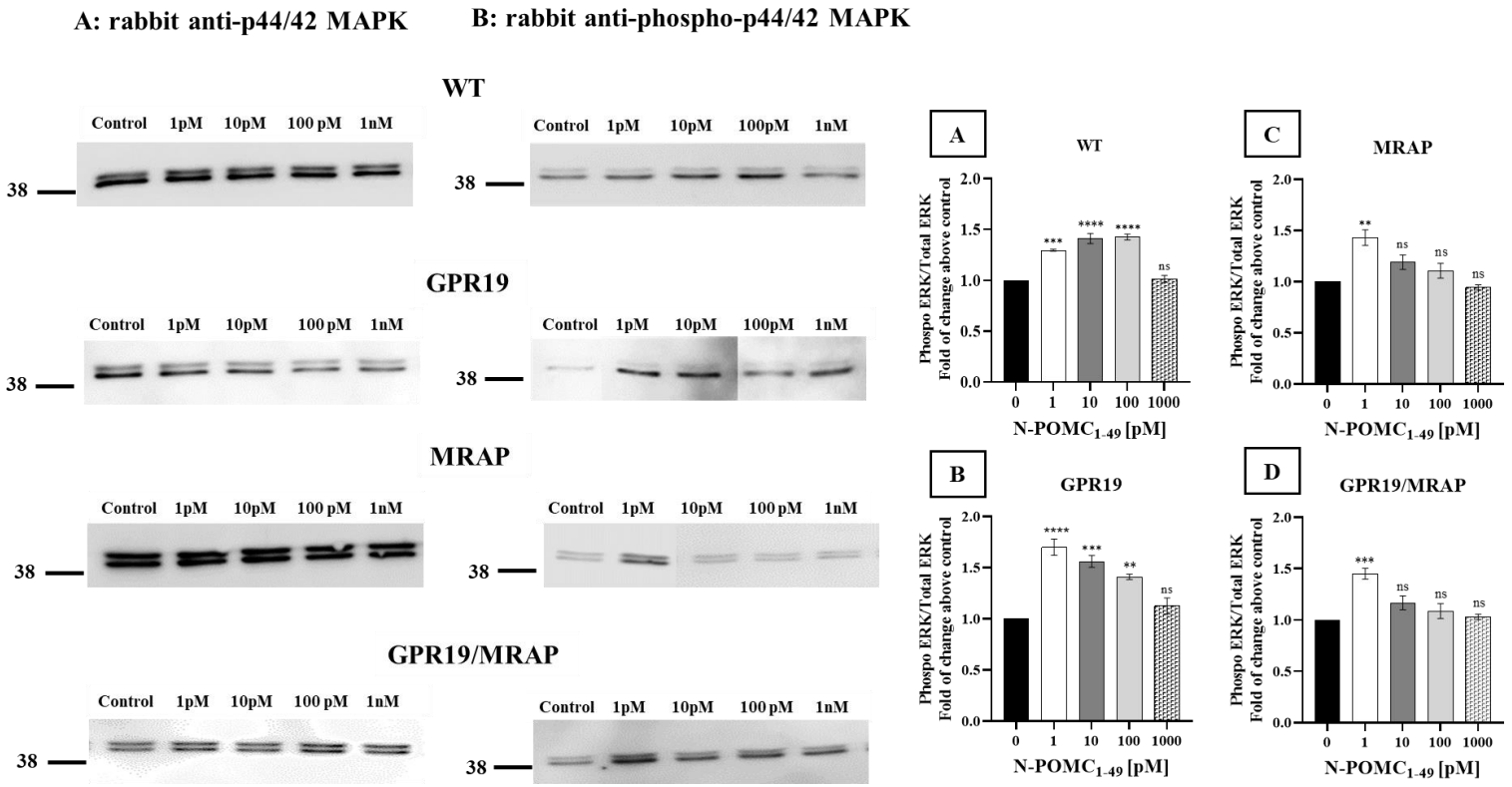

Fig. 6.8. Western blot analysis of total ERK1/2 and phosphorylated ERK1/2 using rabbit anti-p44/42 MAPK and rabbit anti-phospho-p44/42 MAPK, respectively, in HEK-293 (WT) and transformed cells with MRAP, GPR19 and GPR19/MRAP. The cells are treated for 10 min with serial dilutions of N-POMC$_{1-49}$ starting from 1 *p*M to 1 nM with 10X dilution factors. The control cells are treated with 0.1% BSA DMEM media. One-way ANOVA followed by Dunnett's multiple comparisons test was used to compare the findings within the same cell line. Data are expressed as mean ± SEM of three independent experiments. Results were considered statistically significant if the p-value was < 0.05. ns: not significant, * p-value > 0.03, ** p-value > 0.002, *** p-value > 0.0002 **** p-value > 0.0001.

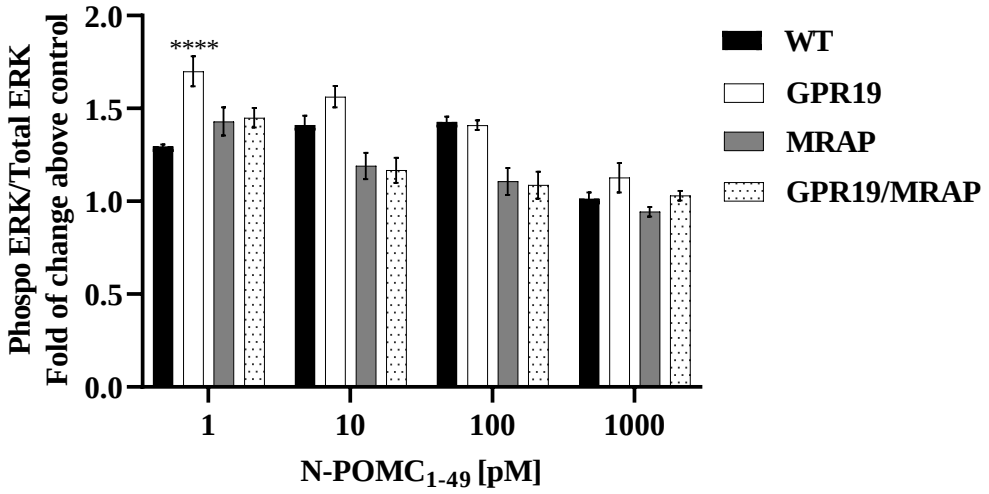

Fig. 6.9. Comparing the dose-dependent treated cells with N-POMC$_{1-49}$ within the four cell lines using two-way ANOVA followed by Dunnett's multiple comparisons test. Results were considered statistically significant if the p-value was < 0.05. * p-value > 0.03, ** p-value > 0.002, *** p-value > 0.0002 **** p-value > 0.0001.

The time-dependent effect of N-POMC$_{1-28}$ treatment on ERK1/2 phosphorylation was then investigated. The cells were treated with 1 *p*M of N-POMC$_{1-28}$, as this concentration shows a significant increase in the ERK1/2 phosphorylation in the three transfected cell lines in comparison to the wild-type cell line in a dose-dependent experiment (Fig. 6.7), for 30 sec, 5, 10, 20, 30 and 60 min. The fold above control of the treated cells with N-POMC$_{1-28}$ for a specific period was compared using multiple unpaired t-tests of three independent experiments. The results of the WT cell line show a significant increase in the ERK1/2 phosphorylation within 5 min of treatment of 1 *p*M N-POMC$_{1-28}$ and returned to the basal level within 10 min (Fig. 6.10). This could explain the non-significant response in the dose-dependent experiment as the signal is ended before 10 min. Moreover, this finding indicates that the HEK-293 responded in a different manner to N-POMC$_{1-28}$ than the Y1 cell line (Pepper & Bicknell, 2009).

Interestingly, the cells that overexpress GPR19 showed a longer response to 1 *p*M N-POMC$_{1-28}$ in comparison to the WT cell line. The signal was at a maximum at the 30 sec time and reduced over time to reach a basal level after 60 min of N-POMC$_{1-28}$ induction (Fig. 6.11). The cells that expressed MRAP showed a longer response to the 1 *p*M N-POMC$_{1-28}$ compared to the cells that overexpress GPR19 but with a different pattern of response over time. ERK1/2 phosphorylation was significantly increased from 30 sec time to reach a maximum at 20 min, after which the signal decreased over time, but it was still significant in comparison to the control cells (Fig. 6.12). The cell line that overexpresses GPR19 and MRAP showed a similar response pattern to the cells that expressed MRAP, with the response slightly faster as the ERK1/2 phosphorylation increased from the 30 sec time and reached a maximum after 10 min, not 20 min as in the MRAP expressing cell line, then start to decrease over time (Fig. 6.13). This result shows that the expression of GPR19 and MRAP changes the response of the cells to N-POMC$_{1-28}$.

Comparing the time-dependent results within the four cell lines using two-way ANOVA followed by Tukey's multiple comparisons test revealed that the cells that express MRAP showed a longer phosphorylation period of ERK1/2 in comparison to the cells that do not express MRAP (Fig. 6.14). This difference in response to N-POMC$_{1-28}$ between the cells that express MRAP and the cells that are not expressing it gives strong evidence that MRAP plays a role in the binding and response of the cells to N-POMC$_{1-28}$.

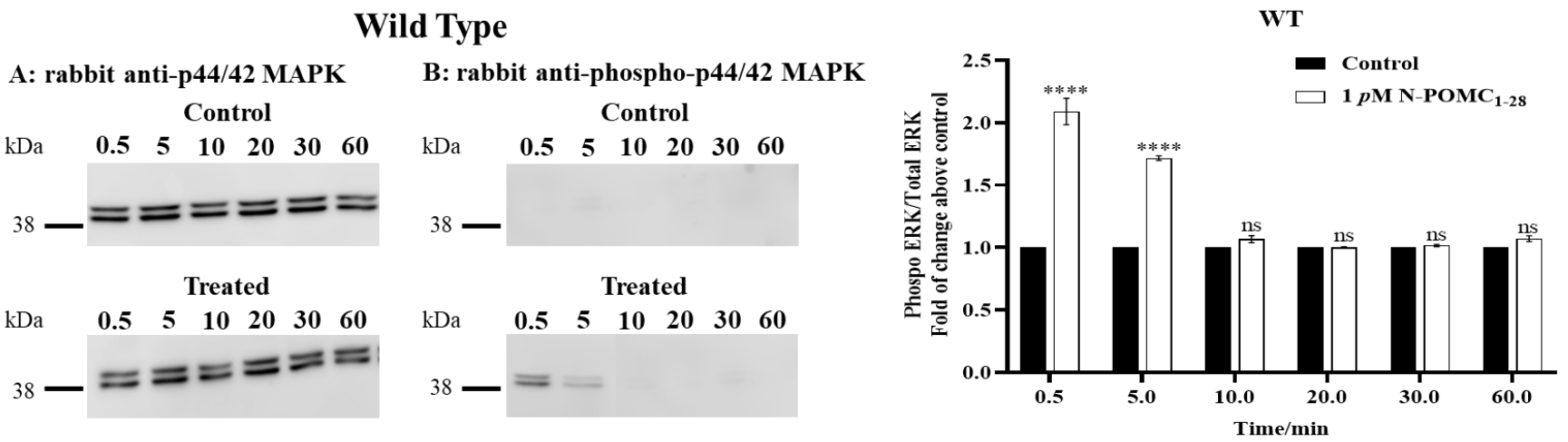

Fig. 6.10. Western blot analysis of total ERK1/2 and phosphorylated ERK1/2 using rabbit anti-p44/42 MAPK and rabbit anti-phospho-p44/42 MAPK, respectively, in HEK-293. The cells were treated with 1 *p*M N-POMC$_{1-28}$ for 0.5, 5, 10, 20, 30, and 60 min. The control cells were treated with 0.1% BSA DMEM media and incubated for the same period as the treated samples. The fold above control of the treated cells with N-POMC$_{1-28}$ was compared using multiple unpaired t-tests. Data are expressed as mean ± SEM of three independent experiments. Results were considered statistically significant if the p-value was < 0.05. ns: not significant, * p-value > 0.03, ** p-value > 0.002, *** p-value > 0.0002 **** p-value > 0.0001.

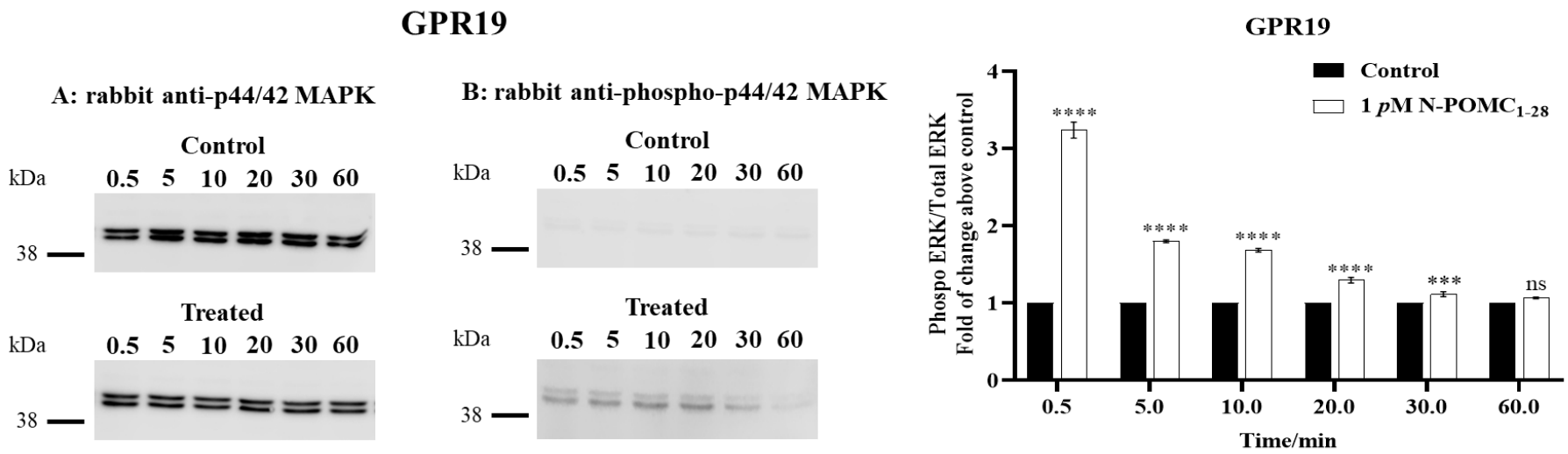

Fig. 6.11. Western blot analysis of total ERK1/2 and phosphorylated ERK1/2 using rabbit anti-p44/42 MAPK and rabbit anti-phospho-p44/42 MAPK, respectively, in HEK-93/GPR19. The cells were treated with 1 *p*M N-POMC$_{1-28}$ for 0.5, 5, 10, 20, 30, and 60 min. The control cells were treated with 0.1% BSA DMEM media and incubated for the same period as the treated samples. The fold above control of the treated cells with N-POMC$_{1-28}$ was compared using multiple unpaired t-tests. Data are expressed as mean ± SEM of three independent experiments. Results were considered statistically significant if the p-value was < 0.05. ns: not significant, * p-value > 0.03, ** p-value > 0.002, *** p-value > 0.0002 **** p-value > 0.0001.

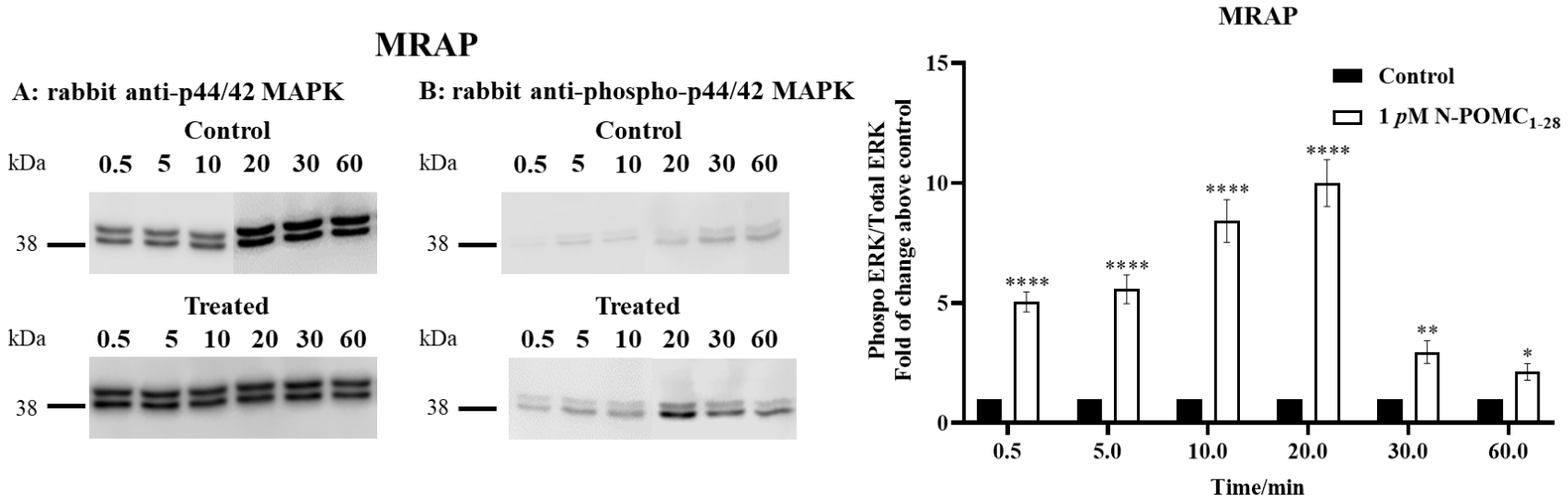

Fig. 6.12. Western blot analysis of total ERK1/2 and phosphorylated ERK1/2 using rabbit anti-p44/42 MAPK and rabbit anti-phospho-p44/42 MAPK, respectively, in HEK-293/MRAP. The cells were treated with 1 *p*M N-POMC$_{1-28}$ for 0.5, 5, 10, 20, 30, and 60 min. The control cells were treated with 0.1% BSA DMEM media and incubated for the same period as the treated samples. The fold above control of the treated cells with N-POMC$_{1-28}$ was compared using multiple unpaired t-tests. Data are expressed as mean ± SEM of three independent experiments. Results were considered statistically significant if the p-value was < 0.05. ns: not significant, * p-value > 0.03, ** p-value > 0.002, *** p-value > 0.0002 **** p-value > 0.0001.

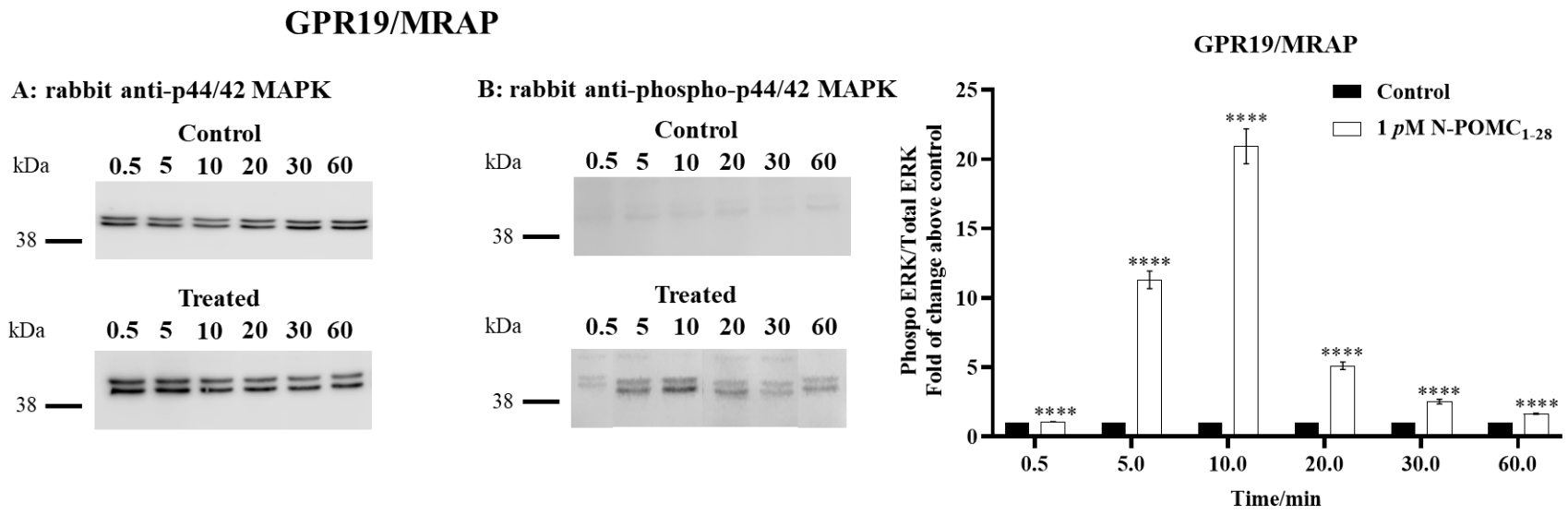

Fig. 6.13. Western blot analysis of total ERK1/2 and phosphorylated ERK1/2 using rabbit anti-p44/42 MAPK and rabbit anti-phospho-p44/42 MAPK, respectively, in HEK-293/GPR19/MRAP. The cells were treated with 1 *p*M N-POMC$_{1-28}$ for 0.5, 5, 10, 20, 30, and 60 min. The control cells were treated with 0.1% BSA DMEM media and incubated for the same period as the treated samples. The fold above control of the treated cells with N-POMC$_{1-28}$ was compared using multiple unpaired t-tests. Data are expressed as mean ± SEM of three independent experiments. Results were considered statistically significant if the p-value was < 0.05. ns: not significant, * p-value > 0.03, ** p-value > 0.002, *** p-value > 0.0002 **** p-value > 0.0001.

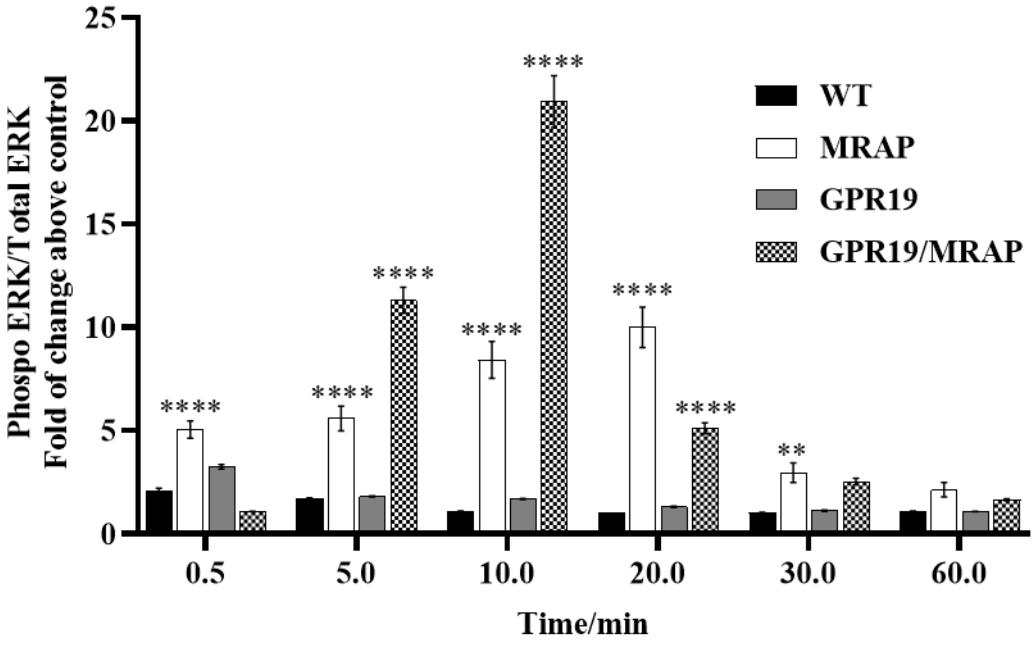

Fig. 6.14. Comparing the time-dependent treated cells with N-POMC$_{1-28}$ within the four cell lines using two-way ANOVA followed by Dunnett's multiple comparisons test. Results were considered statistically significant if the p-value was < 0.05. * p-value > 0.03, ** p-value > 0.002, *** p-value > 0.0002 **** p-value > 0.0001.

6.4.1.2. Determination of Downstream ERK1/2 Phosphorylation Using pSRE-SEAP

In this assay, the reporter vector pSRE-SEAP is used to study the induction of the SRE through the MAPK signal transduction pathway, which is also known as the Ras-Raf-MEK-ERK signal transduction cascade (Roskoski, 2012). This cascade is responsible for the regulation, i.e., activation or inhibition, of various transcription factors and enzymes that are involved in cell adhesion, cell cycle progression, migration, survival, differentiation, metabolism, proliferation, and transcription. In the previous section, it has been confirmed that N-POMC$_{1-28}$ can induce the phosphorylation of the ERK1/2 in the WT cell line and the transfected cells with GPR19, MRAP and

GPR19/MRAP. The activated ERK1/2 will be translocated to the nucleus, where it phosphorylates and activates transcription factors, including Elk1. The phosphorylated Elk1 will then form a complex with a dimer of serum response factor (SRF) to generate a ternary complex. The ternary Elk1-SRF complex binds to SRE, which had been identified as an essential regulatory element of the c-fos proto-oncogene promoter, and thus activates the SRE-controlled *c-FOS* gene that is involved in cell proliferation and division (Thiel et al., 2021; Treisman, 1992; Yang et al., 2013). Therefore, we were interested in investigating if treatment of the cells with N-POMC$_{1-28}$ will lead to the activation of this pathway by following the activity of the reporter gene SEAP that is linked to the response element SRE. Activation of the SRE will activate the synthesis of the SEAP protein that will be subsequently secreted into the cell culture media.

At first, preliminary experiments were performed to standardise the transfection and the detection methods of the SEAP expressing vectors (pSEAP2 and pSRE-SEAP) and the β-galactosidase expressing vector (pSV-β-galactosidase). The WT and GPR19/MRAP cell lines were transfected with the SEAP expressing vectors, one vector at a time, and then co-transfected with the pSV-β-galactosidase to monitor transfection efficiencies of the SEAP vectors for 24 hrs followed with 16-18 hrs of serum starvation to reduce the serum-induced activation of the SRE to a minimum. Cells that were transfected with the pSV-β-galactosidase vector alone were used as a negative control to monitor the background SEAP activity in the cell culture media. The cells were then treated with 0.1% (w/v) BSA DMEM, and 50 µl of the culture media were collected at different time intervals to measure the minimum and the maximum level of SEAP activity that can be detected by the used chemiluminescence assay.

In the Great EscAPe™ SEAP User Manual (Clontech Laboratories, 2005), it is mentioned that the SEAP activity is detectable in the cell culture medium after 12 to 18

hrs of transfection and reaches a maximum level after 48 to 72 hrs of transfection. This means the zero time where the experiment started, after 40 to 42 hrs of transfection, there is SEAP secreted in the culture medium. Therefore, the culture media was discarded, and fresh 0.1% (w/v) BSA DMEM was added to the cells. The zero time was started from this point, and the samples were collected afterwards. The measured SEAP activity was normalised to the β-galactosidase activity and to the protein level of the cells. The results (Fig. 6.15) showed that the SEAP activity reached saturation after 24 hrs of sample collection, which equals 64 to 66 hrs post-transfection, and plateaus after that. Therefore, 24 hrs after treatment was chosen as the time point for studying the effect of N-POMC$_{1-28}$ induction on the cell's SEAP activity. The cells that were transfected with the two vectors pSRE-SEAP and pSV-β-galactosidase and the cells that were transfected with the pSV-β-galactosidase alone showed very low SEAP activity in the culture medium as expected. This means the background activity of alkaline phosphatase present in the culture media can be easily differentiated from the effect of N-POMC$_{1-28}$ induced SEAP activity by having control cells run side-by-side to the treated cells with N-POMC$_{1-28}$. The SEAP activity of the control cells was subtracted from the SEAP activity of the treated cells.

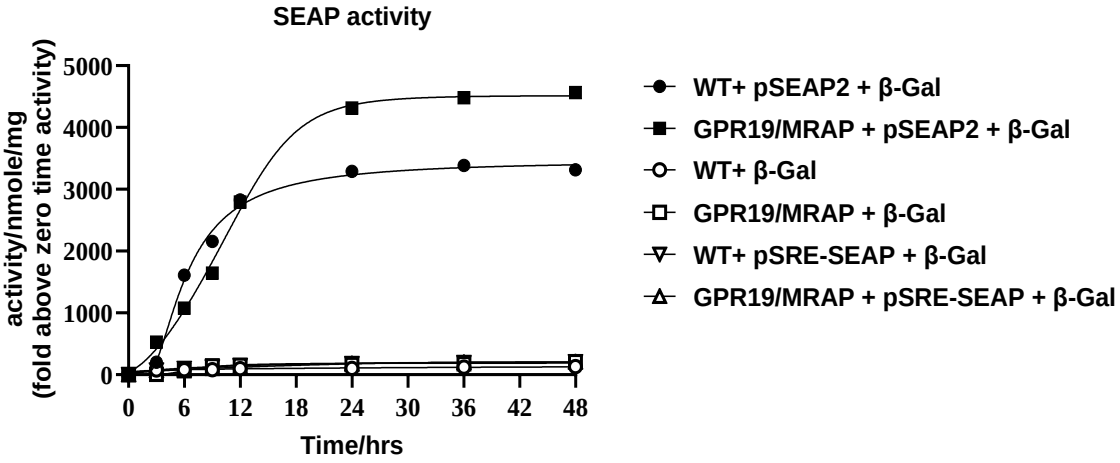

Fig. 6.15. SEAP activity in the WT cell line (HEK-293) and the GPR19/MRAP transfected cell line using the pSEAP2 (Cat No. 631717, Clontech Laboratories, Inc.) as a positive SEAP secreting vector and the profiling vector pSRE-SEAP (Cat No. 631901, Clontech Laboratories, Inc.) that are co-transfected with the pSV-β-galactosidase vector (E1081, Promega). The cells were transfected with the vectors for 24 hrs, then serum starved for 16-18 hrs. The media was discarded, and the cells were maintained in 0.1% BSA DMEM media, and then 50 µl of the media was collected at different time intervals and for 48 hrs. The cells that were transfected with the pSEAP2 vector showed high SEAP activity in the media and reached saturation after 24 hrs of sample collection. The cells that were transfected with the pSRE-SEAP and the pSV-β-galactosidase vector alone, which was used as a negative control, showed very low levels of SEAP activity over time.

The transfection parameters and the detection assays have been optimised, and then the cells were transfected with the pSRE-SEAP and the pSV-β-galactosidase vectors. After serum starving for 16 to 18 hrs, the cells were treated for 24 hrs with 1 nM N-POMC$_{1-28}$, the control samples maintained in 0.1% (w/v) BSA DMEM that was used to prepare the N-POMC$_{1-28}$ solution, and then the samples collected and analysed. As shown in Fig 6.16, the SEAP activity was significantly increased in all four cell lines

above the control samples of the same cell lines. This finding confirms the previous data that N-POMC$_{1-28}$ activates the ERK pathway, which leads to the activation of the transcription factors, which in turn activates the SRE-dependent pathway that will increase cell proliferation and differentiation.

To investigate if the overexpression of GPR19 or MRAP and the overexpression of GPR19 and MRAP together could exhibit an effect on the response of the cells to the N-POMC$_{1-28}$, the results were compared by Two-way ANOVA and followed by Šídák's multiple comparisons test. The results revealed that the cell lines that overexpressed GPR19 (GPR19 and GPR19/MRAP) showed a significant increase in SEAP activity in comparison to the WT cell line. This finding indicates that overexpression of GPR19 increases the sensitivity of the cells to N-POMC$_{1-28}$, which may lead to an increase in cell proliferation. Surprisingly, the cell line that expressed MRAP showed a non-significant response in comparison to the WT cell line. This cell line showed a significant time-dependent increase in ERK1/2 phosphorylation (Fig. 6.14), and it was predicted that the effect of the phosphorylated ERK1/2 that built up inside the cells would increase the stimulation of the downstream transcription factors.

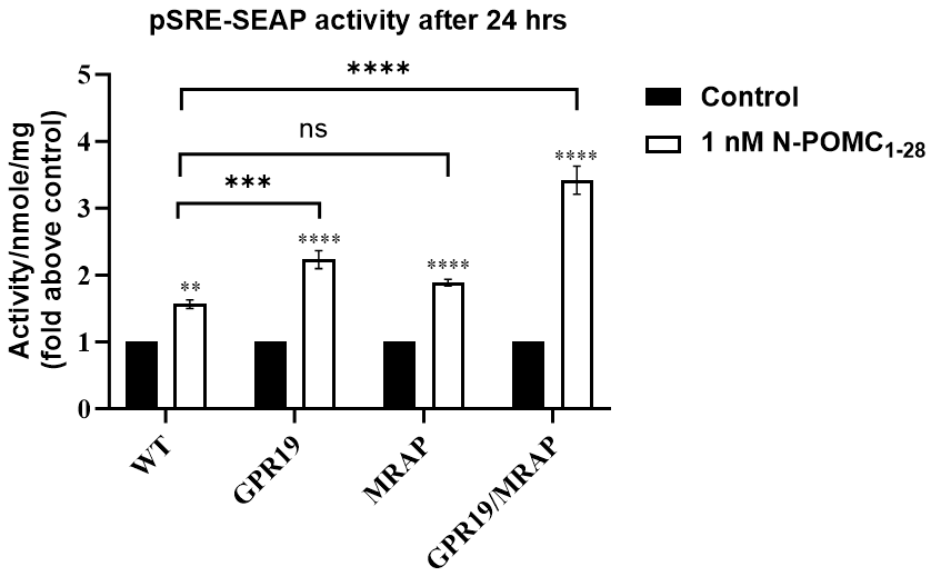

Fig. 6.16. N-POMC$_{1-28}$ induced SEAP expression of pSRE-SEAP vector transiently transfected in WT cell line (HEK-293), GPR19 overexpressing cell line, MRAP expressing cell line and GPR19/MRAP expressing cell line. The cells transfected with pSRE-SEAP (Cat No. 631901, Clontech Laboratories, Inc.) vector and pSV-β-galactosidase vector (E1081, Promega) work as a transfection control vector. After 24 hrs of transfection, the cells were serum starved for 16-18 hrs, then treated with 1 nM N-POMC$_{1-28}$ for 24 hrs. The control samples were treated with 0.1% BSA DMEM. The alkaline phosphatase activity in the media is measured and normalised to the β-galactosidase activity of the cells and to the protein content. Two-way ANOVA followed by Šídák's multiple comparisons test were applied to compare the different cell lines. Data are expressed as mean ± SEM of three independent experiments of three replicates. Results were considered statistically significant if the p-value was < 0.05. ns: not significant, * p-value > 0.03, ** p-value > 0.002, *** p-value > 0.0002 **** p-value > 0.0001.

6.4.2. Effect of N-POMC and Adropin Treatment on cAMP Levels

GPR19 is linked to the inhibitory Gα subunits (Gαi) that, upon activation, suppress adenylyl cyclase activity, resulting in decreased intracellular cAMP levels (Bresnick et al., 2003; Hossain et al., 2016; Rao & Herr 2017). In this study, the cellular cAMP levels were analysed once after treating the cells with N-POMC$_{1-28}$ and adropin to assess their effect on cAMP levels via GPR19. First, the cellular level of cAMP was increased by treating the cells with forskolin and IBMX. Forskolin is a direct activator of adenylyl cyclase that will increase cAMP accumulation inside the cells (Seamon et al., 1981) prior to the treatment of the cells with the GPR19 activators. IBMX is a nonselective inhibitor of cAMP and cGMP phosphodiesterases (PDEs), which are the enzymes responsible for cAMP degradation inside the cells (Beavo et al., 1970). The cAMP levels of the control cells treated with media only were attributed to 100% cAMP levels, and the reduction in cAMP induced by treatment with either N-POMC$_{1-28}$ or adropin, compared to this.

The results demonstrated that stimulation of the cells with N-POMC$_{1-28}$ (Fig. 6. 17) leads to a dose-dependent and time-dependent decrease in the cAMP accumulation in all the cell lines that are used to perform this experiment. In all the cell lines, the cAMP levels reduced between 10% and 20% after 1 min of treatment with 0.1 nM N-POMC$_{1-28}$. In the WT cell line, around 40% reduction of cAMP levels was measured after treating the cells with 10 nM N-POMC$_{1-28}$ for 3 min (Fig. 6.17 A), and this is the lowest percentage that is determined for this cell line over the different N-POMC$_{1-28}$ concentrations and times. The cAMP levels in the cell line overexpressing GPR19 (Fig. 6. 17 B) reduced to more than 50% after 1 min of treating the cells with 10 nM N-POMC$_{1-28}$ in comparison to the control cells and continued to reduce to 70% after 5 min of treatment with the same N-POMC$_{1-28}$ concentration. The cAMP levels in the MRAP (Fig. 6. 17 C) and

GPR19/MRAP (Fig. 6. 17 D) cell lines were reduced from 10% to 40% after treating the cells with serial N-POMC$_{1-28}$ concentrations for 1 min and continued to decrease to around 50% to 60% that of the control over the time.

Interestingly, adropin showed a similar effect on cAMP levels as N-POMC$_{1-28}$, where the cAMP levels were reduced in a dose-dependent and time-dependent manner (Fig. 6.18 A). In the WT cells, adropin seemed to have a larger effect in reducing cAMP levels compared to N-POMC$_{1-28}$ treated cells. Fig. 6.18 A shows that adropin reduced cAMP levels to 40% of the control cells after treating the cells with 10 nM adropin for 1 min, whereas N-POMC$_{1-28}$ reduced it to 20%. Adropin continues its effect on lowering cAMP levels to 70% less than the control samples after 3 min of treatment. The cAMP levels in the GPR19 overexpressing cell lines (Fig. 6.18 B) were reduced to more than 50% after treating the cells for 1 min with 10 nM adropin, and this is the lowest reading recorded for this cell line. From Fig. 6 18 B, we noticed that treatment of the cells for 1 min with different adropin concentrations leads to a reduction in cAMP levels. In contrast, after 3 min, it seems that the cAMP levels have increased again, and that could be explained by the continuous effect of IBMX on the cells as it continues to increase cAMP levels inside the cells (Beavo et al., 1970; Klotz et al., 1977) while the peptide is reducing it. In the two cell lines that express MRAP (Fig. 6 18 C and D), the cAMP levels reduced between 20% and 40% over time with different adropin concentrations. It seems that expression of MRAP slows the response of the cells to adropin as the cAMP levels in the WT cell lines reduced to 70% after treating the cells with 10 nM adropin for 3 min (Fig. 6.18 A).

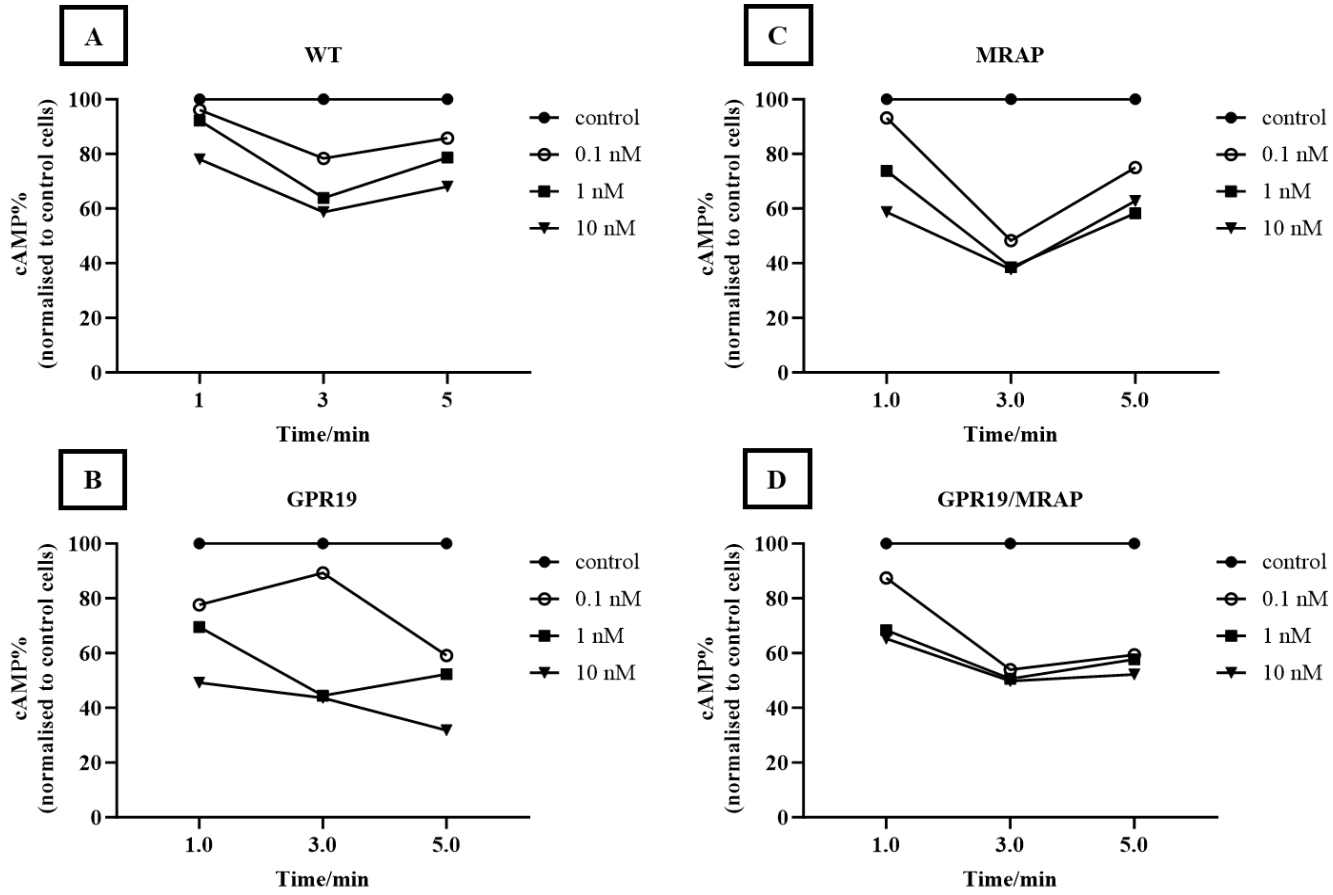

Fig. 6.17. cAMP% of the cells treated with N-POMC$_{1-28}$. The cells were treated with 0.5 mM IBMX and 5 µM forskolin to increase cAMP levels inside the cells for 20 min. Then, the cells were treated with 0.1, 1, and 10 nM N-POMC$_{1-28}$ for 1, 3 or 5 min. The control cells are incubated with 0.1% BSA DMEM media for the same time as the treated samples. The results of the control samples were assumed to be 100% cAMP, and based on that, the effect of the different N-POMC$_{1-28}$ concentrations on cAMP reduction over time was calculated. This experiment was only performed once.

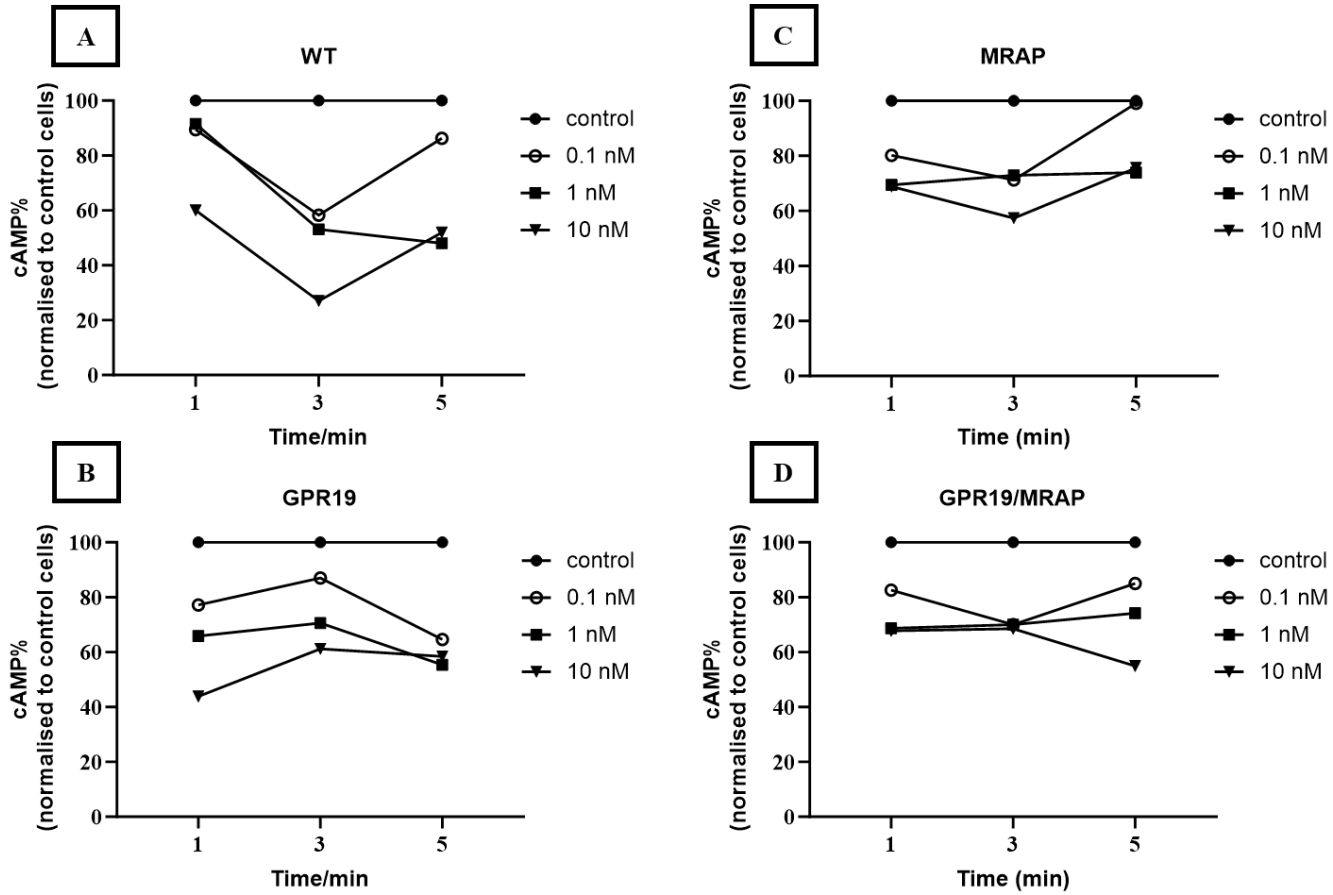

Fig. 6.18. cAMP% of the cells treated with adropin. The cells were treated with 0.5 mM IBMX and 5 µM forskolin to increase cAMP levels inside the cells for 20 min. Then, the cells were treated with 0.1, 1, and 10 nM adropin for 1, 3 or 5 min. The control cells were incubated with 0.1% BSA DMEM media for the same time as the treated samples. The results of the control samples were assumed to be 100% cAMP, and based on that, the effect of the different adropin concentrations on cAMP reduction over time was calculated. This experiment was only performed once.

6.4.3. GPR19 β-arrestin-dependent Signalling

It has been reported that β-arrestins are recruited to activate GPR19 (Southern et al., 2013). The classical function of β-arrestins is to bind to a phosphorylated GPCR, which either leads to desensitisation of the receptor due to hindered interaction with heterotrimeric G proteins or results in receptor internalisation. Once a GPCR is internalised, it either recycles back to the plasma membrane or is sorted for degradation via the endosome-lysosome pathway (Smith & Pack, 2021). To test whether β-arrestin regulates agonist-promoted GPR19 degradation, the cells were transiently transfected with GFP-tagged β-arrestin. The early endosome antigen-1 (EEA-1), which is exclusively localised in the early endosome (Wilson et al., 2000), was used to assess the co-localisation of β-arrestin in the early endosomes to confirm the recruitment of β-arrestin in GPR19 degradation due to N-POMC$_{1-28}$ activation. Fig. 6.19 shows the localisation of the GFP-tagged β-arrestin, and EEA-1 in the control and 1 nM N-POMC$_{1-28}$ treated HEK-293 cell line. Unexpectedly, the images of the control cells (Fig. 6.19 A) showed high levels of EEA-1 co-localised with the GFP-tagged β-arrestin. To evaluate if treating the cells with N-POMC$_{1-28}$ could change the co-localisation of those two proteins, the cells were treated with 1 nM N-POMC$_{1-28}$ for 10 min then the co-localisation between the two proteins was determined.

The same results were detected (Fig. 6.19 B), which led to the modification of the sample preparation protocol. Serum starving influenced the cell signalling pathways, and therefore, the serum starving period was reduced to 6 hrs rather than 24 hrs or no serum starving, but this produced similar results (images not shown). The experiment was performed on a different cell line, the GPR19/MRAP cell line, with 0 hrs, 6 hrs, and 24 hrs serum starving. Similar results were detected in all the conditions. The images of serum-starved GPR19/MRAP cells for 24 hrs are shown in Fig. 6.20. It revealed that both

the GFP-tagged β-arrestin and the EEA-1 were co-localised in both the control and treated cells. The retention of the inserted GFP-tagged β-arrestin on early endosome suggests its role in the endocytosis or degradation of other receptors.

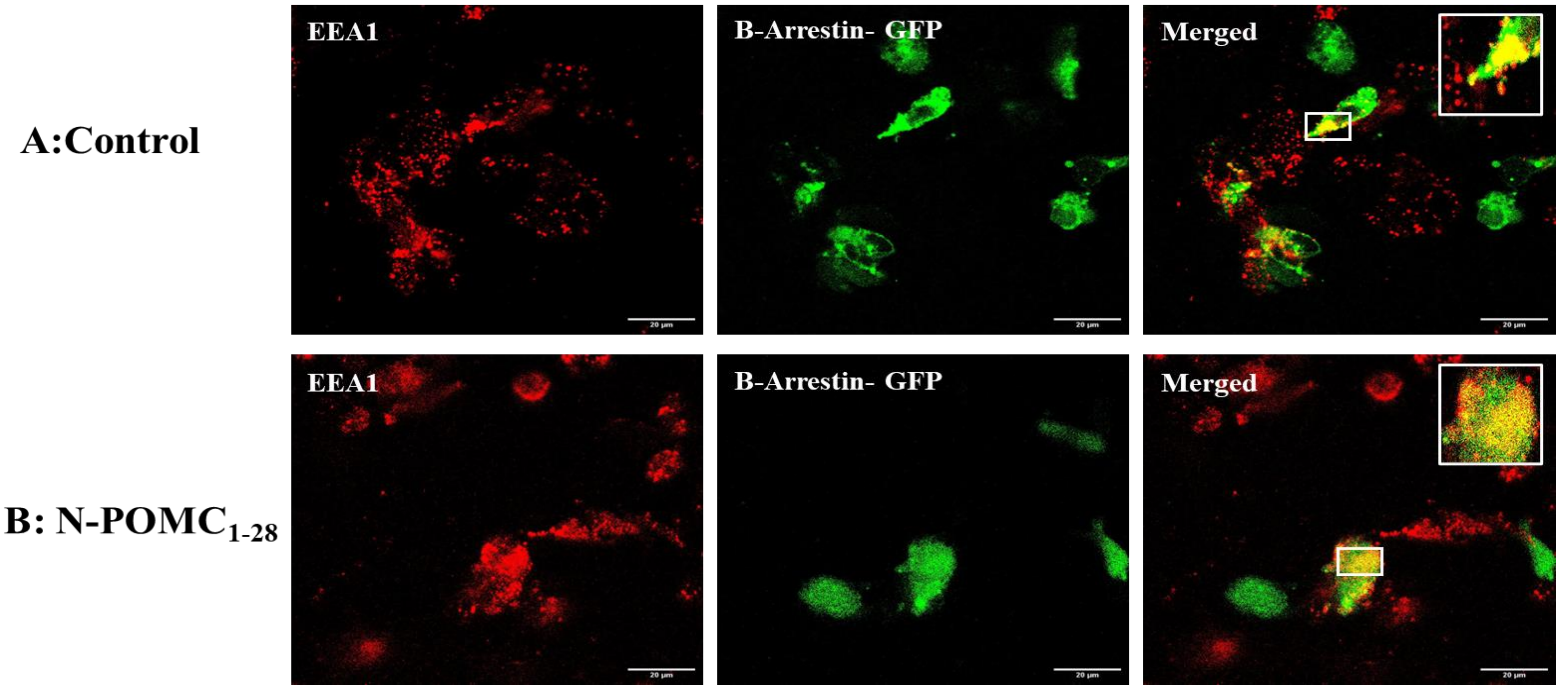

Fig. 6.19. Co-localisation of GFP-tagged β-arrestin and EEA-1 in the WT (HEK-293) cell line. The cells were transiently transfected with GFP-beta-arrestin, and then serum starved for 24 hrs. The cells were treated with 1 nM N-POMC$_{1-28}$ prepared in 0.1% BSA DMEM and incubated for 10 min, and the control cells were incubated with 0.1% BSA DMEM. The cells were fixed with 4% (w/v) PFA for 5 min and permeabilised with 0.2% (v/v) Tween-20 for 5 min. Cells were blocked with 10% (v/v) goat serum in 1X PBS for 60 min at RT and then incubated overnight at 4°C with mouse anti-EEA1 primary antibody (cat. 610457, BD Transduction Laboratories™) at 1:200 in 1% (v/v) goat serum in 1X PBS. The next day, the coverslips were incubated with 300 µl of goat anti-mouse secondary antibody conjugated to Alexa Fluor-555 (A-21422, Invitrogen) prepared in 1% (v/v) goat serum in 1X PBS for 2 hrs at RT. Then, the cells were mounted in a fluorescent mounting medium without DAPI (Vector Laboratories, Inc, UK). Images taken with a Nikon A1 Plus confocal microscope using NIS Elements software. Scale bar = 20 µm.

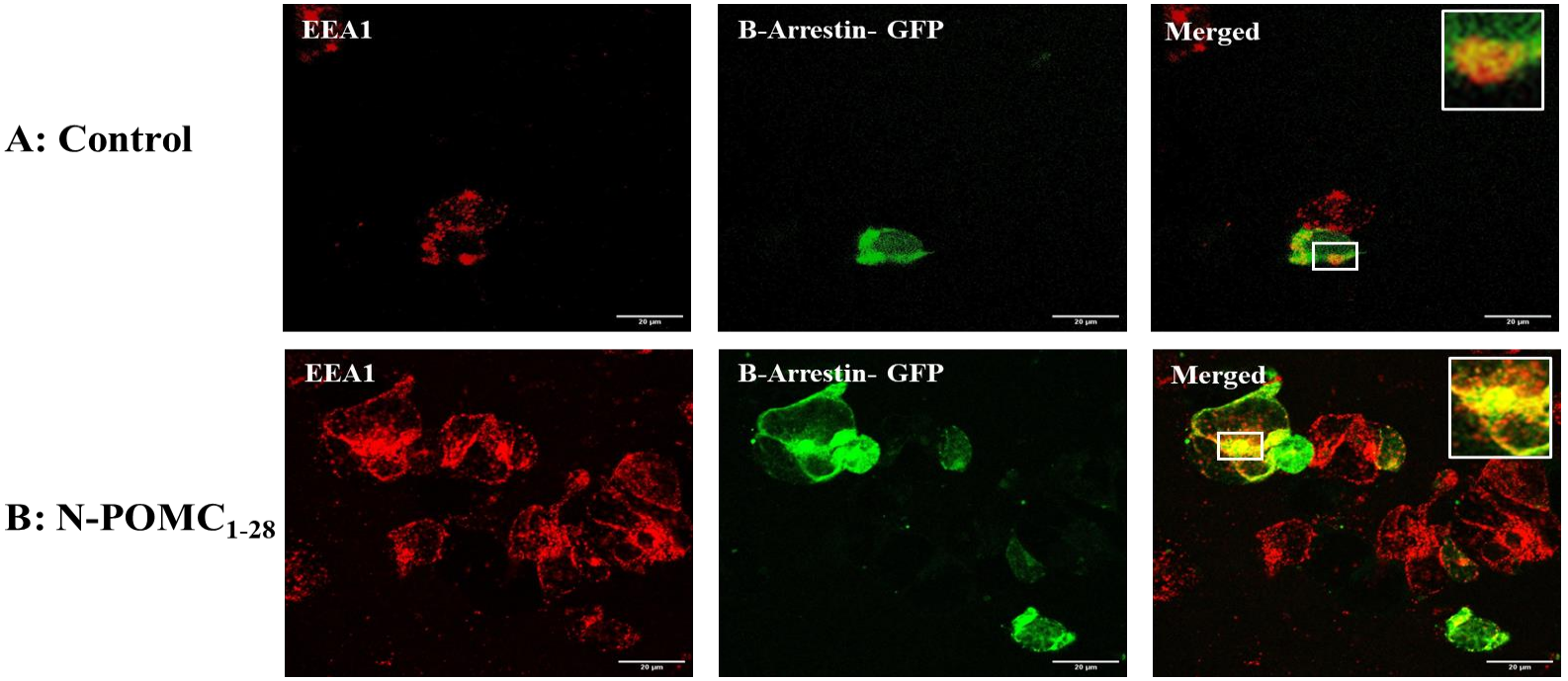

Fig. 6.20. Co-localisation of GFP-tagged β-arrestin and EEA-1 in the GPR19/MRAP cell line. The cells were transiently transfected with GFP-beta-arrestin, and then serum starved for 24 hrs. The cells were treated with 1 nM N-POMC$_{1-28}$ prepared in 0.1% BSA DMEM and incubated for 10 min, and the control cells were incubated with 0.1% BSA DMEM. The cells were fixed with 4% (w/v) PFA for 5 min and permeabilised with 0.2% (v/v) Tween-20 for 5 min. Cells were blocked with 10% (v/v) goat serum in 1X PBS for 60 min at RT and then incubated overnight at 4°C with mouse anti-EEA1 primary antibody (cat. 610457, BD Transduction Laboratories™) at 1:200 in 1% (v/v) goat serum in 1X PBS. The next day, the coverslips were incubated with 300 µl of goat anti-mouse secondary antibody conjugated to Alexa Fluor-555 (A-21422, Invitrogen) prepared in 1% (v/v) goat serum in 1X PBS for 2 hrs at RT. Then, the cells were mounted in a fluorescent mounting medium without DAPI (Vector Laboratories, Inc, UK). Images taken with a Nikon A1 Plus confocal microscope using NIS Elements software. Scale bar = 20 µm.

6.5. Discussion

The proliferative effect of N-POMC peptides, which are co-secreted with ACTH from the anterior pituitary, on the adrenal glands has been reported since the beginning of the 1980s. Estivariz et al. (1982) reported that treatment of rat adrenal cells with the smaller fragments of N-POMC$_{1-76}$: N-POMC$_{1-28}$ and N-POMC$_{2-59}$ increased DNA synthesis in a dose-dependent manner, while treatment with the intact N-POMC$_{1-76}$ had no effect. The mitogenic activity of the smaller N-POMC fragments was further confirmed by Lowry et al. (1983), Estivariz, Carino et al. (1988) and Estivariz, Morano, et al. (1988). In the study that was conducted by Lowry et al. (1983), they found that treatment of rats with anti-POMC$_{1-76}$ and anti-POMC$_{1-28}$ antisera 2 hrs before unilateral adrenalectomy inhibited DNA synthesis, suggesting a decrease in hyperplasia, which explains the compensatory adrenal growth, i.e., increase in adrenal weight, seen after unilateral adrenalectomy. Moreover, they found that N-POMC$_{1-48/49}$ could stimulate DNA synthesis and mitogenesis in rat adrenal following unilateral adrenalectomy. The results of Estivariz and coworkers demonstrated that injection of N-POMC$_{1-28}$, after removing the pituitaries, increased the mitotic index in rat adrenals. Moreover, they investigated whether N-POMC peptides were involved in the regeneration of the adrenal cortex after bilateral adrenal enucleation. Interestingly, they found that administration of purified human N-POMC$_{1-28}$ in rats partially reversed the adrenal growth regression that occurs after hypophysectomy in enucleated rats (Estivariz, Carino, et al., 1988; Estivariz et al., 1982; Estivariz, Morano, et al., 1988).

Further studies have shown that N-POMC$_{1-28}$ elicits its mitogenic effect by activating the MAPK: ERK1/2. MAPK cascades consist of three kinases: MAPK kinase kinases (MAPKKKs), MAPK kinases (MAPKKs) and MAPKs. The MAPKs are activated by the sequential phosphorylation process of the upstream kinases (Roskoski,

2012). The most widely studied MAPK pathways are ERK1/2, c-Jun N terminal kinase (JNK), and p38 pathways. The ERK1/2 pathway is mainly activated by mitogenic stimuli such as growth factors, serum and hormones, while JNK and p38 are predominantly activated by stress stimuli (Yang et al., 2013). The activated MAPKs catalyse the phosphorylation of several proteins, including transcription factors, protein kinases and phosphatases that contribute to the regulation of diverse cellular processes, including cell cycle progression, migration, survival, differentiation, proliferation, and transcription. Moreover, it has been reported that those pathways are upregulated in various cancers, and MAPK inhibitors work as a promising anti-cancer target (Pereira, Monteiro, Costa, Ferreira et al., 2019; Roskoski, 2012). Activation of ERK1/2 is regulated by the signalling cascade RAS-RAF-MEK transduction pathway that phosphorylates ERK at specific threonine and tyrosine amino acid residues.

The first report that studied how N-POMC stimulates adrenal proliferation at the molecular level was published by Fassnacht et al. (2003). First, they confirmed the findings of the previous studies by following the proliferation effect of N-POMC peptides on three different cell lines. They found that treatment of the human adrenocortical cancer cell line NCI-h295 with N-POMC$_{1\text{-}28}$ significantly increased cell proliferation and cell number in a dose-dependent manner. They reported a similar effect when using the mouse Y-1 adrenocortical cancer cells and non-neoplastic bovine adrenocortical cells. Moreover, the larger N-POMC fragments, 1-48 and 1-74, increased NCI-h295 cells and mouse Y-1 cells' proliferation significantly compared to untreated cells. Then, they studied the signalling pathway that N-POMC activated to increase cell proliferation. As mentioned earlier, the activation of MAPK pathways leads to cell proliferation. Therefore, they followed activation of the MAPK pathways ERK1/2, JNK and p38 by incubating the adrenocortical tumour cell lines that were serum starved for 36 hrs, with

1000 nM N-POMC$_{1-28}$ for a period from 5 min to 60 min. They found that N-POMC$_{1-28}$ increased ERK1/2 phosphorylation in a time-dependent manner with maximum activation after 10 to 20 min of cell stimulation with 1000 nM N-POMC$_{1-28}$, while the levels of phosphorylated JNK and p38 were not altered.

Interestingly, recent studies have shown that activated GPR19 transduced downstream signals through the phosphorylation of ERK1/2 and Akt (Bresnick et al., 2003; Hossain et al., 2016; Rao & Herr, 2017; Stelcer et al., 2020; Thapa et al., 2018). As shown in Chapter 5, the binding capacity of N-POMC fragments increased in the cell lines that are overexpressing GPR19 and/or expressing MRAP. That raised the question of whether N-POMC$_{1-28}$, as previously reported, exert its proliferation effect on adrenal cells, following ERK1/2 phosphorylation, through the activation of GPR19 and whether the expression of MRAP could play a role in this pathway.

The present study showed a significant increase in ERK1/2 phosphorylation in the cell line that was overexpressing GPR19, in comparison to the WT cell line, after treating the cells with 1 *p*M N-POMC$_{1-28}$ for 10 min (Fig. 6.7). Moreover, ERK1/2 phosphorylation increased significantly in the cell line overexpressing GPR19 in a time-dependent manner (Fig. 6.9) after treating the cells with 1 *p*M N-POMC$_{1-28}$ for up to 60 min. The phosphorylation signal increased dramatically after treating the cells for less than a minute, then started to decrease with time but was still significant in comparison to the control cells after 30 min of stimulation. Moreover, following ERK1/2 phosphorylation using SEAP as a reporter gene, the GPR19 overexpressed cell line showed a significant increase in SEAP activity in the media in comparison to the WT cell line. From this data, it is reasonable to suggest that N-POMC$_{1-28}$ acts as a ligand to activate GPR19 via the ERK1/2 pathway.

However, the WT cell line showed a significant increase in ERK1/2 phosphorylation only when the cells were treated with 1 *p*M N-POMC$_{1-28}$ and for a time interval of less than 10 min (Fig. 6.8), which is in agreement with the finding reported by Mattos et al. (2011) and in contrast with the findings described by Fassnacht et al. (2003) and Pepper and Bicknell (2009). This contrast could be related to the cell line that was used to perform the experiment in each study and to the concentrations of N-POMC$_{1-28}$ that were used to stimulate the cells.

Regarding the cell line, it has been published that metastatic tissue of the adrenal, breast, lung, pancreas, and brain express significantly higher GPR19 levels in comparison to primary cancer tissues and normal tissues (Kastner et al., 2012; Rao & Herr, 2017; Riker et al., 2008; Stelcer et al., 2020). The cell lines that were used by Fassnacht et al. (2003) and Pepper and Bicknell (2009) are tumour cell lines, the NCI-H295 human adrenal tumour cell line and the mouse Y1 adrenocortical cell line, respectively, that are characterised by high GPR19 expression in comparison to normal cells, i.e., HEK-293 used in this study and normal adrenal ZG and ZF/R cells used by Mattos et al. (2011). This explains the shorter stimulation time in the normal cells, as they express lower GPR19 levels, where the signal lasts for less than 10 min after N-POMC$_{1-28}$ treatment (this study and Mattos et al. (2011)) while in the tumour cells (that express high GPR19 levels) the ERK1/2 phosphorylation reaches maximum after 10-20 min of stimulation and lasts for up to 60 min after treatment (Fassnacht et al., 2003; Pepper & Bicknell, 2009).

Regarding N-POMC$_{1-28}$ concentration, we noticed that treatment of the four cell lines with 1 nM of N-POMC$_{1-28}$ for 10 min showed a non-significant effect on ERK1/2 phosphorylation while lower concentrations, e.g., 1 *p*M, showed significant effect on the used cell lines (Fig. 6.6). This finding is also interesting because Mattos et al. (2011)

reported that only the highest dose 10 μM N-POMC$_{1-28}$ significantly phosphorylated ERK1/2 pathway and the lower concentrations, 100 nM, 1 nM and 10 *p*M, did not activate this pathway. In comparison, Fassnacht et al. (2003) reported a significant effect of 1000 nM of N-POMC$_{1-28}$ on ERK1/2 phosphorylation. In contrast, Pepper and Bicknell (2009) reported a time-dependent increase in ERK1/2 phosphorylation when the cells were treated with 1 nM N-POMC$_{1-28}$. From this finding, we can conclude that the response of the cells to N-POMC$_{1-28}$ stimulation does not depend only on the concentration of N-POMC$_{1-28}$ that was used to perform the experiment but also depends on the levels of GPR19 expressed in the used cell line.

Moreover, it is well-established that agonist stimulation of GPCR induces desensitisation by phosphorylation of the receptor and subsequently internalisation to endosomes (endocytosis) (Rajagopal & Shenoy, 2018; Thompson et al., 2014). This is a protective measure that is tightly regulated by the cell to block overstimulation and sustain normal physiology. It seems that incubation of the cells with 1 nM N-POMC$_{1-28}$ for 10 min resulted in GPR19 desensitisation due to overstimulation, and that could explain the non-significant ERK1/2 phosphorylation in all the cell lines (Fig. 6.7) at high concentrations.

In addition, the adrenal cells used in the above-mentioned studies express MRAP (Chan et al., 2009; Metherell et al., 2005), whereas the HEK-293, which was used in this study, do not naturally express MRAP. Therefore, those adrenal cells are more represented by the MRAP and GPR19/MRAP cell lines that were used in this study, which revealed a similar result. The data showed that N-POMC$_{1-28}$ increased the ERK1/2 phosphorylation in a dose-dependent and time-dependent manner in both MRAP and GPR19/MRAP cell lines. Both cell lines give a significant increase of ERK1/2 phosphorylation when treated with 1 *p*M, 10 *p*M and 100 *p*M N-POMC$_{1-28}$ for 10 min

(Fig. 6.7) in comparison to the WT cell line. Moreover, the cell line that expressed MRAP showed a significant increase of ERK1/2 phosphorylation with time when the cells were treated with 1 *p*M N-POMC$_{1-28}$ and reached a maximum after 20 min of treatment, and then the signal reduced but was still significantly above that of the control cells. Similar results are reported in the cell line that overexpressed GPR19/MRAP, where the signal reaches a maximum after 10 min of treatment with 1 *p*M of N-POMC$_{1-28}$ and then reduced with time. In addition, the SEAP activity increased significantly in the GPR19/MRAP cell lines in comparison to the WT cell line but not in the cell line that expressed MRAP. These data suggest that overexpression of GPR19 with the expression of MRAP increases ERK1/2 phosphorylation in response to N-POMC$_{1-28}$ stimulation, and that could be explained as the expression of MRAP increased the cell membrane expression of GPR19 as shown in the confocal images that are discussed in chapter 3.

The results showed that N-POMC$_{1-49}$ phosphorylate ERK1/2 in a slightly different manner than N-POMC$_{1–28}$. We found that N-POMC$_{1-49}$ significantly increased ERK1/2 phosphorylation in a dose-dependent manner in the WT cell line (Fig. 6.13 A), which indicates that the response of the WT cell lines to N-POMC$_{1-49}$ is longer than its response to N-POMC$_{1-28}$, which has been shown earlier to end before 10 min of stimulation. Moreover, the overexpressing GPR19 cell lines showed a similar response to N-POMC$_{1-49}$ stimulation as the WT cell line (Fig 6.13 B). Moreover, the two cell lines that were expressing MRAP showed a significant response in comparison to the control cells, only after treatment with 1 *p*M N-POMC$_{1-49}$ but not with the higher concentrations (Fig 6.13 C and D). These results suggest that the two peptides stimulate the ERK1/2 signalling pathway in a different way. This is supported by the observation that the response of Y1 cell lines to N-POMC$_{1-49}$ leads to a strong and longer Akt phosphorylation that lasts up to 60 min of stimulation in comparison to their weak response to N-POMC$_{1-28}$, which

started after 10 min of stimulation and ended after 15 min of stimulation (Pepper & Bicknell, 2009). Interestingly, it has been reported that activation of Akt inhibited Raf and MEK phosphorylation, which consequently reduced ERK1/2 phosphorylation (Rommel et al., 1999). The effect of both peptides on Akt activation and ERK1/2 phosphorylation on the cell lines that overexpressed GPR19 require further investigation.

The MAPK pathway, RAS/RAF/MEK/ERK, crosstalk with other signalling pathways, among them the PI3K/Akt. The MAPK pathway plays a role in cell growth and differentiation, while the PI3K/Akt pathway is associated with cell survival and apoptosis. RAS acts as an upstream positive effector of both pathways. Oncogenic RAS mutations are detected in 30% of all cancers, leading to the activation of both pathways and resulting in uncontrolled cellular proliferation (Lauth, 2011). The levels of phosphorylated ERK1/2 were found to be higher in malignant adrenal tumours compared to benign tumours or normal adrenal glands, which suggests the role of this pathway in the transformation of normal adrenal cells into tumours (Pereira, Monteiro, Costa, Moreira, et al., 2019).

Moreover, the expression of GPR19, which was found to signal through the activation of the ERK1/2 and PI3K/Akt pathways (Hossain et al., 2016), is highly increased in metastatic tissues of adrenal, breast, lung, pancreas, and brain in comparison to primary cancer tissues and normal tissues (Kastner et al., 2012; Rao & Herr, 2017; Riker et al., 2008; Stelcer et al., 2020). Where the phosphorylated ERK1/2 regulate the cell cycle progression, differentiation, and survival by activating various substrates such as the cytosolic signalling proteins: p90 RSK and the MAPK-interacting serine/threonine kinase (MNK), the transcription factors that are located in the nucleus: ETS domain-containing protein Elk-1, the proto-oncogenes c-Fos, c-Jun and c-Myc, and cAMP-dependent transcription factor ATF2. These factors support unlimited cell proliferation,

which is a feature of cancer cells (Sugiura et al., 2021). The upregulation of GPR19 in the metastatic tissues can be linked to increased cell proliferation by triggering the activity of those two pathways, and that clarifies the association of GPR19 with breast and lung cancer-related death, according to the GEIPA data. Thus, the use of MAPK inhibitors separately or in combination with PI3K/Akt inhibitors is under clinical assessment to improve different cancer therapies (He et al., 2021).

Patients with FGD present with adrenal atrophy of both the ZF and ZR with preservation of ZG and have cortisol deficiency due to poor response of the adrenal cells to ACTH. FGD is an autosomal recessive disorder with 25% of the cases linked to different MC2R mutations (FGD-1) (Weber & Clark, 1994), 20% were linked to mutations in the MRAP sequence (FGD-2) (Metherell et al., 2005), 5% of cases related to mutations in the steroidogenic acute regulatory protein (StAR) (FGD-3) (Metherell et al., 2009), but around 50% of the FGD cases had an unidentified genetic background. Moreover, mutations in the mini chromosome maintenance-deficient 4 homologue (MCM4) and nicotinamide nucleotide transhydrogenase (NNT) genes that are involved in DNA replication and antioxidant defence, respectively, have been recognised in FGD cohorts (Meimaridou et al., 2013). Interestingly, the detection of *Gpr19* mRNA by *in situ* hybridisation in rat adrenal and GPR19 protein by immunohistochemistry in mouse adrenal revealed the expression of GPR19 across all the adrenal cortex zones and the adrenal capsule (unpublished data of Bicknell lab). Additionally, the knockdown of *Gpr19* leads to a reduction in lung cancer-derived cell line proliferation and an increase in the number of dead cells (Kastner et al., 2012). Accordingly, this suggests the role of GPR19 in the cases of FGD with unidentified mutations that certainly warrant further investigation.

It has been shown in this study that both N-POMC$_{1-28}$ and adropin reduce cAMP levels in a dose-dependent and time-dependent manner. Unfortunately, we were not able to confirm if this reduction was significant or not, as this experiment was performed only once. This finding is still interesting, as we showed in Chapter 5, that only the cell lines that overexpress GPR19 give a significant dose-dependent increase of adropin binding in comparison to the WT cell line. Moreover, the binding capacity data (shown in Chapter 5) revealed that the N-POMC fragments 1-28, 1-49 and 1-77 could compete with adropin binding while adropin could not compete with N-POMC$_{1-28}$. Based on this finding, we hypothesised that only the cell line that overexpressed GPR19 would produce a lower cAMP level after treatment with adropin, but this is not the case. In addition, the results showed a slower response of the cells that express MRAP to adropin, which suggests a role of MRAP in converting the GPR19 to a more N-POMC-specific receptor. On the other hand, it could suggest that adropin could bind to GPR19 or to a different receptor that its expression depends on GPR19 as they could form a dimer and/or translocated to the cell membrane together and the activation of any of them alter the function of the other receptor. This hypothesis requires further investigation to add to our understanding of how GPR19 could act as an N-POMC and/or adropin receptor.

Recruitment of β-arrestin has been used by researchers to identify the natural ligands for the orphan GPCRs using the reverse pharmacology approach. β-arrestins are a family of proteins that regulate the signal pathway of various GPCRs and are involved in the adjustment of cell proliferation, migration, invasion, anti-apoptotic, and drug resistance pathways. Southern et al. (2013) reported that GPR19 signal by recruitment of β-arrestin. In this study, we took a similar approach by transiently transfected cells with GPF-β-arrestin and then followed the localisation of this protein in the early endosomes, using anti-EEA1, after treating the cells with N-POMC$_{1-28}$. Unfortunately, the control

cells showed that the transiently transfected GPF-β-arrestin is already co-localised in the early endosomes. That made the identification of N-POMC$_{1-28}$ effects on cells difficult to measure. Considerable effort was made to improve the protocol, but still, the same was detected in all experiments.

In summary, we show, for the first time, that N-POMC$_{1-28}$ binds to and activates GPR19, which reduces cAMP levels in the cells, increases ERK1/2 phosphorylation, and activates the down-stream transcription factors Elk-1 that activate the SRE of the SRE-SEAP vector, consequently stimulating cell proliferation.

Chapter 7: General Discussion and Future Work

7.1. General Discussion

Over the years, several studies have reported the role of pro-γ-MSH (N-POMC), which is co-secreted with ACTH from the anterior pituitary during the stress response, in adrenal development, growth, and steroidogenesis. N-POMC is cleaved following secretion from the anterior pituitary by AsP expressed by the adrenal gland to release the shorter mitogenic N-POMC peptide. Until now, it has been unclear how N-POMC elicits its action on adrenal cells. Unpublished data from the Bicknell group identified the receptor GPR19 as a possible receptor for N-POMC in adrenal cells.

During stress, the hypothalamus releases CRH, which stimulates the release of ACTH and pro-γ-MSH from the anterior pituitary. ACTH stimulates the ZF of the adrenal cortex to produce glucocorticoid hormones and ZR to release androgens. Studies showed that the full-length N-POMC, 1-76 fragment in humans, exhibit no steroidogenic activity (Seidah et al., 1980) or mitogenic activity in adrenal cells (Estivariz, Morano et al., 1988; Lowry et al., 1983). Several studies have reported the role of the N-POMC fragments 2-59, 1-49, and 1-28 in adrenal growth (Al-Dujaili et al., 1981; Estivariz, Carino et al., 1988; Estivariz et al., 1982; Estivariz, Morano, et al., 1988; Fassnacht et al., 2003; Lowry et al., 1983; Torres et al., 2010). It is believed that pro-γ-MSH undergoes a post-secretion cleavage by AsP expressed by the adrenal to release the mitogenic N-POMC fragment N-POMC$_{1-52}$ and/or N-POMC$_{1-49}$ (Bicknell, 2003; Bicknell et al., 2001).

Moreover, there is evidence that the extended N-terminal γ-MSH (N-POMC$_{1-61}$) that is referred to by Lowry (2016) as "big γ-MSH" appears to have an adrenal mitogenic activity. McLean et al. (1981) reported that they extracted N-POMC$_{2-59}$ from human pituitaries and that it has been shown to be the most potent adrenal mitogen factor among

the other N-POMC fragments (Estivariz et al., 1982). Moreover, this is supported by the finding that injecting rats with an antiserum raised against a synthetic γ-MSH peptide leads to an inhibition of compensatory adrenal growth following unilateral adrenalectomy (Lowry et al., 1983). It seems likely that the extracted fraction that is used to perform those experiments contains a heterogeneous mixture of big γ-MSH and N-POMC$_{2-59}$.

In this study, we used the HEK-293 cell line as a cellular model to characterise GPR19 as an N-POMC receptor. This cell line was chosen since it has been used to express several types of GPCR receptors, which makes it a suitable host cell to express GPCRs, especially if post-translational modifications are essential for GPCR function (Markovic & Challiss, 2009). Moreover, various types of GPCR signalling-related gene products such as the G proteins, α, β, and γ, and their targets and downstream effectors, as well as the proteins that regulate GPCR signalling, are expressed in this cell line (Thomas & Smart, 2005).

The mRNA expression of the GPR19 in the HEK-293 has been reported by Atwood et al. (2011). The reported results here agree with this finding as the mRNA and protein expression of human GPR19 is confirmed in this study by RT-PCR and western blotting, respectively. Expression of GPR19 in HEK-293 could be considered a disadvantage, especially when performing the ligand-receptor experiments, as a negative control cell line that does not express GPR19 is ideally required. On the other hand, it can be considered as an advantage to achieve transfection-mediated functional expression of a receptor. It was suggested that as the HEK-293 expresses GPR19, overexpression of GPR19 in HEK-293 cells will lead to an increase in the localisation of GPR19 in the cell surface. The ICC images of the cell line that over-express rGPR19 revealed that the GPR19 protein mainly accumulated inside the cell, with little staining detected in the cell membrane, suggesting that the trafficking of GPR19 to the cell membrane was

interrupted. Similar results had been reported before for the MC2R, where it accumulates inside cells that do not express MRAP (Metherell et al., 2005).

The *Mrap* null mice and the *Pomc* null mice both show a disrupted adrenal phenotype. MRAP is required for normal adrenal differentiation and proliferation (Gorrigan et al., 2011), and mutations in Mrap have been reported to cause FGD type 2 (Novoselova et al., 2018) and lead to obesity (Novoselova et al., 2016). In addition, the *Pomc* null mice developed obesity, adrenal atrophy and altered pigmentation (Karpac et al., 2005; Yaswen et al., 1999). Those findings showed that both MRAP and POMC peptides are essential for adrenal growth. This suggested that expression of MRAP in the HEK-293 cell, which does not express MRAP (Roy et al., 2007), might be required for GPR19 translocation to the cell membrane.

First, RT-PCR was used to confirm that MRAP is not expressed in the HEK-293 cell line. This then led to the development of two cell lines, one that stably expressed mMRAP and the second that overexpressed rGPR19/mMRAP. The expression of the inserted mMRAP gene was confirmed by RT-PCR, and the protein expression was confirmed by western blotting using a HA-Tag antibody, as the inserted mMRAP gene was tagged with HA-Tag at its C-terminus. The statistical analysis of the ICC images showed that the amount of GPR19 localised to the cell membrane increased significantly in the cell lines that expressed mMRAP and that overexpressed rGPR19/mMRAP in comparison to the cell lines that did not express MRAP. It is important to stress that MRAP expression does not increase the expression of GPR19 but only increases its cell surface expression. Furthermore, the ICC images showed that GPR19 and MRAP proteins were co-localised in the cell membrane and inside the cells. In addition, the results of the Co-IP experiments showed that both GPR19 and MRAP formed a complex, and the GPR19 bands could be precipitated using an anti-N-POMC$_{1\text{-}28}$ antibody after

treating the cells with N-POMC$_{1-28}$ and using the crosslinker DST. These findings strongly suggest that GPR19 and MRAP form a complex to increase GPR19 cell surface expression, and N-POMC$_{1-28}$ binds to GPR19.

Subsequently, we studied the binding ability of N-POMC$_{1-28}$ to the cell lines and the effect of MRAP on the ligand-receptor interaction. Our data showed that the WT and the three transformed cell lines had binding capacity for N-POMC$_{1-28}$ either if it was unlabelled, fluorescently labelled or biotin labelled. The N-POMC$_{1-28}$ peptide was labelled with Alexa Fluor-488, and then the cells were treated with 1 nM of this peptide; the results revealed that the binding capacity of the cell lines that overexpress GPR19, MRAP and GPR19/MRAP to N-POMC$_{1-28}$ was statistically significant in comparison to the WT cell line. Moreover, the cell lines that express MRAP and GPR19/MRAP showed a significant dose-dependent response to the unlabelled N-POMC$_{1-28}$ in comparison to the WT and to the cell line that overexpressed GPR19. Interestingly, similar results were found when using biotin labelled N-POMC$_{1-28}$. Moreover, the longer N-POMC fragments 1-49 and 1-77 showed a binding capacity to GPR19 by competing with the biotinylated N-POMC$_{1-28}$. These findings strongly suggested that GPR19 is the receptor for N-POMC, and the expression of MRAP not only increases GPR19 cell surface expression but also increases the binding ability of N-POMC to GPR19.

An interesting observation was that the full-length N-POMC$_{1-77}$ bound to the receptor. Early studies showed that this fragment had no effect on adrenal growth (Estivariz et al., 1982) and was involved indirectly in adrenal steroidogenesis by increasing free cholesterol levels in the cells (Pedersen & Brownie, 1979; Pedersen et al., 1980). Moreover, treatment of rat and human adrenal cells with both ACTH and pro-γ-MSH leads to an increase in cortisol and aldosterone secretion in comparison to the cells treated with ACTH only (Al-Dujaili et al., 1981). On the other hand, it has been reported

that pro-γ-MSH has a suppression effect on adrenal steroidogenesis (Coulter et al., 2000; Fassnacht et al., 2003) and treatment of the cancer cells NCI-h295 with 10 nM recombinant rat N-POMC$_{1-74}$ stimulated cells proliferation (Fassnacht et al., 2003). The ability of N-POMC$_{1-77}$ to compete for the binding site with N-POMC$_{1-28}$ strongly suggests that both fragments bind to the same receptor.

Interestingly, a new finding reported by Li et al. (2021) showed that GPR19 dimerised with the MC3R. The MC3R has a binding affinity for the POMC peptides α-, β-, γ-MSH and ACTH, with the γ-MSH showing a high binding affinity for MC3R among the other MCRs (Dores et al., 2016; Gantz et al., 1993; Slominski et al., 2000). MC3R is not expressed in HEK-293 cells (Atwood et al., 2011), so the high molecular weight GPR19 band that is detected by western blotting in this study could not be a dimer between GPR19 and MC3R. The results regarding the expression of MC3R in the adrenal cells are in conflict. Dhillo et al. (2003) confirmed the expression of MC3R in rat adrenal cells, while the previous studies reported that MC3R is not expressed in the adrenal gland (Gantz et al., 1993; Roselli-Rehfuss et al., 1993).

The results of Tilemans et al. (1997) showed that treatment of lactotrophs cells with γ3-MSH leads to an increase in cell proliferation that is like the effect of the human POMC$_{1–76}$ on those cells, but the potency of γ3-MSH was lower than that of human POMC$_{1–76}$. The role of γ-MSH as a mitogenic factor was suggested earlier by Lowry et al. (1983). Moreover, Tilemans et al. (1997) reported that γ3-MSH stimulated cAMP formation in the HEK-293 cell line, overexpressing MC3R, while human POMC$_{1–76}$ did not. This finding suggested that the human POMC$_{1–76}$ is not an agonist of MC3R, and its mitogenic activity is performed by another receptor. Interestingly, treatment of the HEK-293 cell line overexpressing MC3R with glycosylated human N-POMC$_{1-76}$ showed no effect on cAMP levels, whereas the recombinant non-glycosylated rat N-POMC$_{1-74}$

increased cAMP level in a dose-dependent manner (Bert et al., 1999). Overexpression of MC3R in HEK-293 leads to an increase in the surface expression of GPR19 (Li et al., 2021). Moreover, MC3R is a $G\alpha_s$ coupled receptor whereas GPR19 is a $G\alpha_i$ coupled receptor and dimerisation between MC3R and GPR19 will lead to crosstalk between the two activated pathways and alter the levels of cAMP levels inside the cells (Selbie & Hill, 1998). It seems that the glycosylated form of N-$POMC_{1-76}$ binds to GPR19, which is why it shows no cAMP activity, while the non-glycosylated form binds to MC3R and leads to an increase in cAMP level. It is also possible that the non-glycosylated form of N-$POMC_{1-76}$ binds to both receptors, the N-terminal part of the peptide binds to GPR19, and the γ3-MSH part of the peptide binds to MC3R.

Both GPR19 and MC3R are highly expressed in the brain (O'Dowd et al., 1996; Roselli-Rehfuss et al., 1993), both have a role in food intake regulation and energy homeostasis and the *Mc3r* null mice and *Gpr19* null mice are characterised with a metabolic disorder syndrome. The *Mc3r* null mice develop metabolic syndrome characterised by increased weight, specifically in females, and increased adipose mass observed in both sexes with no effect on feeding behaviour (Butler et al., 2000). The *Gpr19* knockout (KO) mice showed an increase in fat mass and decreased physical activity, particularly in female mice. Male *Gpr19* KO mice show decreased whole-body glucose tolerance, combined with decreased expression of key hepatic glucose production enzymes, under obese conditions (Mushala et al., 2023). This result suggests that GPR19/MC3R played a role in the development of obesity-related metabolic dysfunction.

The dimerisation of GPR19 with other receptors and the crosstalk between the signalling pathways they activated is an important research area that requires investigation before exploring the biological function of GPR19 in adrenal cells and in

the other peripheral tissues. The findings of this study and linking it with other studies define the fundamental role of the GPR19/MC3R in the regulation of energy homeostasis by N-POMC peptides and thus highlight a potential target for therapeutic interventions in metabolic disorders that trigger obesity.

It has been reported that GPR19 receptor signals by reducing cAMP levels inside the cells (Bresnick et al., 2003), increasing the phosphorylation of ERK1/2 and Akt (Hossain et al., 2016; Rao & Herr, 2017) and GPR19 stimulation leads to receptor internalisation into clathrin-coated vesicles and that involves the recruitment of β-arrestin (Southern et al., 2013). As mentioned earlier, the binding ability of N-POMC$_{1-28}$ increased in a dose-dependent manner in the cell lines that are overexpressed GPR19, MRAP and GPR19/MRAP; therefore, we investigated whether treatment of those cells with N-POMC peptides, 1-28 or 1-49, could influence those pathways.

We found that N-POMC$_{1-28}$ reduced cAMP levels in a dose-dependent and time-dependent manner in all the cellular models. The cAMP % reduction is different between the cell lines, but the overall cAMP levels reduced between 10% to 20% after 1 min of treatment with 0.1 nM N-POMC$_{1-28}$. The % reduction increased as the time of treatment increased and as the concentration of N-POMC$_{1-28}$ increased.

The N-POMC peptides 1-28 and 1-49 mediate mitogenic activity on adrenal cells (Estivariz, Carino, et al., 1988; Estivariz et al., 1982; Estivariz, Morano, et al., 1988; Lowry et al., 1983) through phosphorylation of ERK1/2 (Fassnacht et al., 2003; Mattos et al., 2011; Pepper & Bicknell, 2009). ERK1/2 phosphorylation is regulated by the protein kinases of the transduction pathway RAS-RAF-MEK that phosphorylates ERK at specific threonine and tyrosine amino acid residues. Pepper and Bicknell (2009) reported that both N-POMC peptides 1-28 and 1-49 could stimulate the phosphorylation of RAF and MEK, the upstream regulator of ERK1/2, in a time-dependent manner. The

signalling cascade RAS-RAF-MEK-ERK1/2 is upregulated in a variety of cancers, among them adrenocortical carcinomas, and inhibitors of those protein kinases work as a target for anti-cancer therapy (Pereira, Monteiro, Costa, Ferreira, et al., 2019; Roskoski, 2012).

The present study confirms that both N-POMC peptides, 1-28 and 1-49, stimulate ERK1/2 phosphorylation in the WT and the stably transfected cell lines, but the pattern of the response in those cell lines is different. As the WT cells are expressing very low GPR19 protein levels at the cell membrane, the ERK1/2 phosphorylation was detected for a time interval of less than 10 min and only when the cells were treated with low concentrations (1 *p*M) of N-POMC$_{1-28}$. The cell line that overexpressed GPR19 showed a time-dependent increase of ERK1/2 phosphorylation for up to 30 min of stimulation with 1 *p*M N-POMC$_{1-28}$. In the dose-dependent experiment, this cell line showed a significant increase of ERK1/2 phosphorylation with 1 *p*M and 10 *p*M of N-POMC$_{1-28}$ but not with the higher concentrations. As expected, the cell lines that express MRAP showed higher N-POMC$_{1-28}$ binding ability than the WT and overexpressing GPR19 cell lines showed a time-dependent increase of ERK1/2 phosphorylation for up to 60 min of stimulation with 1 *p*M N-POMC$_{1-28}$ and a dose-dependent increase of ERK1/2 phosphorylation with N-POMC$_{1-28}$ concentrations up to 100 *p*M.

We found that the response of the cells to N-POMC$_{1-49}$ stimulation showed a different pattern than the response of the cells to N-POMC$_{1-28}$. The WT cell line showed a significant dose-dependent increase in ERK1/2 phosphorylation with concentrations less than 1 nM, and a similar result was detected for the cell line that overexpressed GPR19. On the other hand, the cell lines that are expressing MRAP showed a significant response only with 1 *p*M N-POMC$_{1-49}$. This difference in the response between the cells to the N-POMC fragments could be due to the difference in the peptide structure and

could reflect the role of the accessory protein in mediating the receptor response to its ligand.

Torres et al. (2010) studied the role of N-POMC$_{1-28}$ in cell proliferation by treating rats with N-POMC$_{1-28,}$ and they reported that N-POMC$_{1-28}$ leads to the induction of S phase entry in all zones of the adrenal cortex. The effect of N-POMC$_{1-28}$ is mediated through the upregulation of cyclins D2, D3, and E that regulate the cell cycle progression from the G1 to the S phase (de Mendonca et al., 2013; Mendonca & Lotfi, 2011). In this study, we investigated the effect of N-POMC$_{1-28}$ in cell proliferation and cell cycle differentiation using a pSRE-SEAP profiling vector. The SRE has been identified as an essential regulatory element of the c-Fos proto-oncogene promoter, thus activating the SRE-controlled *c-FOS* gene that is involved in unlimited cell proliferation (Thiel et al., 2021; Treisman, 1992; Yang et al., 2013). As N-POMC$_{1-28}$ increases ERK1/2 phosphorylation, transcription factors such as p90RSK and Elk-1 will be activated (Sugiura et al., 2021). The phosphorylated Elk1 binds to and activates the SRE of the pSRE-SEAP vector, which consequently leads to the transcription and release of the SEAP in the culture media. The results of this assay showed that N-POMC$_{1-28}$ increases SEAP release in all the cellular models in comparison to the control cells. Moreover, we found that the cell lines that overexpressed GPR19, both the ones that overexpressed GPR19 alone or with MRAP, showed a significant increase in SEAP activity in comparison to the WT, while the cell line that expressed MRAP alone did not.

This indicates that overexpression of GPR19 impacts the downstream growth regulators led to an increase in cell proliferation, which is a characteristic of adrenocortical carcinomas and other carcinomas (Chen et al., 2021; Gerlach et al., 2023; Stelcer et al., 2020). The GPR19 expression level is suggested to be used as an oncogenic factor (Chen et al., 2021; Pu et al., 2022). The results in this study provide evidence that

both overexpression of GPR19 and treatment of cells with N-POMC$_{1-28}$ increase cell proliferation and thus highlight a potential therapeutic target.

This study was initially designed with the aim of characterising GPR19 as a possible N-POMC receptor. Some studies have reported that the peptide hormone adropin is an agonist of GPR19 (Jasaszwili et al., 2019; Rao & Herr, 2017; Stein et al., 2016; Stelcer et al., 2020; Thapa et al., 2018). The first study suggesting that GPR19 is a receptor for adropin was published by Stein et al. (2016). They used the deductive reasoning strategy to suggest that GPR19 is an adropin receptor. First, they identified the cell lines that were responsive to adropin. Then, they generated an orphan GPCR expression profile using PCR to identify shared populations of orphan receptors, and they identified five potential candidates, including GPR19. This was followed by studying the expression patterns of those receptors and conducting laboratory experiments (*in vivo* and *in vitro*). They found that adropin inhibited the action of water deprivation-induced drinking behaviour and administration of GPR19 siRNA in male rats for 2 days, which significantly lowered GPR19 mRNA levels in the hypothalamus and prevented adropin action. Clearly, in this study, there is no direct evidence of the association of adropin with GPR19. The following studies do not provide any direct evidence of adropin binding ability to GPR19, and the de-orphanisation study performed by Foster et al. (2019) could not confirm the binding of adropin to GPR19.

In fact, the idea that GPR19 could act as a receptor of both the N-POMC fragments and the adropin is perhaps possible as both have amino acid sequence similarities, and both have a disulphide bridge that triggers C-shape structure. Moreover, both peptides act as an adrenal mitogenic factor and reduce adrenal steroidogenesis. Fassnacht et al. (2003) reported that N-POMC$_{1-28}$ stimulated cell proliferation in normal and cancer human adrenocortical cells in a concentration-dependent manner. Moreover,

N-POMC$_{1-28}$ decreased steroid hormone production, e.g., cortisol, 17-hydroxyprogesterone, and dehydroepiandrosterone sulphate, in NCI-h295 cells in a concentration-dependent manner. However, treatment of cells with N-POMC$_{1-28}$ does not affect the protein levels of the steroidogenesis regulators SF1, DAX1, StAR and P450scc. Stelcer et al. (2020) reported that the proliferation rate of HAC15 cells incubated with adropin increased significantly after 48 hrs of incubation, and the cell proliferation via ERK1/2 and Akt pathway was completely inhibited when the HAC15 cells treated with adropin in the presence of ERK1/2 and PI3K/Akt inhibitors, U0126 and LY294002, respectively. Moreover, treatment of HAC15 cells with 10^{-8} M adropin for 24 hrs leads to a significant decrease in forskolin-stimulated aldosterone and cortisol secretion in relation to untreated cells. The difference reported here is that adropin decreases the expression of the StAR protein and the enzyme CYP11A1. Based on those findings, we performed experiments to study if adropin could bind to GPR19.

The HEK-293 cells that were used in this study to characterise GPR19 as an N-POMC receptor were reported to express and secret adropin (Kumar et al., 2011) and that was confirmed in this study (data not shown). Therefore, we labelled adropin with biotin, and this peptide was used to study its binding to the cellular models. Results showed that the binding of the biotin-labelled adropin was linear in all the cellular models used to perform the experiment and did not reach saturation as in the N-POMC$_{1-28}$ binding assay even though we used up to 500 nM of biotin-labelled adropin. The linear, rather than saturation, specific adropin binding supports the idea that GPR19 is not the adropin receptor as GPR19 is expressed in low levels in the WT, and we used very high adropin concentrations (up to 500 nM) and does not reach saturation while in N-POMC$_{1-28}$ it reaches saturation with 15 nM. On the other hand, an important result is reported here, which is the cell line that overexpressed GPR19 showed a significant dose-dependent

increase in adropin binding in comparison to the WT cell line. The binding curve is linear and not saturable, which could be explained as the overexpression of GPR19 increasing adropin binding ability to its receptor rather than binding to GPR19, and its cell membrane expression increases as GPR19 expression increases in the cells.

In the same assay, the cell lines that overexpress GPR19 and MRAP did not show a significant increase in adropin binding in comparison to the WT; instead, both cell lines that express MRAP showed similar or less adropin binding in comparison to the WT cells. This finding suggests that the expression of MRAP reduces the ability of adropin to bind to its receptor. If adropin binds to GPR19, it seems that MRAP converts GPR19 to a more N-POMC receptor as the competitive binding assay data showed that adropin could not compete with N-POMC$_{1\text{-}28}$ binding, whereas the N-POMC peptides, 1-28, 1-49 and 1-77, were found to compete with adropin binding. If adropin binds to a receptor other than GPR19 and that forms a dimer with GPR19, it seems that co-expression of MRAP suppresses this dimer formation. Such an effect of MRAP expression was reported by Wang et al. (2022), where they found that the expression of MRAP inhibits the dimerisation of SSTR2 with SSTR3 and SSTR5.

As mentioned earlier, GPR19 forms a dimer with the MC3R (Li et al., 2021). In this study, we showed that expression of MRAP increased the cell surface expression of GPR19, while expression of MRAP does not affect MC3R cell surface expression, but it has an inhibitory effect on its signalling (Chan et al., 2009). The receptors GPR19 (Mushala et al., 2023) and MC3R (Butler et al., 2000) play a role in energy homeostasis through activation by adropin and POMC peptides. The receptors, MC3R and GPR19, accessory protein MRAP and the ligands, adropin and the POMC fragments: α-, β-, γ-MSH and N-POMC, are all expressed in the hypothalamus. Further work will be required to provide more evidence about the role of GPR19, MC3R, MRAP and their ligands as a

potential regulator of energy homeostasis and thus highlight a possible target for therapeutic applications in metabolic-associated diseases such as obesity.

7.2. Future Work

As discussed throughout the thesis, based on the results and the limitations identified, there is still much to be investigated.

7.2.1. GPR19 Gene Manipulation: Knockdown and Knockout

The development of a cellular model with Grp19 knockdown and an animal model with Grp19 knockout will provide an ideal model to study the effect of GPR19 expression at the cellular level and its effect on animal health.

The gene knockdown (silencing) could be performed using small interfering RNA (siRNA) or short hairpin RNA (shRNA) to inactivate mRNA for a specific gene, *Grp19* in this case, that will effectively suppress mRNA translation to protein. The reduction of GPR19 protein levels can be confirmed using ICC and/or western blotting. Regarding the cellular models that were used in this study, *Grp19* knockdown should be performed in the WT and the cell line that was stably transfected with MRAP. The *Grp19* knockdown cell lines could then be used to confirm that the N-POMC binding is due to GPR19 expression and not due to the expression of another receptor in the HEK-293 cell line. The binding ability of N-POMC could be measured and if the binding ability of N-POMC in those cell lines is undetectable or lower than the cells that are expressing GPR19, this would support GPR19 being the receptor for N-POMC. Moreover, this would confirm that expression of MRAP without GPR19 will also lead to a similar result and exclude the possibility that N-POMC acts through another receptor that is expressed in the HEK-293 cells and the expression of MRAP increases its cell membrane translocation and leads to an increase in N-POMC binding. In addition, it will be used to confirm if adropin binds to GPR19 or not by treating the cells with serial biotin-labelled adropin concentrations and measuring the cell response. If GPR19 is the receptor of adropin, it will show a lower binding ability to the cell lines with *Grp19* knockdown in comparison to the WT cell

lines. Otherwise, it means that adropin may perform its biological activity through different receptors.

Knockout mice are commonly used in research to study the effects of genes that may have significance in human health. *Grp19* knockout mice had been used by Mushala et al. (2023) to study the metabolic function of GPR19 *in vivo*. They found that knockout of *Grp19* leads to an increase in total energy expenditure in male mice under a low-fat diet and in female mice under both a low and high-fat diet, which suggests a role of GPR19 in the body's energy homeostasis. In male mice that were fed a high-fat diet, they noticed a significant increase in the circulating glucose levels and a significant increase in absolute liver weight with decreased expression of key hepatic glucose production enzymes. This finding suggests that GPR19 impacts whole-body energy metabolism in diet-induced obese mice in a sex-dependent manner. It is expected that knockout of *Grp19* in an animal may lead to defective adrenal development and adrenal atrophy after birth, as in the *Pomc* knockout mice (Karpac et al., 2005; Yaswen et al., 1999), as the N-POMC fragments are required for normal adrenal cell growth and development during pregnancy (Fassnacht et al., 2003; Ross et al., 2000; Saphier et al., 1993; Torres et al., 2010).

7.2.2. Dimerisation between GPR19 and other receptors

The fact that GPCRs form a dimer, either as a homodimer or heterodimer, is acknowledged in many studies, and it has been found that heterodimerisation between different GPCRs could alter their ligand binding affinity, the second messenger pathway they activated and their trafficking to the cell membrane (Bouvier, 2001; Li et al., 2021; Selbie & Hill, 1998). Li et al. (2021) reported that MC3R dimerised with GPR19 in the mouse hypothalamus cells, and the cell surface expression of GPR19 increased as the expression ratio of MC3R increased in the cells. Moreover, they transfected cells with a

fixed amount of MC3R and different ratios of GPR19 and followed the cAMP accumulation inside the cells as MC3R is a Gαs coupled receptor, whereas GPR19 is a $G\alpha_i$ coupled receptor. They found that dimerisation between MC3R and GPR19 slightly enhanced cAMP accumulation. This finding is in accordance with the finding of Tilemans et al. (1997) as they reported that both the γ-3-MSH (MC3R agonist) and non-glycosylated rat N-$POMC_{1-74}$ stimulated cAMP formation in HEK-293 stably transfected with MC3R. On the other hand, the glycosylated human N-$POMC_{1-76}$ did not stimulate cAMP formation, and that could be due to the activation of GPR19 by this N-POMC fragment that, upon activation, leads to the reduction of cAMP inside the cells, which leads to crosstalk between the two activated pathways by those receptors.

In this study, we detected two GPR19 bands by western blotting at 50 kDa, which is the predicted size of GPR19, and at 90 kDa, which was explained as a dimer of GPR19, perhaps with another receptor. MC3R is not expressed in the HEK-293 (Atwood et al., 2011), while its expression in adrenal cells is in conflict. Dhillo et al. (2003) confirmed the expression of MC3R in rat adrenal cells, while the previous studies reported that MC3R is not expressed in the adrenal gland (Gantz et al., 1993; Roselli-Rehfuss et al., 1993). That raises the question of whether GPR19 dimerises with other receptors inside HEK-293 cells and in the adrenal cells; if MC3R is not expressed in those cells, that may influence its biological function. The dimerisation of GPR19 with other receptors and the effect of that on the signalling pathways they activated is an interesting research area that requires investigation before exploring the biological function of GPR19 in adrenal cells and in other peripheral tissues.

7.2.3. Role of GPR19 in Adrenal Atrophy

Different studies have shown that the N-POMC fragments are required for normal adrenal cell growth and development during pregnancy (Fassnacht et al., 2003; Ross et

al., 2000; Saphier et al., 1993; Torres et al., 2010) and that patients with FGD are characterised with both atrophy of adrenal ZF and ZR with preservation of ZG and by cortisol deficiency due to poor response of adrenal cells to ACTH. It was found that 25% of the cases of FGD are linked to different MC2R mutations (Weber & Clark, 1994), 20% are linked to mutations in the MRAP sequence (Metherell et al., 2005), 5% of cases related to mutations in StAR (Metherell et al., 2009) and around 50% of the FGD cases had an unidentified genetic background. Unpublished data from the Bicknell lab found that the GPR19 protein is expressed across all the adrenal cortex zones and the adrenal capsule. Moreover, a study performed by Kastner et al. (2012) reported that the knockdown of Grp19 leads to a reduction in the proliferation of lung cancer-derived cell lines and an increase in the number of dead cells. Accordingly, this suggests a role of GPR19 in the cases of FGD with unidentified mutations that certainly require investigation.

7.2.4. N-POMC Fragments and Adropin as GPR19 Ligands

In this study, we showed that the cell lines that overexpressed GPR19 and/or MRAP showed a significant increase, in comparison to the WT, in N-POMC$_{1-28}$ binding capacity and the longer fragments: N-POMC$_{1-49}$ and N-POMC$_{1-77}$, can compete with N-POMC$_{1-28}$ for its binding site. Moreover, those cells showed a significant increase in the ERK1/2 phosphorylation when treated with serial N-POMC$_{1-28}$ concentrations and at different time intervals. In addition, the cell lines that overexpress GPR19, GPR19 alone or with MRAP, showed a significant increase in their ability to stimulate the cell proliferation pathway by following SEAP release from the cells. On the other hand, adropin showed a linear binding curve rather than a saturation curve in all four cell lines that were used in this study and did not compete with the N-POMC$_{1-28}$ specific binding site. In contrast, the N-POMC fragments 1-28, 1-49 and 1-77 can compete with the

adropin binding site. This finding suggests that adropin could bind to a receptor other than GPR19 and may dimerise with GPR19. The slight increase in the binding ability of adropin to the cell lines that overexpress GPR19 in comparison to the WT could suggest that overexpression of GPR19 may influence the binding ability of adropin to its receptor and expression of MRAP obstruct this feature of GPR19. We showed that both N-$POMC_{1-28}$ and adropin could reduce cAMP in all the cellular models that were used, but we could not confirm the significance of this finding due to lab limitations. Those findings are not enough to confirm that both peptides could act as GPR19 agonists.

Moreover, it was reported that non-glycosylated rat N-$POMC_{1-74}$ stimulates cAMP formation in HEK-293 stably transfected with the MC3R, while the glycosylated human N-$POMC_{1-76}$ does not stimulate cAMP formation (Tilemans et al., 1997). While the non-glycosylated rat N-$POMC_{1-74}$ stimulates cell proliferation of the human NCI-h295 cell line (Fassnacht et al., 2003). It seems that the natural form of $POMC_{1–74}$, which is glycosylated, is unlikely to act through the MC3R receptor, and glycosylation prevents this interaction, suggesting that it is acting through a different receptor. The above-mentioned results are performed in HEK-293 that overexpressed MC3R. HEK-293 expresses GPR19 and its cell surface expression increased with MC3R overexpression (Li et al., 2021). These results supported our finding that N-POMC binds to and signals through GPR19. Moreover, it highlighted the difference between using a natural fragment of N-POMC and a synthetic form. The widely used N-$POMC_{1-28}$, which is not a natural product and is described as an extraction artefact (Lowry, 2016), in many published studies on the effect of this peptide on adrenal cells does not reflect the role of the natural N-POMC in adrenal growth and steroidogenesis completely.

Moreover, the reports investigating the effect of N-POMC fragments on adrenal cells depend on the experimental system that is used to perform the experiment and the

extraction and preparations of the natural N-POMC fragment. The extracted fragment may contain a mixture of structurally similar fragments of N-POMC (Lowry, 2016) and either be glycosylated or not and does it contain the disulphide bridges or not. The isolated human N-$POMC_{2-59}$ from pituitaries was shown to be the most potent adrenal mitogenic factor among the other N-POMC fragments and ACTH (Estivariz et al., 1982). This finding needs to be studied more to answer the question of which N-POMC fragment is the natural ligand of GPR19.

7.2.5. PI-3K/Akt Signalling Pathway of GPR19 and Internalisation through β-arrestin.

Pepper and Bicknell (2009) reported that both N-POMC peptides:1-28 and 1-49, could stimulate the phosphorylation of Akt, a key molecule in the PI3 kinase pathway, with the phosphorylation response to be weaker in the cells treated with $POMC_{1–28}$ in comparison to the cells treated with N-$POMC_{1-49}$. This also confirms the fact that the cells are responding in a different manner to different N-POMC fragments that should be investigated, as mentioned in section 7.2.4. The same signalling pathway has been reported to be activated when GPR19 is stimulated with PIs to prevent neuronal cell death (Hossain et al., 2016). Interestingly, adropin was found to stimulate this pathway through GPR19 activation in HAC15 cells (Stelcer et al., 2020). Activation of this pathway using different N-POMC fragments and adropin in the four cellular models that were used in this study, in addition to a *Grp19* knockdown cell line, will add to our understanding of how those fragments modulate cell growth and how they act through GPR19.

As mentioned in Chapter 6, we tried to study the effect of N-POMC on GPR19 internalisation following β-arrestin as it is a feature of GPR19 desensitisation (Southern et al., 2013). Unfortunately, in the control cells, a high background was always detected, and although different modifications were applied to the protocol, the same results were

detected. Therefore, it is best to perform this experiment using a different protocol, such as PathHunter β-Arrestin assay for GPCR cell lines.

7.3. Summary

In summary, from the findings of this study and previous studies, the involvement of N-POMC and its receptor GPR19 in maintaining the integrity of normal adrenal gland growth can be proposed. First, pro-γ-MSH released from the anterior pituitary, which will be cleaved by AsP that is expressed in the cell membrane of the adrenal cells to produce the active adrenal mitogenic factor: N-POMC$_{1-52}$ (Bicknell et al., 2001) and/or N-POMC$_{1-49}$ (Bicknell, 2016; Seger & Bennett, 1986). The active form of N-POMC binds to GPR19, which requires MRAP to increase its cell membrane expression and convert it to an N-POMC-specific receptor (finding of this study).

Activation of GPR19 leads to the activation of $G\alpha_i$ that inhibits the activity of adenylyl cyclase, which leads to the reduction in cAMP levels (finding of this study and Rao and Herr (2017)). The activated G_i is found to mediate downstream signals through the activation of PI3K (Shah et al., 2005), which explains how N-POMC fragments, 1-28 and 1-49 (Pepper & Bicknell, 2009), and GPR19 (Hossain et al., 2016) signal by activating the PI3K/Akt pathway. In addition, activation of GPR19 leads to dissociation of the βγ subunit that will phosphorylate RAS, which will sequentially activate the cascade: c-RAF to MEK (Pepper & Bicknell, 2009) to ERK1/2 (this study, Fassnacht et al. (2003) and Pepper and Bicknell (2009)). This could be followed by the phosphorylation of GPR19 by GRK and the binding of β-arrestin to GPR19 and its internalisation (Southern et al., 2013). Unfortunately, this is not completely confirmed by this study.

Subsequently, the phosphorylated ERK1/2 induces the cytosolic signalling protein p90RSK (Thapa et al., 2018) that probably induces the proto-oncogenes: c-Fos

and c-Jun, like ACTH (this study and Torres and Lotfi (2007)), Which will lead to the activation of the key mediators in the initiation of the cell cycle: cyclin D2, D3, and E and degradation of the cyclin-dependent kinase inhibitory protein P27kip1 (de Mendonca et al., 2013; Mendonca & Lotfi, 2011) and maintaining normal adrenal cell proliferation. Consequently, the knockdown of Grp19 could lead to adrenal atrophy, while overexpression of GPR19 could trigger uncontrolled cell proliferation, which is a characteristic of cancer cells (Chen et al., 2021; Gerlach et al., 2023; Pu et al., 2022).

Chapter 8: Appendixes

Appendix. A

A.1. Luria-Bertani Medium (LB)

20 g of LB broth is dissolved in 1 L ddH_2O and then sterilised by autoclaving.

A.2. 0.5 M PIPES

17.3 g of PIPES is dissolved in 80 ml of ultra-pure water. The pH is adjusted to 6.7 with concentrated HCl, and then the volume is increased to 100 ml of ultra-pure water.

A.3. Inoue Transformation Buffer

2.72 g Mn.Cl_2.4H_2O, 0.55 g $CaCl_2$.2H_2O, and 4.66 g KCl are dissolved in 150 ml ultra-pure water. Then, 5 ml of 0.5 M PIPES (pH 6.7) is added, and the volume is increased to 250 ml with ultra-pure water.

A.4. LB Agar Plate

17.5 g of LB agar is added to 500 ml ddH2O and autoclaved to dissolve and sterilise the mixture. The LB agar bottle is kept in a 55 °C water bath to cool down to 55 °C. Aseptically, 0.1 mg/ml ampicillin or 0.05 mg/ml kanamycin was added and mixed well. The mixture was poured into 90 MM petri dishes to approx. 1 cm and the plates were left to set at RT and then stored upside down at 4 °C.

A.5. 5 X Reaction Buffer

For 1L: 250 mM Tris-HCl (pH 8.3), 250 mM KCl, 20 mM $MgCl_2$, and 50 mM DTT.

A.6. 4% (w/v) Paraformaldehyde (PFA)

PFA is toxic, and the preparation steps should be performed in a fume hood.

4g PFA is dissolved in 80 ml 1X PBS with continuous stirring and heating at 50-60°C till the PFA powder is completely dissolved. The pH was adjusted to 6.9, and the volume was made up to 100 ml. Then, the solution was filtered and aliquoted as appropriate and stored at -20°C.

A.7. 1 M Tris Stock

121.1 g Tris-base is dissolved in 800 ml of ddH_2O. Then, the pH is adjusted to 7 with concentrated HCl, and the volume is increased to 1 L with ddH_2O.

A.8. 2X SDS Sample Buffer (Non-Reducing)

5 ml of 1 M Tris stock (pH 7) is mixed with 25 ml 20% SDS, 20 ml glycerol, and 2 mg bromophenol blue. Then, the volume is increased to 100 ml with ddH_2O.

A.9. 2X SDS Sample Buffer (Reducing)

950 µl of 2X SDS sample buffer is mixed with 50 µl β-mercaptoethanol.

A.10. 4X Resolving Gel Buffer

187 g Tris-base (1.5 M) is dissolved in 800 ml ddH_2O. The pH is adjusted to 8.8 with HCl. Then, 4.0 g SDS (0.4%) is dissolved in the solution, and the volume is increased to 1 L with ddH2O.

A.11. 10% Resolving Gel

3.33 ml Protogel (National diagnostics) is mixed with 2.5 ml 4X Resolving gel buffer, 4.06 ml ddH_2O, 150 µl 10% APS (ammonium persulfate) and 10 µl TEMED (N,N,N′,N′-Tetramethylethylenediamine).

A.12. 4% Stacking Gel

1.3 ml Protogel (National diagnostics) is mixed with 2.5 ml 4X Stacking buffer (0.5 M Tris-HCl, 0.4% SDS, pH 6.8, Melford, UK), 6.1 ml ddH_2O, 100 µl 10% APS, and 10 µl TEMED.

A.13. 5X Tris-Glycine Running Buffer

15.1 g Tris-base and 49 g glycine were dissolved in 900 ml ddH_2O. Then, 50 ml 10% SDS is added and dissolved well, and the volume increased to 1 L with ddH_2O.

A.14. 1X Tris-Glycine Electrophoresis (Running Buffer)

200 ml of 5X Tris-glycine electrophoresis (Running Buffer) is mixed with 800 ml of ddH_2O. The pH is checked and adjusted to pH 8.3.

A.15. 10X Transfer Buffer

30.2 g Tris-base and 144 g glycine were dissolved in 800 ddH_2O. Then, the volume is increased to 1 L with ddH_2O.

A.16. 1X Transfer buffer

700 ml cold ddH_2O is mixed with 100 ml 10X Transfer buffer and 200 ml methanol.

A.17. 10X Tris Buffer Saline (TBS)

80 g of NaCl, 2 g KCl and 30 g Tris-base were dissolved in 800 ml ddH_2O. The pH is adjusted to 7.4 using concentrated HCl, and then the volume is increased to 1 L by ddH_2O.

A.18. 1X Tris Buffer Saline (TBS)

100 ml of 10X TBS is mixed with 900 ml ddH_2O.

A.19. 1X Tris Buffer Saline Tween (TBST)

100 ml of 10X TBS is mixed with 900 ml of ddH_2O. Then, 1 ml of Tween-20 is added and mixed well.

Appendix. B

A

NTNGCAGAGCTCTCTGGCTAACTAGAGANCCACTGCTTACTGGCTTATCGAAATTAATACGACTCACTATAGGGAGACCCAAGCTGG
CTAGCGTTTAAACTTAAGCTTCGAATTCGCCACCATGGGTTTTGATCACAGAATGGAGACCGACCAGCCCCCTGTGGTTACTGCTAC
CCTGCTGGTGCCCCTTCAGAATGGCAGCTGTGTGGAAGCGGCCGAGGCCCTGCTGCCCCATGGCCTGATGGAATTGCATGAGGAAC
ACAGCTGGATGAGCAACAGGACAGACCTTCAGTACGAGCTGAACCCCGGAGAGGTGGCCACAGCCAGCATTTTCTTTGGCGCTTTG
TGGTTGTTCTCTATCTTTGGCAATTCCCTTGTGTGTCTGGTCATCCATAGGAGCCGGAGGACTCAGTCCACCACCAACTACTTTGTGG
TCTCCATGGCGTGTGCTGACCTTCTCATCAGTGTGGCCAGCACACCGTTTGTCGTGCTGCAGTTCACTACCGGGAGGTGGACCCTC
GGGAGCGCCATGTGCAAGGTGGTCCGCTACTTCCAGTATCTCACCCCAGGCGTCCAGATCTACGTGCTGCTCTCCATCTGCATAGAC
CGCTTCTACACCATCGTCTACCCTCTGAGCTTCAAGGTGTCCAGAGAAAAGGCCAAGAGAATGATCGCAGCCTCCTGGATCTTGGAC
GCAGCCCTCGTGACGCCTGTCTTCTTTTTCTACGGCTCTAACTGGGATAGCCACTGTAACTACTTCCTCCCACCCTCCTGGGAGGGA
ACTGCCTATACTGTTATCCACTTCTTGGTGGGCTTTGTGATTCCCTCTGTCCTCATAATCCTGTTTTACCAGAAAGTCATAAAGTATAT
CTGGAGAATAGGCACGGACGGGCGGACCCTGAGGAGGACAATGAACATTGTCCCCAGGACCAAGGTGAAGACGGTCAAGATGTTT
CTGCTCTTGAACCTTGTGTTCCTGTTCTCCTGGCTGCCTTTCCATGTGGCTCAGCTCTGGCATCCCCATGAGCAAGACTACAGGAAG
AGCTCCCCTGTTTTCACAGCAGTCACGTGGGTGTCTTTCAGCTCTTCGGCCTCTAAACCCACTCTGTACTCTATTTATAACGCCAATT
TTCGGAGAGGGATGAAAGAGACTTTCTGCATGTCCTCAACGAAATGTTACCGCAGCAATGCCTACACCATCACGACCAGTTCAAGGA
TGGCCAAAAGAAACTATGTGGGCATTTCGGAAATCCCTCCCGTGAGCAGGACGATAACCAAAGACTCCATCTATGACTCATTTGACC
GTGAGGCCAGGGAGAAGAAGCTCGCCTGGCCCATCAACTCAAACCCACCAAACACTTTTGTCTAATTTCTAAGAACTCCTTCACTGT
TATGGATCCACTAGTCCAGTGTGGTGGAATTCTGCAGATATCCAGCACAGTGGCGGCCGCTCGAGNCTAGAGGCCCNNANCNCTCCC
NNGAGCAGGNNGATAACCAAAGACTCCATCTATGACTCANTNGACCGTGAGGCCAGGGAGAAGAAGCTCGCCTGGTCCATCAANTC
AAACCCACCAAACACNNN

B

MGFDHRMETDQPPVVTATLLVPLQNGSCVEAAEALLPHGLMELHEEHSWMSNRTDLQYELNPGEVATASIFFGALWLFSIFGNSLVCLVI
HRSRRTQSTTNYFVVSMACADLLISVASTPFVVLQFTTGRWTLGSAMCKVVRYFQYLTPGVQIYVLLSICIDRFYTIVYPLSFKVSREKAKR
MIAASWILDAALVTPVFFFYGSNWDSHCNYFLPPSWEGTAYTVIHFLVGFVIPSVLIILFYQKVIKYIWRIGTDGRTLRRTMNIVPRTKVKTV
KMFLLLNLVFLFSWLPFHVAQLWHPHEQDYRKSSPVFTAVTWVSFSSSASKPTLYSIYNANFRRGMKETFCMSSTKCYRSNAYTITTSSRM
AKRNYVGISEIPPVSRTITKDSIYDSFDREAREKKLAWPINSNPPNTFV

B.1. Rat GPR19 (rGPR19) Gene and Protein Sequence.

A) rGPR19 gene sequence that is inserted in the pcDNA5 plasmid using the Flp Recombinase-Mediated Integration technique showing the starting and stopping codon. B) The protein sequence of the rGPR19 has 415 amino acid residues with a molecular weight of 47.5 kDa.

B.2. Mouse MRAP (mMRAP) Gene and Protein Sequence.

A) mMRAP gene sequence that is inserted in the pcDNA5 plasmid using the Flp Recombinase-Mediated Integration technique showing the starting and stopping codon. B) The protein sequence of the mouse MRAP with HA-Tag at the C-terminus having a molecular weight of 15.3 kDa.

Appendix. C

C.1. Peptide Extraction Buffer

1 M HCl is mixed with 5% (v/v) Formic acid, 1% (v/v) Trifluoroacetic acid (TFA) and 0.15 M NaCl together and increase the volume to 1 L with ddH_2O.

C.2. TMB Solution

270 mg TMB was dissolved in 400 ml methanol. In a separate beaker, 50 mM sodium acetate anhydrous and 3.6 g citric acid were dissolved in 600 ml ddH_2O. Then, mix the two solutions together and store them in the dark at 4ºC.

To prepare the working solution of TMB, add 5 µl 30% (v/v) H_2O_2 to every 10 ml of TMB and mix well.

Appendix. D

D.1. Alkaline Phosphatase (ALP) Buffer

To 83 ml ddH_2O, 2 ml 5 M NaCl (final concentration 100 mM), 5 ml 1 M $MgCl_2$ (final concentration 50 mM), 10 ml 1 M Tris-Cl (pH 9.5, final concentration 100 mM) and 200 µl β-mercaptoethanol were added, mixed well, and stored at RT.

D.2. Buffer A

To 2.6 ml ddH_2O, 400 µl 1 M NaH_2PO_4, 400 µl 100 mM KCl, 400 µl 10 mM $MgSO_4$, and 200 µl β-mercaptoethanol were added, mixed well. This buffer should be prepared freshly on the day of the experiment.

Chapter 9: References

Achour, L., Labbé-Jullié, C., Scott, M. G., & Marullo, S. (2008). An escort for GPCRs: implications for regulation of receptor density at the cell surface. *Trends in Pharmacological Sciences*, *29*(10), 528-535.

Akil, H., Shiomi, H., & Matthews, J. (1985). Induction of the intermediate pituitary by stress: synthesis and release of a nonopioid form of beta-endorphin. *Science*, *227*(4685), 424-426.

Alam, J., & Cook, J. (2003). Reporter genes for monitoring gene expression in mammalian cells. *New Comprehensive Biochemistry*, *38*(3), 291–308.

Al-Dujaili, E. A., Hope, J., Estivariz, F. E., Lowry, P. J., & Edwards, C. R. (1981). Circulating human pituitary pro-gamma-melanotropin enhances the adrenal response to ACTH. *Nature*, *291*(5811), 156-159.

Ali, II, D'Souza, C., Singh, J., & Adeghate, E. (2022). Adropin's Role in Energy Homeostasis and Metabolic Disorders. *International journal of molecular sciences.*, *23*(15), 8318.

Almeida, M. Q., Silva, G. V., & Drager, L. F. (2020). What Is the Most Common Cause of Secondary Hypertension? An Interdisciplinary Discussion. *Current Hypertension Reports*, *22*(12), 101.

Ames, M. K., Atkins, C. E., & Pitt, B. (2019). The renin-angiotensin-aldosterone system and its suppression. *Journal of Veterinary Internal Medicine*, *33*(2), 363-382.

Asai, M., Ramachandrappa, S., Joachim, M., Shen, Y., Zhang, R., Nuthalapati, N., Ramanathan, V., Strochlic, D. E., Ferket, P., Linhart, K., Ho, C., Novoselova, T. V., Garg, S., Ridderstråle, M., Marcus, C., Hirschhorn, J. N., Keogh, J. M., O'Rahilly, S., Chan, L. F., . . . Majzoub, J. A. (2013). Loss of function of the

melanocortin 2 receptor accessory protein 2 is associated with mammalian obesity. *Science, 341*(6143), 275-278.

Attie, A. D., & Raines, R. T. (1995). Analysis of Receptor-Ligand Interactions. *Journal of chemical education*, *72*(2), 119-124.

Atwood, B. K., Lopez, J., Wager-Miller, J., Mackie, K., & Straiker, A. (2011). Expression of G protein-coupled receptors and related proteins in HEK293, AtT20, BV2, and N18 cell lines as revealed by microarray analysis. *BioMed Central Genomics*, *12*, 14.

Aumo, L., Rusten, M., Mellgren, G., Bakke, M., & Lewis, A. E. (2010). Functional roles of protein kinase A (PKA) and exchange protein directly activated by 3',5'-cyclic adenosine 5'-monophosphate (cAMP) 2 (EPAC2) in cAMP-mediated actions in adrenocortical cells. *Endocrinology*, *151*(5), 2151-2161.

Azimzadeh, P., Olson, J. A., Jr., & Balenga, N. (2017). Reporter gene assays for investigating GPCR signaling. *Methods Cell Biology*, *142*, 89-99.

Babischkin, J. S., Aberdeen, G. W., Pepe, G. J., & Albrecht, E. D. (2016). Estrogen Suppresses Interaction of Melanocortin 2 Receptor and Its Accessory Protein in the Primate Fetal Adrenal Cortex. *Endocrinology*, *157*(12), 4588-4601.

Bandiera, R., Sacco, S., Vidal, V. P., Chaboissier, M. C., & Schedl, A. (2015). Steroidogenic organ development and homeostasis: A WT1-centric view. *Molecular and cellular endocrinology*, *408*, 145-155.

Bandiera, R., Vidal, V. P., Motamedi, F. J., Clarkson, M., Sahut-Barnola, I., von Gise, A., Pu, W. T., Hohenstein, P., Martinez, A., & Schedl, A. (2013). WT1 maintains adrenal-gonadal primordium identity and marks a population of AGP-like progenitors within the adrenal gland. *Developmental Cell*, *27*(1), 5-18.

Barnard, L., du Toit, T., & Swart, A. C. (2021). Back where it belongs: 11β-hydroxyandrostenedione compels the re-assessment of C11-oxy androgens in steroidogenesis. *Molecular and cellular endocrinology*, *525*, 111189.

Beavo, J. A., Rogers, N. L., Crofford, O. B., Hardman, J. G., Sutherland, E. W., & Newman, E. V. (1970). Effects of xanthine derivatives on lipolysis and on adenosine 3',5'-monophosphate phosphodiesterase activity. *Molecular pharmacology*, *6*(6), 597-603.

Bennett, H. P., Seidah, N. G., Benjannet, S., Solomon, S., & Chrétien, M. (1986). Reinvestigation of the disulfide bridge arrangement in human pro-opiomelanocortin N-terminal segment (hNT 1-76). *International journal of protein research*, *27*(3), 306-313.

Berggård, T., Linse, S., & James, P. (2007). Methods for the detection and analysis of protein-protein interactions. *Proteomics*, *7*(16), 2833-2842.

Bert, C., Vande Vijver, V., Andries, M., Verhaert, P., Proost, P., De Vreese, B., Van Beeumen, J., Vankelecom, H., & Denef, C. (1999). Production of recombinant rat proopiomelanocortin1-74 and characterization of its mitogenic action on pituitary lactotrophs. *Molecular and cellular endocrinology*, *154*(1-2), 111-122.

Bertagna, X., Camus, F., Lenne, F., Girard, F., & Luton, J. P. (1988). Human joining peptide: a proopiomelanocortin product secreted as a homodimer. *Molecular endocrinology*, *2*(11), 1108-1114.

Bicknell, A. B. (2003). Identification of a serine protease involved with the regulation of adrenal growth. *Annals of the New York Academy of Sciences*, *994*, 118-122.

Bicknell, A. B. (2008). The tissue-specific processing of pro-opiomelanocortin. *Journal of neuroendocrinology*, *20*(6), 692-699.

Bicknell, A. B. (2016). 60 YEARS OF POMC: N-terminal POMC peptides and adrenal growth. *Journal of molecular endocrinology*, *56*(4), 39-48.

Bicknell, A. B., Lomthaisong, K., Woods, R. J., Hutchinson, E. G., Bennett, H. P., Gladwell, R. T., & Lowry, P. J. (2001). Characterization of a serine protease that cleaves pro-gamma-melanotropin at the adrenal to stimulate growth. *Cell*, *105*(7), 903-912.

Bioletto, F., Bollati, M., Lopez, C., Arata, S., Procopio, M., Ponzetto, F., Ghigo, E., Maccario, M., & Parasiliti-Caprino, M. (2022). Primary Aldosteronism and Resistant Hypertension: A Pathophysiological Insight. *International journal of molecular sciences.*, *23*(9), 4803.

Böhme, I., & Beck-Sickinger, A. G. (2009). Illuminating the life of GPCRs. *Cell Communication and Signaling*, *7*(1), 16.

Bouvier, M. (2001). Oligomerization of G-protein-coupled transmitter receptors. *Nature Reviews Neuroscience*, *2*(4), 274-286.

Brady, A. E., & Limbird, L. E. (2002). G protein-coupled receptor interacting proteins: emerging roles in localization and signal transduction. *Cell Signalling*, *14*(4), 297-309.

Bresnick, J. N., Skynner, H. A., Chapman, K. L., Jack, A. D., Zamiara, E., Negulescu, P., Beaumont, K., Patel, S., & McAllister, G. (2003). Identification of signal transduction pathways used by orphan g protein-coupled receptors. *Assay and drug development technologies*, *1*(2), 239-249.

Brewster, U. C., & Perazella, M. A. (2004). The renin-angiotensin-aldosterone system and the kidney: effects on kidney disease. *The American Journal of Medicine*, *116*(4), 263-272.

Butler, A. A., Kesterson, R. A., Khong, K., Cullen, M. J., Pelleymounter, M. A., Dekoning, J., Baetscher, M., & Cone, R. D. (2000). A unique metabolic syndrome causes obesity in the melanocortin-3 receptor-deficient mouse. *Endocrinology*, *141*(9), 3518-3521.

Cawley, N. X., Li, Z., & Loh, Y. P. (2016). 60 YEARS OF POMC: Biosynthesis, trafficking, and secretion of pro-opiomelanocortin-derived peptides. *Journal of molecular endocrinology*, *56*(4), 77-97.

Chaly, A. L., Srisai, D., Gardner, E. E., & Sebag, J. A. (2016). The Melanocortin Receptor Accessory Protein 2 promotes food intake through inhibition of the Prokineticin Receptor-1. *E-life*, *5*, e12397.

Chan, L. F., Webb, T. R., Chung, T. T., Meimaridou, E., Cooray, S. N., Guasti, L., Chapple, J. P., Egertova, M., Elphick, M. R., Cheetham, M. E., Metherell, L. A., & Clark, A. J. (2009). MRAP and MRAP2 are bidirectional regulators of the melanocortin receptor family. *Proceedings of the National Academy of Sciences of the USA*, *106*(15), 6146-6151.

Chen, L., Li, J., Wu, X., & Zheng, Z. (2021). Identification of Somatic Genetic Alterations Using Whole-Exome Sequencing of Uterine Leiomyosarcoma Tumors. *Frontiers in Oncology*, *11*, 687899.

Chen, W., Kelly, M. A., Opitz-Araya, X., Thomas, R. E., Low, M. J., & Cone, R. D. (1997). Exocrine gland dysfunction in MC5-R-deficient mice: evidence for coordinated regulation of exocrine gland function by melanocortin peptides. *Cell*, *91*(6), 789-798.

Chida, D., Nakagawa, S., Nagai, S., Sagara, H., Katsumata, H., Imaki, T., Suzuki, H., Mitani, F., Ogishima, T., Shimizu, C., Kotaki, H., Kakuta, S., Sudo, K., Koike, T., Kubo, M., & Iwakura, Y. (2007). Melanocortin 2 receptor is required for

adrenal gland development, steroidogenesis, and neonatal gluconeogenesis. *Proceedings of the National Academy of Sciences, 104*(46), 18205-18210.

Ching, S., & Vilain, E. (2009). Targeted disruption of Sonic Hedgehog in the mouse adrenal leads to adrenocortical hypoplasia. *Genesis, 47*(9), 628-637.

Chrétien, M., Benjannet, S., Gossard, F., Gianoulakis, C., Crine, P., Lis, M., & Seidah, N. G. (1979). From beta-lipotropin to beta-endorphin and 'pro-opio-melanocortin'. *Canadian journal of biochemistry, 57*(9), 1111-1121.

Chung, S., Son, G. H., & Kim, K. (2011). Circadian rhythm of adrenal glucocorticoid: its regulation and clinical implications. *International journal of biochemistry and biophysics, 1812*(5), 581-591.

Civelli, O., Reinscheid, R. K., Zhang, Y., Wang, Z., Fredriksson, R., & Schiöth, H. B. (2013). G Protein–Coupled Receptor Deorphanizations. *Annual Review of Pharmacology and Toxicology, 53*(1), 127-146.

Clark, A. J., Forfar, R., Hussain, M., Jerman, J., McIver, E., Taylor, D., & Chan, L. (2016). ACTH Antagonists. *Frontiers in Endocrinology, 7*, 101.

Clontech Laboratories, I. (1999). pSRE-SEAP Vector Information. In *PT3277-5* (Vol. PT3277-5, pp. PT3277-3275).

Clontech Laboratories, I. (2005). Great EscAPe™ SEAP User Manual. In *PT3057-1* (Vol. PT3057-1, pp. PT3057-3051).

Coble, J. P., Grobe, J. L., Johnson, A. K., & Sigmund, C. D. (2015). Mechanisms of brain renin angiotensin system-induced drinking and blood pressure: importance of the subfornical organ. *American Journal of Physiology-Regulatory, Integrative and Comparative Physiology, 308*(4), R238-R249.

Coll, A. P., Challis, B. G., Yeo, G. S., Snell, K., Piper, S. J., Halsall, D., Thresher, R. R., & O'Rahilly, S. (2004). The effects of proopiomelanocortin deficiency on murine

adrenal development and responsiveness to adrenocorticotropin. *Endocrinology*, *145*(10), 4721-4727.

Coll, A. P., Fassnacht, M., Klammer, S., Hahner, S., Schulte, D. M., Piper, S., Tung, Y. C., Challis, B. G., Weinstein, Y., Allolio, B., O'Rahilly, S., & Beuschlein, F. (2006). Peripheral administration of the N-terminal pro-opiomelanocortin fragment 1-28 to Pomc-/- mice reduces food intake and weight but does not affect adrenal growth or corticosterone production. *The Journal of endocrinology*, *190*(2), 515-525.

Cone, R. D. (2006). Studies on the physiological functions of the melanocortin system. *Endocrine Reviews*, *27*(7), 736-749.

Cool, D. R., & Loh, Y. P. (1994). Identification of a sorting signal for the regulated secretory pathway at the N-terminus of pro-opiomelanocortin. *Biochimie*, *76*(3-4), 265-270.

Cool, D. R., Fenger, M., Snell, C. R., & Loh, Y. P. (1995). Identification of the sorting signal motif within pro-opiomelanocortin for the regulated secretory pathway. *The Journal of biological chemistry*, *270*(15), 8723-8729.

Coulter, C. L., Ross, J. T., Salkeld, M. D., Bennett, H. P., James, S., & McMillen, I. C. (2000). N-proopiomelanocortin (1-77) suppresses expression of steroidogenic acute regulatory protein (StAR) mRNA in the adrenal gland of the fetal sheep. *Endocrine Research*, *26*(4), 523-529.

Cullen, B. R. (2000). Utility of the secreted placental alkaline phosphatase reporter enzyme. *Methods in enzymology*, *326*, 159-164.

Dallman, M. F., Engeland, W. C., Holzwarth, M. A., & Scholz, P. M. (1980). Adrenocorticotropin inhibits compensatory adrenal growth after unilateral adrenalectomy. *Endocrinology*, *107*(5), 1397-1404.

de Mendonca, P. O., Liria, C. W., Machini, M. T., & Lotfi, C. F. (2013). N-POMC1-28 increases cyclin D expression and inhibits P27(kip1) in the adrenal cortex. *Molecular and cellular endocrinology*, *371*(1-2), 166-173.

Denef, C., & Van Bael, A. (1998). A new family of growth and differentiation factors derived from the N-terminal domain of proopiomelanocortin (N-POMC). *Comparative biochemistry and physiology. Part C, Pharmacology, toxicology and endocrinology*, *119*(3), 317-324.

Dhillo, W. S., Small, C. J., Gardiner, J. V., Bewick, G. A., Whitworth, E. J., Jethwa, P. H., Seal, L. J., Ghatei, M. A., Hinson, J. P., & Bloom, S. R. (2003). Agouti-related protein has an inhibitory paracrine role in the rat adrenal gland. *Biochemical and biophysical research communications*, *301*(1), 102-107.

Doghman, M., Karpova, T., Rodrigues, G. A., Arhatte, M., De Moura, J., Cavalli, L. R., Virolle, V., Barbry, P., Zambetti, G. P., Figueiredo, B. C., Heckert, L. L., & Lalli, E. (2007). Increased steroidogenic factor-1 dosage triggers adrenocortical cell proliferation and cancer. *Molecular endocrinology*, *21*(12), 2968-2987.

Dong, C., Liu, Z., & Wang, F. (2015). Radioligand saturation binding for quantitative analysis of ligand-receptor interactions. *Biophysics Reports*, *1*(3), 148-155.

Dores, R. M., Liang, L., Davis, P., Thomas, A. L., & Petko, B. (2016). 60 YEARS OF POMC: Melanocortin receptors: evolution of ligand selectivity for melanocortin peptides. *Journal of molecular endocrinology*, *56*(4), T119-T133.

Dumontet, T., & Martinez, A. (2021). Adrenal androgens, adrenarche, and zona reticularis: A human affair? *Molecular and cellular endocrinology*, *528*, 111239.

Ehrhart-Bornstein, M., Hinson, J. P., Bornstein, S. R., Scherbaum, W. A., & Vinson, G. P. (1998). Intraadrenal interactions in the regulation of adrenocortical steroidogenesis. *Endocrine Reviews*, *19*(2), 101-143.

Eipper, B. A., & Mains, R. E. (1980). Structure and biosynthesis of pro-adrenocorticotropin/endorphin and related peptides. *Endocrine Reviews*, *1*(1), 1-27.

Elustondo, P., Martin, L. A., & Karten, B. (2017). Mitochondrial cholesterol import. *Molecular and cell biology of lipids*, *1862*(1), 90-101.

Estivariz, F. E., Carino, M., Lowry, P. J., & Jackson, S. (1988). Further evidence that N-terminal pro-opiomelanocortin peptides are involved in adrenal mitogenesis. *The Journal of endocrinology*, *116*(2), 201-206.

Estivariz, F. E., Iturriza, F., McLean, C., Hope, J., & Lowry, P. J. (1982). Stimulation of adrenal mitogenesis by N-terminal proopiocortin peptides. *Nature*, *297*(5865), 419-422.

Estivariz, F. E., Morano, M. I., Carino, M., Jackson, S., & Lowry, P. J. (1988). Adrenal regeneration in the rat is mediated by mitogenic N-terminal pro-opiomelanocortin peptides generated by changes in precursor processing in the anterior pituitary. *The Journal of endocrinology*, *116*(2), 207-216.

Fagerberg, L., Hallström, B. M., Oksvold, P., Kampf, C., Djureinovic, D., Odeberg, J., Habuka, M., Tahmasebpoor, S., Danielsson, A., Edlund, K., Asplund, A., Sjöstedt, E., Lundberg, E., Szigyarto, C. A., Skogs, M., Takanen, J. O., Berling, H., Tegel, H., Mulder, J., . . . Uhlén, M. (2014). Analysis of the human tissue-specific expression by genome-wide integration of transcriptomics and antibody-based proteomics. *Molecular and cellular proteomics*, *13*(2), 397-406.

Fassnacht, M., Hahner, S., Hansen, I. A., Kreutzberger, T., Zink, M., Adermann, K., Jakob, F., Troppmair, J., & Allolio, B. (2003). N-terminal proopiomelanocortin acts as a mitogen in adrenocortical tumor cells and decreases adrenal

steroidogenesis. *The Journal of clinical endocrinology and metabolism*, *88*(5), 2171-2179.

Finco, I., Lerario, A. M., & Hammer, G. D. (2018). Sonic Hedgehog and WNT Signaling Promote Adrenal Gland Regeneration in Male Mice. *Endocrinology*, *159*(2), 579-596.

Finlay, D. B., Duffull, S. B., & Glass, M. (2020). 100 years of modelling ligand-receptor binding and response: A focus on GPCRs. *British journal of pharmacology*, *177*(7), 1472-1484.

Flanagan, C. A. (2016). GPCR-radioligand binding assays. *Methods in cell biology*, *132*, 191-215.

Foster, S. R., Hauser, A. S., Vedel, L., Strachan, R. T., Huang, X. P., Gavin, A. C., Shah, S. D., Nayak, A. P., Haugaard-Kedström, L. M., Penn, R. B., Roth, B. L., Bräuner-Osborne, H., & Gloriam, D. E. (2019). Discovery of Human Signaling Systems: Pairing Peptides to G Protein-Coupled Receptors. *Cell*, *179*(4), 895-908.

Freed, S. C., Brownfield, B., & Evans, H. M. (1931). Effect of Adrenalectomy on the Testes of the Rat. *Proceedings of the Society for Experimental Biology and Medicine*, *29*(1), 1-3.

Fukuda, T. R. (1952). On bilateral adrenalectomy in rabbits. *The Japanese journal of physiology*, *2*(3), 208-212.

Galasko, G. (2015). Hyperaldosteronism. In *Reference Module in Biomedical Sciences*. Elsevier.

Gallo-Payet, N. (2016). 60 YEARS OF POMC: Adrenal and extra-adrenal functions of ACTH. *Journal of molecular endocrinology*, *56*(4), T135-T156.

Ganesh Kumar, K., Zhang, J., Gao, S., Rossi, J., McGuinness, O. P., Halem, H. H., Culler, M. D., Mynatt, R. L., & Butler, A. A. (2012). Adropin deficiency is associated

with increased adiposity and insulin resistance. *Obesity (Silver Spring)*, *20*(7), 1394-1402.

Gantz, I., Konda, Y., Tashiro, T., Shimoto, Y., Miwa, H., Munzert, G., Watson, S. J., DelValle, J., & Yamada, T. (1993). Molecular cloning of a novel melanocortin receptor. *The Journal of biological chemistry*, *268*(11), 8246-8250.

Gao, X., Li, F., Liu, B., Wang, Y., Wang, Y., & Zhou, H. (2021). Cellular Senescence in Adrenocortical Biology and Its Disorders. *Cells*, *10*(12), 3474.

Gaunt, R. (1933). Adrenalectomy in the rat. *American Journal of Physiology-Legacy Content*, *103*(2), 494-510.

Geller, S. A. (1964). ACTH production by non-pituitary tumors: a review. *Journal of the National Medical Association*, *56*(5), 415-418.

Gerlach, L., Beyer, A. L., Kaemmerer, D., Sänger, J., Evert, K., Schulz, S., & Lupp, A. (2023). Expression of G protein-coupled receptor GPR19 in normal and neoplastic human tissues. *Scientific reports*, *13*(1), 18993.

Ghayee, H. K., & Auchus, R. J. (2007). Basic concepts and recent developments in human steroid hormone biosynthesis. *Reviews in endocrine and metabolic disorders*, *8*(4), 289-300.

Gorrigan, R. J., Guasti, L., King, P., Clark, A. J., & Chan, L. F. (2011). Localisation of the melanocortin-2-receptor and its accessory proteins in the developing and adult adrenal gland. *Journal of molecular endocrinology*, *46*(3), 227-232.

Gossard, F., Seidah, N. G., Crine, P., Routhier, R., & Chrétien, M. (1980). Partial N-terminal amino acid sequence of pro-opio-melanocortin (ACTH/beta-LPH precursor) from rat pars intermedia. *Biochemical and biophysical research communications*, *92*(3), 1042-1051.

Goto, M., Piper Hanley, K., Marcos, J., Wood, P. J., Wright, S., Postle, A. D., Cameron, I. T., Mason, J. I., Wilson, D. I., & Hanley, N. A. (2006). In humans, early cortisol biosynthesis provides a mechanism to safeguard female sexual development. *The Journal of clinical investigation*, *116*(4), 953-960.

Groskreutz, D., & Schenborn, E. T. (1997). Reporter systems. *Methods in molecular biology*, *63*, 11-30.

Gurevich, V. V., & Gurevich, E. V. (2018). GPCRs and Signal Transducers: Interaction Stoichiometry. *Trends in Pharmacological Sciences*, *39*(7), 672-684.

Haber, D. A., & Housman, D. E. (1992). The genetics of Wilms' tumor. *Advances in cancer research*, *59*, 41-68.

Hammer, G. D., & Basham, K. J. (2021). Stem cell function and plasticity in the normal physiology of the adrenal cortex. *Molecular and cellular endocrinology*, *519*, 111043.

Hammer, G. D., Parker, K. L., & Schimmer, B. P. (2005). Minireview: transcriptional regulation of adrenocortical development. *Endocrinology*, *146*(3), 1018-1024.

Hanley, N. A., Ball, S. G., Clement-Jones, M., Hagan, D. M., Strachan, T., Lindsay, S., Robson, S., Ostrer, H., Parker, K. L., & Wilson, D. I. (1999). Expression of steroidogenic factor 1 and Wilms' tumour 1 during early human gonadal development and sex determination. *Mechanisms of Development*, *87*(1-2), 175-180.

Harmer, S. C., & Bicknell, A. B. (2004). The role of the melanocortin 3 receptor in mediating the effects of gamma-MSH peptides on the adrenal. *Endocrine Research*, *30*(4), 629-635.

Harmer, S. C., & Bicknell, A. B. (2005). Role of gamma-MSH peptides in the regulation of adrenal steroidogenesis. *Peptides*, *26*(10), 1944-1951.

Harno, E., Gali Ramamoorthy, T., Coll, A. P., & White, A. (2018). POMC: The Physiological Power of Hormone Processing. *Physiological reviews*, *98*(4), 2381-2430.

Hatano, O., Takakusu, A., Nomura, M., & Morohashi, K. (1996). Identical origin of adrenal cortex and gonad revealed by expression profiles of Ad4BP/SF-1. *Genes Cells*, *1*(7), 663-671.

He, Y., Sun, M. M., Zhang, G. G., Yang, J., Chen, K. S., Xu, W. W., & Li, B. (2021). Targeting PI3K/Akt signal transduction for cancer therapy. *Signal transduction and targeted therapy*, *6*(1), 425.

Hermanson, G. T., & ebrary, I. (2013). *Bioconjugate techniques [electronic resource] Greg T. Hermanson* (3rd ed ed.). Academic Press.

Hinze, C., & Boucrot, E. (2018). Endocytosis in proliferating, quiescent and terminally differentiated cells. *Journal of cell science*, *131*(23), jcs216804.

Hoffmeister-Ullerich, S. A., Susens, U., & Schaller, H. C. (2004). The orphan G-protein-coupled receptor GPR19 is expressed predominantly in neuronal cells during mouse embryogenesis. *Cell and tissue research*, *318*(2), 459-463.

Holtbäck, U., Brismar, H., DiBona, G. F., Fu, M., Greengard, P., & Aperia, A. (1999). Receptor recruitment: a mechanism for interactions between G protein-coupled receptors. *Proceedings of the National Academy of Sciences of the USA*, *96*(13), 7271-7275.

Hornsby, P. J. (1984). Regulation of adrenocortical cell proliferation in culture. *Endocrine Research*, *10*(3-4), 259-281.

Hossain, M. S., Mineno, K., & Katafuchi, T. (2016). Neuronal Orphan G-Protein Coupled Receptor Proteins Mediate Plasmalogens-Induced Activation of ERK and Akt Signaling. *Public Library of Science one*, *11*(3), e0150846.

Huang, C. C., Miyagawa, S., Matsumaru, D., Parker, K. L., & Yao, H. H. (2010). Progenitor cell expansion and organ size of mouse adrenal is regulated by sonic hedgehog. *Endocrinology*, *151*(3), 1119-1128.

Hulme, E. C., & Trevethick, M. A. (2010). Ligand binding assays at equilibrium: validation and interpretation. *British journal of pharmacology*, *161*(6), 1219-1237.

Husebye, E. S., Pearce, S. H., Krone, N. P., & Kämpe, O. (2021). Adrenal insufficiency. *Lancet*, *397*(10274), 613-629.

Invitrogen. (2010). Flp-In™ System: For Generating Stable Mammalian Expression Cell Lines by Flp Recombinase-Mediated Integration. In *User Manual: K6010–01* (Vol. Version E, pp. K6010–6002).

Jackson, D. S., Ramachandrappa, S., Clark, A. J., & Chan, L. F. (2015). Melanocortin receptor accessory proteins in adrenal disease and obesity. *Frontiers in neuroscience*, *9*, 213.

Jahnke, G. D., Soldato, C. M., Erisman, M. D., DiAugustine, R. P., & Lazarus, L. H. (1983). "Joining peptide" of pro-opiomelanocortin. II. Interspecies heterogeneity of the joining peptide fragment. *Peptides*, *4*(4), 483-492.

Jasaszwili, M., Wojciechowicz, T., Billert, M., Strowski, M. Z., Nowak, K. W., & Skrzypski, M. (2019). Effects of adropin on proliferation and differentiation of 3T3-L1 cells and rat primary preadipocytes. *Molecular and cellular endocrinology*, *496*, 110532.

Jež, M., Bas, T., Veber, M., Košir, A., Dominko, T., Page, R., & Rožman, P. (2013). The hazards of DAPI photoconversion: effects of dye, mounting media and fixative, and how to minimize the problem. *Histochemistry and Cell Biology*, *139*(1), 195-204.

Jones, B. W., Song, G. J., Greuber, E. K., & Hinkle, P. M. (2007). Phosphorylation of the Endogenous Thyrotropin-releasing Hormone Receptor in Pituitary GH3 Cells and Pituitary Tissue Revealed by Phosphosite-specific Antibodies. *Journal of Biological Chemistry*, *282*(17), 12893-12906.

Kain, S. R. (1997). Use of secreted alkaline phosphatase as a reporter of gene expression in mammalian cells. *Methods in molecular biology*, *63*, 49-60.

Karpac, J., Ostwald, D., Bui, S., Hunnewell, P., Shankar, M., & Hochgeschwender, U. (2005). Development, Maintenance, and Function of the Adrenal Gland in Early Postnatal Proopiomelanocortin-Null Mutant Mice. *Endocrinology*, *146*(6), 2555-2562.

Kasai, R. S., Ito, S. V., Awane, R. M., Fujiwara, T. K., & Kusumi, A. (2018). The Class-A GPCR Dopamine D2 Receptor Forms Transient Dimers Stabilized by Agonists: Detection by Single-Molecule Tracking. *Cell biochemistry and biophysics*, *76*(1-2), 29-37.

Kastner, S., Voss, T., Keuerleber, S., Glockel, C., Freissmuth, M., & Sommergruber, W. (2012). Expression of G protein-coupled receptor 19 in human lung cancer cells is triggered by entry into S-phase and supports G(2)-M cell-cycle progression. *Molecular cancer research*, *10*(10), 1343-1358.

Kempná, P., & Flück, C. E. (2008). Adrenal gland development and defects. *Best practice and research. Clinical endocrinology and metabolism*, *22*(1), 77-93.

Kim, J. H., & Choi, M. H. (2020). Embryonic Development and Adult Regeneration of the Adrenal Gland. *Endocrinology and metabolism*, *35*(4), 765-773.

Kimura, E., & Armelin, H. A. (1990). Phorbol ester mimics ACTH action in corticoadrenal cells stimulating steroidogenesis, blocking cell cycle, changing

cell shape, and inducing c-fos proto-oncogene expression. *The Journal of biological chemistry*, *265*(6), 3518-3521.

Kimura, E., Sonobe, M. H., Armelin, M. C., & Armelin, H. A. (1993). Induction of FOS and JUN proteins by adrenocorticotropin and phorbol ester but not by 3',5'-cyclic adenosine monophosphate derivatives. *Molecular Endocrinology*, *7*(11), 1463-1471.

King, P., Paul, A., & Laufer, E. (2009). Shh signaling regulates adrenocortical development and identifies progenitors of steroidogenic lineages. *Proceedings of the National Academy of Sciences of the USA*, *106*(50), 21185-21190.

Kiss, A. L., & Botos, E. (2009). Endocytosis via caveolae: alternative pathway with distinct cellular compartments to avoid lysosomal degradation? *Journal of cellular and molecular medicine*, *13*(7), 1228-1237.

Klotz, U., Antonin, K. H., & Bieck, P. (1977). Cyclic nucleotide phosphodiesterases of human and rat gastric mucosa. *Naunyn-Schmiedeberg's archives of pharmacology*, *296*(2), 187-190.

Kumar, K. G., Trevaskis, J. L., Lam, D. D., Sutton, G. M., Koza, R. A., Chouljenko, V. N., Kousoulas, K. G., Rogers, P. M., Kesterson, R. A., Thearle, M., Ferrante, A. W., Jr., Mynatt, R. L., Burris, T. P., Dong, J. Z., Halem, H. A., Culler, M. D., Heisler, L. K., Stephens, J. M., & Butler, A. A. (2008). Identification of adropin as a secreted factor linking dietary macronutrient intake with energy homeostasis and lipid metabolism. *Cell Metabolism*, *8*(6), 468-481.

Kumar, K., Kumar, S., Kurupati, R. K., Seth, M. K., Mohan, A., Hussain, M. E., & Pasha, S. (2011). Intracellular cAMP assay and Eu-GTP-γS binding studies of chimeric opioid peptide YFa. *European journal of pharmacology*, *650*(1), 28-33.

Kunselman, J. M., Lott, J., & Puthenveedu, M. A. (2021). Mechanisms of selective G protein-coupled receptor localization and trafficking. *Current opinion in cell biology*, *71*, 158-165.

Lacroix, A. P., Feelders, R. A. M. D., Stratakis, C. A. M. D., & Nieman, L. K. M. D. (2015). Cushing's syndrome. *The Lancet (British edition)*, *386*(9996), 913-927.

Lala, D. S., Rice, D. A., & Parker, K. L. (1992). Steroidogenic factor I, a key regulator of steroidogenic enzyme expression, is the mouse homolog of fushi tarazu-factor I. *Molecular Endocrinology*, *6*(8), 1249-1258.

Lauth, M. (2011). RAS and Hedgehog--partners in crime. *Frontiers in bioscience (Landmark edition)*, *16*(6), 2259-2270.

Le, T., & Schimmer, B. P. (2001). The regulation of MAPKs in Y1 mouse adrenocortical tumor cells. *Endocrinology*, *142*(10), 4282-4287.

Legros, F., & Lehoux, J. G. (1983). Changes in characteristics of rat adrenal glomerulosa cells under acute and chronic treatment with ACTH. *Canadian journal of biochemistry and cell biology*, *61*(7), 538-546.

Lepique, A. P., Moraes, M. S., Rocha, K. M., Eichler, C. B., Hajj, G. N., Schwindt, T. T., & Armelin, H. A. (2004). c-Myc protein is stabilized by fibroblast growth factor 2 and destabilized by ACTH to control cell cycle in mouse Y1 adrenocortical cells. *Journal of molecular endocrinology*, *33*(3), 623-638.

Li, Y., Wang, X., Lu, L., Wang, M., Zhai, Y., Tai, X., Dilimulati, D., Lei, X., Xu, J., Zhang, C., Fu, Y., Qu, S., Li, Q., & Zhang, C. (2021). Identification of novel GPCR partners of the central melanocortin signaling. *Molecular metabolism*, *53*, 101317.

Liddington, R. C. (2004). Structural basis of protein-protein interactions. *Methods in molecular biology*, *261*, 3-14.

Little, D. W., 3rd, Dumontet, T., LaPensee, C. R., & Hammer, G. D. (2021). β-catenin in adrenal zonation and disease. *Molecular and cellular endocrinology*, *522*, 111120.

Liu, N., Wang, Y., Li, T., & Feng, X. (2021). G-Protein Coupled Receptors (GPCRs): Signaling Pathways, Characterization, and Functions in Insect Physiology and Toxicology. *International journal of molecular sciences*, *22*(10), 5260.

Lorsignol, A., Vande Vijver, V., Ramaekers, D., Vankelecom, H., & Denef, C. (1999). Detection of melanocortin-3 receptor mRNA in immature rat pituitary: functional relation to gamma3-MSH-induced changes in intracellular Ca2+ concentration? *Journal of neuroendocrinology*, *11*(3), 171-179.

Lotfi, C. F., Todorovic, Z., Armelin, H. A., & Schimmer, B. P. (1997). Unmasking a growth-promoting effect of the adrenocorticotropic hormone in Y1 mouse adrenocortical tumor cells. *The Journal of biological chemistry*, *272*(47), 29886-29891.

Lourenço, E. V., & Roque-Barreira, M. C. (2010). Immunoenzymatic quantitative analysis of antigens expressed on the cell surface (cell-ELISA). *Methods in molecular biology*, *588*, 301-309.

Lovren, F., Pan, Y., Quan, A., Singh, K. K., Shukla, P. C., Gupta, M., Al-Omran, M., Teoh, H., & Verma, S. (2010). Adropin is a novel regulator of endothelial function. *Circulation*, *122*(11 Suppl), S185-S192.

Lowry, P. (2016). 60 YEARS OF POMC: Purification and biological characterisation of melanotrophins and corticotrophins. *Journal of molecular endocrinology*, *56*(4), T1-T12.

Lowry, P. J., Silas, L., McLean, C., Linton, E. A., & Estivariz, F. E. (1983). Pro-gamma-melanocyte-stimulating hormone cleavage in adrenal gland undergoing compensatory growth. *Nature*, *306*(5938), 70-73.

Lowry, P. J., Silman, R. E., Hope, J., & Scott, A. P. (1977). Structure and biosynthesis of peptides related to corticotropins and beta-melanotropins. *Annals of the New York Academy of Sciences*, *297*, 49-62.

Luo, X., Ikeda, Y., & Parker, K. L. (1994). A cell-specific nuclear receptor is essential for adrenal and gonadal development and sexual differentiation. *Cell*, *77*(4), 481-490.

Magalhaes, A. C., Dunn, H., & Ferguson, S. S. (2012). Regulation of GPCR activity, trafficking and localization by GPCR-interacting proteins. *British journal of pharmacology*, *165*(6), 1717-1736.

Maguire, J. J., Kuc, R. E., & Davenport, A. P. (2012). Radioligand binding assays and their analysis. *Methods in molecular biology*, *897*, 31-77.

Malik, S., Dolan, T. M., Maben, Z. J., & Hinkle, P. M. (2015). Adrenocorticotropic Hormone (ACTH) Responses Require Actions of the Melanocortin-2 Receptor Accessory Protein on the Extracellular Surface of the Plasma Membrane. *The Journal of biological chemistry*, *290*(46), 27972-27985.

Markovic, D., & Challiss, R. A. (2009). Alternative splicing of G protein-coupled receptors: physiology and pathophysiology. *Cellular and molecular life sciences*, *66*(20), 3337-3352.

Martin, A. L., Steurer, M. A., & Aronstam, R. S. (2015). Constitutive Activity among Orphan Class-A G Protein Coupled Receptors. *Public Library of Science one*, *10*(9), e0138463.

Marti-Solano, M. (2023). A multi-dimensional view of context-dependent G protein-coupled receptor function. *Biochemical Society transactions*, *51*(1), 13-20.

Masui, H., & Garren, L. D. (1971). Inhibition of replication in functional mouse adrenal tumor cells by adrenocorticotropic hormone mediated by adenosine 3':5'-cyclic monophosphate. *Proceedings of the National Academy of Sciences of the USA*, *68*(12), 3206-3210.

Mateska, I. (2024). Primary cilia and Sonic hedgehog signaling in adrenal gland physiology and cancer. *Current Opinion in Endocrine and Metabolic Research*, *34*, 100507.

Mattos, G. E., Jacysyn, J. F., Amarante-Mendes, G. P., & Lotfi, C. F. P. (2011). Comparative effect of FGF2, synthetic peptides 1-28 N-POMC and ACTH on proliferation in rat adrenal cell primary cultures. *Cell and tissue research*, *345*(3), 343-356.

McLean, C., Hope, J., Salacinski, P., Estivariz, F., & Lowry, P. J. (1981). Purification and characterization of amino-terminal pro-opiocortin peptides from human pituitary glands. *Bioscience Reports*, *1*(11), 843-849.

Meimaridou, E., Hughes, C. R., Kowalczyk, J., Guasti, L., Chapple, J. P., King, P. J., Chan, L. F., Clark, A. J., & Metherell, L. A. (2013). Familial glucocorticoid deficiency: New genes and mechanisms. *Molecular and cellular endocrinology*, *371*(1-2), 195-200.

Mendonca, P. O., & Lotfi, C. F. (2011). The proliferative effect of synthetic N-POMC (1-28) peptides in rat adrenal cortex: a possible role for cyclin E. *Molecular and cellular endocrinology*, *336*(1-2), 156-161.

Mesiano, S., Mellon, S. H., & Jaffe, R. B. (1993). Mitogenic action, regulation, and localization of insulin-like growth factors in the human fetal adrenal gland. *The Journal of clinical endocrinology and metabolism*, *76*(4), 968-976.

Metherell, L. A., Chapple, J. P., Cooray, S., David, A., Becker, C., Ruschendorf, F., Naville, D., Begeot, M., Khoo, B., Nurnberg, P., Huebner, A., Cheetham, M. E., & Clark, A. J. (2005). Mutations in MRAP, encoding a new interacting partner of the ACTH receptor, cause familial glucocorticoid deficiency type 2. *Nature genetics*, *37*(2), 166-170.

Metherell, L. A., Naville, D., Halaby, G., Begeot, M., Huebner, A., Nürnberg, G., Nürnberg, P., Green, J., Tomlinson, J. W., Krone, N. P., Lin, L., Racine, M., Berney, D. M., Achermann, J. C., Arlt, W., & Clark, A. J. (2009). Nonclassic lipoid congenital adrenal hyperplasia masquerading as familial glucocorticoid deficiency. *The Journal of clinical endocrinology and metabolism*, *94*(10), 3865-3871.

Milligan, G. (2001). Oligomerisation of G-protein-coupled receptors. *Journal of cell science*, *114*(Pt 7), 1265-1271.

Milligan, G. (2009). G protein-coupled receptor hetero-dimerization: contribution to pharmacology and function. *British journal of pharmacology*, *158*(1), 5-14.

Milligan, G., Ward, R. J., & Marsango, S. (2019). GPCR homo-oligomerization. *Current opinion in cell biology*, *57*, 40-47.

Montpetit, A., & Sinnett, D. (1999). Physical mapping of the G-protein coupled receptor 19 (GPR19) in the chromosome 12p12.3 region frequently rearranged in cancer cells. *Human Genetics*, *105*(1-2), 162-164.

Motiejunaite, J., Amar, L., & Vidal-Petiot, E. (2021). Adrenergic receptors and cardiovascular effects of catecholamines. *Annales Endocrinol (Paris)*, *82*(3-4), 193-197.

Motulsky, H. J., & Neubig, R. R. (2010). Analyzing binding data. *Current protocols in neuroscience*, *Chapter 7*, Unit 7.5.

Mushala, B. A. S., Xie, B., Sipula, I. J., Stoner, M. W., Thapa, D., Manning, J. R., Bugga, P., Vandevender, A. M., Jurczak, M. J., & Scott, I. (2023). G-protein coupled receptor 19 (GPR19) knockout mice display sex-dependent metabolic dysfunction. *Scientific reports*, *13*(1), 6134.

Novoselova, T. V., Hussain, M., King, P. J., Guasti, L., Metherell, L. A., Charalambous, M., Clark, A. J. L., & Chan, L. F. (2018). MRAP deficiency impairs adrenal progenitor cell differentiation and gland zonation. *Federation of American Societies for Experimental Biology journal*, *32*(11), fj201701274RR.

Novoselova, T. V., Larder, R., Rimmington, D., Lelliott, C., Wynn, E. H., Gorrigan, R. J., Tate, P. H., Guasti, L., Sanger Mouse Genetics, P., O'Rahilly, S., Clark, A. J., Logan, D. W., Coll, A. P., & Chan, L. F. (2016). Loss of Mrap2 is associated with Sim1 deficiency and increased circulating cholesterol. *The Journal of endocrinology*, *230*(1), 13-26.

O'Dowd, B. F., Nguyen, T., Lynch, K. R., Kolakowski, L. F., Jr., Thompson, M., Cheng, R., Marchese, A., Ng, G., Heng, H. H., & George, S. R. (1996). A novel gene codes for a putative G protein-coupled receptor with an abundant expression in brain. *Federation of European Biochemical Societies letters*, *394*(3), 325-329.

Oliver, C., & Jamur, M. C. (2010). Immunocytochemical methods and protocols. *Methods in molecular biology*, *588*, iv-v.

Ortiz, R., Kluwe, B., Lazarus, S., Teruel, M. N., & Joseph, J. J. (2022). Cortisol and cardiometabolic disease: a target for advancing health equity. *Trends in endocrinology and metabolism*, *33*(11), 786-797.

Payne, A. H., & Hales, D. B. (2004). Overview of steroidogenic enzymes in the pathway from cholesterol to active steroid hormones. *Endocrine Reviews*, *25*(6), 947-970.

Pedersen, R. C., & Brownie, A. C. (1979). Failure of ACTH to mimic the stress-induced activation of rat adrenocortical cholesterol ester hydrolase in vivo. *Journal of steroid biochemistry*, *11*(4), 1393-1400.

Pedersen, R. C., & Brownie, A. C. (1980). Adrenocortical response to corticotropin is potentiated by part of the amino-terminal region of pro-corticotropin/endorphin. *Proceedings of the National Academy of Sciences of the USA*, *77*(4), 2239-2243.

Pedersen, R. C., & Brownie, A. C. (1983). Lys-gamma 3-melanotropin binds with high affinity to the rat adrenal cortex. *Endocrinology*, *112*(4), 1279-1287.

Pedersen, R. C., Brownie, A. C., & Ling, N. (1980). Pro-adrenocorticotropin/endorphin-derived peptides: coordinate action on adrenal steroidogenesis. *Science*, *208*(4447), 1044-1046.

Pepper, D. J., & Bicknell, A. B. (2009). The stimulation of mitogenic signaling pathways by N-POMC peptides. *Molecular and cellular endocrinology*, *300*(1-2), 77-82.

Pereira, S. S., Monteiro, M. P., Costa, M. M., Ferreira, J., Alves, M. G., Oliveira, P. F., Jarak, I., & Pignatelli, D. (2019). MAPK/ERK pathway inhibition is a promising treatment target for adrenocortical tumors. *Journal of cellular biochemistry*, *120*(1), 894-906.

Pereira, S. S., Monteiro, M. P., Costa, M. M., Moreira, Â., Alves, M. G., Oliveira, P. F., Jarak, I., & Pignatelli, D. (2019). IGF2 role in adrenocortical carcinoma biology. *Endocrine*, *66*(2), 326-337.

Pihlajoki, M., Dörner, J., Cochran, R. S., Heikinheimo, M., & Wilson, D. B. (2015). Adrenocortical zonation, renewal, and remodeling. *Frontiers in endocrinology (Lausanne)*, *6*, 27.

Pirkmajer, S., & Chibalin, A. V. (2011). Serum starvation: caveat emptor. *American journal of physiology. Cell physiology*, *301*(2), C272-C279.

Pu, S., Zhou, Y., Xie, P., Gao, X., Liu, Y., Ren, Y., He, J., & Hao, N. (2022). Identification of necroptosis-related subtypes and prognosis model in triple negative breast cancer. *Frontiers in immunology*, *13*, 964118.

Rajagopal, S., & Shenoy, S. K. (2018). GPCR desensitization: Acute and prolonged phases. *Cellular signalling*, *41*, 9-16.

Rao, A., & Herr, D. R. (2017). G protein-coupled receptor GPR19 regulates E-cadherin expression and invasion of breast cancer cells. *Biochimica et biophysica acta. Molecular cell research*, *1864*(7), 1318-1327.

Rao, V. S., Srinivas, K., Sujini, G. N., & Kumar, G. N. (2014). Protein-protein interaction detection: methods and analysis. *International journal of proteomics*, *2014*, 147648.

Rege, J., Garber, S., Conley, A. J., Elsey, R. M., Turcu, A. F., Auchus, R. J., & Rainey, W. E. (2019). Circulating 11-oxygenated androgens across species. *The Journal of steroid biochemistry and molecular biology*, *190*, 242-249.

Relav, L., Doghman-Bouguerra, M., Ruggiero, C., Muzzi, J. C. D., Figueiredo, B. C., & Lalli, E. (2023). Steroidogenic Factor 1, a Goldilocks Transcription Factor from Adrenocortical Organogenesis to Malignancy. *International journal of molecular sciences*, *24*(4), 3585.

Riker, A. I., Enkemann, S. A., Fodstad, O., Liu, S., Ren, S., Morris, C., Xi, Y., Howell, P., Metge, B., Samant, R. S., Shevde, L. A., Li, W., Eschrich, S., Daud, A., Ju, J.,

& Matta, J. (2008). The gene expression profiles of primary and metastatic melanoma yields a transition point of tumor progression and metastasis. *BMC medical genomics, 1*, 13.

Roberts, L. M. (2019). Tips for Avoiding Artifacts from UV Photoconversion of DAPI. *Microscopy Today*, *27*(5), 18-24.

Rocha, K. M., Forti, F. L., Lepique, A. P., & Armelin, H. A. (2003). Deconstructing the molecular mechanisms of cell cycle control in a mouse adrenocortical cell line: roles of ACTH. *Microscopy Research and Technique*, *61*(3), 268-274.

Rommel, C., Clarke, B. A., Zimmermann, S., Nuñez, L., Rossman, R., Reid, K., Moelling, K., Yancopoulos, G. D., & Glass, D. J. (1999). Differentiation stage-specific inhibition of the Raf-MEK-ERK pathway by Akt. *Science, 286*(5445), 1738-1741.

Roselli-Rehfuss, L., Mountjoy, K. G., Robbins, L. S., Mortrud, M. T., Low, M. J., Tatro, J. B., Entwistle, M. L., Simerly, R. B., & Cone, R. D. (1993). Identification of a receptor for gamma melanotropin and other proopiomelanocortin peptides in the hypothalamus and limbic system. *Proceedings of the National Academy of Sciences of the USA*, *90*(19), 8856-8860.

Roskoski, R., Jr. (2012). MEK1/2 dual-specificity protein kinases: structure and regulation. *Biochemical and biophysical research communications, 417*(1), 5-10.

Ross, J. T., Bennett, H. P., James, S., & McMillen, I. C. (2000). Infusion of N-proopiomelanocortin-(1-77) increases adrenal weight and messenger ribonucleic acid levels of cytochrome P450 17alpha-hydroxylase in the sheep fetus during late gestation. *Endocrinology*, *141*(6), 2153-2158.

Rouault, A. A. J., Lee, A. A., & Sebag, J. A. (2017). Regions of MRAP2 required for the inhibition of orexin and prokineticin receptor signaling. *Biochimica et biophysica acta. Molecular cell research*, *1864*(12), 2322-2329.

Roux, B. T., & Cottrell, G. S. (2014). G protein-coupled receptors: what a difference a 'partner' makes. *International journal of molecular sciences*, *15*(1), 1112-1142.

Roy, S., Pinard, S., Chouinard, L., & Gallo-Payet, N. (2011). Adrenocorticotropin hormone (ACTH) effects on MAPK phosphorylation in human fasciculata cells and in embryonic kidney 293 cells expressing human melanocortin 2 receptor (MC2R) and MC2R accessory protein (MRAP)beta. *Molecular and cellular endocrinology*, *336*(1-2), 31-40.

Roy, S., Rached, M., & Gallo-Payet, N. (2007). Differential regulation of the human adrenocorticotropin receptor [melanocortin-2 receptor (MC2R)] by human MC2R accessory protein isoforms alpha and beta in isogenic human embryonic kidney 293 cells. *Molecular endocrinology*, *21*(7), 1656-1669.

Sambrook, J., & Russell, D. W. (2006). The inoue method for preparation and transformation of competent e. Coli: "ultra-competent" cells. *Cold Spring Harbor protocols*, *2006*(1), pdb.prot3944.

Saphier, P. W., Glynn, B. P., Woods, R. J., Shepherd, D. A., Jeacock, M. K., & Lowry, P. J. (1993). Elevated levels of N-terminal pro-opiomelanocortin peptides in fetal sheep plasma may contribute to fetal adrenal gland development and the pre-parturient cortisol surge. *Endocrinology*, *133*(3), 1459-1461.

Scott, M., & Laporte, S. (2019). *Beta-Arrestins Methods and Protocols: Methods and Protocols*.

Seamon, K. B., Padgett, W., & Daly, J. W. (1981). Forskolin: unique diterpene activator of adenylate cyclase in membranes and in intact cells. *Proceedings of the National Academy of Sciences of the USA*, *78*(6), 3363-3367.

Sebag, J. A., & Hinkle, P. M. (2007). Melanocortin-2 receptor accessory protein MRAP forms antiparallel homodimers. *Proceedings of the National Academy of Sciences of the USA*, *104*(51), 20244-20249.

Sebag, J. A., Zhang, C., Hinkle, P. M., Bradshaw, A. M., & Cone, R. D. (2013). Developmental control of the melanocortin-4 receptor by MRAP2 proteins in zebrafish. *Science*, *341*(6143), 278-281.

Seger, M. A., & Bennett, H. P. (1986). Structure and bioactivity of the amino-terminal fragment of pro-opiomelanocortin. *Journal of steroid biochemistry*, *25*(5b), 703-710.

Seidah, N. G., & Chrétien, M. (1981). Complete amino acid sequence of a human pituitary glycopeptide: an important maturation product of pro-opiomelanocortin. *Proceedings of the National Academy of Sciences of the USA*, *78*(7), 4236-4240.

Seidah, N. G., Benjannet, S., Routhier, R., De Serres, G., Rochemont, J., Lis, M., & Chrétien, M. (1980). Purification and characterization of the N-terminal fragment of pro-opiomelanocortin from human pituitaries: homology to the bovine sequence. *Biochemical and biophysical research communications*, *95*(4), 1417-1424.

Seidah, N. G., Rochemont, J., Hamelin, J., Benjannet, S., & Chrétien, M. (1981). The missing fragment of the pro-sequence of human pro-opiomelanocortin: sequence and evidence for C-terminal amidation. *Biochemical and biophysical research communications*, *102*(2), 710-716.

Seidah, N. G., Rochemont, J., Hamelin, J., Lis, M., & Chrétien, M. (1981). Primary structure of the major human pituitary pro-opiomelanocortin NH2-terminal glycopeptide. Evidence for an aldosterone-stimulating activity. *The Journal of biological chemistry*, *256*(15), 7977-7984.

Selbie, L. A., & Hill, S. J. (1998). G protein-coupled-receptor cross-talk: the fine-tuning of multiple receptor-signalling pathways. *Trends in Pharmacological Sciences*, *19*(3), 87-93.

Shah, B. H., Baukal, A. J., Shah, F. B., & Catt, K. J. (2005). Mechanisms of extracellularly regulated kinases 1/2 activation in adrenal glomerulosa cells by lysophosphatidic acid and epidermal growth factor. *Molecular endocrinology*, *19*(10), 2535-2548.

Sleno, R., & Hébert, T. E. (2018). The Dynamics of GPCR Oligomerization and Their Functional Consequences. *International review of cell and molecular biology*, *338*, 141-171.

Slominski, A., Wortsman, J., Luger, T., Paus, R., & Solomon, S. (2000). Corticotropin releasing hormone and proopiomelanocortin involvement in the cutaneous response to stress. *Physiological reviews*, *80*(3), 979-1020.

Smith, A. I., & Funder, J. W. (1988). Proopiomelanocortin processing in the pituitary, central nervous system, and peripheral tissues. *Endocrine Reviews*, *9*(1), 159-179.

Smith, J. S., & Pack, T. F. (2021). Noncanonical interactions of G proteins and β-arrestins: from competitors to companions. *Federation of European Biochemical Societies journal*, *288*(8), 2550-2561.

Smrcka, A. V., Lehmann, D. M., & Dessal, A. L. (2008). G protein betagamma subunits as targets for small molecule therapeutic development. *Combinatorial chemistry and high throughput screening*, *11*(5), 382-395.

Southern, C., Cook, J. M., Neetoo-Isseljee, Z., Taylor, D. L., Kettleborough, C. A., Merritt, A., Bassoni, D. L., Raab, W. J., Quinn, E., Wehrman, T. S., Davenport, A. P., Brown, A. J., Green, A., Wigglesworth, M. J., & Rees, S. (2013). Screening β-Arrestin Recruitment for the Identification of Natural Ligands for Orphan G-Protein–Coupled Receptors. *Journal of Biomolecular Screening*, *18*(5), 599-609.

Srisai, D., Yin, T. C., Lee, A. A., Rouault, A. A. J., Pearson, N. A., Grobe, J. L., & Sebag, J. A. (2017). MRAP2 regulates ghrelin receptor signaling and hunger sensing. *Nature communications*, *8*(1), 713.

Stein, L. M., Yosten, G. L., & Samson, W. K. (2016). Adropin acts in brain to inhibit water drinking: potential interaction with the orphan G protein-coupled receptor, GPR19. *American journal of physiology. Regulatory, integrative and comparative physiology*, *310*(6), R476-R480.

Stelcer, E., Milecka, P., Komarowska, H., Jopek, K., Tyczewska, M., Szyszka, M., Lesniczak, M., Suchorska, W., Bekova, K., Szczepaniak, B., Ruchala, M., Karczewski, M., Wierzbicki, T., Szaflarski, W., Malendowicz, L. K., & Rucinski, M. (2020). Adropin Stimulates Proliferation and Inhibits Adrenocortical Steroidogenesis in the Human Adrenal Carcinoma (HAC15) Cell Line. *Frontiers in endocrinology (Lausanne)*, *11*, 561370.

Steven, A., Friedrich, M., Jank, P., Heimer, N., Budczies, J., Denkert, C., & Seliger, B. (2020). What turns CREB on? And off? And why does it matter? *Cellular and molecular life sciences*, *77*(20), 4049-4067.

St-Jean, M., Ghorayeb, N. E., Bourdeau, I., & Lacroix, A. (2018). Aberrant G-protein coupled hormone receptor in adrenal diseases. *Best practice and research. Clinical endocrinology and metabolism*, *32*(2), 165-187.

Sugiura, R., Satoh, R., & Takasaki, T. (2021). ERK: A Double-Edged Sword in Cancer. ERK-Dependent Apoptosis as a Potential Therapeutic Strategy for Cancer. *Cells*, *10*(10), 2509.

Suntharalingham, J. P., Buonocore, F., Duncan, A. J., & Achermann, J. C. (2015). DAX-1 (NR0B1) and steroidogenic factor-1 (SF-1, NR5A1) in human disease. *Best practice and research. Clinical endocrinology and metabolism*, *29*(4), 607-619.

Swaim, W. D. (2010). Overview of confocal microscopy. *Methods in molecular biology*, *588*, 187-201.

Tabor, A., Weisenburger, S., Banerjee, A., Purkayastha, N., Kaindl, J. M., Hübner, H., Wei, L., Grömer, T. W., Kornhuber, J., Tschammer, N., Birdsall, N. J., Mashanov, G. I., Sandoghdar, V., & Gmeiner, P. (2016). Visualization and ligand-induced modulation of dopamine receptor dimerization at the single molecule level. *Scientific reports*, *6*, 33233.

Tang, C., Zelenak, C., Völkl, J., Eichenmüller, M., Regel, I., Fröhlich, H., Kempe, D., Jimenez, L., Le Bellego, L., Vergne, S., & Lang, F. (2011). Hydration-sensitive gene expression in brain. *Cellular physiology and biochemistry*, *27*(6), 757-768.

Terrillon, S., & Bouvier, M. (2004). Roles of G-protein-coupled receptor dimerization. *European Molecular Biology Organization reports*, *5*(1), 30-34.

Thapa, D., Stoner, M. W., Zhang, M., Xie, B., Manning, J. R., Guimaraes, D., Shiva, S., Jurczak, M. J., & Scott, I. (2018). Adropin regulates pyruvate dehydrogenase in cardiac cells via a novel GPCR-MAPK-PDK4 signaling pathway. *Redox biology*, *18*, 25-32.

Thapa, D., Xie, B., Manning, J. R., Zhang, M., Stoner, M. W., Huckestein, B. R., Edmunds, L. R., Zhang, X., Dedousis, N. L., O'Doherty, R. M., Jurczak, M. J., &

Scott, I. (2019). Adropin reduces blood glucose levels in mice by limiting hepatic glucose production. *Physiological reports*, *7*(8), e14043.

Thapa, D., Xie, B., Zhang, M., Stoner, M. W., Manning, J. R., Huckestein, B. R., Edmunds, L. R., Mullett, S. J., McTiernan, C. F., Wendell, S. G., Jurczak, M. J., & Scott, I. (2019). Adropin treatment restores cardiac glucose oxidation in pre-diabetic obese mice. *Journal of molecular and cellular cardiology*, *129*, 174-178.

Thiel, G., Backes, T. M., Guethlein, L. A., & Rössler, O. G. (2021). Critical Protein-Protein Interactions Determine the Biological Activity of Elk-1, a Master Regulator of Stimulus-Induced Gene Transcription. *Molecules*, *26*(20), 6125.

Thomas, M., Keramidas, M., Monchaux, E., & Feige, J. J. (2004). Dual hormonal regulation of endocrine tissue mass and vasculature by adrenocorticotropin in the adrenal cortex. *Endocrinology*, *145*(9), 4320-4329.

Thomas, P., & Smart, T. G. (2005). HEK293 cell line: a vehicle for the expression of recombinant proteins. *Journal of pharmacological and toxicological methods*, *51*(3), 187-200.

Thompson, M. D., Cole, D. E., Jose, P. A., & Chidiac, P. (2014). G protein-coupled receptor accessory proteins and signaling: pharmacogenomic insights. *Methods in molecular biology*, *1175*, 121-152.

Tilemans, D., Ramaekers, D., Andries, M., & Denef, C. (1997). Effect of POMC (1-76), its C-terminal fragment gamma3-MSH and anti-POMC (1-76) antibodies on DNA replication in lactotrophs in aggregate cell cultures of immature rat pituitary. *Journal of neuroendocrinology*, *9*(8), 627-637.

Torres, T. E., & Lotfi, C. F. (2007). Distribution of cells expressing Jun and Fos proteins and synthesizing DNA in the adrenal cortex of hypophysectomized rats: regulation by ACTH and FGF2. *Cell and tissue research*, *329*(3), 443-455.

Torres, T. E., de Mendonca, P. O., & Lotfi, C. F. (2010). Synthetic modified N-POMC(1-28) controls in vivo proliferation and blocks apoptosis in rat adrenal cortex. *Cell and tissue research*, *341*(2), 239-250.

Treisman, R. (1992). The serum response element. *Trends in biochemical sciences*, *17*(10), 423-426.

Turcu, A., Smith, J. M., Auchus, R., & Rainey, W. E. (2014). Adrenal androgens and androgen precursors-definition, synthesis, regulation and physiologic actions. *Comprehensive Physiology*, *4*(4), 1369-1381.

Ulloa-Aguirre, A., Zariñán, T., Gutiérrez-Sagal, R., & Tao, Y. X. (2022). Targeting trafficking as a therapeutic avenue for misfolded GPCRs leading to endocrine diseases. *Frontiers in endocrinology (Lausanne)*, *13*, 934685.

Ulrich-Lai, Y. M., Figueiredo, H. F., Ostrander, M. M., Choi, D. C., Engeland, W. C., & Herman, J. P. (2006). Chronic stress induces adrenal hyperplasia and hypertrophy in a subregion-specific manner. *American journal of physiology. Endocrinology and metabolism*, *291*(5), E965-E973.

Val, P., Martinez-Barbera, J. P., & Swain, A. (2007). Adrenal development is initiated by Cited2 and Wt1 through modulation of Sf-1 dosage. *Development*, *134*(12), 2349-2358.

van Biesen, T., Luttrell, L. M., Hawes, B. E., & Lefkowitz, R. J. (1996). Mitogenic signaling via G protein-coupled receptors. *Endocrine Reviews*, *17*(6), 698-714.

Vassilatis, D. K., Hohmann, J. G., Zeng, H., Li, F., Ranchalis, J. E., Mortrud, M. T., Brown, A., Rodriguez, S. S., Weller, J. R., Wright, A. C., Bergmann, J. E., & Gaitanaris, G. A. (2003). The G protein-coupled receptor repertoires of human and mouse. *Proceedings of the National Academy of Sciences of the USA*, *100*(8), 4903-4908.

von Kleist, L., Stahlschmidt, W., Bulut, H., Gromova, K., Puchkov, D., Robertson, M. J., MacGregor, K. A., Tomilin, N., Pechstein, A., Chau, N., Chircop, M., Sakoff, J., von Kries, J. P., Saenger, W., Kräusslich, H. G., Shupliakov, O., Robinson, P. J., McCluskey, A., & Haucke, V. (2011). Role of the clathrin terminal domain in regulating coated pit dynamics revealed by small molecule inhibition. *Cell*, *146*(3), 471-484.

Wang, M., Xu, J., Lei, X. W., Zhang, C., Liu, S. Y., Jin, L. N., & Zhang, C. (2022). Selective Interactions of Mouse Melanocortin Receptor Accessory Proteins with Somatostatin Receptors. *Cells*, *11*(2), 267.

Webb, T. R., & Clark, A. J. (2010). Minireview: the melanocortin 2 receptor accessory proteins. *Molecular endocrinology*, *24*(3), 475-484.

Webb, T. R., Chan, L., Cooray, S. N., Cheetham, M. E., Chapple, J. P., & Clark, A. J. (2009). Distinct melanocortin 2 receptor accessory protein domains are required for melanocortin 2 receptor interaction and promotion of receptor trafficking. *Endocrinology*, *150*(2), 720-726.

Weber, A., & Clark, A. J. (1994). Mutations of the ACTH receptor gene are only one cause of familial glucocorticoid deficiency. *Human molecular genetics*, *3*(4), 585-588.

Weinberg, Z. Y., & Puthenveedu, M. A. (2019). Regulation of G protein-coupled receptor signaling by plasma membrane organization and endocytosis. *Traffic*, *20*(2), 121-129.

Wilhelm, D., & Englert, C. (2002). The Wilms tumor suppressor WT1 regulates early gonad development by activation of Sf1. *Genes and Development*, *16*(14), 1839-1851.

Wilson, J. M., de Hoop, M., Zorzi, N., Toh, B. H., Dotti, C. G., & Parton, R. G. (2000). EEA1, a tethering protein of the early sorting endosome, shows a polarized distribution in hippocampal neurons, epithelial cells, and fibroblasts. *Molecular biology of the cell*, *11*(8), 2657-2671.

Wong, C. M., Wang, Y., Lee, J. T., Huang, Z., Wu, D., Xu, A., & Lam, K. S. (2014). Adropin is a brain membrane-bound protein regulating physical activity via the NB-3/Notch signaling pathway in mice. *The Journal of biological chemistry*, *289*(37), 25976-25986.

Worzfeld, T., Wettschureck, N., & Offermanns, S. (2008). G(12)/G(13)-mediated signalling in mammalian physiology and disease. *Trends in Pharmacological Sciences*, *29*(11), 582-589.

Wright, N. A., Appleton, D. R., & Morley, A. R. (1974). Effect of dexamethasone on cell population kinetics in the adrenal cortex of the prepubertal male rat. *The Journal of endocrinology*, *62*(3), 527-536.

Yabu, M., Senda, T., Nonaka, Y., Matsukawa, N., Okamoto, M., & Fujita, H. (1991). Localization of the gene transcripts of 11 beta-hydroxylase and aldosterone synthase in the rat adrenal cortex by in situ hybridization. *Histochemistry*, *96*(5), 391-394.

Yang, S. H., Sharrocks, A. D., & Whitmarsh, A. J. (2013). MAP kinase signalling cascades and transcriptional regulation. *Gene*, *513*(1), 1-13.

Yaswen, L., Diehl, N., Brennan, M. B., & Hochgeschwender, U. (1999). Obesity in the mouse model of pro-opiomelanocortin deficiency responds to peripheral melanocortin. *Nature medicine*, *5*(9), 1066-1070.

Yates, R., Katugampola, H., Cavlan, D., Cogger, K., Meimaridou, E., Hughes, C., Metherell, L., Guasti, L., & King, P. (2013). Adrenocortical development, maintenance, and disease. *Current topics in developmental biology*, *106*, 239-312.

Zhang, S., Chen, Q., Lin, X., Chen, M., & Liu, Q. (2020). A Review of Adropin as the Medium of Dialogue between Energy Regulation and Immune Regulation. *Oxidative Medicine and Cellular Longevity*, *2020*, 3947806.

Zhang, X., Saarinen, A. M., Campbell, L. E., De Filippis, E. A., & Liu, J. (2018). Regulation of Lipolytic Response and Energy Balance by Melanocortin 2 Receptor Accessory Protein (MRAP) in Adipocytes. *Diabetes*, *67*(2), 222-234.

Zhou, A., Bloomquist, B. T., & Mains, R. E. (1993). The prohormone convertases PC1 and PC2 mediate distinct endoproteolytic cleavages in a strict temporal order during proopiomelanocortin biosynthetic processing. *The Journal of biological chemistry*, *268*(3), 1763-1769.

Zinchuk, V., Zinchuk, O., & Okada, T. (2007). Quantitative colocalization analysis of multicolor confocal immunofluorescence microscopy images: pushing pixels to explore biological phenomena. *Acta histochemica et cytochemica*, *40*(4), 101-111.